



UNIVERSITY OF TRENTO - Italy

International PhD Program in Biomolecular Sciences

Centre for Integrative Biology

29th Cycle

**Characterization of Small Molecules Inhibiting the RNA
Binding Protein HuR**

Tutor: Dr. Alessandro PROVENZANI

Advisor: Dr. Vito Giuseppe D'AGOSTINO

Centre for Integrative Biology, CIBIO

Laboratory of Genomic Screening

Ph.D. Thesis of

Preet LAL

Centre for Integrative Biology, CIBIO

Laboratory of Genomic Screening

Academic year

2015-16

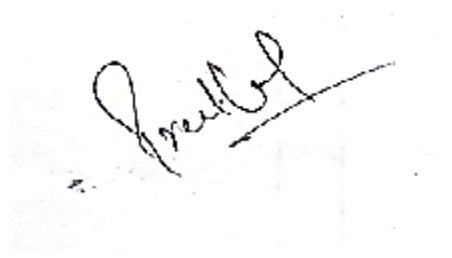
ABSTRACT

HuR, the ubiquitously expressed member of the ELAV (embryonic lethal abnormal vision) family of RNA binding proteins, selectively binds to AREs (AU-rich elements) and mainly stabilizes ARE-containing mRNAs, e.g. TNF α , VEGF, c-FOS, favoring specific protein translation. TNF α mRNA is one of the most important target mRNA of HuR since the protein encoded by this gene mediates the inflammatory response and its overexpression is correlated with autoimmune diseases and cancer-related inflammation. Specific drugs are already available that can inhibit TNF α protein but cause important side-effects, as insurgence of tumoral pathologies, due to high immunodepression. Therefore, inhibition of TNF α mRNA translation by specific inhibitors targeting HuR, only in those cells undergoing pathological anomalies, is an alternative, intriguing novel therapeutic approach that deserves investigation. By REMSA and AlphaScreen assays we identified a family of low molecular weight inhibitors, called Tanshinones, among which DHTS-I (Dihydrotanshinone – I) was the most potent. Tanshinones are well known in the traditional Chinese Medicine Practice, and these anti-inflammatory agents possess the ability to prevent HuR-RNA complex formation *in vitro*. We further identified structural determinants of HuR and DHTS interaction using RRM1&RRM2 tandem domains. EMSA and AlphaScreen experiments, with truncated Δ RRM1 and mutants revealed that DHTS is a competitive binder of HuR with respect of target RNA. To ameliorate the solubility of DHTS, we synthesized a number of DHTS analogs, of which the most potent and soluble compound was named MFM49. We evaluated the anti-inflammatory potential of DHTS and DHTS analogs and the HuR-dependent mechanism of action, revealing that, at least in part, DHTS and DHTS analogs rely on HuR to exert their mechanism of action. Influence on NF-kB activation by DHTS and MFM49 upon LPS co-stimulation was not seen in immunofluorescence studies. So here, we disclose a previously unrecognized molecular mechanism of action exerted by DHTS, and anti-inflammatory potential of DHTS analogs opening new perspectives to therapeutically target the HuR mediated, post-transcriptional control in inflammation and cancer like anomalies.

ORIGINAL AUTHORSHIP

Declaration

I *Preet Lal*, confirm that this is my own work and the use of all material from other sources has been properly and fully acknowledged.

A handwritten signature in black ink, appearing to read "Preet Lal", is written over a faint grid background.

CONTENTS

#Page

ABSTRACT.....	2
ABBREVIATIONS.....	9-10
INTRODUCTION	12
<i>Elav-like genes a conserved family in vertebrates.....</i>	12
<i>HuR structural feature.....</i>	14
<i>Signals that converge to HuR.....</i>	16
<i>p38 MAPK Pathway influence on HuR and TTP.....</i>	18
<i>NF-kB pathway.....</i>	19
ROLES OF HUR	20
<i>HuR in pre-mRNA processing.....</i>	20
<i>HuR in Cancer</i>	23
<i>HuR in Inflammation</i>	26
<i>Nuclear or Cytoplasmic: Does it endow any prognostic role?.....</i>	30
<i>Current state of the art on the Pharmacology of HuR and Small Molecules Inhibiting HuR....</i>	32
<i>Focusing on Tanshinones/DHTS to target HuR in vitro and in vivo.....</i>	35
<i>Why to inhibit HuR.....</i>	38
MATERIAL AND METHODS	41
RESULTS.....	49
<i>DHTS is an Inhibitor of HuR-RNA Interaction</i>	50
<i>DHTS binds to M1M2 domains of rHuR.....</i>	51
<i>DHTS selective profile against other RBPs.....</i>	53
<i>Inter-domain linker region of HuR structure is crucial for binding to target RNA and therefore for DHTS activity.....</i>	54
<i>Single point mutations in the HuR-DHTS interacting region abolishes DHTS efficacy.....</i>	57
<i>Single point mutation causes dimerizing aggregation behavior of Muteins.....</i>	60

<i>DHTS downregulates TNFα and VEGF in breast cancer cells.....</i>	<i>61</i>
<i>DHTS efficacy depends upon HuR expression.....</i>	<i>64</i>
<i>DHTS is effective on HuR positive models invitro and invivo.....</i>	<i>64</i>
BIOCHEMICAL CHARACTERIZATION OF DHTS ANALOGS.....	66
<i>MFM49 is most potent inhibitor of rHuR-RNA interaction invitro.....</i>	<i>68</i>
<i>DHTS analogs are the potential inhibitors of HuR RNA: Complex formation.....</i>	<i>69</i>
<i>MFM49 and DHTS do not influence nucleocytoplasmic level of HuR in MCF-7 cells.....</i>	<i>71</i>
<i>MFM49 and DHTS do not influence substantial nucleocytoplasmic level of NF-kB and HuR in RAW264.7 cells.....</i>	<i>73</i>
ANTI-INFLAMMATORY PROPERTIES OF DHTS ANALOGS.....	75
<i>Cell Viability assays.....</i>	<i>75</i>
<i>DHTS analogs down-regulates LPS induced cytokines in RAW264.7 cells.....</i>	<i>76</i>
<i>DHTS downregulates TNFα and TTP levels.....</i>	<i>78</i>
<i>Down regulation of major cytokines by DHTS and MFM49 is HuR-dependent.....</i>	<i>79</i>
<i>TNFα down-regulation by DHTS and DHTS analogs is independent of TTP in TTP-KO macrophages.....</i>	<i>80</i>
Preliminary Results.....	81
<i>NF-kB activation is not influenced by DHTS analogs in RAW264.7 cells</i>	<i>81</i>
<i>MAPK pathway activation upon co-treatment our with compounds.....</i>	<i>84</i>
<i>Analysis of p38 MAPK pathway in TTP-KO cells.....</i>	<i>85</i>
<i>Polysomal analysis in RAW264.7 upon LPS stimulation.....</i>	<i>85</i>
<i>Effect on mRNA Stability after transcriptional inhibition with Actinomycin D.....</i>	<i>87</i>
OTHER DHTS ANALOGS.....	88
DISCUSSION.....	91
CONCLUSIONS.....	98
REFERENCES.....	99

APPENDIX.....	112
Acknowledgements.....	144

LIST OF FIGURES

Figure 1 Schematic representation of the biological processes where HuR plays crucial role...14	
Figure 2 (i) Crystal structure of free RRM1/2.....15	
Figure 2 (ii) Dynamic properties of RRM1/2.....15	
Figure 3 MAPK signalling pathways affecting properties of cytokine mRNAs.....17	
Figure 4 Schematic of regulation of TNF α mRNA and TNF α release by p38 and MK2/3.....18	
Figure 5 Schematic of NF- κ B pathway and the Mechanism of NF- κ B action.....20	
Figure 6 HuR function in controlling cell fate by controlling mRNAs.....25	
Figure 7 Schematic diagram of HuR target and their influence in cells.....26	
Figure 8 The immunostaining of HuR from histological and cytological specimen32	
Figure 9 Schematic representation of Synthesis HuR-FNP preparation.....34	
Figure 10 Chemical structure of tanshinones.....37	
Figure 11 Densitometric comparison of Tanshinones activity by EMSA38	
Figure 12 Biochemical screening and characterization of DHTS in-vitro..... 50	
Figure 13 DHTS interfere with HuR-RNA complex and lowers the cell viability..... 51	
Figure 14 Effects of DHTS on RRM1/2 and RRM2/3.....51	
Figure 15 Limited effects of DHTS on individual RRMs.....53	
Figure 16 Determination of selective profile for DHTS in panel of other well-known RBPs.....53	
Figure 17 EMSAs using individual RRMs and Δ RRM1 to dictate probe binding upon DHTS addition.....56	
Figure 18 Single point mutations in the HuR-DHTS interacting region abolish DHTS efficacy 58	

Figure 19 CD and NMR spectra of TNF α	59
Figure 20 Calculation of Kd of muteins by AlphaScreen assay.....	59
Figure 21 Calculation of Kd for RRM1/2, and positions of mutated residues in HuR.....	60
Figure 22 Aggregation of HuR muteins.....	61
Figure 23 DHTS downregulates TNF α and VEGF in breast cancer cells.....	62
Figure 24 Efficacy of DHTS is HuR dependent	63
Figure 25 DHTS efficacy relies on HuR presence in vivo.....	65-66
Figure 26 Screening of other potent HuR inhibitors.....	67
Figure 27 MFM49 is most potent inhibitor of rHuR-RNA interaction.....	68-69
Figure 28 AlphaScreen assays to evaluate DHTS analogs activity.....	70
Figure 29 Nucleocytoplasmic levels of HuR upon MFM49 and DHTS treatment.....	72
Figure 30 Nucleocytoplasmic levels of HuR & NF- κ B upon co-treatment with LPS and DMSO, MFM49, DHTS and ActD	73-74
Figure 31 Dose Response curve for DHTS analogs and DHTS.....	76
Figure 32 DHTS analogs down-regulates cytokines produced after LPS stimulation.....	76-77
Figure 33 DHTS downregulates TNF α and TTP levels.....	78
Figure 34 Down regulation of major cytokines by DHTS and MFM49 is HuR-dependent...79-80	
Figure 35 TNF α levels counteracted by DHTS analogs independent of TTP in TTP KO cells.....	81
Figure 36 NF- κ B activation is not influenced by DHTS analogs in RAW264.7 cells	82
Figure 37 Activation of p-MK2 and α -TTP levels in RAW.264.7 cells.....	83
Figure 38 Analysis of p38 MAPK pathway in TTP-KO cells.....	85
Figure 39 RT-qPCR analysis of actin and TNF α mRNA levels in Polysomal Profile.....	86
Figure 40 Influence of DHTS and MFM49 on the stability of major cytokines in LPS-exposed RAW 264.7.....	88

Figure 41 Cell viability assays done on various cell line using HuR inhibitors.....	89
Figure 42 (1 & 2) Cytokines levels upon DHTS and MFM49 treatment.....	114

LIST OF TABLES

TABLE 1 <i>K</i> (obs) values for HuR and its isoforms in FP.....	56
TABLE 2 <i>K_i</i> values obtained for DHTS Analogs by Alphascreen assay.....	70-71
TABLE 3 IC-50 values for DHTS and its analogs.....	112
TABLE 4 qPCR Primer sequences.....	112
TABLE 5 HuR RRM's Primer and HuR mutants Primers.....	113

ABBREVIATIONS

Act D	Actinomycin
ALEs	Alternative Last Exons
AREs	AU-Rich Elements
ATP	Adenosine Tri-Phosphate
Bi-TNF	Biotinylated TNF
BMDMs	Bone marrow derived macrophages
CALM-2	Calmodulin 2
CCL	C-C Motif Chemokine Ligand
CD	Circular Dichroism
CENPN	Centromere Protein N
Chk2	Checkpoint Kinase 2
clAP-2	Cellular Inhibitor of Apoptosis
COX-2	Cyclooxygenase 2
CSF-2	Colony Stimulating Factor 2
CXCL	The chemokine (C-X-C motif) ligand
CXCR-4	C-X-C Motif Chemokine Receptor 4
DHTS-I	Dihydratanshinone-I
Dlst	Dihydrolipoamide-Succinyl transferase
ELAVL-1	Embryonic Lethal Abnormal Vision like-1
EMSA	Electrophoretic Mobility shift Assay
FNP	Folate Nanoparticles
GATA3	GATA-Binding Factor 3
HDACs	Histone deacetylases
HuR	Human Antigen R
IC50	Inhibitory Concentration 50
i-CLIP	individual-Nucleotide Resolution UV Crosslinking and Immunoprecipitation
IFN- γ	Interferon- γ
MAPK	Mitogen Activated protein Kinases
MK-2	MAP kinase-activated protein kinase

MMPs	Matrix Metalloproteinase
NF-1	Neuro Fibromin-1
Ni-NTA	Ni-Nitrilo Triacetic Acid
NMR	Nuclear Magnetic Resonance
OSCC	Oral squamous cell carcinoma
PAR-iCLIP	Photoactivatable ribonucleoside-enhanced Crosslinking and Immunoprecipitation
PCR	Polymerase Chain Reaction
p-gp	p-Glycoprotein
Pro-T α	Pro-Thymosin A
qPCR	Quantitative Polymerase Chain Reaction
RBP	RNA binding Protein
RIP	RNA-Immunoprecipitation
AUBPs	AU-rich Binding Proteins
RRMs	RNA recognition motifs
SDS-PAGE	Sodium Dodecylsulphate-Polyacrylamide Gel Electrophoresis
SIRT	Deacetylase Sirtuin
SNPs	Single Nucleotide Polymorphisms
SPR	Surface Plasmon Resonance
TGF- β 1	Transforming Growth Factor beta 1
TIA -1	T-cell restricted Intracellular Antigen -1
TIAR-1	T-cell restricted Intracellular Antigen 1-related protein
TNF α	Tumor Necrosis Factor
TRA	T-cell Receptors
TTP	Tristetraprolin
u-PA	Plasminogen Activator, urokinase
VEGF	Vascular Endothelial Growth Factor
α -KGDH	Alpha-Ketoglutarate Dehydrogenase

CHAPTER 1

Introduction

INTRODUCTION

Thousands of RBPs have been found to evolve during evolution, possessing unique properties to process newly formed RNA elements within eukaryotic cells regulating post-transcriptional gene expression. RNA molecules with RNA binding proteins (RBPs) further comprise ribonucleoprotein (RNP) complexes. These complexes play vital roles in cellular processes such as stability, splicing, transport, polyadenylation, cellular localization, and translation [1]. RBPs contains distinct RNA binding domains (RBDs), categorized in RNA recognition motifs (RRMs) or RNP domains, K Homology (KH) domain, Zinc finger (mainly C-x8-C-x5-C-x3-H type), DEAD/DEAH box, Pumilio/FBF (PUF) domain, double-stranded RNA binding domain (DS-RBD), Piwi/Argonaute/Zwille (PAZ) domain, Sm domain, and few others. These domains usually consist of 90-100 amino acids domains which bind to pre-mRNA, mRNA, pre-ribosomal RNA (rRNA), and small nuclear RNAs (snRNA) [2].

Many RNA binding motif indicates the molecular function of the RBP, e.g., DEAD/DEAH box is responsible for RNA helicase activity, PAZ domain binds to short single-stranded RNA in RNAi or microRNAs processing, and Sm domain binds to snRNA during splicing and also involved in tRNA processing. However, for other RBPs their RNA binding domains doesn't indicate the aspect of RNA metabolism they engage [3].

One key feature of these RNA motifs is the RNP consensus sequence which is mainly composed of hydrophobic conserved amino acids distributed in each motif. These amino acids are well conserved and play an important role in the RNA binding function of these numerous RBPs. Most of the RBPs bind to multiple RNA types and these multi-RNA binding domain proteins possess amino acids at the terminal region of the RBDs are highly conserved and indicate that they are responsible for sequence-specific RNA contacts [2].

Elav-like genes a conserved family in vertebrates

Eukaryotes employ many posttranscriptional mechanisms to regulate gene expression [4]. A distinct family of genes encodes proteins that have RNA binding domain or RNA recognition motifs, which binds RNA and regulate their post-transcriptional function. The elav embryonic lethal abnormal vision like / Hu-protein family of RBPs is one of them, which is neuronal specific and is necessary for differentiation and maintenance of neurons in *Drosophila melanogaster*. It was identified after characterization of fly mutants of lethal embryonic with abnormal vision phenotype, suggesting that the gene function during embryogenesis is pivotal

for normal neuronal differentiation [5] [6]. Later human ELAV orthologues have been discovered after the elav gene has been found to be linked with small cell lung carcinoma and paraneoplastic encephalomyelitis (elavl1 and elavl4) [7]. Similar genes have been found in other species *Xenopus laevis*, zebrafish, frogs, mouse and classified into elrA, elrB, elrC, and elrD [8].

ELAV-like or Hu antigens caused autoimmune response leading to numerous neurological defects in human also known as Hu-syndrome [9]. In mammals these four proteins are HuA (erlA), HuB (erlB), HuC (erlC) and HuD (erlD) shows homology of 70-85% between themselves. HuB (erlB), HuC (erlC) and HuD (erlD) are confined to be expressed in the neuronal tissue and generally localized in cytoplasm whereas the HuA (erlA) or HuR is ubiquitously expressed in and localized in nucleus as was found in fly *Drosophila* [10] [11]. However, in the presence of nucleo-cytoplasmic signals, HuR can shuttle between nucleus and cytoplasm.

Ma *et al.*, in 1996 first cloned and characterized Human HuR protein showing tight binding to AREs present in c-fos, n-myc, c-myc and IL3 mRNAs. HuR mainly binds to AU rich (ARE) sites at the 3' prime of the mRNA of several cell-cycle regulators, growth factors, and transcription-regulating proteins and transports the mRNA to the cytoplasm for protein translation. Localization of the HuR was confirmed on to human chromosome 19p13.2. Protein corresponds to 326 amino acid with molecular weight of 36 kDa [11].

HuR regulates many transcripts based on their AU-sequences available at the 3' or 5' UTR sequences. Excessive dysregulation of these transcripts via this protein can cause inflammation and further physiological dysregulation [12]. Comparing the sequence identity, AU-rich 3' UTR was found to be conserved in most of the cytokine and oncogenic mRNA [13]. It was also shown that the ARE of TNF mRNA is important for regulating its expression, is one of the targets of HuR and plays a crucial role in causing chronic inflammatory diseases [14].

Specifically, HuR-dependent stabilization was evident at the pre-mRNA level, suggesting that HuR-binding is a very early step in the life of an mRNA. HuR is a major player in regulating the post-transcriptional regulation of thousands of transcripts (**Figure 1**). Considering this fate, it has been proposed that the stabilization of pre-mRNA by HuR ensures proper mRNA processing, akin to the effect of Pol II transcription which was HuR mediated [15].

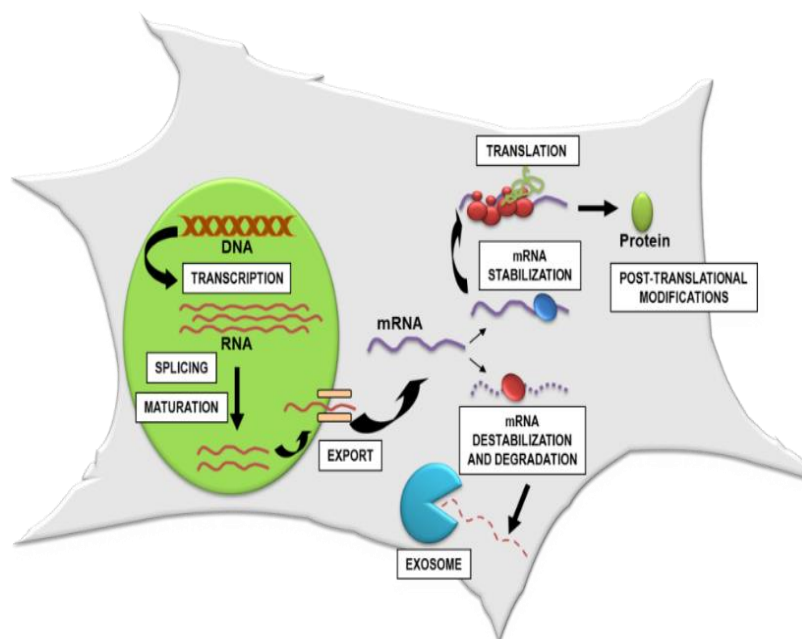


Figure 1 Schematic representation of the biological processes, where HuR plays the crucial roles, i.e., in splicing of pre-mRNA, nucleo-cytoplasmic export, stabilization, and recruitment of bound transcript on active translating polysomes [16].

HuR Structural Features

HuR protein has three RRMs (RRM1, RRM2, and RRM3), the N-terminal RRMs are arranged in tandem (RRM1–RRM2), whereas RRM2 and RRM3 are joined by a hinge region. First two regions were shown to bind tightly to target RNAs [17]. RRM3 has been demonstrated to bind to poly-A tail and further involved in oligomerization [18] [19]. Crystal structure of the first two HuR domains was solved by Wang, H. *et al.*, 2013, both in RNA free and RNA bound form. By comparing both structures of RRM1/2, it was revealed that it undergoes conformational changes after RNA binding. A region exists between two domains called as inter-domain linker comprised of 12-residue (Tyr95–Ala106) forming a short helix and maintains the distance within the two RRM motifs with a length of 13Å. RRM1 can recognize at least 4 or 5 consecutive uracil's (U) residues, which further confers strong binding affinity towards RNA, inter-domain linker was also found to interact with 1 or 2 uracil residues. To further confirm this they have done mutational analysis in RRM1/2 domains, and CD experiments revealed that two structures of those mutants changed as compared to WT RRM1/2. The open (RNA-free form **Figure 2 (i)**), and closed (RNA bound- form), however the protein folding are same,-

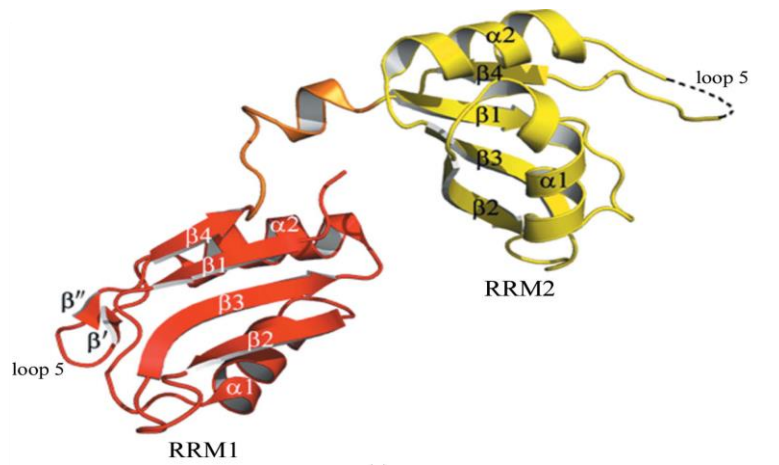


Figure 2 (i) crystal structure of free RRM1/2 [20].

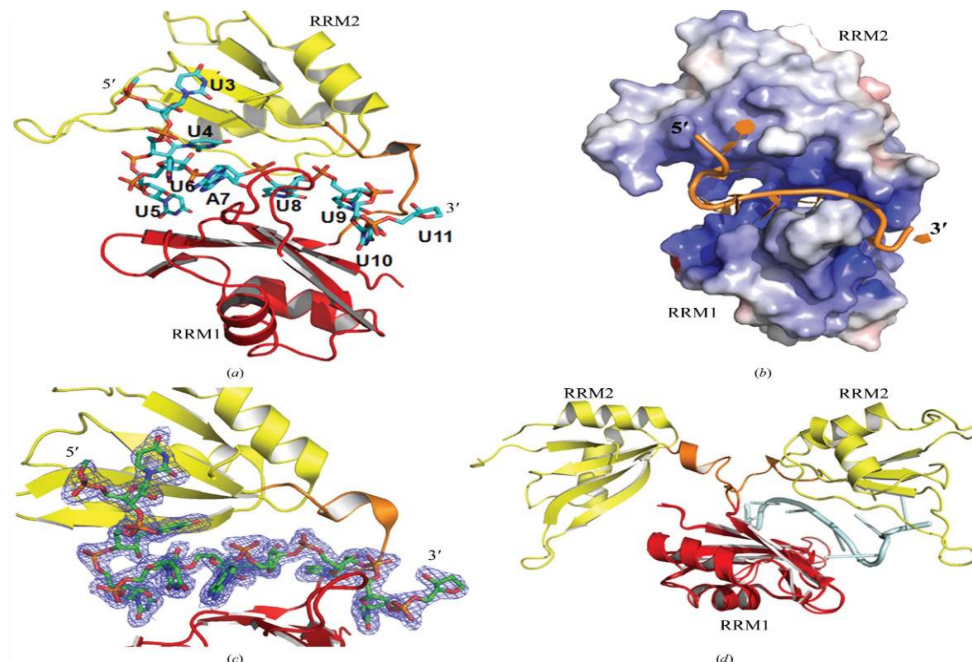


Figure 2 (ii) Dynamic properties of RRM1/2 a) HuR RRM1/2–RNA bound structure, RNA-interacting residues (bases) are labeled accordingly. b) The RNA is shown in a positively charged cavity formed upon conformational changes in HuR RRM1/2. c) Schematic view of RNA element covered with a 2Fo-Fc electron-density map contoured at 1σ . The RNA is represented as ball-and-stick representation. d) Super positioned structure of RRM1 in bound and free form together with RRM2 [20].

-but there were dramatic changes in tertiary protein structure as represented by the attached figure above. Conformational changes were noticeable upon superimposition, as RRM2 has undergone a rotation of 137.3 rad, to form an RNA binding cleft [20].

Signals that converge to HuR

Mechanisms regulating HuR expression are still unknown. However, HuR functions primarily related to its subcellular localization [21]. Generally, HuR is present in the nucleus of unstimulated cells, where it binds to other protein ligands such as SET α/β , pp32, and APRIL, but can be transported to the cytoplasmic compartment in response to stress stimuli. In the presence of leptomycin increased binding with pp32 and APRIL was observed along with increased crosslinking of HuR to nuclear Poly (A) mRNA, suggesting ligand binding stabilized HuR's association with ARE bearing mRNAs. Heat-induced activation of HuR has resulted in the cytoplasmic export of the hsp70 mRNA and importantly through its association with protein ligands pp32 and APRIL [17]. Moreover, AMPK (AMP-activated protein kinase) activity decreased the abundance of HuR vice versa and led to HuR dependent regulation of mRNA targets [22].

MAPK cascades as the sensor of stress-activated pathways have been already found to regulate the abundance of cytoplasmic HuR and RNA complex formation activity in stimulated cells (**Figure 3**) [23] [24]. Activated MAP kinases p38 and ERK has enhanced the stability of uPA and p21 mRNAs along with an abundant cytoplasmic accumulation of HuR confirming the role of HuR in these signaling pathways [24] [25]. Accordingly, MAPK activation by ionizing radiation resulted in upregulation of the cyclin-dependent kinase inhibitor p21^{Cip1} and following arrest of cell cycle at G1 phase leading to accumulation of p21^{Cip1} mRNA. This was due to phosphorylation of HuR on Thr118, causing cytoplasmic accumulation of HuR and enhanced binding to the p21^{Cip1} mRNA [26].

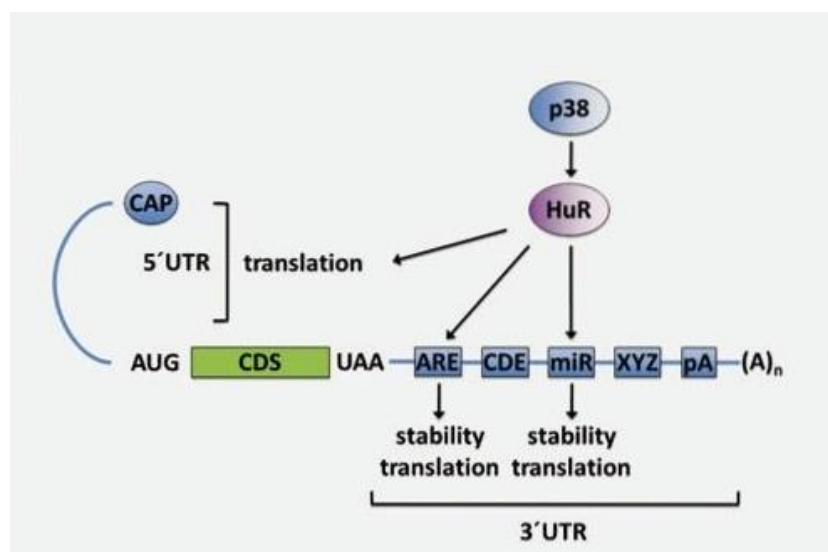


Figure 3 MAPK-signaling pathway affecting properties of cytokine mRNAs via phosphorylation of HuR, different MAPKs and consequent mRNA stabilization and translation mediated by their interaction with distinct 3' or 5' UTR elements is shown. AUG start codon; UAA stop codon; CDS, coding sequence; UTR, non-translated region; (A)_n, poly(A) tail of variable length; ARE, AU-rich element, class I, II, and III; CDE, constitutive decay element; pA, polyadenylation signal; miR, miRNA-binding site; XYZ, any other element such as cytoplasmic polyadenylation element (CPE), differentiation control element (DICE), CU-rich or an upstream sequence element (USE), and others; pre-miR, precursor miRNA (Figure adapted from Tiedje et al, 2014 [23]).

Phospho-regulation at the HuR RRM1 notably at S88 in RRM1, S158 in RRM2, and S100 in hinge region; strongly affect the binding to mRNA. However, there was no influence in the general structure of HuR [27].

Cyclins are the central engines of the cell cycle machinery, which interacts with cyclin-dependent kinases (cdks) to form the cyclin-cdk complexes. It has been found that important cyclin A2 (for progression through the S and G2 phases) and cyclin B1 (for progression through G2/M phases) interact with HuR in human, mouse cells and cancerous cells thus can play a critical role in growth progression, at least in part by mediating the cell cycle-dependent stabilization of these mRNAs. It is known previously that HuR phospho-regulation by cdk1 at S202 within hinge region is necessary for increased association with 14-3-3 and causes its nuclear retention. In case of cell cycle residue S242 phosphorylation causes HuR's cytoplasmic accumulation with enhanced cyclin expression, modulating cell proliferation thus suggesting an important role of HuR in cell division [28] [29]. Chk2 (checkpoint kinase 2) also phosphorylate HuR at S88, S100, and T118, leading to dissociation of HuR from the target RNA probe, further triggering the growth arrest with enhanced cell survival [30]. In *in vitro* kinase assays HuR serines (Ser) 158, 221 and 318 have been identified as targets of protein kinase C (PKC), further validation by phosphomimetic mutation at S221D and data from electrophoretic mobility shift assays indicated that S221 is not relevant for binding to target mRNAs. Whereas S158D and S318D have shown specific binding to all ARE-RNA types, suggesting the differential binding of HuR upon phosphorylation by PKCs [31]. Protein arginine methyltransferases (PRMTs) or member of PRMTs family, protein coactivator-associated arginine methyltransferase (CARM1/PRMT4) has been shown to methylate HuR protein, at arginine 217(R217) under the influence of LPS in macrophages and in HeLa cells, by stabilizing the stability of mRNAs encoding cyclin A, cyclin B1, c-fos, SIRT1, and p16 [32] [33]. Increased ubiquitination of the HuR at K182 was associated with tumor suppressor esophageal cancer-

related gene 2 (ERCG2), upon DNA damage. In this report, XIAP, an inhibitor of apoptosis whose expression levels were decreased as the HuR was degraded [34]. Thus HuR activity with in cells is influenced by all these major upstream regulators in cellular pathways.

p38 MAPK pathway influence on HuR and TTP

p38 MAP kinase pathway is essential during the stress responses, e.g., heat shock, UV radiation exposure, LPS- stimulation, etc. [35]. Regulation of TNF α biosynthesis mediated via AU-rich element (ARE) post-transcriptionally under the influence of p38 MAPK pathway [14] [36]. p38 MAPK kinase targets various RNA binding protein including TTP, hnRNP, KSRP, PABP1 [37][40].

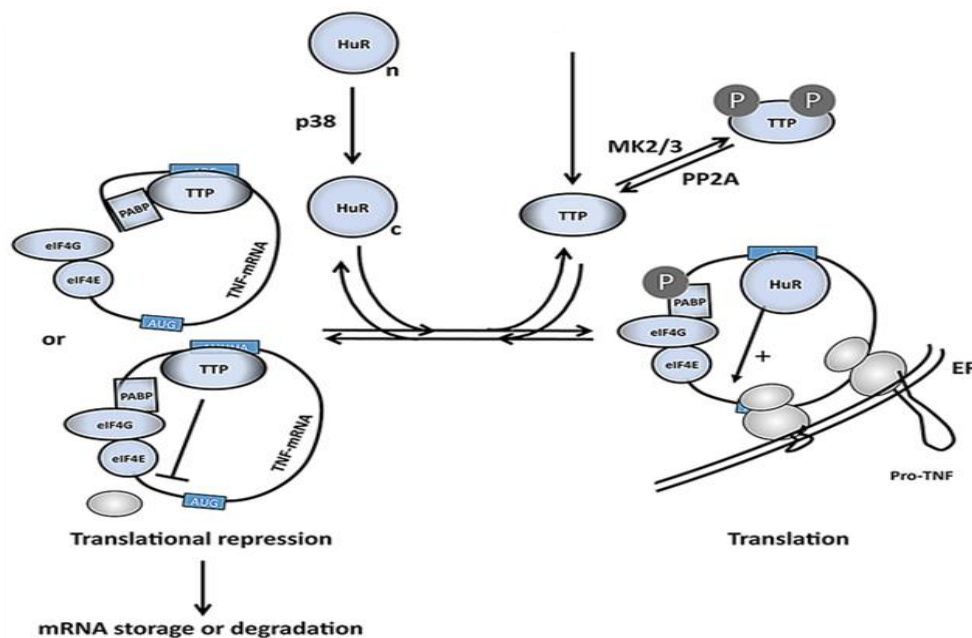


Figure 4 Schematic of the regulation of TNF mRNA and TNF release by p38 and MK2/3. TTP expression is induced upon LPS treatment followed by activation of p38 and MK2/3 kinases. MK2 phosphorylates downstream targets TTP and PABP [37], [40] and [41]. p38 and MK2 phosphorylate HuR directly and get distributed in its subcellular localization from the nucleus (n) to the cytoplasm (c) [24] [42]. HuR involved in translation of ARE bearing mRNA, whereas on the opposite phosphorylation of TTP by MK2/3 leave TTP unable to compete with cytoplasmic HuR (right side of picture). Non-phosphorylated TTP competes with HuR and stops the translational initiation by competition with eIF4G binding to PABP1 or by blocking association of the 43S pre-initiation complex. Therefore TTP interferes with expression of AU rich -containing mRNAs [43].

HuR and other RBPs are mainly involved in the control of the cytokine production under the control of p38 pathway [44] (**Figure 4**). HuR an RBP takes part in the nuclear and cytoplasmic

stabilization of ARE-mRNAs[45], [46]. HuR has been found to be associated with the translation of control of ARE bearing mRNA and has been shown as a negative posttranscriptional modulator in inflammation [47] [48]. MAPK MK-2 as an inducer of HuR function, after subjecting cells to oxidative stress, activated p38 MAPK pathway resulting in phosphorylation of HuR and consequently enhanced HuR binding to AREs of uPA in BT-549 and MDA-MB-231 cells [24]. TTP in p38 MAPK pathway plays an opposite role to that of HuR, via deadenylation of colony-stimulating factor or other ARE bearing mRNA, including its own mRNA [37] [49]. MK-2 phosphorylates TTP which further binds with 14-3-3 proteins and TTP is not able to degrade target mRNA [40]. p38 MAPK pathway activation and influence on TTP protein level has been checked in normal and TTP-KO RAW264.7 cells, upon LPS co-stimulation with DHTS and DHTS analogs has been monitored and described in the result section (**Figure 37 and 38**).

NF-kB Pathway:

The inflammatory response is a coordinated program, which through several proteins come into the function via the specific use of DNA elements that can be selectively recognized by the transcription factors [50]. Nuclear factor (NF) kB belongs to the family of seven homologs vertebrate transcription factors that usually serve in various combinations in response to external stimuli and move from cytoplasm to the nucleus in macrophages and T-cells, e.g., cytokines, ROS, bacterial lipopolysaccharides, viral infection and DNA damage. This family has Rel Homology domain (RHD) of 300 amino acids which displays homology 35-61% between themselves. RHD decides IκB binding to DNA with identical or others members of the family [51]. The Rel/NF-IκB are grouped into two classes: one comprised of p105 and p100 precursor protein, which proteolytically changed to p50 and p52 forms [52]–[54]. Second class contains c-Rel, v-Rel, Rel A (p65) and Rel B proteins [55] [56]. First class members are known as weak or inert gene activators whereas dimeric forms NF-kB containing at least one form of subunit from a second-class function as a strong activator of gene expression in human [57].

In recent studies, NF-kB has been indicated as the primary mediator of vascular inflammation, cardiovascular hypertrophy, and cellular stress responses [51]. HuR has been found as a direct transcription target of NF-kB and its activation in gastric cancer cell lines strongly linked with phosphatidylinositol 3-kinase/AKT signaling. HuR activation of this pathway has led to increased nucleo-cytoplasmic shuttling and subsequent proliferation of the tumor cells and

transition from the G1 phase to the S phase, finally showing the anti-apoptotic behavior of the gastric cancer cells [58]. Influence on the translocation of NF- κ B upon LPS co-stimulation with DHTS and DHTS analogs has been checked and described in result section (**Figure 30 and in preliminary results Figure 36**).

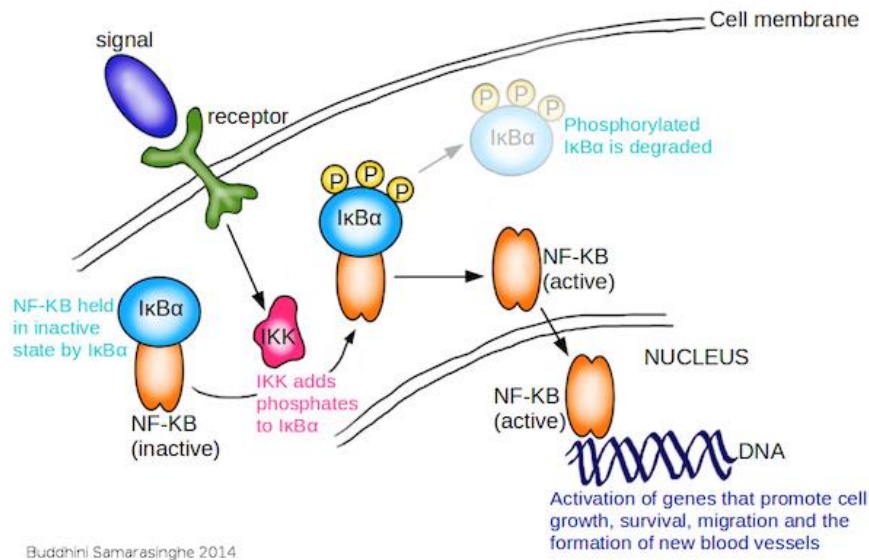


Figure 5 Schematic of NF- κ B pathway and the Mechanism of NF- κ B action. The NF- κ B, a heterodimer of Rel and p50 proteins, is usually found in cells in an inactivated state located in the cytoplasm complexed to I κ B α the inhibitory protein. Membrane receptors, through a variety of extracellular signals (stress, UV, TNF) can activate the enzyme IKK, which phosphorylates, I κ B α inhibitory protein, which later degraded via ubiquitin-mediated proteasomal degradation. The NF- κ B components Rel A and p50 together shifted to the nucleus where it binds to RE (Response Elements) of DNA particular sequence, where other coactivators and RNA Polymerase proteins are involved in the transcription of the same DNA elements and further active translation of the transcripts on the polysomal translation machinery, which further determine the cell fate. [51], [59] [60] and [61].

Roles of HuR

HuR role in Pre-mRNA processing:

Genome-wide analysis has revealed that a maximum number of human pre-mRNAs undergo RNA processing [62]. Hu Protein's nuclear function was also discovered by Hui Zhu *et al.* in 2006 as they function as RNA processing regulators in the nucleus, moreover they found that these proteins halt the activity of TIA-1/TIAR at the exon junction of several mRNAs. In 2008 they reported that Hu proteins check the production of short protein NF1, in this case by blocking the inclusion of 23a NF1 exon by the TIA-1/TIAR proteins. *In vitro* experiments done

using nuclear extract showed that Hu protein block the binding of U1 and U6 snRNPs at 5' splicing site, on the opposite TIA-1/TIAR increased this binding [63].

Proteomic analysis of assembled pre-mRNA revealed that HuR was found for the first time with spliceosome complex, ENSEMBL Accession number ENSGALG00000000726) [64]. HuR's role in splicing was confirmed by *in vitro* splicing assays in which *in vitro* produced *fas* mRNA containing sequences between 5 and 6 including a 30 nucleotides sequences were incubated with extracts from HeLa cells, along with splicing machinery, so there was the inclusion of exon 5 and 6 in an ATP dependent manner. On the other hand, when recombinant HuR was transfected into cells, the cells extract didn't show any accumulation of exon 5 and 6 splicing product, to further confirm this recombinant TIA-1 and TIAR were added to reaction mixture, and again it rescued exon 5 and 6 from skipping. Exon 6 skipping by splicing of *fas* transcript further produces soluble form of its protein which is apoptosis receptor and is engaged in preventing programmed cell death [65].

Zhao *et al.*, 2014 showed that HuR is also involved in splicing of SIRT1, which is also known as histone 3 deacetylases (HDACs), by skipping exon 8 from the spliced SIRT1 transcript. Here they measured the levels of SIRT1-FL and SIRT1-ΔExon8 by PCR and qPCR based experiments, in HuR overexpressing cells HEK293T cells. They found an increase in the level of SIRT1-ΔExon8 and in HuR ablation conditions apparently this event was not observed at all, similar experiments were also done in the U251 cells, and the same pattern of outcomes was seen. Previously it was known that HuR regulates the SIRT mRNA and stabilize it upon HuR phosphorylation by Chk2 but how it is regulated was discovered by Wenhui and colleagues [67].

PAR-CLIP and RIP-Chip Seq analysis have shown that HuR was involved in regulating the fate of transcripts by binding to intronic and 3' UTR of many sequences. Further investigation to confirm this specific probes to the intronic region, considered as HuR binding sites were correlated with their stabilization [15].

In a transcriptome-wide analysis of the HuR interactome, almost 26,000 binding sites were identified, and specifically, most of them were found in the intronic region. They also showed that HuR binds ssRNA preferentially and having no preference for Hairpins, by computationally folded HuR binding motif in almost 30 UTRs and resulting base pairing

probabilities were averaged. These studies confirm that HuR finely binds to transcripts immediately after or during transcription and further cooperate in splicing, cytoplasmic export of the target RNA, in this regard, it further stabilizes these mRNA transcripts [68].

Dutertre group in 2013 elucidated the nuclear function of HuR and its consequent role in alternative splicing. Upon doxorubicin treatment, alternative polyadenylation pattern changed and led to the inclusion of intronic poly (A) sites, normally HuR was responsible for binding to the conserved region which was repressed by doxorubicin and resulted in reduced production of CENPN, MBD1 mRNAs. These transcripts are thought to be involved in the G2/M passage and DNA damage response. On the other hand, it was observed that HuR translocate to the cytoplasm and get engaged in 3'UTRs binding and stabilization of various mRNAs. Therefore Internal ALEs in a subset of human premature mRNAs depend on HuR binding for inclusion in matured mRNA. Upon DNA damage, this unique binding is inhibited and results in isoforms like CENPN-pA12 [69].

Naipauer J. *et al.*, 2013, explained about the short and full-length mRNA encoding the $\beta 1$ subunit (Itgb1) based on alternative functional cleavage and polyadenylation site which yielded a new Itgb1 mRNA isoform corresponding to 578 bp shorter than that previously discovered. These forms are expressed in a variety of tissues. $\beta 1$ integrins play a significant role in the maintenance of mammary gland tissue integrity and function. Itgb1-S (short) isoform was decreased during the pregnancy and lactation where Itgb1-L (long) isoform remained unchanged, Actinomycin D chase experiments revealed that Itgb1-L was more stable as compared to Itgb1-S isoform, in differentiating and proliferating HC11 cells. This was probably due to the presence of AUBPs (AU-rich Binding Proteins) at Itgb1-L 3' UTRs. Meanwhile, the level of HuR correlated to the increased level of the Itgb1-L, both at mRNA and protein levels. To confirm the role of HuR in all of these events transfection of HC11 cells with the HuR siRNAs after following Act D treatment was performed and the mRNA levels of Itgb1-L mRNA isoform were measured by RT-PCR. As expected the level of the Itgb1-L were decreased in the Si-HuR as compared to control [70]. Munoz, MD *et al.*, 2015 showed that HuR is required for the normal B-cell antibody response, besides this they also explained the B-cells transcriptome regulation by HuR. Using i-CLIP it was discovered that HuR dependent splicing had affected thousands of transcripts, one particular gene they have described was Dlst (Dihydrolipoamide-S-succinyltransferase) which is a subunit of the 2-oxoglutarate

22

dehydrogenase (α-KGDH) complex. In HuR KO mice B-cells defective mitochondrial metabolism was observed along with abundant secretion of ROS, leading to B-cell death. Splicing alteration which has occurred upon HuR deletion was retention of intron 10 and followed by alternative inclusion of a cryptic exon linking exons 10 and 11. To explore this matter mechanistically they further analyzed the i-CLIP data, which verified that 75% of the HuR crosslinking sites were related to the intronic region. So merely HuR cross-linked at the exon-intron boundaries indicating that HuR specifically binds to introns 3' UTR primarily bond within branch point and 3' splice site [71].

All these data together suggest that HuR might be a splicing regulator, regulating all events described above.

Further, HuR was also exploited for its participation in alternative splicing of the TRA2β gene in human colon cancer cells under the oxidative stress. TRA2β is a splicing factor transformer 2, and it produces 5 mRNA isoforms (TRA2β 1 to -5) via alternative splicing. In HCT116 colon cancer cell line, Chk2 and p-38 MAPK kinase were induced by sodium arsenite treatment, and further phosphorylated HuR at positions S88 and T118, this caused HuR to bind to TRA2β at exon 2 and resulting in TRA2β4 isoform that bears exon 2 with multiple stop codons. Upon deletion or HuR Chk2/p38 MAPK double knockdown and after following sodium arsenite stimulation came out with TRA2β and in return protein levels of TRA2β. These results were validated further by using mutant HuR S88A, S100A, and T118A as expected this obstructed association of TRA2β4 with HuR and consequently TRA2β4 generation [72].

HuR in Cancer

In cancer-like conditions, RNA binding proteins function is perturbed, notably TTP (zfp36) and HuR are involved in these pathological conditions. Overexpression of AU-rich sequences is coupled to low activity or deficiency of Tristetraprolin (TTP, zfp36), and high activity of HuR in controlling the fate of these numerous transcripts and causing irrelevant pathologic conditions (**Figure 6**). This was confirmed in TTP-KO mouse fibroblasts, in this context HuR-zfp36 has been correlated with cancer invasive gene expression. Moreover, miR29a specifically target TTP and miR29a expression is usually higher in breast cancer, when it was inhibited by the permeable miR29a inhibitor, rise in the TTP activity was seen especially towards the HuR 3'UTR, this further affected the expression of mRNAs, uPA, MMP-1, MMP-

13 which are known as cancer-causing invasive factors. This point was highlighted for potential therapeutic approach, focused on TTP-HuR axis [73]. In cancer pathology, HuR is usually correlated with its cellular localization. HuR was overexpressed in seven human cancer cell lines SW480, Caco-2, SW707, HT-29, HRT-18, CX-2, and LoVo, and its localization and expression investigated by immunoblotting and quantitative RT PCR. HuR was found predominantly inside the nucleus of all these lines however after overexpression, HuR cytoplasmic accumulation was observed and correlated with increased COX-2 expression [74]. Robert Calaluce *et al.*, 2011 by using RIP-ChIP assay to find systematic HuR target genes in breast cancer cell lines MCF-7 (estrogen receptor positive, ER⁺) and MDA-MB-231 (estrogen receptor negative, ER⁻), among many subsets of HuR target, they found two unique HuR targets CD9, CALM2, which were previously not known among the HuR targets. These targets were further verified by pull-down assay and qPCR analysis. Quantification of HuR protein levels in both cell lines showed that more or less same level of HuR were seen, however, the cytoplasmic levels of HuR in MDA-MB-231 was higher than in MCF-7 Cells [75].

Nevertheless, HuR expression was also seen in non-tumorous immortalized epithelial cells for e.g., Epithelial HB2, HMT-3522-T4-2, epithelial ductal carcinoma T47D, epithelial carcinoma BT-20, Hs578T cells and in epithelial adenocarcinoma SKBR-3 cells [76]. Further, in 2010, Lauren A. and colleagues showed that HuR is involved in mediating the post-transcriptional processes of GATA3 mRNA, upon HuR silencing, GATA3 levels were significantly lowered, biotin pull-down experiment confirmed that GATA3 3'UTR is the target binding site of HuR.

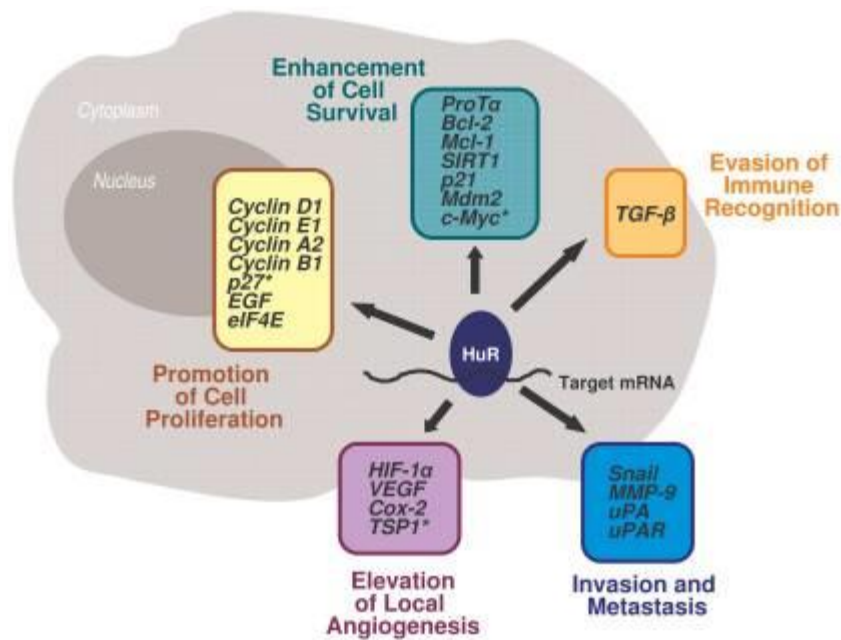


Figure 6 HuR function in controlling the fate of the mRNA involved in various cellular processes. In each case when the respective transcripts levels are altered lead to mentioned pathologic and cancer like conditions [16].

Also, cellular proliferation rate upon inhibition of either HuR or GATA3 were decreased to by 35 and 44%, in MCF-7 cells suggesting the possible role of HuR and GATA3 in invasion and progression of breast cancer [77]. In OSCC, cleavage of HuR was interfered via the increased COX-2 expression by caspase 3. Cyclooxygenase-2 (COX-2) was overexpressed rigorously, which was one of the reason for resistance to paclitaxel treatment within oral cancer cells. After successfully inhibiting the COX-2 via its known inhibitor celecoxib lead to apoptosis in the same cells, which confirmed the cleavage of HuR in resistant oral cancer cells [78]. Baldan *et al.*, 2016, determined the level of HuR in thyroid cancer cells and found the huge altered level of HuR, based on this finding they performed RIP seq and compared the HuR regulated transcripts in tumorigenic and non-tumorigenic cancer cell line, almost 114 mRNA were found bound to HuR, which were absent in non-tumorigenic cell line [79].

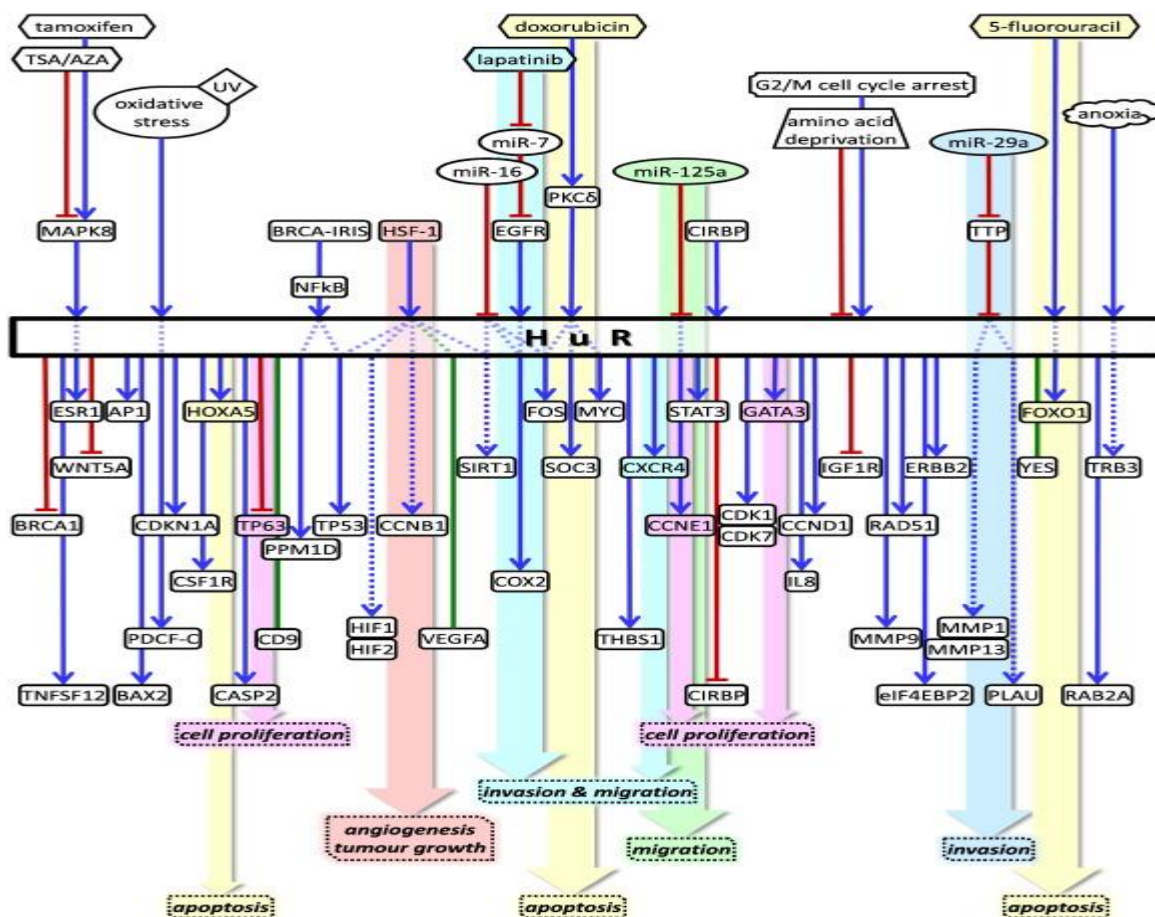


Figure 7 Schematic diagram of HuR targets and their influence in cells, mediated by HuR in breast cancer cells. HuR is depicted as a rectangle in the middle of the arrowheads. The upper part of the diagram from the depicted HuR are drugs, miRNA, factors modulating HuR expressions and in lower are the HuR target and their fate upon HuR regulation [76].

In breast cancer, most of the genes modulated by HuR are involved in cellular processes such as migration, proliferation, and invasion along with tumor and angiogenesis **Figure 7.** demonstrates the link between HuR and these cellular processes and its role in breast cancer [76].

HuR in Inflammation

HuR is the central modulator of inflammation as it is pivotal in the regulation of cytokine synthesis and coordinates the activity of other AREs binding proteins. Cytokines and chemokines secreted by the immune cells exert inflammation and most of them carry 3' UTR ARE sequences and are supposed to be regulated by HuR. The key mediators of inflammation such as TNF, IL-4, IFN γ , and COX2, have already been described to be involved in inflammatory

pathways. However inflammation is a critical component of the immune system, it allows cells to repair the damaged cells by recruiting factors which further cooperate in the recovery of damage but on the other side excessive uncontrolled inflammation can exacerbate tissue damage [80]. Conditional KO mice for HuR has been already tested for the role of HuR in regulating the expression of Gata3, IL4 and IL13 mRNAs with decreased steady-state level and least changes at the protein level [81]. HuR expression in myeloid lineages is important, so as to limit the expression of inflammatory cytokines. Conversely, HuR KO myeloid cells induced systemic inflammation with increase in the levels of pro-inflammatory cytokines TNF, IL-6, CCL2, iNos and IL-10 mRNA. Most of cells expressing abundant IL-12 and IFN- γ resulted in severe colitis. RIP on activated macrophages confirmed that Ccl2, IL10, and TNF α mRNAs interact with HuR whereas other cytokines such as IL12, Ccl7, and IL6 mRNAs did not [82]. This shows the systemic preference of HuR in myeloid lineages.

On the other hand, where HuR is considered as an inducer of inflammation evidenced from the above examples, HuR was also recognized as suppressor of the inflammatory responses *in vivo* in murine macrophages. HuR overexpression caused the translation inhibition of specific cytokine mRNAs without promoting any symbolic effects upon their turnover. Katsanou, V. *et al.*, 2005 demonstrated in a model of abnormal ARE function, that HuR is not inducing any accumulation of ARE transcripts in the absence of destabilizing protein zfp36, besides cooperate with translation silencing protein TIA-1 to decrease the level of cytokines mRNA. Further to explore about the HuR associations they have performed IP analysis for the target mRNA TNF α , COX-2, and TGF- β and IL-1b in RAW 264.7 cells. Upon LPS induction the TNF α level were found associated with HuR whereas COX-2, IL-1b were constitutively present besides their increased mRNA pool, the same fashion was also observed in the Tg632 macrophages, in which they suggested that transgenic HuR can directly alleviate the levels of TNF α , COX-2, and TGF- β but not of IL-1b. Also, actinomycin D chase experiment confirmed the level of TNF α and COX-2 half-life increased in transgenic macrophages whereas this behavior was not observed for the TGF β . Conversely 40% reduced level observed for TGF β 1 transcript produced in induced transgenic cultures, whereas TNF α , COX-2 remained unaffected. Polysomal analysis showed reduced levels of TNF α , COX2, and TGF β 1 in macrophages whereas IL-1b and actin showed the same distribution over the polysomes, this was further clarified as these mRNA TNF α , COX2 share the same ARE-III type, and showed same response to HuR

overexpression. Altogether the results showed HuR targets only specific mRNAs, and overexpression can inhibit the translation of certain inflammatory transcripts, besides differential alteration on their mRNA level, these differences by HuR can be explained on the basis of sequence diversity of different transcripts [48].

Giammanco, A. *et al.*, 2014 also showed HuR role in intestinal homeostasis, by generating HuR-KO mice and confirming that deletion of HuR in intestinal tissues reduce the burden of small intestinal polyposis. They also demonstrated that HuR-KO mice after injection of azoxymethane and dextran sodium sulfate (AOM-DSS), the level of the tumor was three fold lower than the control mice. These two models came to the conclusion that intestinal removal of HuR protected mice against the tumorigenesis by inducing the apoptosis, and regulating the intestinal specific mRNA bearing anti-apoptotic HuR target sequences. They also confirmed that prolonged deletion of HuR for over one year didn't have any impact on the phenotype in fact aged HuR-KO showed similar phenotype to that of control. Despite all these, however, the proliferation of small intestine was not reduced in aged HuR KO mice, also the expression of RNAs (Olfm4, Tp53, and CcnB1) which are involved in the homeostasis, cell growth and survival were unaltered [83].

HuR was also implicated in the IL-17 induced act-1 mediated chemokines (CXCL1 and CXCL5) transcripts stabilization, the absence of HuR markedly lowered the levels of these chemokines which were induced by IL-17 through Act-1 (U-box E3 ubiquitin ligase) ubiquitination of HuR further leading to binding and stabilization. Consequently, HuR deletion has lowered the level of these cytokines. The role of IL-17 is critical as it is involved in organizing local tissue inflammation and further inducing secretion of important chemokines and cytokines IL-6, CSF2, TNF α , IL-1, CXCL1, CCL2, CXCL2, CCL7, and CCL20, and subsequent release of monocytes and lymphocytes including neutrophils in inflamed areas. Upon IL-17 induction HuR was found ubiquitinated, to confirm this they transfected HeLa cells with HA-tagged ubiquitin and then induced with IL-17. IP experiments revealed the association of HA-ubiquitin with HuR after the western blotting. To test further if Act1 was directly ubiquitinating HuR they have performed *in vitro* poly-ubiquitination assay, interestingly Act1 used Ubc13/Uev1A E2 complex to ubiquitinate HuR, merely acting as E3 ubiquitin ligase to HuR, considering all these observations it was noted that HuR's ActD mediated HuR poly-ubiquitination is important for its stabilizing activity on CXCL1 and CXCL5 mRNAs. Accordingly, polysomal analysis also

revealed that upon IL-17 induction, Act1-HuR were found shifted to actively translating polysomes and were responsible for the translation of ARE-bearing transcripts [84].

Auto-immune disease encephalomyelitis was found mainly due to HuR pathology, as HuR was involved in stabilization and translation of the IL-17 mRNA which otherwise was reduced upon HuR ablation [85], [86]. Moreover it was experimentally proved that HuR directly binds to the IL-17 mRNA at 3'UTR by RIP and pull down assays. Th17 cells which are third subset of Th family and are responsible for pathologies in inflammatory and autoimmune diseases for e.g. encephalomyelitis, arthritis and asthma [87] [88]. Jin Chen *et al* in 2013 used an adoptive transfer model HuR-deficient Th17 cells and found delay in onset and less in severity of EAE (Experimental autoimmune encephalomyelitis). They developed EAE by adoptive transfer of MOG-specific CD4+ T cells into naive mice, WT and KO mice. After repeated adoptive transfer, they found significant differences in the onset of encephalomyelitis in WT and KO mice, WT developed encephalomyelitis on the 11 day after transfer and reached extremity at day 23, while in HuR KO, all these onset were delayed. After isolating the monocytes from the CNS and finding the frequency of IL-17 secreting cells by Flow cytometry, this analysis also showed the decreased level of CD4+ and IL-17 positive cells, within HuR KO mice. On the other hand CD4+, T cells proliferation rate from KO and WT mice revealed that cells from KO mice have reduced proliferation rate as compared to WT under Th17-polarization conditions. [85]

Skliris *et al.*, 2014 demonstrated that as HuR is expressed in both neuronal and non-neuronal tissues, it can help in promoting the renewal of neuronal progenitor's cells. They highlighted a neuroprotective role of HuR which was revealed upon genetic ablation of HuR. Conditional KO mice for HuR in the Hippocampal neurons were briefly investigated for the role of HuR in neuronal functionality. Upon kainic acid (KA) administration which is potent agonist of a subtype of glutamate receptors that could lead to epileptic seizures when administered systemically. Seizure rating extent was different in CN-KO mice, as compared to control, where it was increased in 10 min and peaked around 20 or 30 min in control mice, whereas seizure-rating in, female CN-KO mice showed significant decrease in seizure magnitude and sudden muscle convulsion leading to death, this confirmed the participation of HuR in the excitation and elicitation of the epileptic seizures. Further to assess the degree of permanent neuronal damage in both control and CN-KO mice Hematoxylin/eosin and Nissl staining revealed additional KA-induced hippocampal lesions than in control [89].

Taken all this together, HuR coordinates defensive network of RNAs post-transcriptionally to neutralize oxidative metabolism by lowering the expression of potential hazardous genes and further protecting neurons from degradation and necrosis, e.g., Bcl2, NQO1 and Ppargc1a mRNAs and its role in inflammation as explained above cannot be ignored. In our experiments, we have checked HuR-dependent influence on the TNF α , CXCL2 and CXCL10 levels, of our compounds upon treatment with DHTS and MFM49. **(Figure 34)**

Nuclear or cytoplasmic: does it endow any prognostic role?

In last two decades, a lot of studies focused on the role of nuclear and cytoplasmic localization of HuR and further its clinical prognostic outcome in cancer types. Predominantly HuR is localized in the nucleus, but upon external stimulus (stress) to various stress stimuli, including oxidative stress, heat shock, hypoxia, UV light, amino acid starvation, polyamine depletion, and staurosporine, it shuttle from nucleus to the cytoplasm, here it binds to target RNAs and further recruits them on ribosomes for their active translation [90]. HuR interacts with various other proteins such as set PP32 (phosphoprotein-32), APRIL (Acidic protein rich in leucine), and SET α/β . These proteins are believed to be involved in HuR export from the nucleus, modulating its affinity towards its target probes. Further P21 increases expression upon exposure to UV was found to correlate with HuR association with RNPs and silencing of HuR resulted in low level of P21 in RKO colon carcinoma cells. All of these events occurred in the cytoplasmic presence of HuR [91].

Upadhyay, R. *et al.*, 2012 demonstrated about the polymorphism of ELAVL1 (HuR) with poor survival in African-American patients, interestingly ELAVL1 gene has been found with more than 400 SNPs. Most of the SNPs function is still to be exploited; however, some they have a role in as discussed earlier in RNA stability, microRNA recognition and in splicing regulation, moreover HuR was neither found mutated in all studied tumors [92].

In another study, HuR was implicated in carcinogenesis in renal cell carcinoma (RCC), an increase in cytoplasmic HuR and RCC associated survival was poor in the patients who expressed HuR and COX-2 in their tumors. Here they have treated the cell line with siRNA targeting HuR and further reduced the expression of HuR and COX-2. Nevertheless, in esophageal squamous cell carcinoma (ESCC), HuR was proposed as a potential prognostic marker. Immuno-histochemical analysis and clinicopathological studies revealed that

metastasis in lymph node, invasive tumors with an advanced stage was positively associated with HuR. Patients with cytoplasmic HuR had cumulative five years survival rate of 25%, on the other side it was 43.8% for patients with negative cytoplasmic HuR expression [93]. HuR was also found to be associated with the cellular inhibitor of apoptosis (cIAP2) in oral squamous cell carcinoma (OSCC). In this case, HuR was seen overexpressed cytoplasmically in 8 oral cancer cell lines. Consequently in OSCC HuR and cIAP2 expression levels were determined and cIAP expression except for 4.2% specimen cIAP levels overexpressed in 95.8% of OSCC specimens, similarly altered cytoplasmic expression was also found to confer increased expression of COX-2 in OSCC [94].

In gallbladder carcinoma, results showed that increased nuclear HuR expression was related to high tumor number followed by vascular invasion, univariate analysis performed verified that patients with high nuclear expression had poor disease-free survival [95].

A major obstacle in cancer chemotherapy is the HuR induced overexpression of P-glycoprotein (P-gp) in human breast cancer. Immunohistochemistry revealed overexpressed HuR in the cytoplasm, so patients with high cytoplasmic HuR had poor survival as compared to a low expressed level of HuR, as inference cytoplasmic HuR expression was found to be negative prognostic measure in patients with breast cancer [96]. HuR was also found abundantly expressed in non-tumorous immortalized epithelial cells for e.g. Epithelial HB2, HMT-3522-T4-2, epithelial ductal carcinoma T47D, epithelial carcinoma BT-20, Hs578T cells and in epithelial adenocarcinoma SKBR-3 cells [76] (**Figure 8**).

Concerning the above findings, we evaluated the influence of DHTS and MFM49 on the nucleocytoplasmic abundance of HuR within MCF-7 breast cancer cell line (**Result Section: Figure 29**).

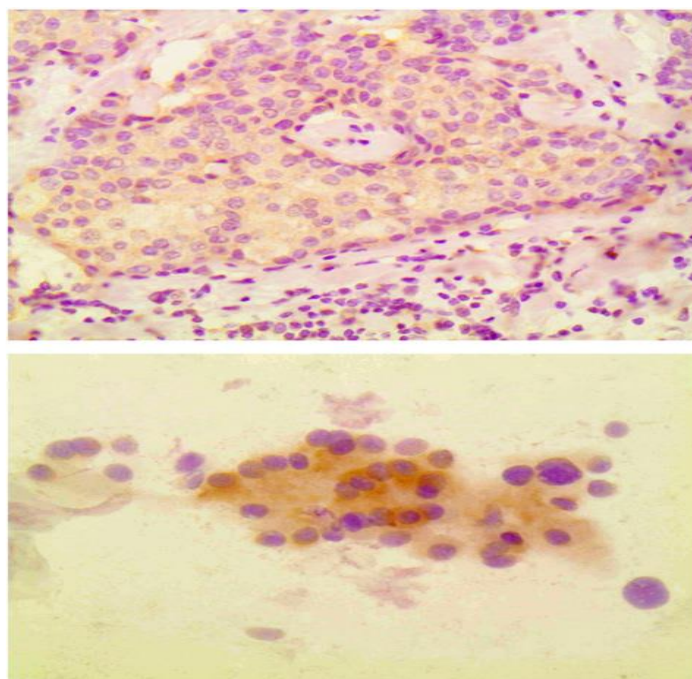


Figure 8 The immunostaining of HuR from the histological and cytological specimen taken from breast cancer patient. Showing the cytoplasmic abundance of HuR and is primary cause of cancer. [76]

Current state of the art on the Pharmacology of HuR and Small Molecules Inhibiting HuR

Since HuR has been predicted as a druggable target, lot of researchers published their research outcomes in recent years. In this regard Chae et al., 2009 showed the role of chemical inhibitors and their efficacy toward HuR, they screened around 179 chemicals, and identified three with IC₅₀ below 10 μM e.g., for quercetin, b-40, and b-41 were 1.4 μM , 0.38 μM , and 6.21 μM , against the binding of HuR and TNF α in *in vitro* EMSA and filter binding assay. Also, they found that Quercetin and b-40 compounds were not effective on *zfp36* and TNF α binding. In RAW264.7 LPS-induced TNF α which is a HuR target, levels were lowered in Act D chase assay. Using our compound we have also determined the half-life of the LPS induced TNF α and other cytokines in RAW264.7 cells (**Figure 40**).

Meisner, N. *et al.*, in 2007 screened 50,000 natural compounds and found most potent, Dehydromutactin, naphthofuranone MS-444, and Okicenone. Mechanistically, MS-444 bound HuR protein within first two RRM and prevented HuR homo-dimerization, thus further block HuR translocation to the cytoplasm, where it is known for its stabilizing function.

D'Agostino *et al.*, 2013 demonstrated a novel assay, to assess HuR and probe binding *in vitro*, and has screened 2000 small molecules, inhibiting the HuR-RNA complex formation, further verified by EMSA assays. He found Cetylpyridinium chloride mitoxantrone, a small molecule abrogating HuR-RNA complex formation [98].

Later on, D'Agostino *et al.* screened 107 commercially available anti-inflammatory compounds, searching for their inhibiting specificity on rHuR-RNA complex formation *in vitro*. Eight potential compounds (DHTS, hydrocortisone acetate, amiprilose, flurbiprofen, deracoxib, fluocinolone, triamcinolone and dexamethasone) from 107 compounds came out to be potential inhibitors, but the most potent hit was given by DHTS (ChEMBL227075 ID in ChEMBL database), which belongs to tanshinones family [99].

Further Wu, X. *et al.*, 2015 screened and validated HuR inhibitors from a group of 6000 novel compounds using FP HTS based assay, after finding lists of potential disruptors they consequently validated them by using AlphaLISA (Amplified Luminescent Proximity Homogeneous Assay), surface plasmon resonance (SPR), ribonucleoprotein immunoprecipitation (RNP-IP) and luciferase reporter assays. These disruptors e.g. CMLD1–6 and NC1-3 were tested on colon cancer cell line HCT-11, pancreatic cell line, MiaPaCa 2, and normal fibroblast cell line WI-38. Among these NC2, was most potent with IC₅₀ of 13.5±0.5, 9.2±1.5 µM in HCT-11 and MiaPaCa2 cell lines. CMLD-1 and CMLD-2 were also analyzed for their blocking function on HuR and its target mRNAs i.e. for, stability of Bcl-2, Msi1, and XIAP mRNAs in HCT-116 cells, by using the Actinomycin D experiments, they significantly decreased levels of these mRNAs. Consequently protein levels of these targets were also lowered indicating that HuR failed to recruit these transcripts on the polysomes in the presence of these molecular disruptors. In addition, the CMLD-2 compound was recognized as potential HuR-mRNA disruptor, with a K_i of 350 nM [100]. Zhonghua and colleagues by using Fluorescence polarization (FP) assay also screened 1597 compounds. They used NMR spectroscopy demonstrating some hit given by potential compounds which disturbed HuR oligomerization *in vitro* [101].

Resveratrol found in the red skin of grapes was found to decrease induced gene expression in T-cells, in a HuR dependent manner. Resveratrol regulated the 3'UTR sequences of the transcripts via favoring KSRP interaction and replacing the HuR from the 3' UTR sequences

hence changing the stability of the transcripts [102]. **Figure 9**, represents the study of folate-based nanoparticle which was transduced with siHuR sequences, forming HuR-FNP (folate nanoparticles) spherical structure giving a protective shield to siRNA from degradation. The most interesting fact with FNP system was the moderate and controlled distribution of siRNA at physiological pH, this was supposed to prolong the efficacy of the treatment and therefore reducing the chances of further treatments [103] (**Figure 9**).

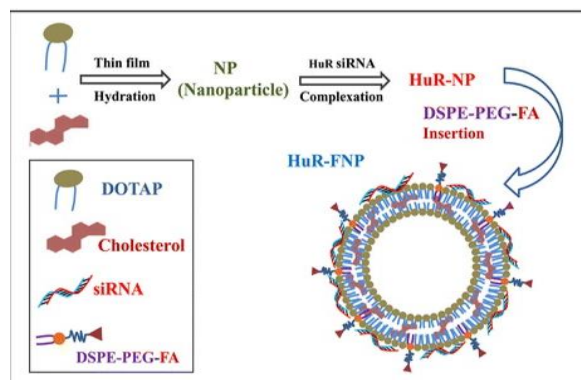


Figure 9 Schematic representation of synthesis HuR-FNP preparation. Nanoparticles are complemented with siRNA for HuR and further inserted via 1, 2-distearoyl-*sn*-glycero-3-phosphoethanolamine-N-[amino (polyethylene glycol)-2000] or DSPE-PEG-FA Mediated delivery [103].

R Muralidharan *et al.*, 2015 used CXCR-4 antagonist AMD3100, together with HuR silencing sequences coupled to FP nanoparticles. This showed repressed CXCR-4 levels and inhibition of cancer cell metastasis. Co-treatment resulted in cell cycle arrest at G1 phase followed by decreased cell viability. Moreover, their physicochemical studies showed that HuR-FNPs were positively charged having zeta potential of 4.3 mV were almost 300 ± 10 nm in size. Cells used for this study were folate receptor (+) positive H1299 lung cancer cells, and the uptake of the FNP was via endocytosis, as they were folate-targeted and were efficient in delivering siRNA into the cells [104].

Jiawei Guo *et al.*, 2016 found a synergistic effect of cisplatin, doxorubicin, vincristine, and oxaliplatin together with a FDA-approved anthelmintic drug, pyrinium pamoate. In this study, this drug appeared to be a novel HuR inhibitor that inhibited HuR cytoplasmic accumulation in a dose-dependent manner. Combined effect enhanced the cytotoxic effect together with the repressed growth of tumor derived from patient's bladder xenografted in mice. Further

investigation confirmed pyrvinium pamoate supported nuclear import of HuR along with inhibition of Chk/Cdk kinase pathway, with these findings this novel compound also downregulated the level of DNA ligase IV and BRCA2, leading to genetic instability and cell death [105]. MPT0B098 is an indoline-sulfonamide compound, a microtubule inhibitor, has the potential to interfere with the HIF-1 α in several cancer cell lines, e.g., H460, A549 and H1299 Non-small cell lung carcinoma (NSLCs). It mainly decreased HuR translocation from the nucleus to the cytoplasm, and efficiently suppressed tumor growth and microvessel density of tumor specimen *in vivo* in low IC₅₀ values, i.e., from 70-150 nmol/L [105] [106]. In another study N-Benzylcantharidinamide a novel cantharidin analog, decreased cytosolic translocation of HuR, resulting in lower mRNA level of matrix metalloproteinase-9 (MMP-9), in a dose-dependent manner. MMP-9 causes invasion and metastasis of hepatocellular carcinoma HepG3 cells [108].

Tripterygium wilfordii, a member of the Celastraceae plant family, in Chinese medicine practice, its extract triptolide inhibited COX-2 mRNA and its expression in NSLC A549 cells, when induced with TNF α by suppressing nucleocytoplasmic shuttling of HuR [109]. Previously triptolide has been shown to, impairs dendritic cell migration by inhibiting COX-2 and CCR7 expression through NF- κ B and phosphatidylinositol-3 kinase (PI3-K)/Akt pathway [110]. Similarly, natural compounds from Green tea and *Kalopanax pictus* has been shown to down-regulate TNF α and MMP9 mRNA stability and protein trafficking by increasing the anti-inflammatory protein TTP [111]–[113]. Finally, a new class of anti-inflammatory methoxyphenolic compounds has been shown to inhibit CCL2, CCL5, IL-6, IL-8, ICAM-1, MIF, CXCL1, CXCL10, and Serpin E1 mRNA levels in Human airway cells when stimulated with TNF- α . This has been confirmed by the specificity of methoxy compound towards HuR-mRNA binding, and the hence have been indicated for their HuR dependent post-transcriptional influence [114].

Focusing on Tanshinone/DHTS to target HuR *in vitro* and *in vivo*

Tanshinones are diterpenes extracted from plant root of *Salvia miltiorrhiza*, also known as red sage, tanshen or danshen. The chemical compositions of tanshinones have been well studied extensively over the last 75 years. They are classified based on their structure, e.g. tanshinone-I has aromatic furan ring, Dihyrotanshinone-I (DHTS) has a reduced dihydrofuran on the right side of the molecule, together with cyclohexane rings [115] (**Figure 10**). According to

differences in their structural, chemical/physical properties, tanshen constituents have been classified into two groups, **I)** first groups contains water-soluble phenolic acids such as lithospermic acid B and salvianolic acid. **II)** The second group has lipophilic diterpene quinones such as tanshinone I, tanshinone IIA; B, Cryptotanshinone etc., where each of them contribute to their biological activities [116].

These Tanshen are well known in Chinese traditional medicine practice for the treatment of the coronary heart diseases such as myocardial infarction and angina pectoris. Besides this they also have been suggested for the treatment of hemorrhage, swelling, insomnia, miscarriage, and dysmenorrhea, as well as inflammatory diseases such as edema, endangitis, and arthritis. Tanshen analogues were tested for their cytotoxicity in KB, HeLa, Colo-205 and Hep2 Carcinoma cell lines. Interestingly they were effective in conc. <1 µg/ml [117]. Moreover, in LPS activated RAW 264.7 macrophages, Tanshinone IIA inhibited iNOS expression and synthesis of TNF-α, IL-1β and IL-6 protein levels [118]. Besides this Tan IIA has been shown to inhibit tumor cell proliferation, intervening tumor cell cycle, initiating tumor cell apoptosis, and suppressing tumor cell invasion and transfer in human lung cancer cell lines [119].

In *in vitro* and *in vivo* experiments tanshinone-I exhibited anti-migrating, invasiveness with reduced tumorigenesis and metastasis in human lung adenocarcinoma and severe combined immunodeficient mice. RT PCR, EMSA experiments confirmed that tanshinone-I reduces IL-8 intracellular levels, a major factor involved in the angiogenesis and cancer metastasis and thus further blocking DNA binding activity of AP-1 and NF-kB [120].

15, 16 Dihydrotanshinone has been found to inhibit the collagen-induced aggregation of rabbit platelets with an IC₅₀ lower than that the active green tea ingredient Catechin. Besides this DHTS inhibited intracellular calcium levels, suppressed collagen-induced liberation of Arachidonic acid and thromboxane B₂ from rabbit platelets. Here DHTS exerted potent anti-platelet activity via suppression of Ca²⁺ mobilization and arachidonic acid liberation and hence possess anti-inflammatory activity [121].

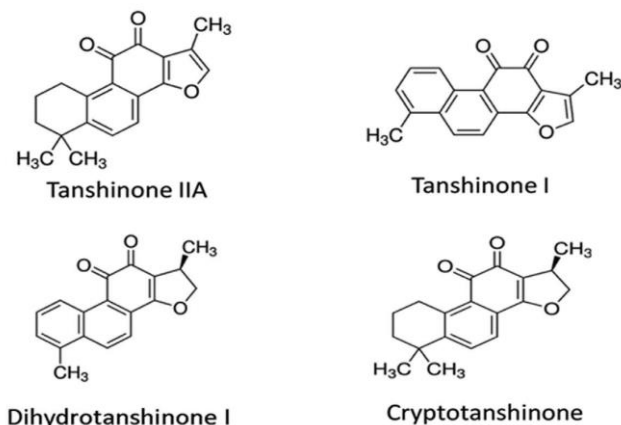


Figure 10 Chemical structures of tanshinones. (Adapted from D'Agostino *et al.*, 2015)

Tanshinone I, Tanshinone IIB, Cryptotanshinone, and DHTS has been shown to possess antibacterial against the broad range of Gram positive bacteria as they generated superoxide radicals, anti-inflammatory, anti-allergic and anti-oxidant properties [122]. DHTS induced autophagy and apoptosis through caspase activation and p53 independent pathway, as well as via intracellular generation and accumulation of ROS, which showed the pro-apoptotic activity of DHTS in colon carcinoma cells [123], [124]. Tumor cells adapt and proliferate in the presence of hypoxia-inducible factor-1 (HIF-1), whose protein translation was inhibited by DHTS in HeLa and its xenograft tumor model *in vivo* mice model. Conclusively the HIF-1 α protein synthesis was blocked via downregulation of the mTOR/p70S6K/4E-BP1 and MEK/ERK pathways [125]. NF- κ B transcription factor which controls many physiological processes e.g., immunity, inflammation, apoptosis, and angiogenesis, was significantly suppressed by DHTS upon TNF α induction in a dose-dependent manner. DHTS also inhibited TNF α induced phosphorylation of I κ B α and p65 and subsequent nuclear translocation of p65. Additionally, DHTS induced the apoptosis and suppressed the TNF α -induced expression of NF- κ B target genes, cIAP-1, COX-2, MMP-9, VEGF and major inflammatory cytokines such as TNF α , IL-6 and MCP1. *The in vivo* model also indicated that Dihydrotanshinone I inhibited the growth of HeLa cells in a xenograft tumor models [126]. Altogether, these findings suggest that Dihydrotanshinone I could be a valuable candidate for therapeutic intervention in the cancer patients. Also among tanshinones, tanshinone-I was found to be most potent, but due to its low solubility and crystal forming property, Dihydrotanshinone-I was better soluble and was

further able to disrupt rHuR-RNA complex formation in in-vitro binding assays, e.g., EMSA (Figure 11) [99].

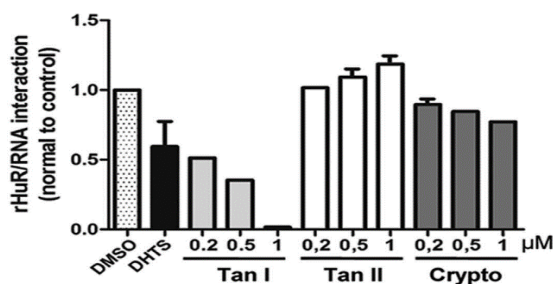


Figure 11 Densitometric comparison of tanshinones activity from EMSA (EMSA Image not shown) for disassociation of HuR–RNA complex formation upon incubation with IC50, 0.2, 0.5 and 1 μM of DHTS, Tan I, Tan II, Cryptotanshinone and IC50 conc. of DHTS [99].

Why to inhibit HuR?

HuR could be a drug target for cancer therapy and its inhibition simultaneously down-regulates multiple oncoproteins resulting in reduced cell migration and tumor progression [127]. Considering HuR is a regulator of many biological pathways responsible for growth, metastasis, tumor formation which contribute to chemo-resistance mechanisms to therapeutic drugs for e.g., tamoxifen thus now it's important that HuR could be considered as a therapeutic target for cancer therapy. Hence, targeting HuR would attenuate the onset of multiple cancer related pathways or delay in disease progression by using the small molecules that act on or via HuR.

We further tried to contribute to the list of potential HuR inhibitors, by testing a specific library of commercially available anti-inflammatory compounds [98], [99]. One potential hit compound was used as a model inhibitor to synthesize further and characterize set of other synthetic analogs and their ability to prevent the rHuR-RNA complex formation, in biochemical and cell-based assays. Also because, these tanshen are widely used in clinics in China, and the exact mechanism behind therapeutic basis is still unknown [128]. Thus to exploit the mechanism of action of DHTS we rigorously worked on our experimental models and published our work as D'Agostino *et al.*, 2015 and Lal *et al.*, 2017 [129] [130].

Regarding above task:

The Aim of my PhD thesis project is **“Characterization of small molecules inhibiting the RNA binding protein HuR”**.

CHAPTER 2

Materials and Methods

Materials and Methods

Media and bacterial strains used

LB (Luria Bertani) broth was used as the medium to grow bacterial strains. The bacterial strain used was Neb α strain of *E.coli* for obtaining the recombinant clones. For prokaryotic expression, the Rosetta BL-21 strain of *E. Coli* was used. For amplification of the desired motif, primer used were forward primer with *NdeI* restriction site and the reverse primer with *XhoI* restriction site for the RRM1/2 and akin for RRM2/3 but with different primer sequences. All Primer used are listed in Table 4.

Protein expression and purification

pET-42a vector containing the full-length sequence of HuR was used as a template for PCR to produce all the individual RRM1s [99], including the Δ RRM1, Primers used for Δ RRM1 are listed in Table 5. All four mutants were produced by using Q5[®] Site-Directed Mutagenesis Kit, following the instructions are given by the manufacturer. Primers used are S94A, N107A, I133A, and N134A are listed in Table 5.

Expression of the all the RRM1s, i.e. RRM1, RRM2, RRM3, RRM1/M2, and Δ RRM1 were done at 37°C for initial growth to reach the OD at 0.5, and then were induced by 0.1mM IPTG at 18°C for at least 6 hrs. Cells were centrifuged at 5000g and later pellets were dissolved in equilibration buffer (20mM Tris-Cl pH 8.0, 100 mM NaCl, 3 mM MgCl₂, 0.5 Mm DTT and 1X Protease inhibitors) and sonicated at 95 kHz amplitude with 7' Pulse ON and 30' OFF for 9 cycles. Centrifuged the lysed solution for 30 min at 13000 rpm, separated the supernatant by filtering with the 0.2 μ M filter. While centrifugation aliquoted 1 ml of the Ni-NTA resins, and centrifuged at 1800 rpm for 30 sec removed the excess 20% ethanol and added 1 ml of the equilibration buffer with imidazole (5mM), inverted the tube gently 2-3 times and centrifuged again at 1800 rpm. Repeated this at least for 3 times. Dissolved the resins in the same buffer (0.5 ml) and transferred to the supernatant, incubated on rotating shaker at the 4°C for 4 hrs. After 4 hrs centrifuged the supernatant (1800 rpm for 1 min) and separated the protein bound resins and dissolved the resins gently in 1 ml of wash buffer (20mM Tris-HCl Buffer pH 8.0, 100 mM NaCl, 2mM MgCl₂, 0.5 Mm DTT and 20 mM Imidazole). Incubate for 10 minutes on rotating shaker at 4°C (cold room). Repeated the wash twice with wash buffer containing 250,

350 mM NaCl and 25 mM Imidazole, now discard washes but keep 50 μ l for coomassie gel analysis. Added the elution buffer 1 (equilibration buffer with 100 mM Glycine and 30 mM Imidazole) 0.3 ml to the microfuge tube containing the resins incubated rotating again for 20 min at 4°C. Repeated the second elution using elution buffer 1 with 60 mM Imidazole and collected in fresh Eppendorf tubes. To both elutions added the glycerol to 10% final concentration. 50 μ l aliquots of all the elution, wash, and add laemlli buffer to 1X final concentration. Expression and purification of WT-HuR and mutants were similar as described above, except for the induction which was done at 30°C with little modification of 20mM imidazole in equilibration buffer and wash buffers with 50 mM, 100 mM and 110 mM and 100mM NaCl in all three washes. All samples of each purified proteins were run on 15% SDS-PAGE gel for RRM1 and 12% SDS-PAGE gel for HuR and its mutants. Stained with the Coomassie blue staining solutions for 2 hrs and destained using destaining solution (40% methanol, 10% acetic acid and 50% water), the gels were analyzed in Odyssey® Infrared Imaging System.

REMSA assays

EMSA was done using the equimolar concentrations, i.e., 0.2 μ M of the recombinant proteins and RNA probe (FAM labelled-AUUAUUUAUUUAUUUAUUUAUUUA), DHTS or DHTS analogs were dissolved in the 1X REMSA buffer to have the required final conc. of the compound in the reaction mixture. After mixing the all the reagents, the vials to incubate for 30 min at room temperature 1 μ l of 100% glycerol was added to each reaction mixture before loading on the native 4% PAGE gel. The native PAGE gel was made in the 0.5x TBE buffer. Now the mixture was loaded on the 4% Native polyacrylamide gel (18 μ l) was run at 80 V constant voltage for about 60 minutes in 0.5X TBE at 4°C (cold room). All the reaction mixtures were run without using the bromophenol loading dye. This is to avoid the interference of the dye while reading the gel, on the other hand, I have used one well with bromophenol loading dye, to check the running front of the free probe. The running apparatus was covered with aluminum foil to avoid direct light exposure. The gel image was developed in Typhoon scanner at high resolution for FAM probe at 488nm or Licor odyssey infra-red apparatus if using DY-681 labeled RNA probe depending on the area the gel was occupying on the gel instrument surface, with high resolution for at least 10 min and then exported and analyzed for the results.

then collected at high-speed centrifugation, sonicated, and supernatants collected were used directly or loaded with Ni-NTA beads for 3-4 hrs and were eluted in elution buffer (20mM Tris-HCl, 100mM NaCl, 3 mM MgCl₂ and 250 mM Imidazole), respective proteins were lysed with Laemmli buffer and were loaded on 12% gel with 0.05% SDS. The separated proteins were then transferred to the nitrocellulose (0.45 μM) membrane, using standard wet transfer protocol. The blotted membrane was then incubated with 5% BSA for 1 hr and followed by Incubation of membrane with the mouse anti-HuR primary antibody (Santacruz (1:1000) overnight at 4°C. Next day after washing three-time (10 min each) membranes with 1x PBST was incubated with secondary antibody (HRP-anti-Mouse IgG) for 1 hr. The membrane was again washed for 3 times (10 min each) with 1X PBST and developed under BioRad ChemiDoc instrument using commercial developing solutions. Image obtained were then analyzed for the outcomes. At least three independent experiments repeated to confirm the dimerization of muteins.

Western blot analysis

Whole cell lysates were collected using Laemmli buffer, afterward separated by running on 12% SDS-PAGE gels and transferred to PVDF membranes. Membranes were incubated with the following primary antibodies: anti-HuR (Santa Cruz biotech), anti-zfp36 (NE2.2/1), anti-p-MAPKAPK-2 T222 (MK-2), anti-MAPKAPK-2 D1E11 (p-MK-2), anti-NFκB, p-IκB-alpha S32/36, anti-pp38-T180/Y182, anti-ATF2, (Cell Signaling) and anti EF2, anti-Actin (Santa Cruz biotech) all were used at dilution 1:1000. The peroxidase-labeled secondary antibody (Santa Cruz Biotechnology) was detected using ECL western blotting reagents from GE Healthcare and were developed under the Bio-Rad developing apparatus.

Fractionation experiments

RAW 264.7 cells (1x10 cm plate) were washed with 1x PBS (4°C) and resuspended in 300 μL Buffer A, collected and transferred to a 1.5ml tube and were put on ice for 15 min. Then Igepal CA 630 (0.5 % (v/v)) was added and vortexed for 10s. Nuclear fraction was isolated by spinning at 4°C for the 20s at 6500 rpm. The transferred supernatant (cytosolic fraction) to a new tube and kept on ice. Added 150 μL Buffer B to the Pellet (nuclear fraction). Rocked this fraction for 30 min at 4°C in an overhead tumbler. Centrifuged for 10 min at 13000rpm at 4°C to separate the nuclear fraction from the cell debris. Nuclear fraction was in the supernatant.

Blot for cytosolic (GAPDH/Actin/Tubulin) and nuclear markers (H3/ATF-2) to control fractionation.

Polysomal analysis

10x10⁶ Cells were seeded in 15cm per plate and next day treated with compounds (DHTS, MFM49, GD041, MB11v) and co-stimulated with 1 µg/ml LPS, for 3 hrs, after 3 hrs cells were washed twice with 10 ml 1X PBS containing 0.1 mg/ml of the CHX further cells were collected in on ice and the pellets obtained were stored at -80°C. On the same day gently made the gradients as was mentioned in protocol, stored the gradients at 4°C and next day lysed the cells in lysis buffer vortexed properly put on ice for 10 min and centrifuged them at a 13000 rpm at 4°C for 10 min collected the supernatant and transferred the clear supernatant on top of the gradient made, now weighed them accurately in very high sensitive weighing balance and then proceeded for centrifugation at 40,000g for 2 hrs 45 min, after the centrifugation separated each monosomal and polysomal fraction numbered 1 to 12, store on ice in a polysome separating at UV visible spectrum in gradient separator instrument . To each 1 ml fraction obtained added 100 µl of sodium acetate and 900 µl absolute isopropanol stored at -20°C. RNA was extracted as explained by [43], then followed by qPCR analysis of each fraction.

RT qPCR Experiments

PCR conditions and Primers conc. for the target sequences were used according to the Mastermix manufacturer instructions. The reaction mixture was prepared with the primer of each target to be tested without the cDNA template. The reaction mixture of the each target added to 96 or 384 well Biorad qPCR plate. At the end diluted cDNA template was added in nanomolar range to each well 96-well plate for q-PCR analysis. The CFX 96 or CFX384 biorad machines were used for quantifying the target levels. The program used for the qPCR analysis was 2 min initial denaturation at 95°C, 10 sec second denaturation at 95°C and 30 sec annealing and extension time at 60°C. This cycle from second denaturation was repeated 40X times to see the differences in the level of each target in each test and control. On completion of the program after 1 hr 9 min, data obtained were analyzed by averaging 3 technical replicates, Ct values were obtained by using formula $2^{-\Delta Ct}$. The mean Ct of the each replicate were exported to MS-excel and then normalized to housekeeping genes GAPDH or 18S or beta-actin gene. Fold enrichment changes were then normalized to DMSO or not treated Ct

values obtained. The standard deviation for each replicate was calculated in MS-Excel and then normalized to the mean of the DMSO control. Primers used for qPCR analysis are listed in Table 4.

Circular Dichroism

All experiments have been done by using a final 10 μ M concentration of TNF-ARE and 10 μ M DHTS, 10 mM sodium phosphate buffer pH 7.3, was used to dilute RNA and DHTS. CD spectra were recorded in a JASCO-700 Spectrophotometer at 240-350nm range (DMSO interfered below 240nm), at 100nm/min speed. The TNF-ARE probe was produced by using AmpliScribe-T7 High Yield Transcription Kit following the manufacturer's instructions. The primer sequences used for the IVT for the TNF probe were:

Forward, 5'-TAATACGACTCACTATAGATTATTTATTATT

Reverse, 5'-TAAATAATAAATAAATAAATAAATAATCTA

RNA Immunoprecipitation experiments

5x10⁶ cells per sample for each RIP experiment were used and followed accordingly as explained in Peritz et al., 2006 [131] without cross-linking step. The cells were treated with DMSO and reference compounds for 3 hrs and then collected in Lysis buffer as given in Peritz *et al.*, 2006 [131]. The anti-HuR antibody or of mouse IgG isotype (negative control) concentration used were 1 μ g/ml. TRIzol was added directly to the beads for isolation of HuR-bound RNA. Data were analyzed by averaging technical triplicates. Fold enrichment changes were calculated by the following formula: $(X - \text{IgG}) / \text{INPUT}$, where X is the Ct value of the target of interest obtained from the immunoprecipitated RNA bound to HuR; IgG is the Ct value of the same RNA sequence obtained from the RNA immunoprecipitated with an IgG antibody (background) and Input is the Ct value obtained from the total RNA before immunoprecipitation.

RTCA proliferation assays

xCELLigence RTCA DP Instrument (Roche) was used to perform the Proliferation assays by plating 5,000 cells/well at time zero (t0) in E-Plate-16 format. Experiments were run for 72 hrs. The cell proliferation rate was automatically recorded on the xCELLigence System (Roche) in real time every 15 minutes by an electronic cell system. The doubling rate of the cells was calculated in accordance with cell index. The cell index is an arbitrary measuring unit which

displays impedance. Treatment of the cells was performed by replacing medium with DHTS dissolved to 1 and 10 μM concentrations or DMSO (v/v) under the same working conditions. Since this system measures the impedance-based sensitivity system, optimization of the cells seeding number was followed before starting the main experiments.

Immunofluorescence experiments

MCF-7 8,000 cells/well in 96 well plate in triplicate and treated with 1 μM DHTS, MFM49 5 μM and ActD 2 μM for 3 hrs, were fixed with 100 μl 4% paraformaldehyde (PFA) for 15 min at RT. Cells were washed with 1X PBS two times. Now Cells were treated for 10 minutes with 100 μl permeabilization buffer (200 mM sucrose, 0.2% Triton X-100) followed by one time wash with 1X PBS and then blocked for 15 min with 100 μl blocking buffer (3% Bovine Serum Albumin in PBS). Primary antibody anti-HuR 1:300, Anti-NF- κB 1:300 (50 μl) were prepared in 3% BSA and allowed to incubate for 1 hour at RT. Now washed twice or thrice with 100 μl 1X PBS. Secondary fluorophore-conjugated (Alexa 594 Red and Alexa 488 Green) antibody (1:500, 50 μl) were diluted in PBS + BSA 0.6% and incubate for 1 hour. Washed 3 times with 1X PBS (100 μl) and then 100 μl of DAPI Blue (1.5 $\mu\text{g}/\text{ml}$) in PBS was used and incubated for 2 minutes. After this followed 3 washes with 1X PBS again and let the labelled cells stay in 200 μl 1X PBS solution overnight or until the image analysis. PerkinElmer image plate reader, Operetta was used for image and evaluation by selecting 13 fields/well. Intensity of HuR and NF- κB in nucleus and cytoplasm were measured. Nucleocytoplasmic ratio of HuR/NF- κB protein analyzed and plotted in comparison with DMSO control. Clear representative images along with DAPI were selected and used for further visual description along with the graph showing N/C ratio.

CHAPTER 3

Results

RESULTS

In 2013, a novel high-throughput AlphaScreen biochemical assay was developed in our laboratory to evaluate HuR protein-RNA complex formation *in vitro* [98]. Based on this strategy, in 2015 again we screened 107 commercially available anti-inflammatory compounds for their potential to target rHuR-RNA complex formation *in vitro* specifically. Out of 107, eight potential positive hit giving compounds named DHTS, hydrocortisone acetate, amiprilose, flurbiprofen, deracoxib, fluocinolone, triamcinolone, dexamethasone, were additionally screened by EMSA. DHTS was the most potent compound (ChEMBL227075 ID in ChEMBL database) among these molecules. Also DHTS did not alter the electrophoretic running behavior of the RNA probe in *in-vitro* EMSA experiments [99].

Considering this molecule as model HuR inhibitor, we further characterized this molecule biochemically *in vitro* and in a panel of breast cancer cell lines, specifically focusing on post-transcriptional role of DHTS, in a HuR dependent manner. With the kind support of our collaborator, for synthesizing new DHTS analogs, from University of Milan, Prof. Pierfausto Seneci and others, we further continued progress of characterizing more precise inhibitors in the context of targeting post-transcriptional control of HuR, in breast cancer cell lines, human monocytic cell line, and in murine macrophage cell lines via *in vitro* biochemical, cytotoxic and proliferation experiments.

Together with DHTS, and its analogs we started testing efficacy of those compounds in our experimental models systematically. All the results collected are reported below.

DHTS is an inhibitor of the rHuR-RNA interaction

We screened a set of anti-inflammatory compounds by using High-throughput AlphaScreen assay [98]. Among 107 tested anti-inflammatory compounds DHTS gave the most potent hit in term of preventing the HuR-RNA complex formation *in vitro* indicated with arrowhead (**Figure 12 A**), it showed a Z-score of -2.69. The chemical structure of the DHTS shows the reduced dihydrofuran ring, on the right side while on left side planar aromatic methyl-substituted cyclohexane ring. Dihydrofuran ring was claimed to be the potential body in this interfering process.

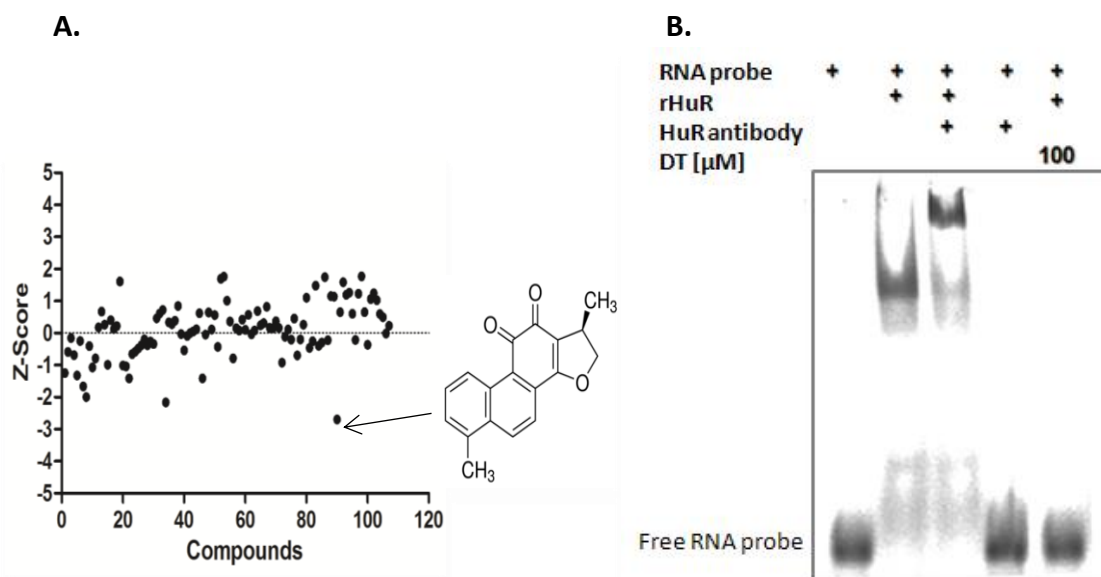


Figure 12 Biochemical characterization of DHTS in-vitro **A)** HTS AlphaScreen carried for 107 anti-inflammatory compounds using 50 nM of each compound with 1 nM of rHuR, 50 nM of Bi-TNF RNA probe. **B)** EMSA showing inhibition of 0.5 μ M of rHuR and 0.5 μ M of Cy-3 RNA probe at equilibrium with DHTS compound *in vitro*, reference DHTS concentration used was 100 μ M. Mean \pm SD refers to three independent experiments ($n = 3$). (Experiment has been performed by Dr. Vito D'Agostino, published in D'Agostino et al., 2015).

DHTS apart from its interfering property further did not alter the electrophoretic mobility of the Cy-3 labelled RNA probe, even at 200 fold more concentration (100 μ M), Anti-HuR antibody was used to confirm the shift acquired, was by HuR itself Lane 3 (**Figure 12B**). To see the DHTS efficacy we have performed competitive binding saturation experiments by using either EMSA or Alphascreen assays. IC₅₀ values obtained for EMSA and AlphaScreen were 149 \pm 34 nM, 68 \pm 16 nM. K_i value, i.e., equilibrium dissociation constant (K_i) calculated for DHTS by AlphaScreen assay was 3.74 \pm 1.63 nM, after using the K_d 2.5 nM [98] (**Figure 13A and 13B**). These values depend upon the different concentration of the constituent used.

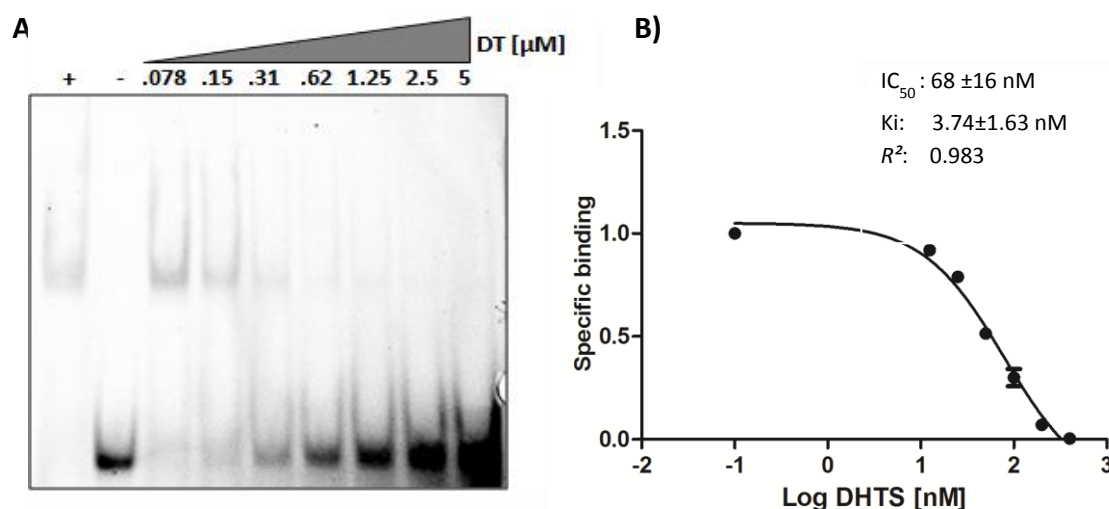


Figure 13 DHTS interfere with HuR-RNA complex and lowers the cell viability. **A)** Titration of the HuR with a gradient of DHTS concentration showing saturation binding. **B)** Evaluation of the DHTS activity in low nanomolar or micromolar range. K_i values was calculated using the GraphPad Prism version 6 with nonlinear regression function in analysis tab and choosing the one site-specific binding or one site-specific K_i function. For the K_i , the K_d value [98] (2.5 nM) of the HuR protein and final conc. of the probe used (50 nM) was needed to put in order to obtain the specific K_i Mean \pm SD refers to three independent experiments (n = 3). (Experiment has been performed by Dr. Vito D'Agostino, published in D'Agostino et al., 2015 [99]).

DHTS binds to M1M2 domain of the rHuR

In HuR main remnant responsible for recognizing the AU-rich RNA elements, are present in its RRM (RNA recognition motif), we constructed and purified recombinant HuR isoforms containing two different arrangement of HuR RRM (Figure 14A). Since we know that RRM1 and RRM2 are rate-limiting domain of HuR for RNA binding activity [20], the RRM1/2 construct was supposed to copy the ability of FL-HuR to bind the target RNA probe, as expected it was the target of the DHTS for its ability to interfere in RNA binding activity in HuR RRM1/2 motifs.

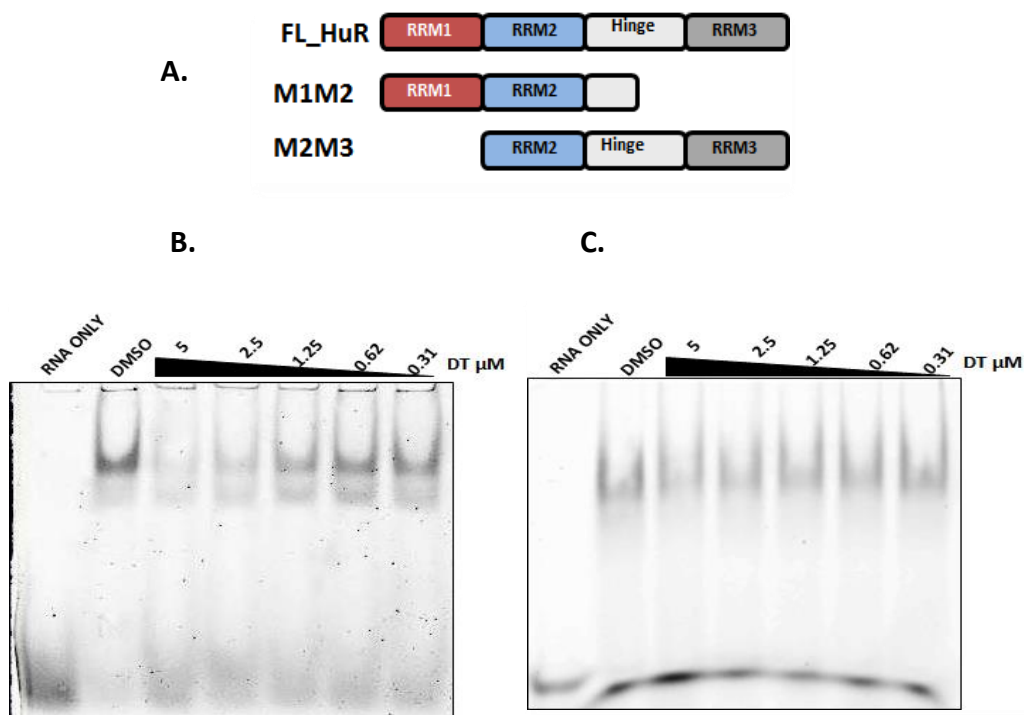


Figure 14 Effects of DHTS on RRM1/2 and RRM2/3 **A)** Schematic representation of strategy used to exploit the DHTS efficacy in HuR RRM. **B)** EMSAs showing inhibition of RRM1/2 binding to TNF α probe, the concentration of protein and probe used were 0.5 μ M respectively. **C)** EMSA for RRM2/3, DHTS could not inhibit the binding of RRM2/3 binding to TNF α probe, conc. of protein and probe used were same as in figure B. Representative REMSAs were repeated with at least three independent protein purification. (Experiment has been performed by me and published in D'Agostino *et al.*, 2015 [99]).

Consequently RRM1/2 isoform reported K_d value 2.66 nM, more or less similar to FL-HuR. DHTS was found to be working on the first two domain RRM1/2-RNA complex formation with

Ki = 4.12 ± 0.81 nM, when titrated with DHTS to upto 5 μM concentration resulted in complete abrogation of the HuR and its ARE binding was observed (**Figure 14B**) (Ki and Kd graphs not shown).

Moreover RRM2/3 HuR isoform was purified and noted to be a labile protein concerning its stability, and represented higher Kd value of 24 nM and only minimal effects of DHTS were seen upon, titration with DHTS in a similar fashion as is done for RRM1/2 (**Figure 14C**).

Additionally each individual motifs (RRM1, RRM2 and RRM3) were constructed and purified from *E. coli* cells (**Figure 15A**). RRM1 and RRM3 were stably expressed at RT, whereas RRM2 showed labile, low expression pattern at RT, lately optimized and was expressed at 16 °C, this may be due to its low molecular weight ≥ 10 kDa or labile conformations (Coomassie gel not shown).

They were analyzed for their binding to FAM labelled AU-RNA probe, in the absence (DMSO only) and presence of DHTS gradient ranging from 0.31-10 μM, remarkably individual RRMs-RNA was strong and was not abrogated by DHTS at reference doses. As expected from RRM1, where it's binding with RNA probe was slightly interfered with 20% displacement observed after densitometric analysis by Image J (**Figure 15B**). Altogether, these results show that DHTS interfere with RNA binding activity of HuR. A correct clarification could be given for DHTS interference with allosteric alteration in conformation of RRM1/2, therefore disturbing the additional association formed with inter-domain linker region during RNA-complex formation [20].

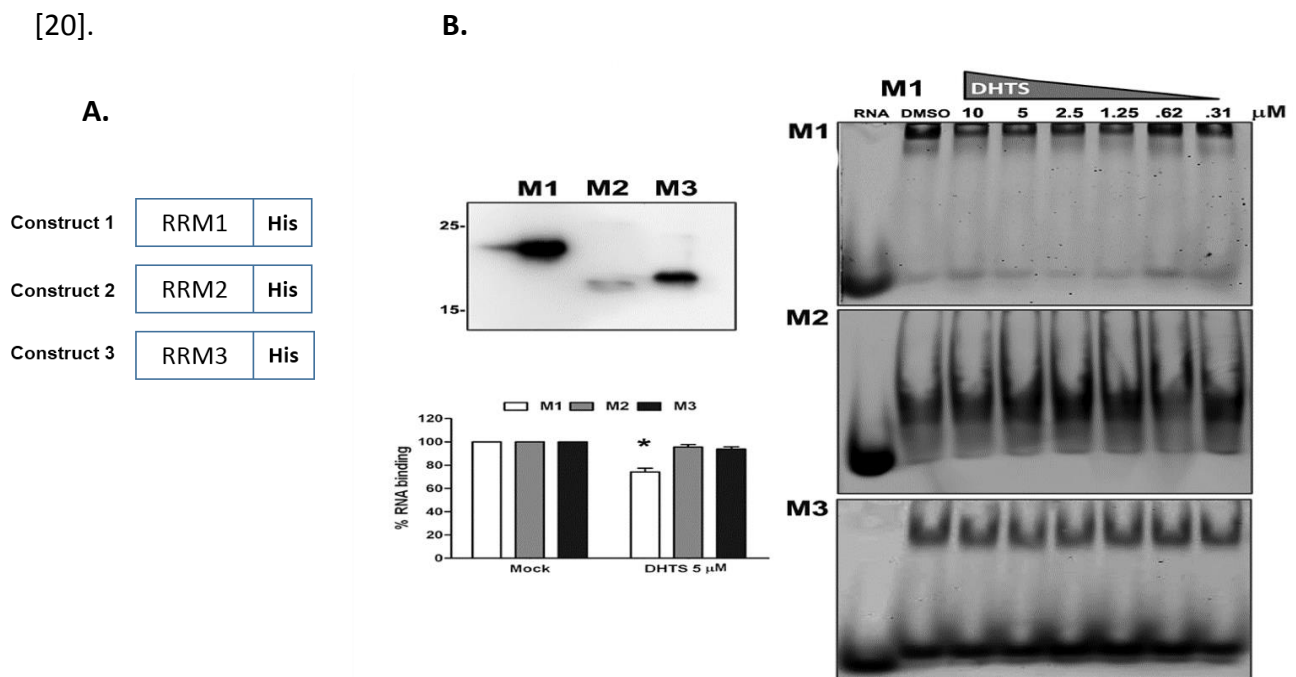


Figure 15 Limited effects of DHTS on individual RRM1 **A)** Schematic of the RRM1 constructs used for DHTS interference analysis (On left). **B)** RRM1 western blot, and densitometry of each RRM1 from EMSA. (Upper and lower pictures, left hand side), Representative EMSAs showed no inhibition by DHTS on individual RRM1, even at 10 μ M, except at for RRM1 (On Right). Mean \pm SD refers from at least 3 independent protein purification independent experiments. (Experiment has been performed by me, published in D'Agostino et al., 2015 [99]).

DHTS selective profile against other RBPs

Since we know that DHTS interferes with HuR-RNA interaction, *in vitro* characterization of the selective profile of DHTS was necessary [99]. For this purpose we selected four RNA binding proteins (RBPs), i.e., HuD/ELAVL-4, TTP, Lin28 and TDP-43, having structural homology of 78%, 50%, 35%, and 24 % with HuR. HuD which selectively expressed in brain and tumor tissue possess 78% homology as it also contains RNA-Binding Domains [7]. *In vitro* HuD-RNA complex formation was interfered by DHTS at 5 μ M concentration, whereas on contrary Lin28b has a cold shock domain and a pair of CCHC zinc finger domains [132]. TTP (Nup475) has two tandemly arranged cysteine and histidine sequences of new heavy metal-binding domain and is known to bind Zn^{2+} and TDP-43 protein has NTD (N-terminal domain, two middle RNA recognition motifs (RRMs) followed by a C-terminal glycine-rich fragment [133]. All protein's except HuD, binding to target probe was not abrogated by DHTS (**Figure 16A, 16B, 16C, 16D**).

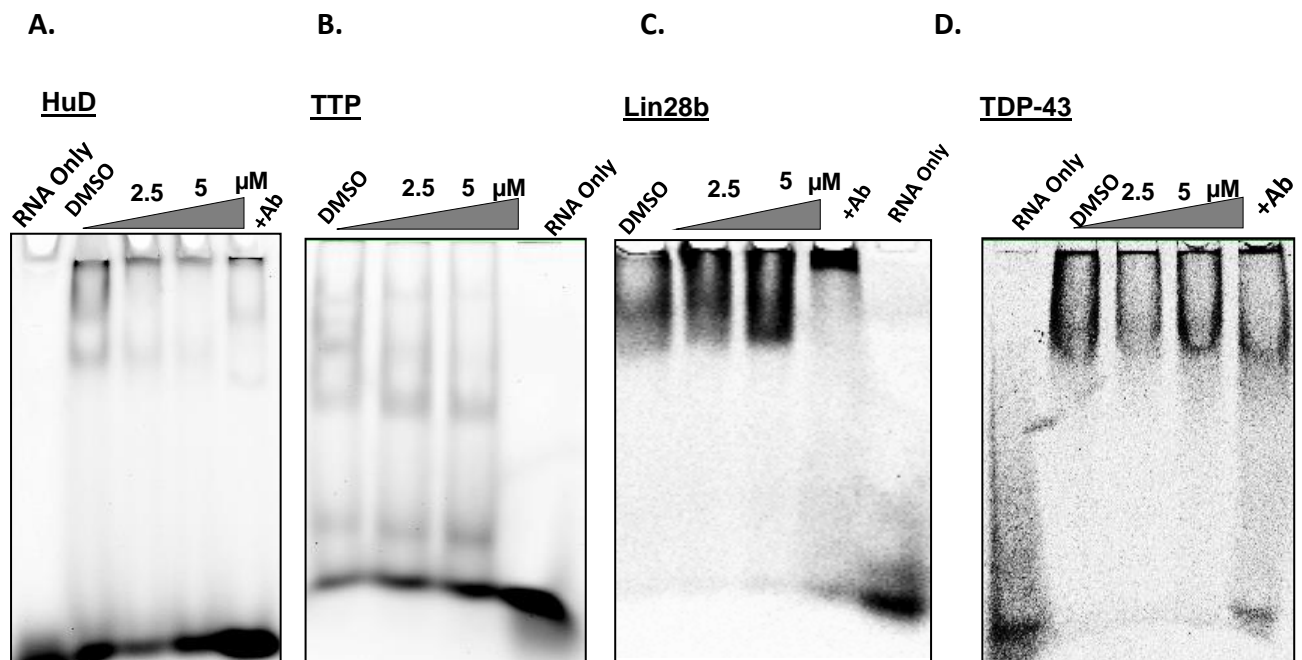


Figure 16 Determination of selective profile for DHTS in panel of other well-known RBPs **A)** EMSA for HuD, DHTS interfered at reference doses. **B, C & D)** EMSA for TTP, Lin28b, TDP-43, no interference by DHTS at reference doses, in all RBPs were detected. Representative EMSAs were repeated with at least three independent protein purification. (Experiment has been performed by me, published in D'Agostino et al., 2015 [99]).

Taken together these set of experiments further led us to determine the DHTS mediated aftermath in *in vitro* and cell model with highest efficacy of the DHTS among other tested compound encompassing a selective profile towards a group of 4 RBPs. We further decided to characterize DHTS additionally in a different set of biochemical experiments which are explained in the following result section.

Inter-domain linker region in HuR structure is crucial for binding to target RNA and therefore for DHTS activity.

We have shown DHTS is somehow interacting with HuR, as it was displacing bound RNA from HuR in low micromolar range, we got a positive hint from the EMSA experiments done in RRM1/2 domains that our DHTS specifically binding in the RRM1/2 domain and inhibiting the RRM1/2-RNA complex formation (**Figure 14A**). Already first two domains of HuR, has been proved experimentally, and are responsible for binding to target RNA probe in a dynamic fashion [20]. To know exactly the amino acid residual information interacting with DHTS, we have done NMR studies on RRM1/2 and DHTS binding with combined efforts of our collaborators Prof. Marco Fragai, from University of Florence.

Surprisingly, NMR studies revealed participating HuR aa residues in binding to DHTS, which lies in the first two domain in β -sheets of HuR protein. They are Thr20, Asn21, Ile52, Ser94, Tyr95, Ala106, Asn107, Leu108, Ile133, Asn134, Val137, Leu138, Arg147, Ile152, Phe154, Asp155, and Lys182 respectively. Further after conducting molecular modeling followed by “tandem” docking calculations and molecular dynamics (MD) simulations in order to know the mechanism of action of DHTS compound, consistently again DHTS was found interacting at the region within RRM1/2 i.e. from Ser 94 aa of RRM1 to N107aa of RRM2. This region is also called inter-domain linker region and together with these RRMs, forms binding cleft of HuR, responsible for binding to target probe [130].

To support NMR and molecular modeling that addressed a specific interacting region on HuR, we produced HuR protein domains made of the first RRM domain (RRM1), second RRM domain (RRM2), RRM1-RRM2 wild-type RRM domains, RRM1 lacking 14 amino acids at the C-terminus Δ RRM1, missing residues from Ser94 to Asn107 and performed *in vitro* RNA binding experiments. Some of these residues belong to the inter-domain linker (Ser99–Asp105) and the others to the β -platform regions of the two domains, where some amino acids

experienced decreased intensity in the presence of DHTS (Ser94–Tyr95 in RRM1 and Ala106–Asn107 in RRM2). HuR domains were produced in *Escherichia coli* using the pET42 plasmid [99]. We obtained the same purity for all the protein isoforms (Figure not shown). As single domains lose RNA-binding activity very quickly, the *in vitro* activity of the single protein domains and their combination was evaluated by REMSA, mixing equimolar concentration of each, freshly prepared, with 0.2 μ M of the FAM-ARE ssRNA probe (**Figure 17A**). The RRM1–RRM2 isoform was used as a positive control because it displayed a similar K_d (2.62 ± 0.6 nM) [99] to the FL HuR protein, and because it was used in the NMR experiments [101]. RRM1 retained the capability to recognize mRNA substrates [20], however with a lower affinity compared to the RRM1–RRM2 construct, probably indicating a change in the stoichiometry of cooperative protein binding (**Figure 17A**) [134][20].

Importantly, the RRM1–RNA complex was still sensitive to DHTS. REMSA performed with RRM2 and *in vitro* complementation of the two domains RRM1 + M2 did not provide information about the contact region of DHTS. After removing 14 amino acids, the binding capacity of Δ RRM1 to RNA was slightly reduced ($\sim 20\%$) in comparison with the RRM1 domain (**Figure 17A**). Conversely, Δ RRM1 became resistant to DHTS, suggesting that this region is essential for DHTS inhibitory activity (**Figure 17B**).

By using fluorescence polarization, we analyzed the binding kinetics of proteins (200 nM) toward the FAM-ARE RNA probe (100 nM). We confirmed that full-length HuR and RRM1–RRM2 tandem domains behave almost similarly (average $K_{obs} \sim 4$ min), reaching equilibrium after 10 min. On the other hand, the RRM1 domain rapidly recognized the substrate ($K_{obs} \sim 1$ min), but this affinity was significantly impaired in the Δ RRM1 construct (K_{obs} of ~ 8 min) (**Figure 17C; TABLE 1**). All these results together explain the importance of interdomain region of HuR for RNA and for DHTS efficacy.

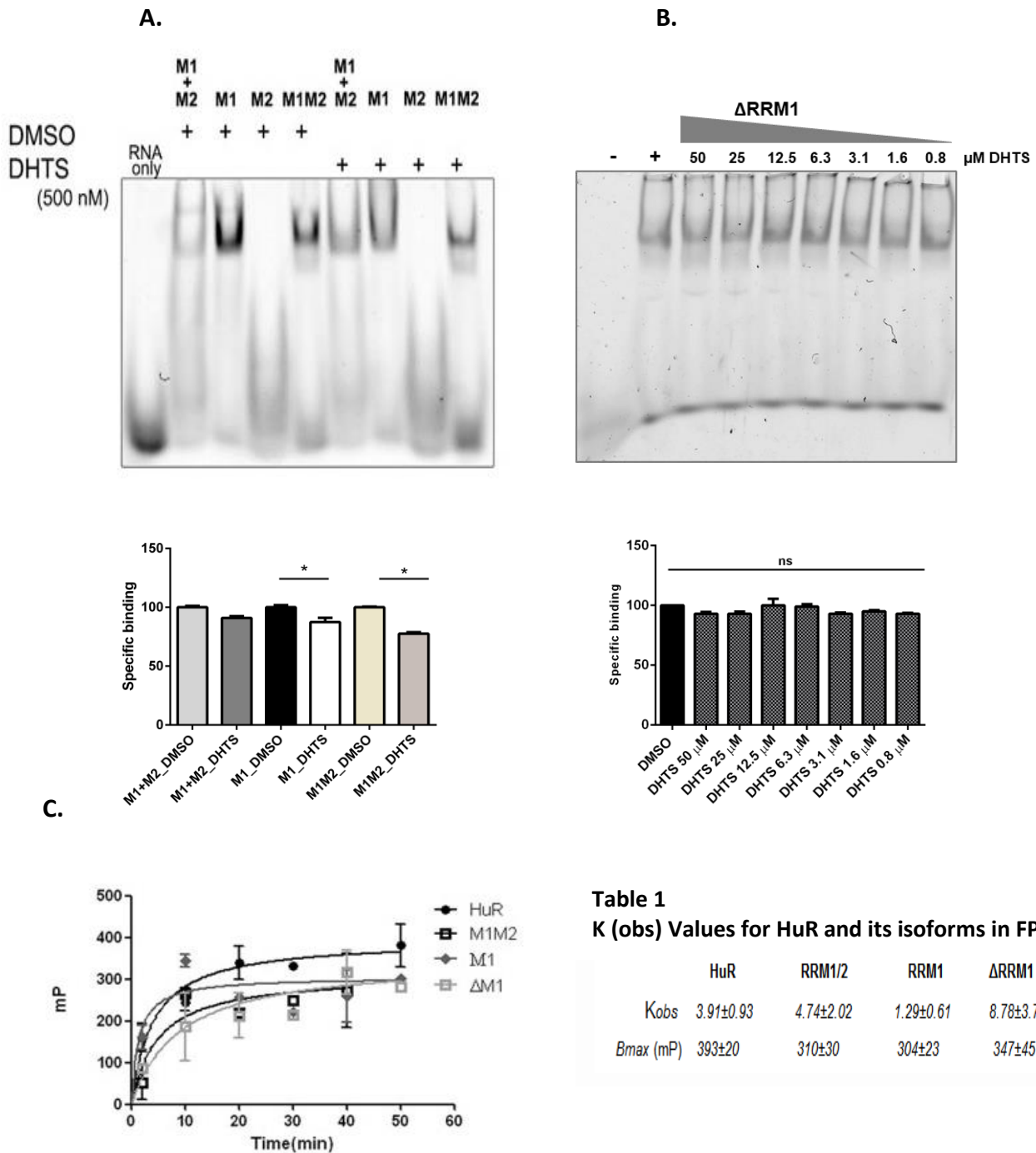


Table 1
K (obs) Values for HuR and its isoforms in FP

	HuR	RRM1/2	RRM1	ΔRRM1
<i>K_{obs}</i>	3.91±0.93	4.74±2.02	1.29±0.61	8.78±3.74
<i>B_{max}</i> (mP)	393±20	310±30	304±23	347±45

Figure 17 EMSAs using individual RRMs and ΔRRM1 to dictate probe binding upon DHTS addition. A) Representative REMSAs of at least three independent protein preparations of recombinant RRM1 + RRM2 (M1 + M2) domains, RRM1 (M1), RRM2 (M2), RRM1–RRM2 (M1M2) HuR proteins. REMSAs were performed with 0.2 μM of protein, 0.2 μM of Cy-3 RNA probe and DMSO or DHTS at indicated doses. **B)** On right Representative REMSA performed with 2.5 μM of ΔRRM1 and 75 fM of probe RNA titrated with DHTS (concentration as shown in the legend). Densitometric quantification plotted below represents specific HuR–RNA binding challenged by DHTS. **C)** Kinetic saturation binding experiment by fluorescence polarization. 200 nM wild-type protein or mutants were incubated with FAM-ARE RNA probe (100 nM). Full-length HuR and RRM1–RRM2 tandem domains (M1M2) have similar *K_{obs}*. RRM1 (M1) is binding faster (*K_{obs}* of ~1 min), but deletion of the inter-domain region abolishes the binding properties of RRM1 (ΔM1) (*K_{obs}* of ~8 min). Mean ± SD refers to three independent experiments (*n* = 3, * indicates *t*-test *P*-value < 0.05). (All experiment has been performed by me, published in Lal et al., 2017 [130]).

Single point mutations in the HuR–DHTS interacting region abolishes DHTS efficacy

Consistent with NMR data, and therefore considering the NMR aa residual information given, as a putative DHTS binding site, we produced mutants of FL-HuR, belonging to the inter-domain region. Together with another participating residues from RRM2, which forms the beta sheets secondary structure in HuR, these mutants were mutated at S94A, N107A, I133A, and N134A. These muteins were produced by site directed mutagenesis, and later purified from *E.coli* cells accordingly [98] [134] (**Figure 18A**). After quantification of the each mutein protein concentrations by densitometry (data not shown), we performed EMSA of these muteins, with 200 nM of each mutein or FL-HuR and 200 nM FAM labelled ARE-RNA probe, as expected we did not see interfering function of DHTS at 5 μ M concentration, whereas in WT FL-HuR dissociation of the RNA probe, was clearly noticed. In addition, we observed a differential qualitative binding behavior of each muteins, which can be seen in the binding profile of FL-HuR alone. From this experiment we found three distinct super-shifts (indicated as arrow head with number 1, 2 and 3) given by individual mutein or possessed fully by FL-HuR, depending on the molecular size on EMSA gel. These single point mutants N107 and N134A possessed noticeable supershift 3. However, S94A and I133A has given supershift similar to that of FL-HuR control. Nevertheless partially they also possessed slight enrichment of supershift 3 explaining the likelihood of these muteins with greater oligomerizing and RNA recognition function compared to FL- HuR, this is also evident from the amount of free RNA probe, both in case of muteins and FL-HuR running front in native EMSA gel (**Figure 18B**).

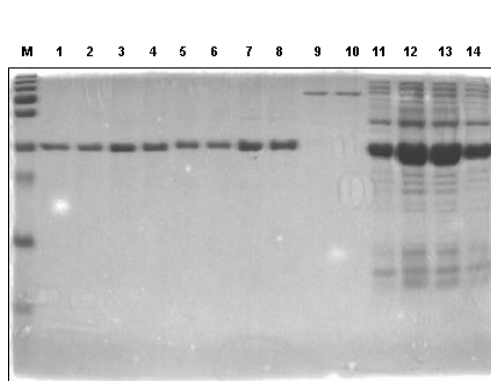
Moreover to find if DHTS interacts with RNA probe we performed, Circular dichroism (CD) experiments at 10 μ M concentration of both reagents similarly 50 μ M RNA + 150 μ M DHTS in NMR measurements. The results obtained ruled out the putative interaction between DHTS and RNA as didn't observe any difference in the spectra obtained (**Figure 19A and 19B**).

Additionally in AlphaScreen assays we found 100 folds lower K_d values i.e. an increased affinity in saturation binding experiments concerning wild-type HuR, when titrated with biotinylated probe's final concentration 3.12, 3.12, 0.78, 1.78 for S94A, N107A, I133A and N134A respectively. Notably the K_d values obtained were 0.22 with R² = 0.84, 0.067 with R² = 0.82, 0.31 with R² = 0.93 and 0.030 with R² = 0.99 for S94A, N107A, I133A and N134A (**Figure 20A, B, C, and D**), Consistently RRM1/2 has given the K_d value of 2.55 \pm 0.744, similar to the k_d obtained by D'Agostino *et al.*, 2013, 2015 (**Figure 21A**) [98], [99]. This shows the critical

57

importance of first two motifs for RNA binding activity. The relative Kd values shown by the N107A and N134A is consistent with previous finding in EMSA experiments (**Figure 20B, 20D** and **Figure 18B**), showing enhanced enrichment of aggregation upon RNA probe addition, considering this profile of binding, we have optimized the RNA probe conc. to be used in these assays which were significantly lower as compared to FL-HuR (50 nM). Accordingly when Ser94, Asn107, Ile133 and Asn134 are mutated into Alanine, DHTS does not bind to any mutein. The four residues are thus crucial in providing the required flexibility to HuR for its mRNA binding function.

A.



B.

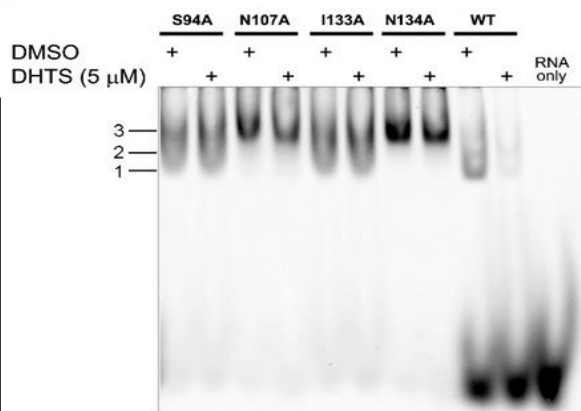
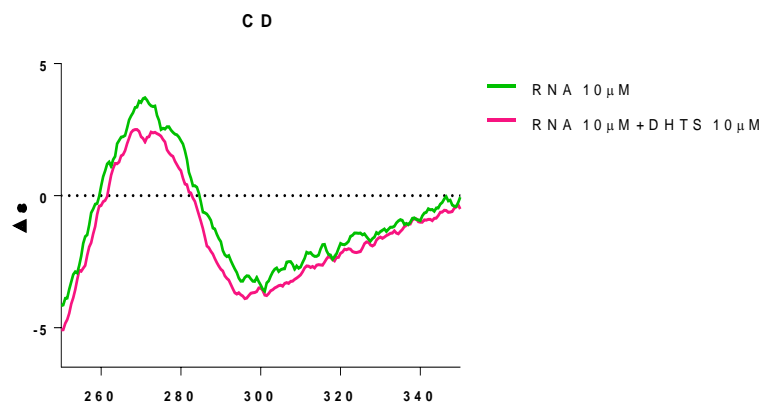


Figure 18 Single point mutations in the HuR–DHTS interacting region abolishes DHTS efficacy. **A)** Coomassie for purification of muteins, M = Marker, Lanes S94A Lanes 1 and 2, N107A Lanes 3 and 4, I133A Lanes 5 and 6, N134A Lanes 7 and 8, BSA 350ng and 450ng Lanes 9 and 10, supernatant of muteins S94A, N107A, I133A, N134A Lanes 11, 12, 13 and 14. Two lanes for each muteins represents the elution with 250 and 500mM imidazole containing elution buffer **B)** RNA and DHTS-interacting amino acids are crucial for DHTS and RNA binding, and for protein dimerization. Representative REMSAs of at least three independent protein preparations of recombinant full-length HuR and indicated muteins. REMSAs were performed with 0.2 μM of protein, 0.2 μM of Cy-3 RNA probe, and DMSO or 5 μM DHTS. Muteins are insensitive to DHTS and show different binding patterns to the RNA probe. Indicated arrows (1, 2 & 3) shows the binding behavior of FL- HuR (DMSO), which is represented by each muteins. Representative REMSA were repeated with at least three independent protein purification. (Experiment has been performed by me, published in Lal et al., 2017 [130]).

A.



B.

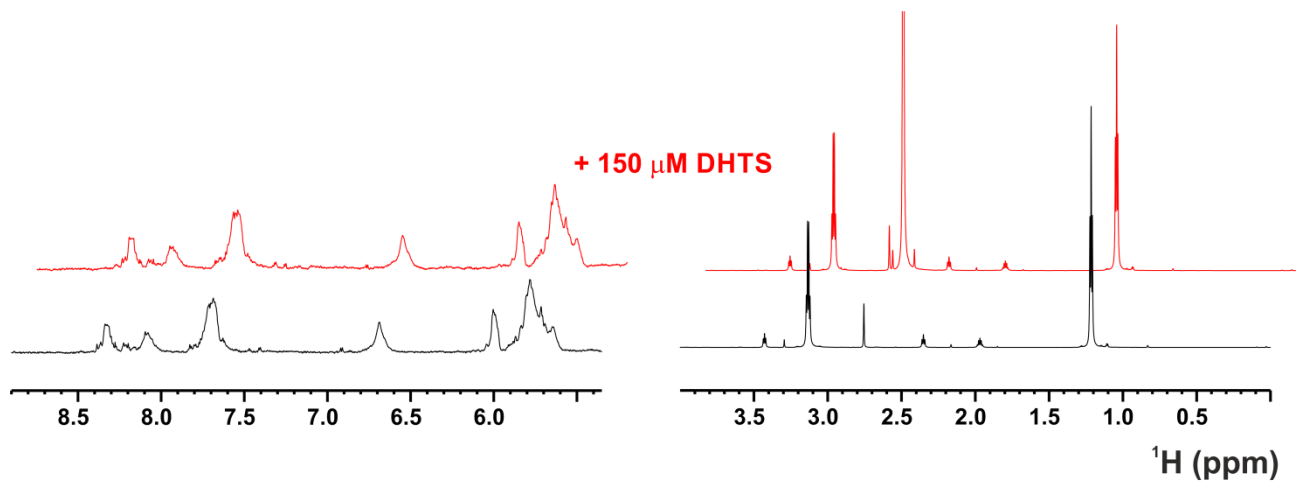


Figure 19 A) Circular Dichroism spectra of TNF α RNA (10 μ M in 200 μ L of buffer indicated as Green line) showing no binding to DHTS (10 μ M in 200 μ L Buffer with DMSO indicated as Red line). **B) 1D 1 H NMR spectra of TNF α RNA (50 μ M) acquired at 298 K on a 950 MHz spectrometer in the absence (black) and the presence of DHTS (150 μ M, red). (Figure A :Experiment has been performed by me, published in Lal et al., 2017 [130]) (Figure B :Experiment has been performed by our collaborator from University of Florence, published in Lal et al., 2017 [130]).**

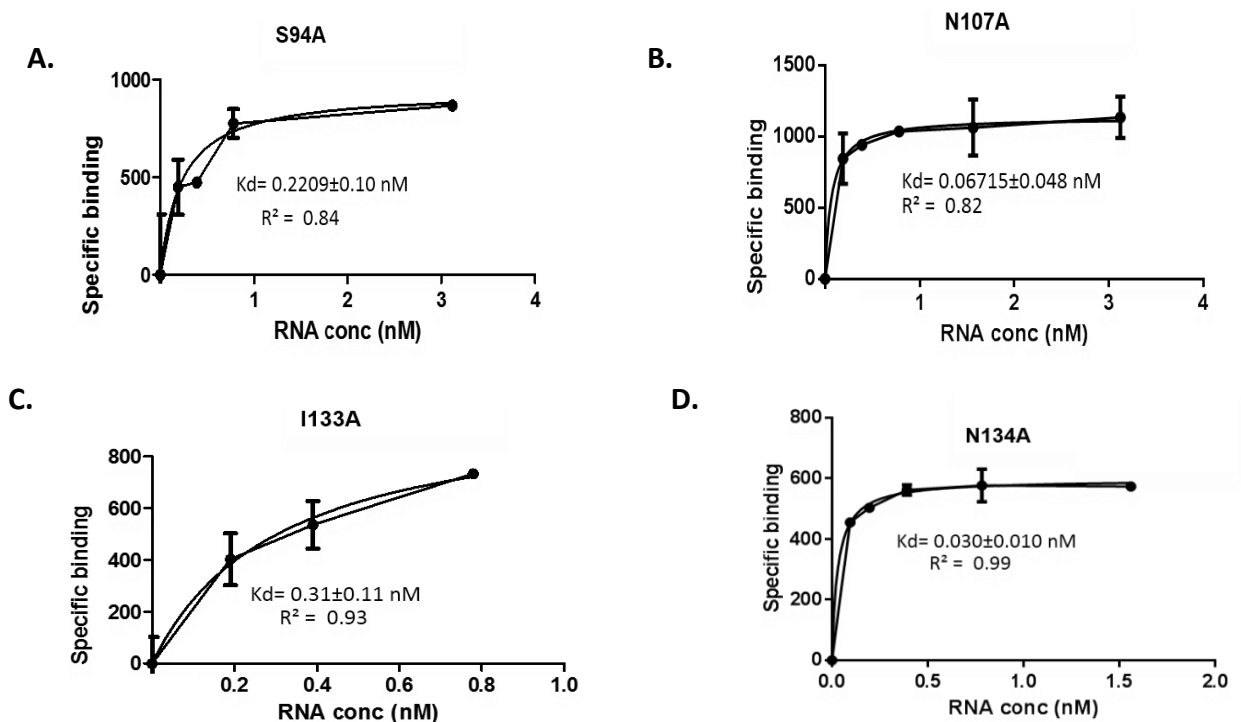


Figure 20 Calculation of kd of Muteins, by AlphaScreen assay. (A) S94A, (B) N107A, (C) I133A and (D) N134A. Differences in the scale used in all Kd's graphs is due to different concentrations of the Bi-RNA probe used to

obtain the respective lowered kds. Mean \pm SD refers to three independent experiments (n = 3) (Experiment has been performed by me, published in Lal et al., 2017 [130]).

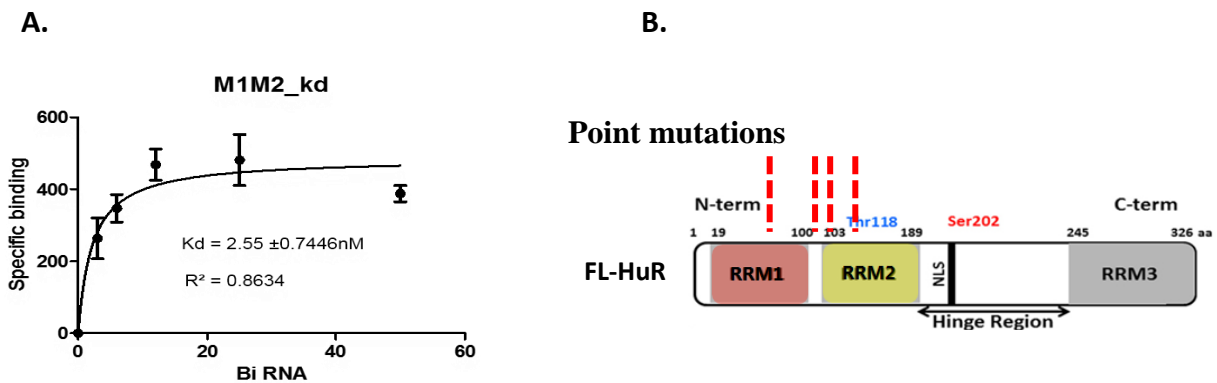


Figure 21 Calculation of Kd for HuR isoform RRM1/2, by AlphaScreen assay. A) Kd value obtained for RRM1/2 **B)** Schematic showing the position of Mutated residue to Alanine in FL-HuR. Mean \pm SD refers to three independent experiments (n = 3) (adapted from Venigalla, RKC *et al.*, 2012). (Figure A: Experiment has been performed by me).

Single point mutation causes dimerizing aggregation behavior of Muteins

As evident from the previous experiments presented in figure 20 and 21, we further performed cross-linking experiment to analyze the constitutional pattern of each muteins deeply. To establish this, we followed direct fixing of the *E. coli* cells expressing FL-HuR and muteins with 2% HCHO (Formaldehyde) in LB growth medium for about 15 minutes, after purification of the cross-linked protein by Ni-NTA beads, were run on 12% SDS-PAGE with 0.05% SDS in the running gel. Notably again N107A and I134A showed the abundant level of both monomer and dimer with particular mol. size (36 and 75kDa) (**data not shown**). REMSA *in vitro* binding assays confirmed the significant N107A and I134A, more likely aggregating behavior as compared to other muteins (**Figure 22A and 22B**). However, S94A and I133A have shown binding differently similar to WT HuR (**Figure 22 C**). This behavior could result from a higher efficiency in recognition and dimerization along the mRNA substrate, or alternatively from an aggregation-prone tendency of muteins that therefore aggregate on the same molecule of RNA probe. Indeed, mutants showed significantly lower Kd values, i.e., an increased affinity in saturation binding experiments with respect to M1M2 (**Figure 20 and 21**).

All these experiments notify that these mutants altogether aggregates due to mutation, also DHTS showed negligible efficacy, and this confirms that these residues are important for RNA binding activity of HuR and therefore, for pure efficacy of DHTS.

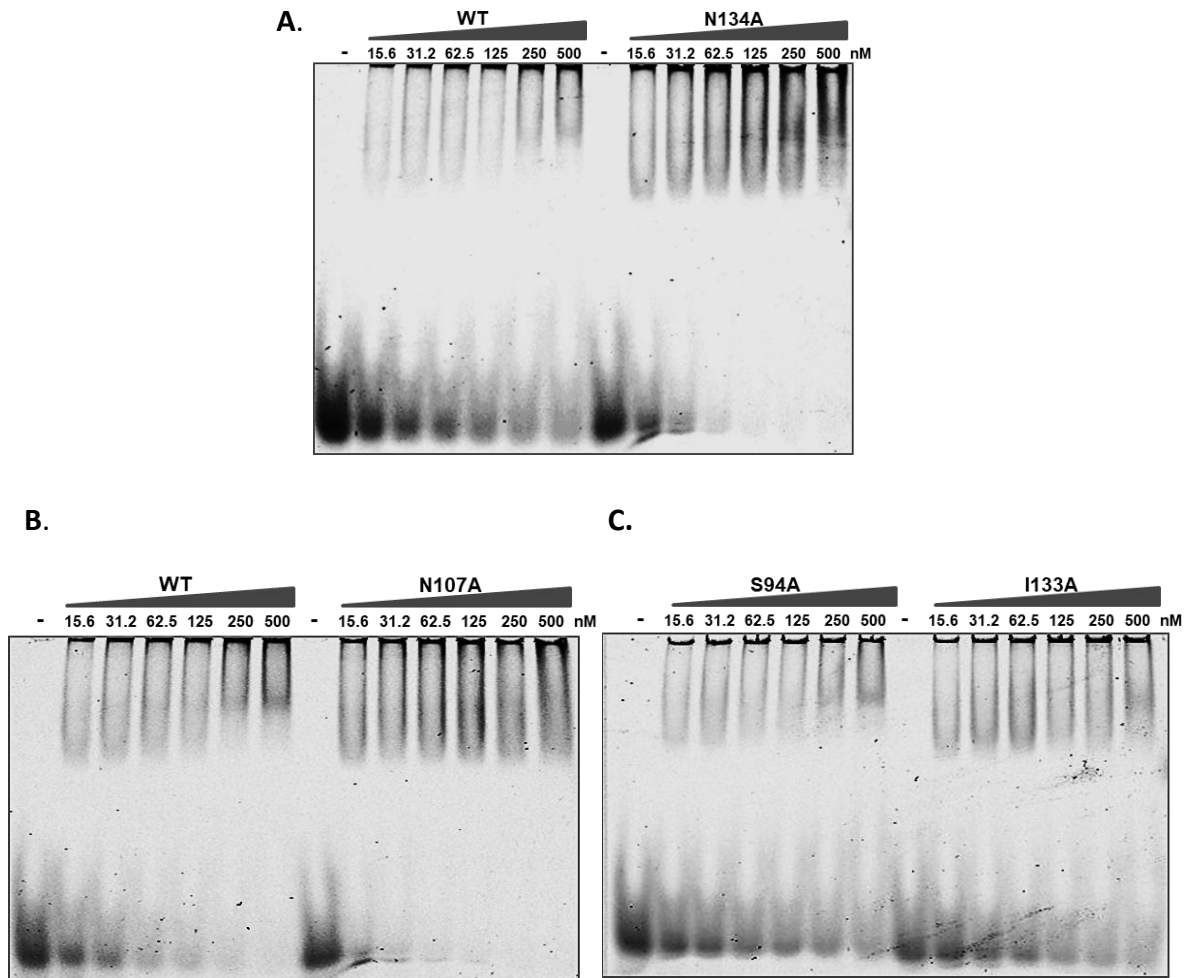


Figure 22 Aggregation of mutants. Representative REMSAs of at least three independent protein purification performed with increasing concentration of WT and HuR single point mutants as indicated in the legends **A)** WT HuR and N134A **B)** WT HuR and N107A and **C)** S94A and I133A with 75 fM of probe RNA. Representative REMSAs were repeated with at least three independent protein purifications. (Experiment has been performed by me, published in Lal et al., 2017 [130]).

DHTS downregulates TNF α and VEGF in breast cancer cells

As tanshinones were found to inhibit the HuR and TNF α binding, confirmed *in vitro* via biochemical experiments [97], we checked the levels of HuR targets TNF α (tumor necrosis factor) and VEGF (vascular endothelial growth factor) in breast cancer cell lines, following treatment for 24 hrs with DHTS (shown in legend as DT). As noted earlier DHTS as strong HuR inhibitor *in vitro*, we observed 50-60% significant decrease in the levels of TNF α in MDA-MB-

231 and SKBR-3 cell line (**Figure 23A**). Another HuR target VEGF (vascular endothelial growth factor) upon DHTS treatment for 24 hrs, was also downregulated to upto 40%. (**Figure 23B**).

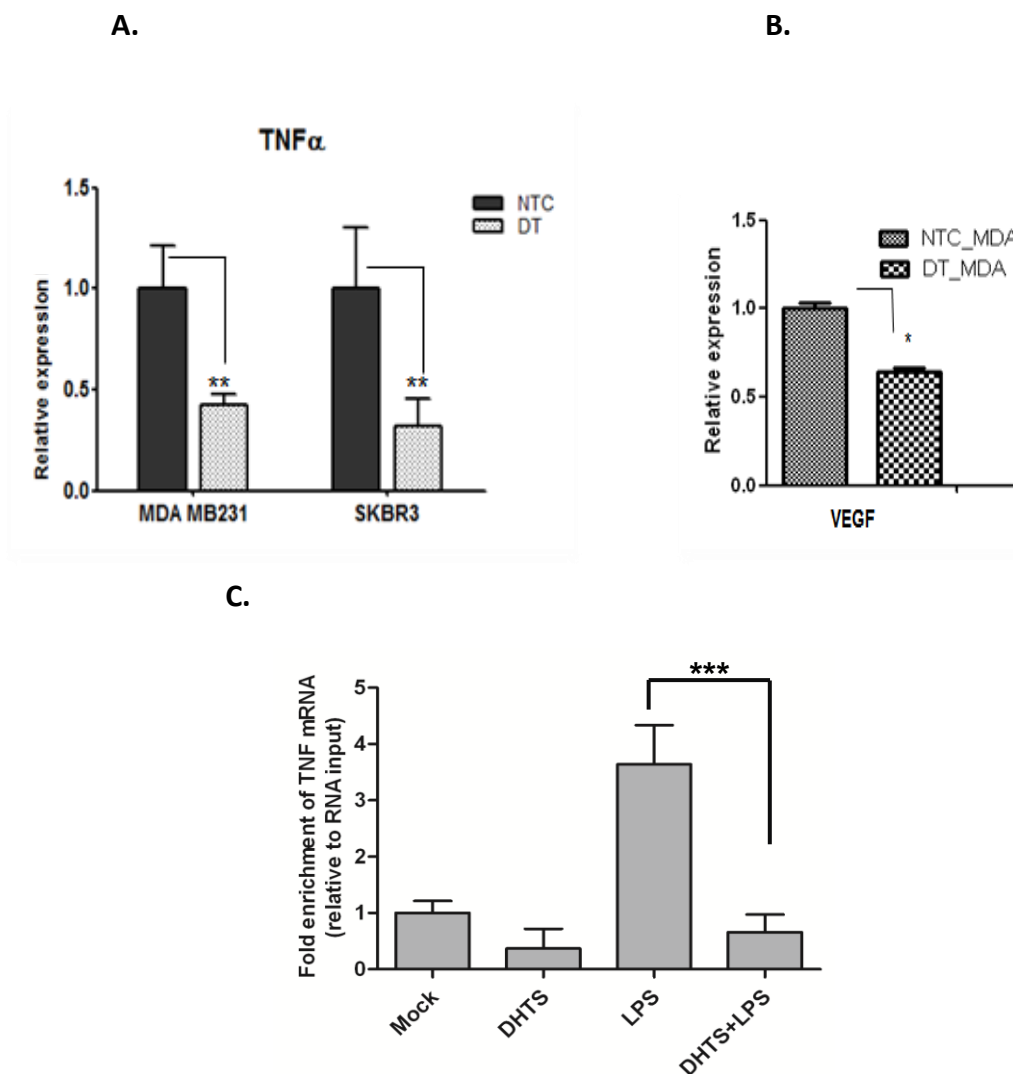


Figure 23 Intracellular effects of DHTS on HuR targets **A)** TNF α level in MDA-MB231 and SKBR3 cell lines after 24 hrs, TNF α level were normalized to actin. **B)** VEGF levels in MDA cell line, normalized to actin. **C)** RNA immunoprecipitation, in MCF-7 cell line, the treatment was for 3 hrs, with LPS (1 μ g/ml), DHTS (1 μ M). Mean \pm SD refer to n= 3 experiments and analyzed by one-way ANOVA. * P \leq 0.05, ** P \leq 0.01 and *** P \leq 0.01. (Figure A & B contributed by me) (**Figure C** contributed by Dr. Vito D’Agostino published in D’Agostino *et al.*, 2015 [99]).

Further, we checked whether DHTS is affecting post-transcriptional control mediated by HuR, using RNA immunoprecipitation (RIP). We co-induced cells with LPS, DHTS and another LPS+DHTS (1 μ M) and DMSO or mock as an independent control. qPCR analysis showed that LPS stimulated the TNF α level, whereas our DHTS has counteracted this increase by lowering TNF α level comparable to mock control. The strong increase observed in LPS-induced cells

further explain the important role of HuR, in controlling post-transcriptionally the fate of TNF α mRNA (**Figure 23C**). Nevertheless, this post-transcriptional control of HuR is not limited to TNF α , but RIP analysis of another HuR regulated transcripts, ERBB2, VEGF, and CCND1 bound copy number, the presence of DHTS is controlled to a different extent (data not shown), but to significant level, with respect to control.

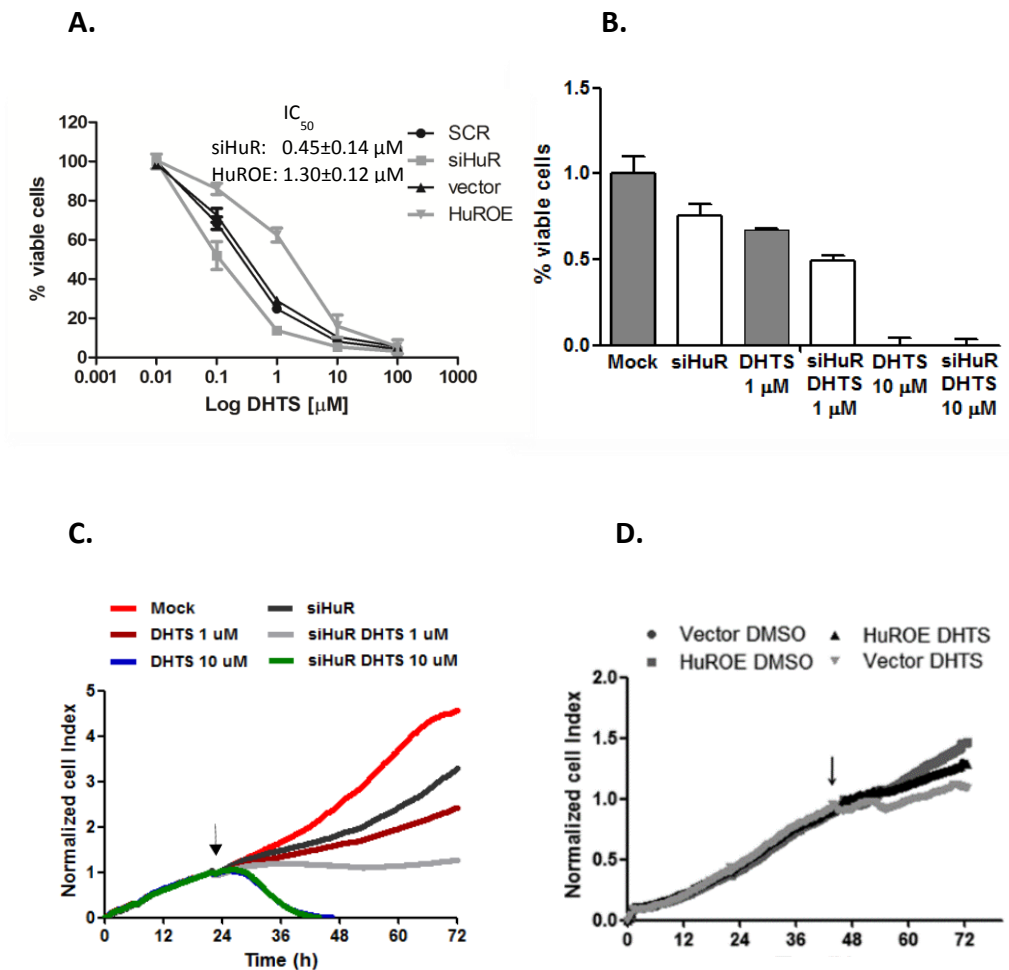


Figure 24 Efficacy of DHTS is HuR dependent **A)** MTT assays on the silenced/overexpressing HuR MCF-7 cells treated with DMSO OR DHTS for 24 hrs. **B)** Relative level of the viable cells in silenced/overexpressing HuR MCF-7 cells treated with DMSO or DHTS for 24 hrs. **C)** Real time cell analysis (RTCA) proliferation assays, done in normal and silenced HuR MCF-7 cells with indicated doses of DHTS in legends. **D)** Real time cell analysis proliferation assays (RTCA), done in normal and overexpressing (OE) HuR MCF-7 cells with 1 μM of DHTS. Mean \pm SD refers to three independent experiments (n = 3). (Experiment contributed by Dr. Vito D'Agostino published in D'Agostino et al., 2015 [99]).

DHTS efficacy depends upon HuR expression

After following the string of biochemical experiments, we also exploited the DHTS influence in HuR silenced or overexpressing HuR transiently in MCF-7 breast cancer cells. To establish this, we started with dose-response assays on HuR silenced or overexpressing MCF-7 cells. After 24 hrs exposure of DHTS to these cell lines, differential level of sensitivity was revealed for siHuR MCF-7, $IC_{50} = 0.45 \mu\text{M}$ or for OE-HuR MCF-7, $IC_{50} = 1.3 \mu\text{M}$ as compared to scramble or vector MCF-7 cells. This information explained the compensatory effect overexpressing HuR versus DHTS in case of siHuR MCF-7 and, OE-HuR MCF-7 (**Figure 24A**). HuR absence increased the sensitivity of MCF-7 cells in DHTS dose dependent manner, from the figure it is clear that even at $1 \mu\text{M}$ DHTS concentration, siHuR MCF-7 cells viability decreased to 50% as compared to mock, however we also observed 20% lower viability rate in case of non-treated siHuR cells after 24 hrs. At higher concentrations undoubtedly DHTS killed the cells surpassing the fact of either silenced HuR or OE-HuR in MCF-7 cells (**Figure 24B**). Real-time cell analysis assays were done in a similar manner but in different set of experiments to study the effect of DHTS on MCF-7 rate i.e. firstly we checked the proliferation rate of siHuR MCF-7 cells together with proliferation normal MCF-7 cells. The anti-proliferative effect of DHTS was evident at low doses, i.e., at $1 \mu\text{M}$, in normal cells, after 12 hrs of treatment time, indicated as the arrowhead. In HuR silenced DHTS completely blocked the cell proliferation, at higher doses, i.e., at $10 \mu\text{M}$ cytotoxic effects of DHTS emerged in this experimental system, later on, were confirmed by MTT. (**Figure 24C**). Secondly, we also checked the proliferative potential of HuR overexpressing MCF-7 cells in the presence of $1 \mu\text{M}$ DHTS concentration, in this case also markedly $1 \mu\text{M}$ DHTS has shown the anti-proliferative potential, further indicating that HuR levels can counteract or modify the phenotypic response of OE-HuR MCF-7 cells at low doses of DHTS. (**Figure 24D**).

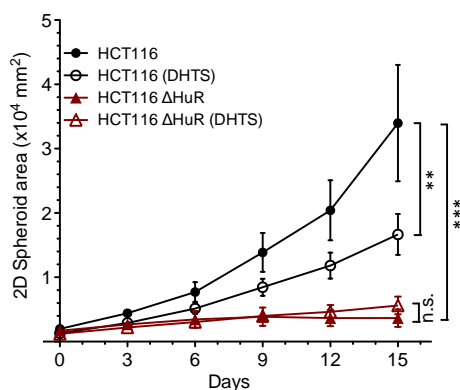
Taken all together these results shows that HuR can rescue phenotypic effects of DHTS, for example viability, proliferation arrest of cancer cells. This further explain that HuR is a central target of DHTS, and collectively effects of DHTS on HuR targets could be demonstrated by blockade of HuR-RNA binding activity.

DHTS is effective on HuR-positive models *in vitro* and *in vivo*

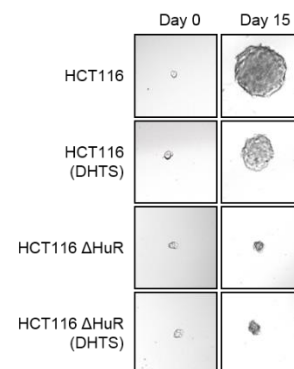
To evaluate this mechanism of action, in which a limited displacement of RNAs from HuR may be effective in HuR-dependent tumor growth, we studied tumor growth *in vitro* and *in vivo*.

HCT116 colon cancer cells were used as a model, based on high endogenous levels of HuR and their sensitivity to HuR inhibition [136]. These experiments were performed by our collaborator in the laboratory of Prof. Dan Dixon from University of Kansas Medical Center, Kansas USA. Creation and characterization of CRISPR/Cas9-mediated knockout of the *ELAVL1* gene in HCT116 cells were accomplished as described in Lal S. et al., 2017[137]. HCT116 and HuR-knockout cells (HCT116 Δ HuR) were grown under anchorage- and serum-independent conditions to facilitate tumor spheroid growth, and HuR was observed to be needed for tumorsphere growth. In the presence of DHTS, the growth of HCT116 spheroids was attenuated 2-fold, whereas DHTS did not impact HCT116 Δ HuR sphere growth (**Figure 25A and 25B**). To test the effects of DHTS on tumor growth *in vivo*, mice bearing HCT116 cell xenografts received IP injections of DHTS (10 mg/kg body weight) or vehicle every 48 h. Over the course of the experiment, DHTS was well tolerated, and mice did not display any signs of acute toxicity and maintained similar weights. Significant anti-tumor effects of DHTS were observed, with approximately a 4-fold reduction in tumor size (**Figure 25C and 25D**).

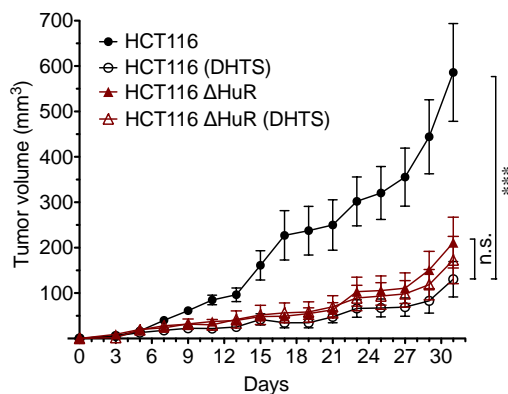
A.



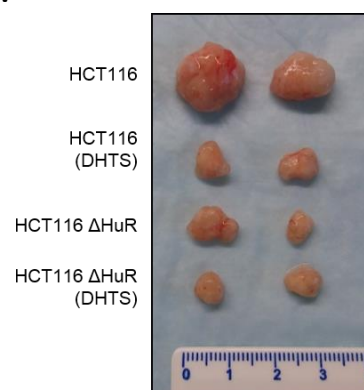
B.



C.



D.



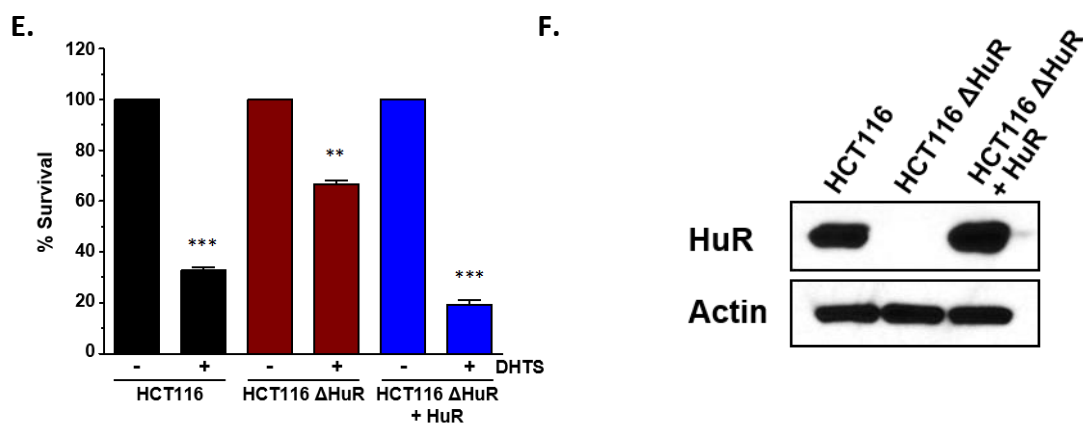


Figure 25 DHTS efficacy relies on HuR presence *in vivo*. **A)** The spheroid growth of parental HCT116 (HCT116) and HuR-knockout cells (HCT116ΔHuR) treated with DHTS (10 μM) or vehicle. DHTS was added after 3 days of culture in spheroid growth medium on ultra-low adherence substrate, and spheroid growth was tracked by imaging for 15 days. *P*-value is **<0.01, ***<0.001, n.s. = not significant. **B)** Representative tumorsphere images from day 0 and day 15 of DHTS treatment. Scale bar = 100 μm. **C)** Tumor growth of parental HCT116 and HuR-knockout cells (HCT116_HuR) xenografts in nude mice treated with 10 mg/kg DHTS or vehicle control every 48 h. *P*-value is ***<0.001, n.s. = not significant. **D)** Representative tumors excised at day 31 are shown. **E)** HuR-knockout cells (HCT116ΔHuR) were transfected a HuR-expression construct (+HuR), along with empty vector transfected parental HCT116 and HCT116ΔHuR cells. Cells were treated with DHTS (10 ΔM) or vehicle, and cell growth was assessed 6 days after the treatment using MTT assay. Cell survival was normalized to the respective control and are the average of three experiments. *P*-value is **<0.01, ***<0.001. **F)** Western blot showing HuR complementation in HCT116ΔHuR+HuR cells and absence of HuR in HCT116ΔHuR cells. Actin was used as a loading control. (Experiment has been contributed by our collaborator from University of Kansas Medical Center, published in Lal et al., 2017 [130]).

Additionally, the efficacy of DHTS was strictly dependent on the presence of HuR. HCT116ΔHuR cells grew significantly more slowly and formed smaller tumors, but were completely insensitive to DHTS. Furthermore, this decreased growth sensitivity of DHTS in HuR deficient cells could be restored with expression of HuR in HCT116ΔHuR cells (**Figure 25E** and **25F**). These results indicate that DHTS has significant antitumor activity *in vitro* and *in vivo* without major systemic toxicity, along with demonstrating the specificity of HuR inhibition.

Biochemical Characterization of DHTS Analogs

As mentioned earlier at the beginning of result section, I am also involved in characterizing another DHTS analogs which we regularly receive from our collaborators. A peculiar property of these analogs is that these are more potent or specific for interfering with binding of HuR-RNA complex formation. Moreover, on the other side, these molecules showed differential cytotoxicity in a panel of model cell lines. Although we had a long list of DHTS analogs, we

started with nine (9) analogs (which are named as MFM49, MB11V, VB062, GD041, MB37, MB39, MB40, MB42, and MB44) by checking their *in vitro* specificity for HuR-RNA binding complex formation. The nomenclature given is random and is meant to identify them structurally, the difference in their RNA binding activity and the most important thing to note is that we could not show the chemical structures of these DHTS analogs due to a confidential agreement with our collaborators.

Nevertheless, we saw their biochemical activity on rHuR and FAM-ARE. We freshly purified rHuR from *E.coli* cells and used to a final concentration of 250 nM along with 25 nM FAM-ARE. As evident from the picture, most potent hit was given by MFM49 and MB39, lanes 4 and 9 (**Figure 26A**). However to be more precise densitometric analysis has confirmed this impression for activity of MFM49 and MB39, where 60-70% displacement of the bound FAM-ARE RNA was observed. Simultaneously other analogs showed displacement of the RNA, but to lesser magnitude than MFM49 and MB39. Looking accordingly, degree of displaced FAM-ARE RNA from rHuR- RNA complex, GD041, VB062, and MB42 showed inhibition activity in decreasing order, for their ability to displace target bound RNA (**Figure 26A** lanes, 7, 6 and 11). Notably, they decreased the binding significantly to 60, 55, and 50% as DMSO control 100%. (**Figure 26B**).

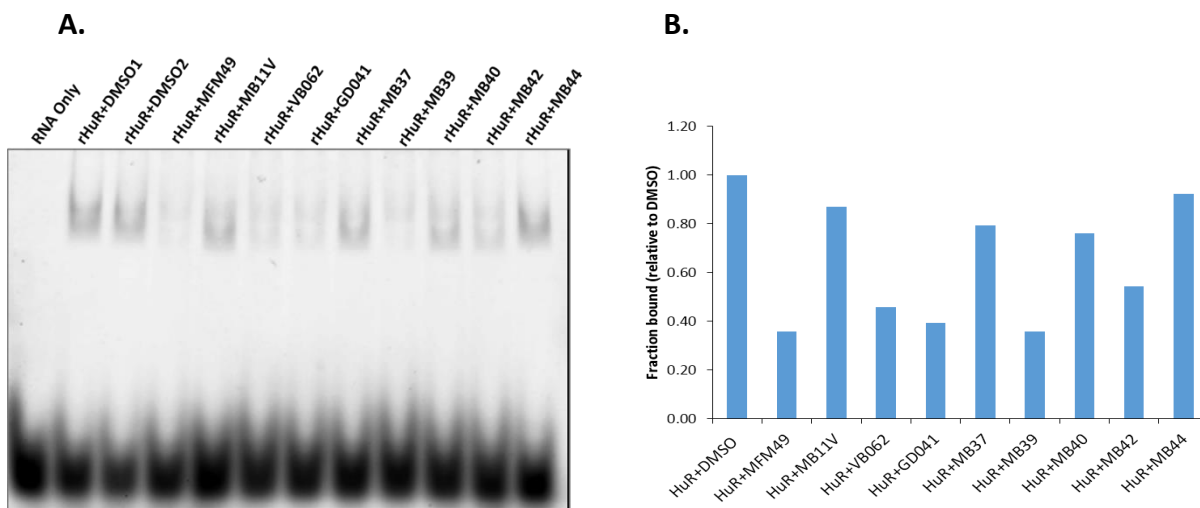


Figure 26: Screening of other potent HuR inhibitors **A)** Representative EMSA for evaluating the activity of DHTS analogs using 250 nM of rHuR and 25 nM of FAM-RNA probe, the concentration of each compound used is 5 μ M. Lanes RNA only (1), rHuR+DMSO1 (2), rHuR+DMSO2 (3), rHuR+MFM49 (4), rHuR+MB11V (5), rHuR+VB062 (6) rHuR+GD041 (7), rHuR+MB37(8) rHuR+MB39 (9) rHuR+MB40 (10), rHuR+ MB42 (11) and rHuR+MB44 (12). **B)** Densitometry of figure A to quantify the level of displaced and bound FAM-RNA probe. (Experiment has been performed by me).

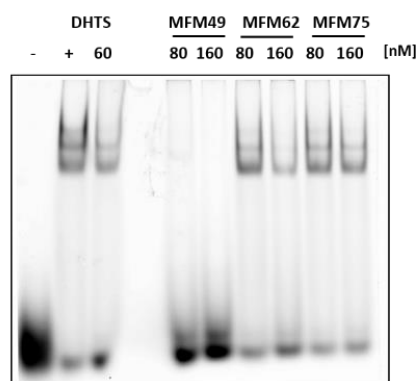
Minor inhibition activity were shown by MB40, MB37, MB44 and MB11V, again in a decreasing order for their ability to halt the RNA-binding activity by rHuR, (**Figure 26A** lanes, 10, 8, 12 and 5) with 30, 20, 15, and 15 percent decrease after quantification by Image J (**Figure 26B**).

Taken all together these results shows that differences in structural moiety can have the significant impact on their ability, to bind or recognize or fit into the RNA binding site of HuR, which selectively bind to the ultimate small molecules possessing the ability to participate at the upfront of binding cleft.

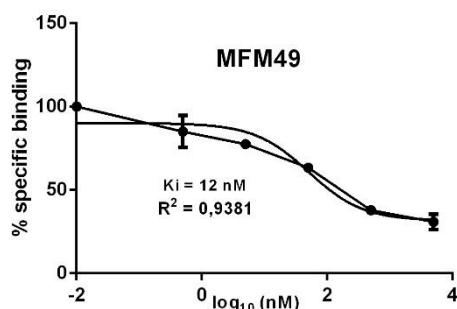
MFM49 is the most potent inhibitor of rHuR-RNA interaction.

I came across a more specific rHuR-RNA complex inhibitor while screening three compounds received together from our collaborators. These inhibitors were soluble in DMSO, firstly we checked by the REMSA for its inhibition function using 0.5 μ M of Cy3-ARE-RNA probe, 400 nM of rHuR protein together with DHTS inhibitor at its IC-50 as positive control lane 2 and 3. Lanes 5 and 6, represented the MFM49 activity at 80 and 160 nM, surprisingly, it showed significant displacement of rHuR-RNA complex formation. Among these we also loaded, reaction mixture for MFM62 and MFM75 incubated with rHuR-RNA, MFM62 showed displacement of rHuR-RNA complex formation, but with less significant level, lanes 7 and 8; whereas MFM75 showed negligible inhibition of rHuR-RNA complex formation function, lanes 9 and 10 (**Figure 27A**). I also checked these compound's activity in AlphaScreen assays described in previous experiments, consistent with EMSA data, these compounds showed, similar efficacy towards rHuR-RNA complex formation, as said earlier the most potent compound is MFM49 which showed K_i of 12 nM (**Figure 27B**).

A.



B.



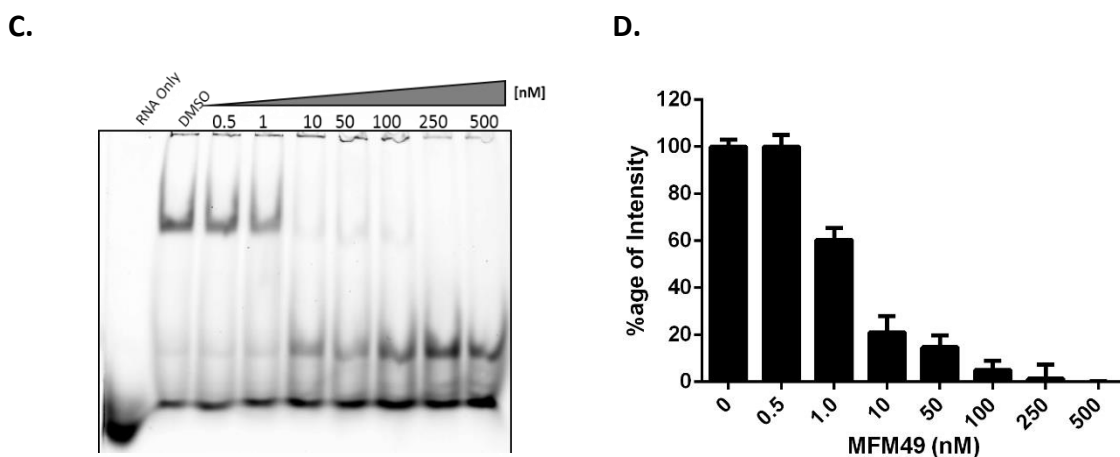


Figure 27 MFM49 is the most potent inhibitor of rHuR-RNA interaction. A) Representative EMSA showing the most potent activity of MFM49 among other analogs. **B)** Alphascreen assay carried out using 25nM of rHuR and 50 nM of biotinylated probe together with 20 ng/ μ l of donor and acceptor beads to evaluate the K_i of MFM49. **C)** Competitive saturation binding EMSA assay with gradient concentrations as shown in legend for MFM49 with 0.5 μ M of Cy3- ARE-RNA probe and 500 nM of rHuR protein. **D)** Densitometric analysis to quantify the proportion of Cy3-RNA displaced upon MFM49 addition in reaction mixtures. Mean \pm SD refer to at least 3 independent experiments. (Experiment has been performed by me).

Consequently complete repeal of the rHuR-Cy3 ARE-RNA formation in competitive binding assays, using equimolar concentration of both ligands with MFM49 as indicated in the legends, was also observed (**Figure 27C, D**). Taken all together these results suggest that MFM49 is most potent compound, based on its preference to displace rHuR-RNA complex formation significantly. Further, this also may suggest that it occupies ARE-RNA binding cleft of HuR tightly and prevent further HuR biochemical function *in vitro*. To test further MFM49 for intracellular effect on HuR targets, we have tested this compound together with DHTS in different cell line models. Results obtained for few of them are described below in coming result sections.

DHTS analogs are the potential inhibitors of HuR RNA:Complex formation

REMSA binding assays confirmed the specificity of these potent inhibitors, nevertheless we also checked this potency in AlphaScreen assays [98], the relative inhibition profile of these inhibitors, as expected these molecules interfered with the apparent binding behavior, to a significant measures, at low nanomolar range (nM). I selected five compounds among 9 compounds, previously known for their potential from EMSA binding assay (**Figure 26**). Also

taking into account their color which could interfere or give false alpha count while plate read, as this assay is based on fluorescence emission events given by close proximity of donor and acceptor beads, specific for the biotinylated probe or His-tagged rHuR protein.

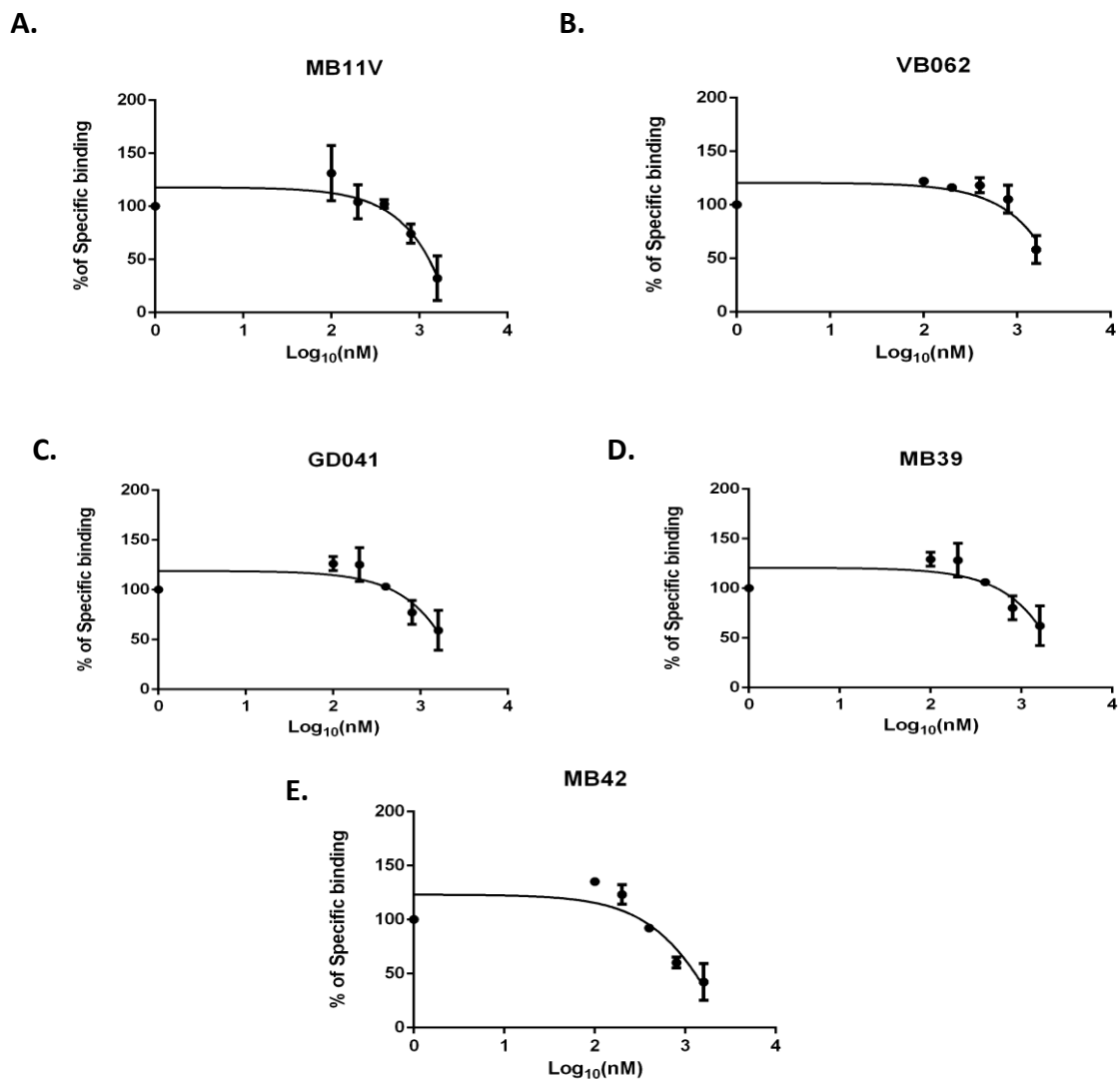


Figure 28 AlphaScreen assays to evaluate DHTS analogs activity, showing Ki curve for, in low nanomolar range or micromolar range A) MB11V, B) GD041 C) VB062, D) MB39 and E) MB42 Mean ±SD obtained from refer to at least 3 independent protein purification. (Experiment has been performed by me).

TABLE 2 Ki values obtained for DHTS Analogs

	DHTS	MB11V	GD041	VB062	MB39	MB42
logKi nM	1,689	~3,442	1,909	~ 5,742	2,462	2,116
R ²	0,9200	0,7896	0,9112	0,7396	0,7365	0,8453

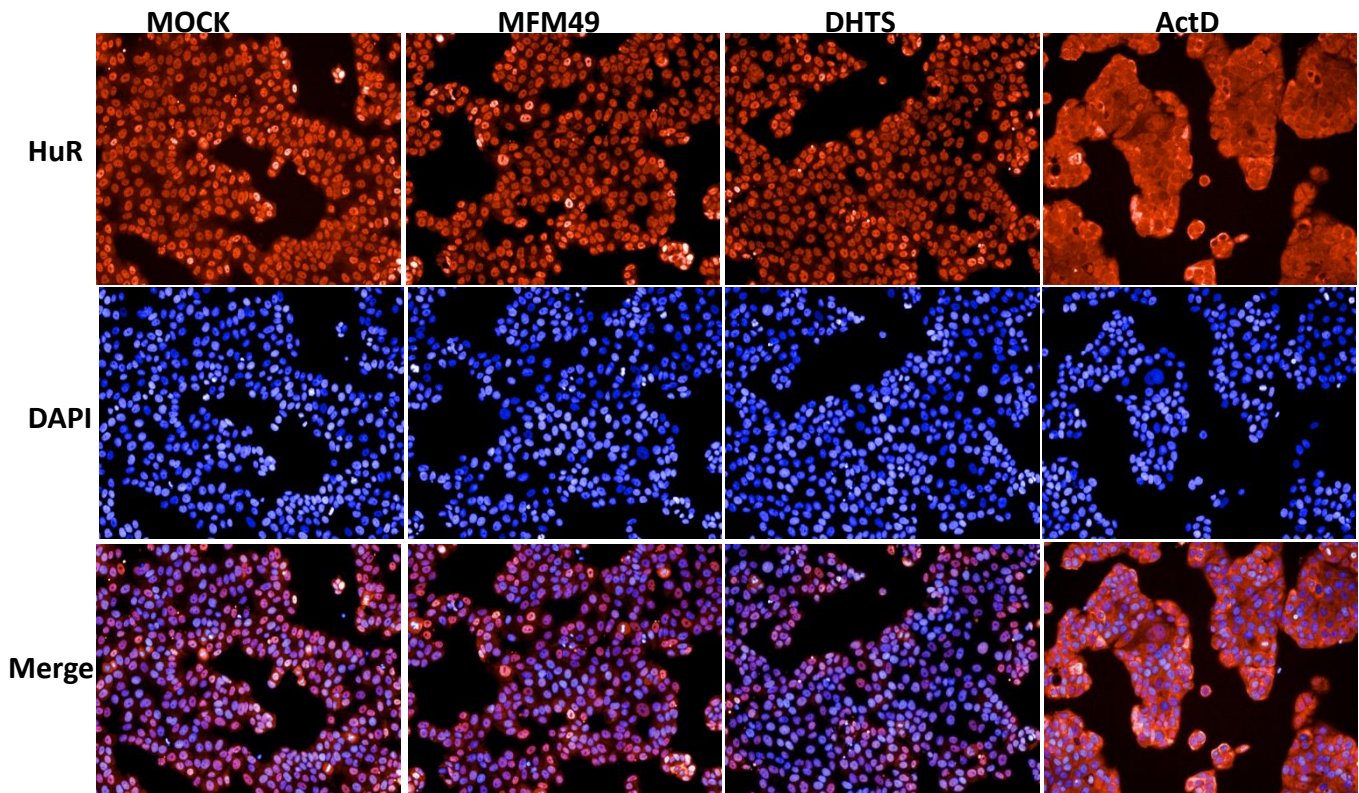
Ki (nM)	48,94	~ 2766,9	81	~ 552077,4	289,7	130,6
Ki (μM)	0,048	~ 2,8	0,081	~ 552,1	0,3	0,1

I firstly optimized the protein-RNA ligands ratio, by keeping constant the final concentration of biotinylated RNA-ligands i.e., 50 nM together with donor and acceptor beads concentration, i.e., 20 ng/μl, and varying rHuR protein levels from 10-100 nM. I obtained an optimal signal at 25 nM as hooking point (data not shown) because after this proportions of alpha-count obtained, started decreasing, due to excess of rHuR molecules oversaturated with donor or acceptor beads. So noting 25 nM protein concentration as optimal for the binding kinetics of rHuR- biotinylated RNA ligands, I further challenged this binding phenomenon with the addition of these novels DHTS analogs. After reading plate in alpha-count reader we calculated Ki of these molecules using kd of 2.5 nM as reported by D' Agostino *et al.*, 2013. (**Table 2**). Although I saw the difference in obtained ki values, to abrogation behavior I observed in our *in vitro*, EMSA assays (**Figure 26**). This outcome may be explained by the different setup of two assays and especially the physical properties of the interfering these molecules. Nonetheless, some of these molecules reported with supposedly full abrogation of rHuR- RNA- complex formation (**Figure 28** for Ki Graphs).

MFM49 and DHTS do not influence substantial nucleocytoplasmic level of HuR in MCF-7 cells

The p38 pathway is the main inducer of HuR nuclear or cytoplasmic localization or re-localization. To check whether this HuR localization is affected by our compounds, I treated MCF-7 cells with MFM49, DHTS and Act D as control, for 3 hrs, after fixing, and following further immunofluorescence protocol; we saw that 1μM DHTS, 5 μM MFM49 did not affect subcellular localization of HuR (**Figure 29A**).

A.



B.

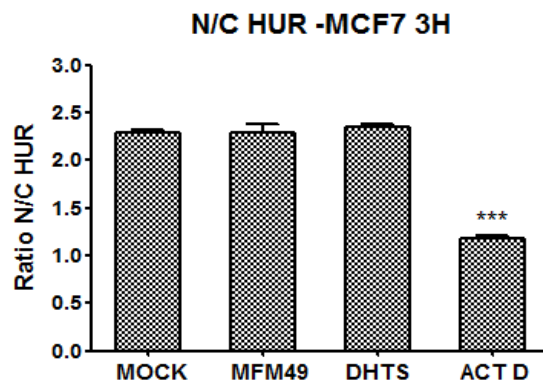


Figure 29 Nucleocytoplasmic levels of HuR upon MFM49 and DHTS treatment A) Immuno- fluorescence images showing HuR (Red) or nuclei (Blue) in MCF7- cells. Actinomycin D was used as control, B) Ratio of N/C HuR level plotted after reading the plate under PerkinElmer image plate reader Operetta, Average of each biological replicates plotted and compared using Dunnett's Multiple Comparison Test showing ns outcome for Mock, MFM49, DHTS, and ActD. The test was only significant with $P < 0.001$ for ActD. (Experiment has been performed by me, Dr. Natthakan Thongon helped in following the protocol).

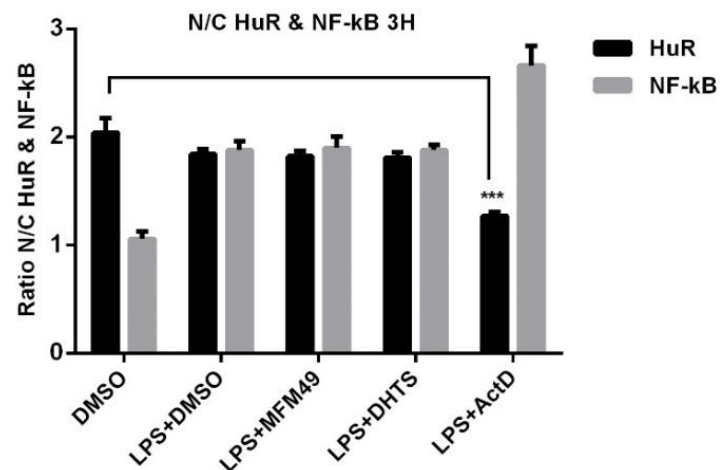
After collection of values given by Operetta plate reader for nuclear-cytoplasmic ratio, I plotted them and compared, to ActD control which significantly impaired the nucleocytoplasmic HuR level to significant amount $P < 0.001$ (Figure 29B). In fact, both of the

compounds have shown their beneficial pharmacological potential by confining the HuR level to the nucleus only.

MFM49 and DHTS do not influence substantial nucleocytoplasmic level of NF-kB and HuR in RAW264.7 cells

As mentioned in the introduction part, NF-kB has been shown to target HuR in Gastric carcinoma [58]. RAW264.7 cells were co-treated with LPS as LPS+DMSO, LPS+DHTS, LPS+MFM49, and LPS+ActD. Predominantly HuR stayed in the nucleus, which upon LPS stimulation localized to the cytoplasm with 10% increment. LPS co-treatment with DHTS (1 μ M) and MFM49 (5 μ M) did not affect these substantial levels after 3 hrs of treatment. LPS+ActD treatment in RAW264.7 cells showed the low level of HuR, with impaired nucleocytoplasmic localization. I have also checked the nuclear translocation of NF-kB upon LPS stimulation. Notably, LPS caused a very strong shift of NF-kB from the cytoplasm to nucleus. Accordingly, co-treatment of LPS and DHTS and MFM49 didn't affect LPS induced NF-kB subcellular localization. Conversely, Actinomycin D treatment has indicated the significant localization of NF-kB to the nucleus after 3 hrs of LPS co-treatment.

A.



B.

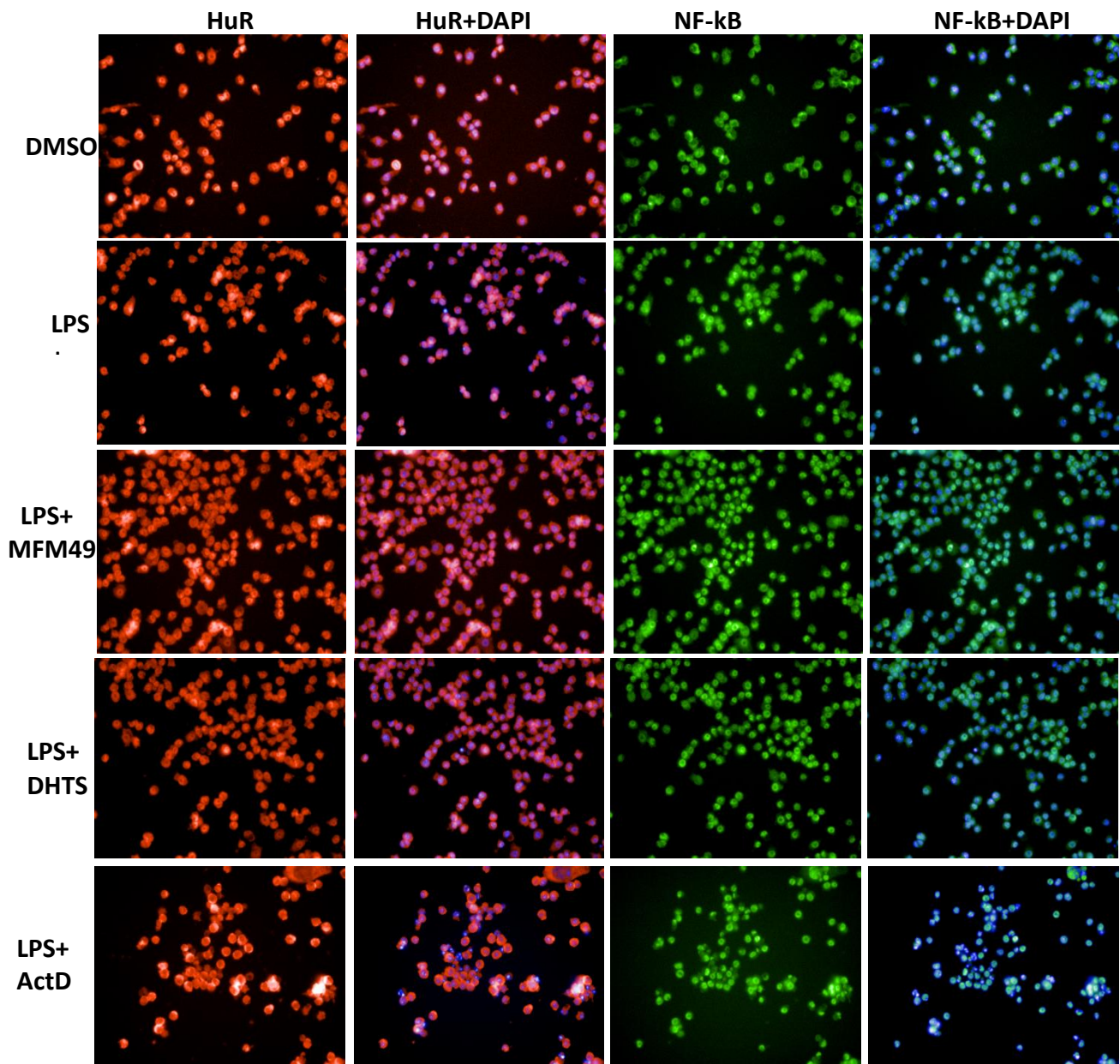


Figure 30 Nucleocytoplasmic levels of HuR & NF-kB upon co-treatment with LPS and DMSO, MFM49, DHTS and ActD A) Ratio of N/C HuR and NF-kB levels plotted after reading the plate under PerkinElmer image plate reader Operetta, Average of each biological replicates plotted and compared using Dunnett's Multiple Comparison Test showing ns outcome for DMSO, LPS, LPS+MFM49, LPS+DHTS, LPS+ActD. The test was only significant with $P < 0.001$ for ActD. B) Immuno- fluorescence images showing HuR (Red), NF-kB (Green) or nuclei (Blue) in RAW264.7 cells. Actinomycin D was used as control. (Experiment has been performed by me, Dr. Natthakan Thongon helped in following the protocol).

Considering the above observation, we can say that DHTS and MFM49 do not influence the nucleocytoplasmic level of HuR and NF- κ B (**Figure 30A** and **30B**). Moreover concerning the Min Ju et al., 2008, we didn't see HuR activation with increased nucleocytoplasmic shuttling upon NF- κ B activation, in RAW 264.7 upon LPS challenge, which otherwise was observed in gastric cancer cell lines. This further confirms that, DHTS and MFM49 do not influence the p38 and NF- κ B axis while targeting HuR, in inflammation, where HuR act as key player.

Anti-Inflammatory Properties of DHTS analogs

RBPs are involved in the post-transcriptional control of genes encoding for cytokines [138]; [139]; [140]; [141]; [142]. AU-rich elements possessing genes are mainly involved in regulatory processes, e.g. cell communications, regulation of cellular physiological processes, nucleobase, nucleoside, nucleotide and nucleic acid metabolism, signal transduction, and transcription [143]. HuR and TTP play a role in stabilization and destabilization of the master cytokines, e.g., TNF, interleukins, etc. [43]. To check the anti-inflammatory properties of the compounds, I did two months internship period at MHH, Germany in prof. Matthias Gaestel lab. In Gaestel Lab, I tested some of these compounds (DHTS, MFM49, GD041, MB11V, VB062, and MB39). The cell lines used were RAW264.7 and TTP-KO RAW264.7. TTP-KO RAW264.7. were recently established and not yet available to the scientific community, the dose-response curves for each compound were determined at 24 and 72 hrs, before starting all the experiments. The IC₅₀ values obtained were in micromolar range for new analogs, based on IC₅₀ values, I picked the relative sub-toxic doses lower than the IC₅₀ values as DHTS = 1 μ M, MFM49 = 5 μ M, GD041 = 10 μ M, MB11V = 5 μ M, MB39 = 5 μ M, and VB062= 10 μ M Representative cell viabilities curve at 24 hrs and 72 hrs are shown in **Figure 31**.

Cell Viability assays

I treated RAW 264.7 cells with respective DHTS and DHTS analogs to up to 50 μ M of each compound. We obtained higher IC-50 values and are listed in **Table 3** in appendix.

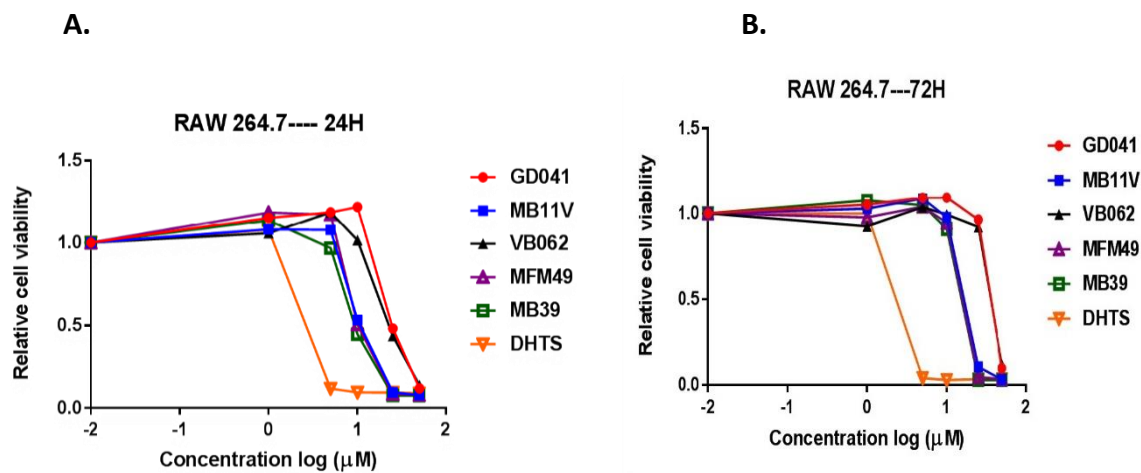
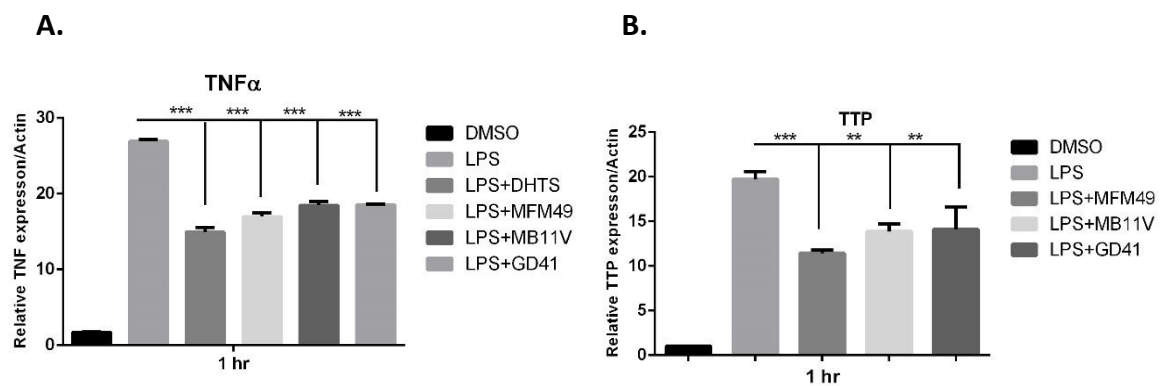


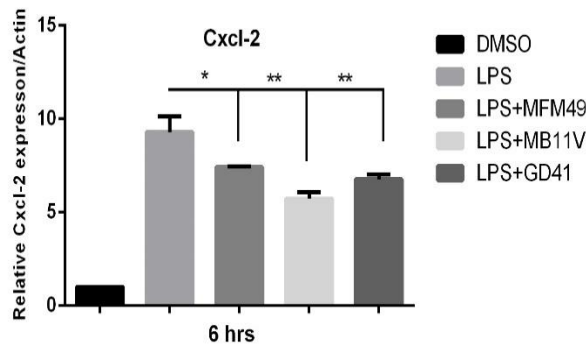
Figure 31 Dose Response curve for DHTS analogs and DHTS itself **A)** at 24 hrs, except DHTS, all showed very less cytotoxicity and the range of IC50 was in micromolar range **B)** At 72 hrs, DHTS is most toxic than analogs, the IC50 conc. obtained were considered as reference for further experimental analysis. (Experiment has been performed by me).

DHTS analogs down-regulates LPS Induced Cytokine Levels in RAW264.7 cells

HuR and TTP are involved in regulation AU containing RNA elements upon activation of p38/MK-2 via LPS stimulation. I decided to check level mRNA of TNF, TTP, CXCL-2, and CXCL-10, upon co-treatment of our compounds with LPS induction at 1, 4, 6 hrs. Also, these cytokines were found bound with HuR upon LPS stimulation in TTP/TTP-AA BMDMs via CLIP studies [144].



C.



D.

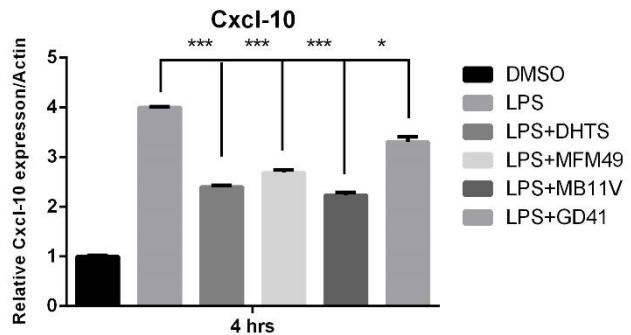


Figure 32 DHTS analogs down-regulates cytokines produced after LPS stimulation mRNA level obtained by RT-PCR analysis at 1 hr after treatment with LPS (1 $\mu\text{g}/\text{ml}$), DHTS (1 μM), MFM49, MB11V and GD041 (all 5 μM). The conditions were as indicated in the legends **A**) TNF α levels obtained RT-PCR analysis at one hour after LPS co-induction **B**) TTP levels obtained RT-PCR analysis at one hour after LPS co-induction **C**) CXCL2 levels obtained at 6 hrs after LPS co-induction **D**) CXCL10 levels obtained at 4 hrs after LPS co-induction TTP. Data expressed as mean \pm s.d. (n= 3), and analyzed using Dunnett's Multiple Comparison Test * $P\leq 0.05$, ** $P\leq 0.01$ and *** $P\leq 0.001$. (Experiment has been performed by me at MHH, Hannover).

I saw almost 40-50% significant decrease in the levels of TNF α in RAW264.7 macrophages after 1 hr LPS stimulation DHTS, MFM49, MB11V, and GD041, showing counteracting action of our DHTS analogs. Consistently at 4 hrs and 6 hrs not 40-50% lowered level but the similar pattern of TNF α level were observed i.e., lower than LPS control (**Figure 32A**). For TTP mRNA, we found 35-45% lowered level as compared to LPS control at one hour for MFM49, MB11V, and GD041. Conversely steady state TTP levels at 4 hrs and 6 hrs remained as they have reached the level of NTC control which was DMSO only (**Figure 32B**). For CXCL-2 mRNA at 1 and 4 hrs, our compounds didn't show any counteraction behavior however at 6 hrs for MFM49, MB11V. GD041, MB11V has significantly lowered the CXCL-2 level as compared to MFM49 (**Figure 32C**).

The cxcl-10 level at 1, 4, 6 hrs differed as compared to TNF, TTP, and CXCL-2. The LPS induced CXCL-10 increased levels were 3 to 4 fold higher, and counteraction behavior of compounds were not seen at one hour, in spite of that DHTS altered the standard of CXCL-10 additively at one hour (not shown in the graph), although all of them lowered CXCL10 level at 4 hrs from 10-30% (**Figure 32D**). At 6 hrs CXCL-10 level also reached steady state level and remained unchanged. HuR inhibitors has significantly decreased CXCL10 levels at 4 hrs, the intracellular mechanism of action of these compounds still needs to be explored, altogether considering the late counteraction pattern observed for CXCL-2 and CXCL10 at 6 hrs and 4 hrs respectively. The difference observed in levels for mRNA depends upon the differential specificity of these

compounds as they are structurally dissimilar. All the mRNA level normalized to 0 hr DMSO control after normalization with housekeeping gene i.e., Actin.

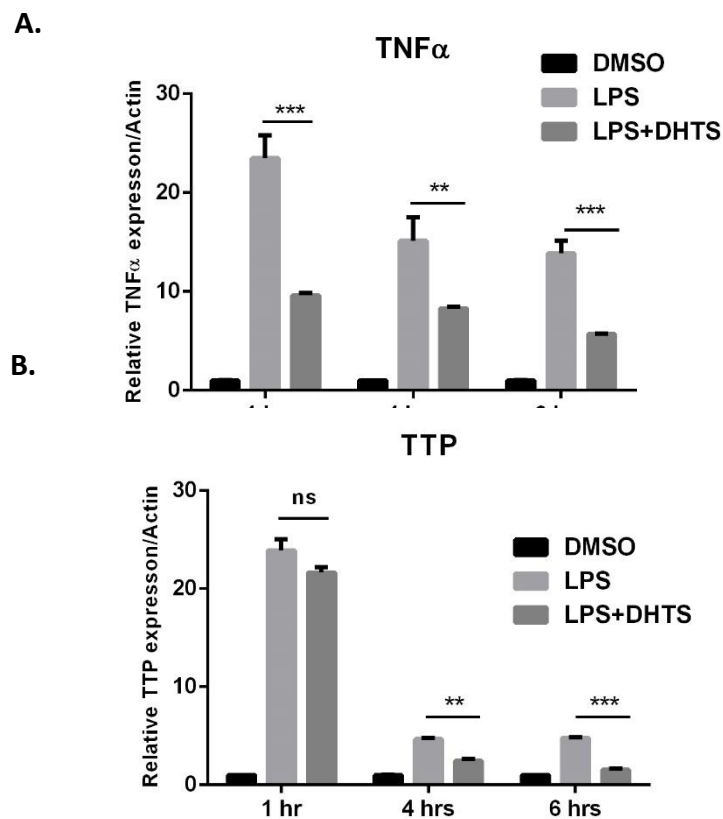


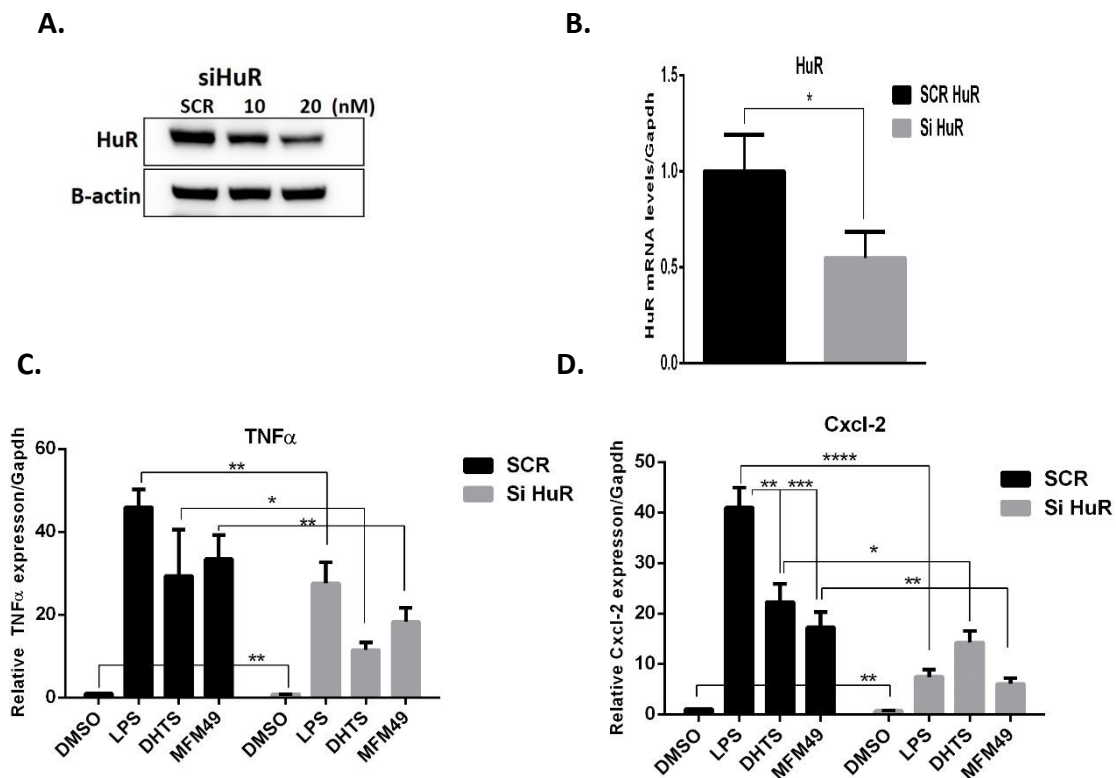
Figure 33 DHTS downregulate TNF α and TTP level **A)** TNF α levels obtained by qPCR analysis upon DHTS treatment at 1, 4 and 6 hrs (DMSO, LPS and LPS+DHTS) **B)** TTP levels obtained by qPCR analysis upon DHTS treatment at 1, 4 and 6 hrs. (DMSO, LPS and LPS+DHTS). Data expressed as mean \pm s.d. (n= 3), and analyzed using Dunnett's Multiple Comparison Test ** P \leq 0.01, *** P \leq 0.001 and ns = not significant. (Experiment has been performed by me, at MHH, Hannover).

DHTS downregulates TNF α and TTP levels

DHTS fresh aliquot was used to check again level of TNF α and TTP. The level of CXCL-2 and CXCL-10 remained unchanged (data not shown) with the new fresh aliquot of DHTS. TNF α level as always were lowered to significant levels at 1, 4 and 6 hrs. Again consistent decrease of 60%, 50% and 60% were observed at 1, 4 and 6 hrs (**Figure 33A**). Then I checked the levels of TTP upon DHTS addition, this time 50%, 60% downregulation of TTP level were obtained at 4 and 6 hrs. At one hour also slightly the level of TTP started decreasing which further resulted in significant reduction of TTP level at all time points checked (**Figure 33B**).

Downregulation of major cytokines by DHTS and MFM49 is HuR-dependent

HuR is responsible for the increase in TNF α , CXCL2 and CXCL10 mRNA level induced by LPS stimulation. RAW 264.7 cells were transfected with siRNA oligos targeting HuR or the control via electroporation and allowed to grow for 72 hrs, and then challenged with LPS and LPS co-treatment using DHTS (1 μ M) and MFM49 (5 μ M) for 3hrs (**Figure 34A**). TNF α , CXCL2 and CXCL10 mRNA levels were determined by real-time PCR. When HuR protein and mRNA expression was silenced (**Figure 34B**) the remaining TNF α , CXCL2 and CXCL10 mRNAs in LPS stimulated cells were further decreased to ~40%, ~80, and ~60%, compared with that of control short interfering RNA (siRNA)-transfected cells.. Interestingly DHTS and MFM49 significantly reduced TNF α , CXCL2 mRNAs stability compared with Si or SCR control ($P \leq 0.05$). Conversely, CXCL10 mRNA levels were not affected ($P = ns$). MFM49 compound also significantly lowered TNF α , CXCL2, and CXCL10 mRNA compared with that of Si or SCR control ($P \leq 0.05$) (**Figure 34C, 34D and 34E**). From these observations we can conclude that HuR absence has impacted on the stability of these cytokines, where upon addition of our compounds has caused a slight additive effect on their stability in siHuR cells, thus suggest the role of HuR in maintaining mRNA stability.



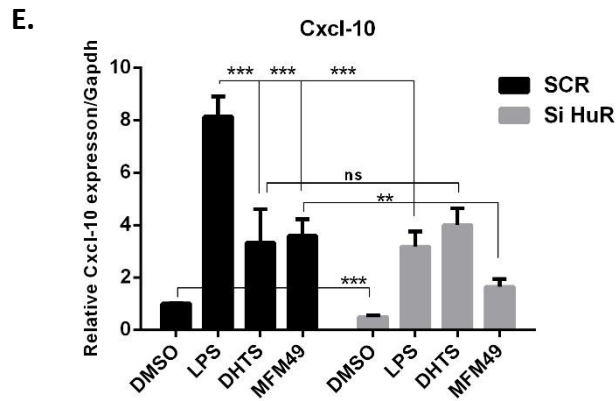


Figure 34 Downregulation of major cytokines by DHTS and MFM49 is HuR-dependent HuR is involved in the increase in cytokine mRNA levels, when induced by LPS stimulation. **A, B)** Western blot and RT-PCR analysis showing siHuR protein and HuR mRNA expression for siHuR and scramble (Si control). **C)** TNF α mRNA levels in siRNA and scramble (SCR) control transfected cells at 3 hrs, the treatment conditions were as indicated in the legends but along with LPS 1 μ g/ml. **D)** CXCL2 mRNA levels in siRNA and scramble (SCR) control transfected cells at 3 hrs, the treatment conditions were as indicated in the legends but along with LPS 1 μ g/ml. **E)** CXCL10 mRNA levels in siRNA and scramble (SCR) control transfected cells at 3 hrs; the treatment conditions were as shown in the legends but along with LPS 1 μ g/ml. Note: DHTS and MFM49 treatment conditions are with LPS (1 μ g/ml) co-treatment. Mean, and SD obtained are from 3 independent experiments and were analyzed by one-way ANOVA. *P \leq 0.05, **P \leq 0.01, ***P \leq 0.001; ns, not significant. (All Experiment has been performed by me).

TNF α downregulation by DHTS and DHTS analogs is independent of TTP in TTP-KO macrophages

Qiu et al., 2015 confirmed the level of TNF in TTP-KO cells, were higher than the control in myeloid specific macrophages [145]. I wanted to check if our compound already has lowered the TNF levels were TTP dependent or independent, we induced TTP-KO macrophages with LPS (1 μ g/ml) together with reference doses of DHTS and DHTS analogs.

qPCR analysis revealed that at one hour, all analogs had lowered TNF α level significantly to 8-10%. At 2 hrs TNF α levels were consistently reduced to 60, 65, 65 and 35 % in case of DHTS, MFM49, MB11V, and GD041 (**Figure 35A**). Further at 4 hrs TNF α fold increase lowered and except the case of MFM49, where it is reducing consistently, for all other analogs including DHTS the level of TNF α repressed as compared to LPS control. Moreover at 6 hrs, the level of TNF α fold increase came to basal level to that of LPS but higher than the DMSO control (data not shown). Nonetheless at 1 and 2 hrs when the LPS stimulation were at its peak even in TTP-KO macrophages and our compounds has counteracted TNF α , which shows that our compounds reduced TNF α level independent of TTP (**Figure 35A**).

A.

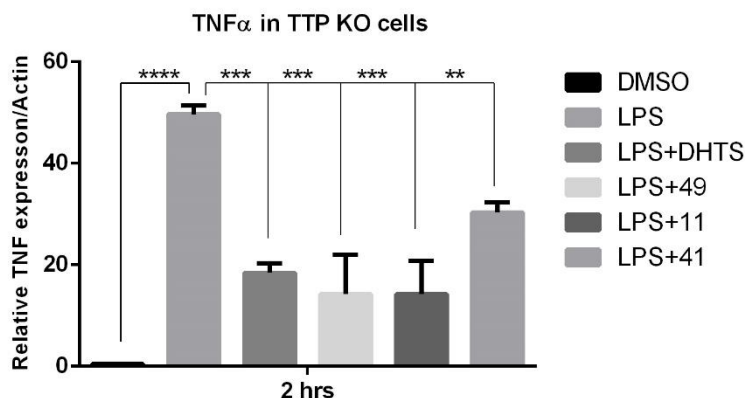


Figure 35 TNF α levels counteracted by DHTS analogs independent of TTP in TTP KO cells TNF α levels obtained by qPCR analysis upon DHTS treatment at 1, 2, 4 and 6 hrs in TTP-KO RAW 264.7 cells. (DMSO, LPS, MFM49, MB11V, and GD041). Data expressed as mean \pm s.d. (n= 3), and analyzed using Dunnett's Multiple Comparison Test ** P \leq 0.01, *** P \leq 0.001 and ns = not significant. (Experiment has been performed by me, at MHH, Hannover).

Preliminary Results

NF- κ B activation is not influenced by DHTS analogs in RAW264.7 cells.

NF- κ B transcription factor is involved in the gene expressions of many immune-modulatory proteins, e.g., TNF, interleukins, iNOS and many others inflammatory proteins. Before the stimulation, a significant level of the Rel/NF- κ B resides in the cytoplasm, along with I κ B α . Multiple numbers of stimuli translocate Rel/NF- κ B protein to the nucleus by induced phosphorylation of the I κ B α , which further lead to proteasomal degradation of the I κ B α [146]. To test the influence of our drugs on NF- κ B activation upon LPS stimulation at 0, 15, 30 and 60 minutes, I did differential fractionation of the RAW264.7 cells.

After confirmation of the differential lysis by western blotting for nuclear and cytoplasmic markers (ATF-2, and GAPDH), we checked levels NF- κ B (p65) and p-I κ B α S32/36. Firstly, NF- κ B translocation were not observed at 0 and 15 min for DMSO, DHTS and LPS. At 30 min the p65 level increased in both DHTS and LPS, followed by a slight decrease in LPS while in DHTS p65 levels remained unaffected at 60 min. Nonetheless, actual activation of p65 is shown by phosphorylation of p-I κ B α S32/36 in the cytoplasm was observed in LPS treated cells. As expected DMSO didn't show any phosphorylation of p-I κ B α S32/36, then I checked the p-I κ B α

S32/36 level in DHTS (1 μ M) presence at 15, 30 and 60 minutes, I κ B α S32/36 level were marginally counteracted by DHTS especially at 15 and 30 minutes, which were increased in LPS control (**Figure 36A**).

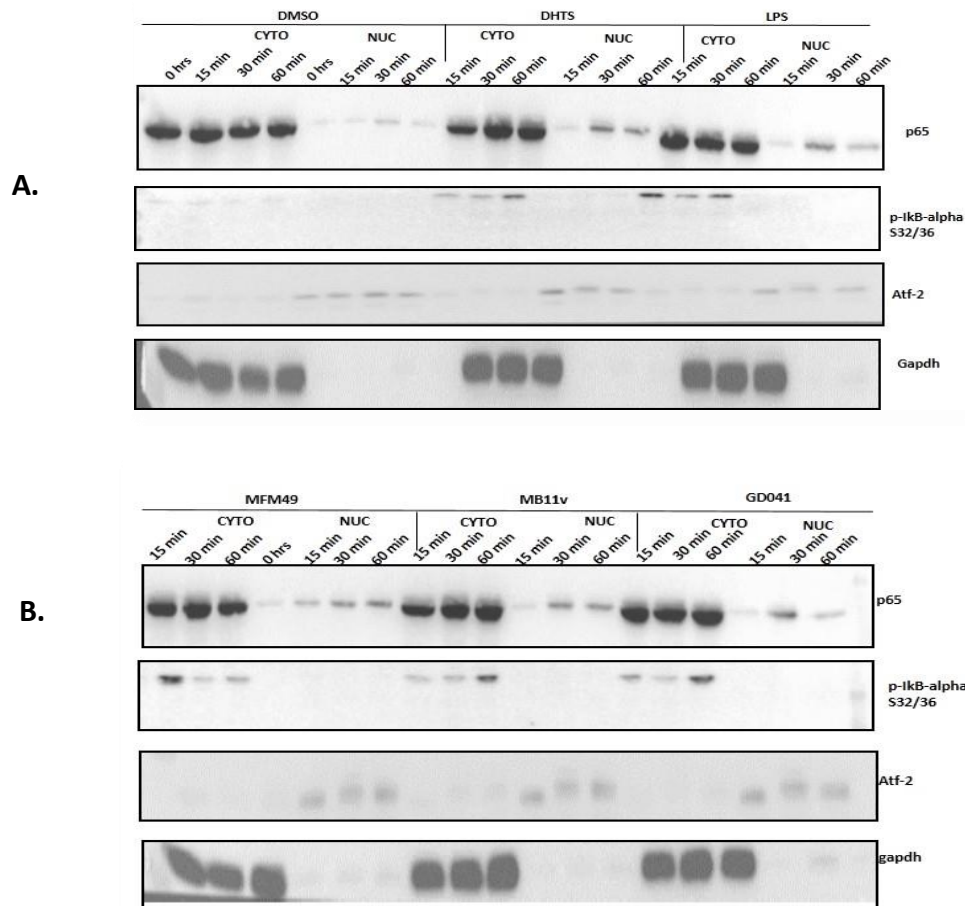


FIGURE 36 NF- κ B activation is not influenced by DHTS analogs in RAW264.7 cells. A) NF κ B activation and I κ B α at 0, 15, 30, 60 min, for DMSO, DHTS (1 μ M)+LPS, LPS (1 μ g/ml). **B)** NF κ B and I κ B α activation at 0, 15, 30 and 60 min, for LPS+MFM49 (5 μ M), LPS+MB11V (5 μ M) and LPS+GD041 (5 μ M), ATF-2 and GAPDH are the nuclear and cytoplasmic marker for differential fractionation confirmation. (Experiment has been performed by me, at MHH Hannover)

If we compare nuclear levels of p65 (NF- κ B) translocation in case of MFM49, MB11V and GD041 treatment, except MFM49, which showed little increase at 15 minutes, was not shown by MB11V and GD041, while at 30 minutes all of them showed increased level. p65 translocation at 60 minutes was same in case of MFM49 and MB11V, whereas GD041 has shown corresponding p65 translocation as to that of LPS control. p-I κ B α S32/36 cytoplasmic activation level for MFM49, MB11V and GD041 treatment were strongly induced in MFM49 treated cells, while indistinguishable pattern was observed for MB11V and GD041 at 15

minutes. Phosphorylation of p-IkBa S32/36 at 30 min was similar in MFM49, MB11V and GDO41, i.e., slightly lowered level than the LPS control. The levels of p-IkBa S32/36 low in MFM49 as compared to MB11V and GDO41, where they showed increased phosphorylation of p-IkBa S32/36, similar to LPS control at 60 min (**Figure 36B**). Thus the p-IkBa S32/36 activation were differentially regulated by DHTS, MFM49, MB11V, and GDO41. So taken all together DHTS, MB11V and GDO41 have shown similar behavior at 15 and 30 min, while in MFM49 as shown in opposite, i.e., fast activation at 15min and then lowered at 30 and 60 min consistently. This may explain that DHTS, MB11V, and GDO41 has the activation at 15 and 30 minutes, and later couldn't surpass the LPS induced action on p-IkBa S32/36. Hence our compounds do not influence the activation of NF- κ B, as also evidenced by the immunofluorescence studies in **Figure 30**.

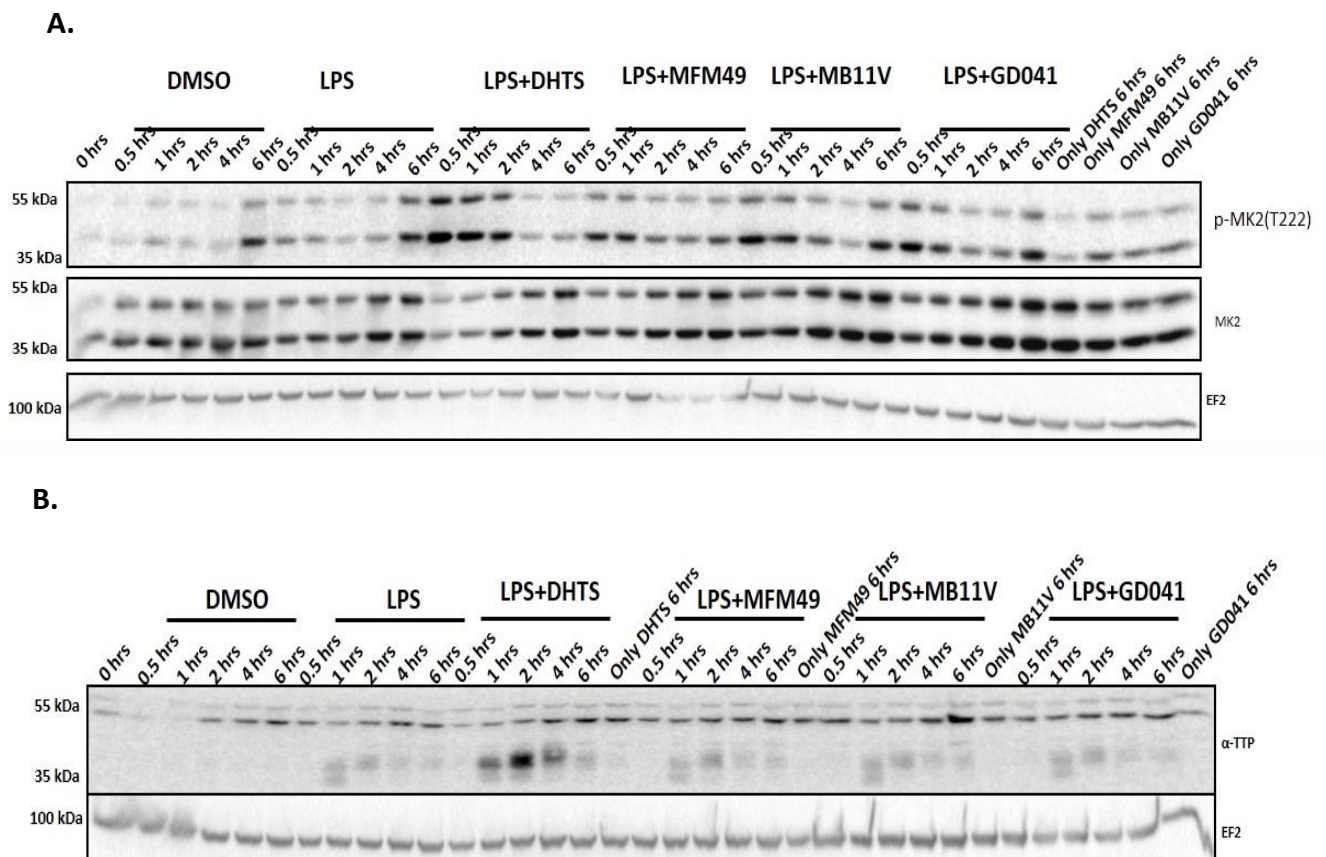


Figure 37: Activation of p-MK2 and α -TTP levels **A)** p-MK2(T222) levels obtained by western blot analysis upon co-treatment LPS and DHTS analogs, in legends only DHTS, MFM49, MB11V, and GDO41 are without LPS treatment incubated for 6 hrs. **B)** α -TTP levels obtained by western blot analysis upon co-treatment LPS and DHTS analogs, only DHTS, MFM49, MB11V, and GDO41 are without LPS treatment incubated for 6 hrs. (Experiment has been performed by me, at MHH Hannover)

MAPK pathway activation upon co-treatment our with compounds

As we know that p38 MAPK activated protein kinase (MAPK) pathway play an important role in the post-transcriptional regulation of inflammatory cytokines such as TNF α and other cytokines based on their cis-elements present in 3' or 5' UTRs. It was proved in MK-2 KO macrophages where no induction of the TNF α was observed, as compared to normal cells [147].

I have seen strong down-regulation of TNF α upon co-treatment of our drugs with LPS. Further to confirm activation of MK-2 we performed western analysis upon co-treatment of our drugs with LPS, to see check activation pattern at different time points, i.e., at 0, 0.5, 1, 2, 4 and 6 hrs. I observed activation of p-MK2 (T222) at 0.5, 1 and 2 hrs with LPS, where as in case of our compounds the MK-2 was activated strongly at 0.5, 1, 2 hrs followed by reactivation at 6 hrs in case of LPS, MB11V and GD041, similarly this activation was also observed in DMSO control. DHTS has already been shown in literature to strongly activate p38 at 0.5 hrs [148]. Therefore we also observed the strong activation of MK-2 at half an hour. Conversely treating cells with our compounds only has activated or phosphorylated MK-2 levels. Total MK-2 level were also checked by western blot analysis which showed differential expression pattern among the LPS and LPS co- treated macrophages. The MK-2 level started to accumulate at 4 and 6hrs for LPS and DHTS, whereas for the MFM49, MB11V and GD041 total MK-2 expression increased at 1, 2, 4 and 6 hrs. At 2, 4, 6 hrs, MK-2 increased exceptionally (**Figure 37A**).

If I report about TTP activation at 0, 0.5, 1, 2, 4 hrs accumulated after MK-2 diverse phosphorylation in LPS and co-LPS treated compounds. I saw abrupt increase TTP level in DHTS treated cells, besides this other 3 compounds (MFM49, MB11V and GD041) did not alter the substantial TTP level upon co-treatment with LPS, tiny differences in TTP could be seen in the TTP levels in but were not evident significantly. (**Figure 37B**). Huge alterered α TTP levels in DHTS treated cells were the stability issue of DHTS, which was later resolved with fresh aliquot of DHTS. (Data not shown).

Taken all together these result shows that our compounds do not influence p38 MAPK pathway as we didn't see an alteration in TTP level upon LPS co-treatment with DHTS analogs.

Analysis of p38 MAPK pathway in TTP-KO cells

p38 MAPK has been known to stabilize transcripts that contain AU-rich sequences [149]. LPS activates p38 MAPK pathway and as a model to check the level of TNF α decrease, if TTP dependent or not, our qPCR analysis showed that decrease was independent of TTP (**Figure 35**), I further investigated by western blot the activation of p38 MAPK pathway, the pattern of and p-MK-2(T222) observed is similar to the normal RAW cells. LPS p-MK-2(T222) activation at 1 hour were same as in LPS co-treated cells with DHTS, MFM49, MB11V, and GD041. Also, pp38-T180/Y182 was strongly induced at 0.5 hrs in all treated RAW264.7 macrophages. The relative decline in the level of p38 MAPK were observed after 2 hrs i.e. at 4 hrs the partial level p38 were detected in case of compound co-treated cells. Total MK-2 levels remained unaltered in RAW264.7 TTP KO cells (**Figure 38**).

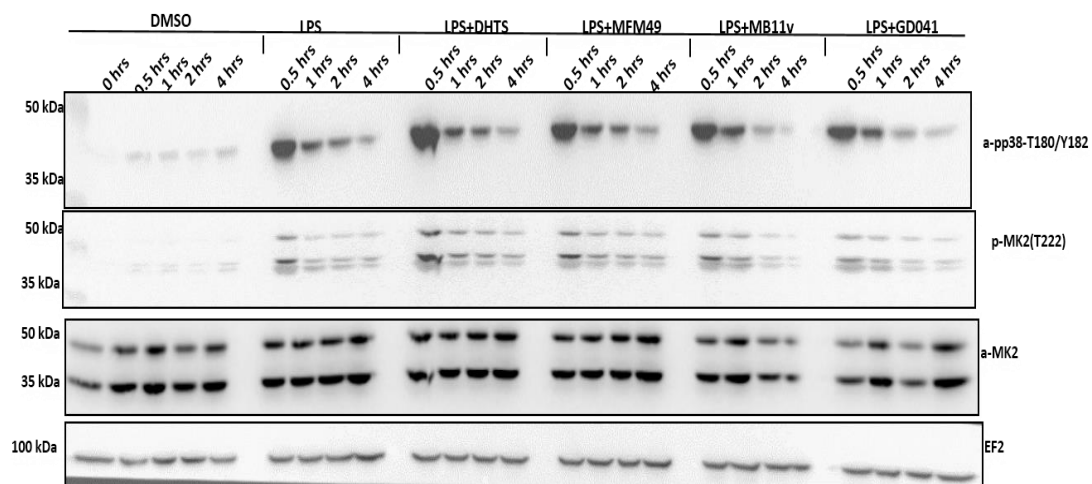


Figure 38: Analysis of p38 MAPK pathway in TTP-KO cells. (Experiment has been performed by me, at MHH Hannover).

Polysomal analysis in RAW264.7 upon LPS stimulation

Polysome determine the fate of mRNAs by participating in mature mRNA translation. Polysomal profiling was done as described by [43]. We know that DHTS reduces the TNF α mRNA translational efficiency [129]. To evaluate if DHTS analogs arrests TNF α mRNA loading

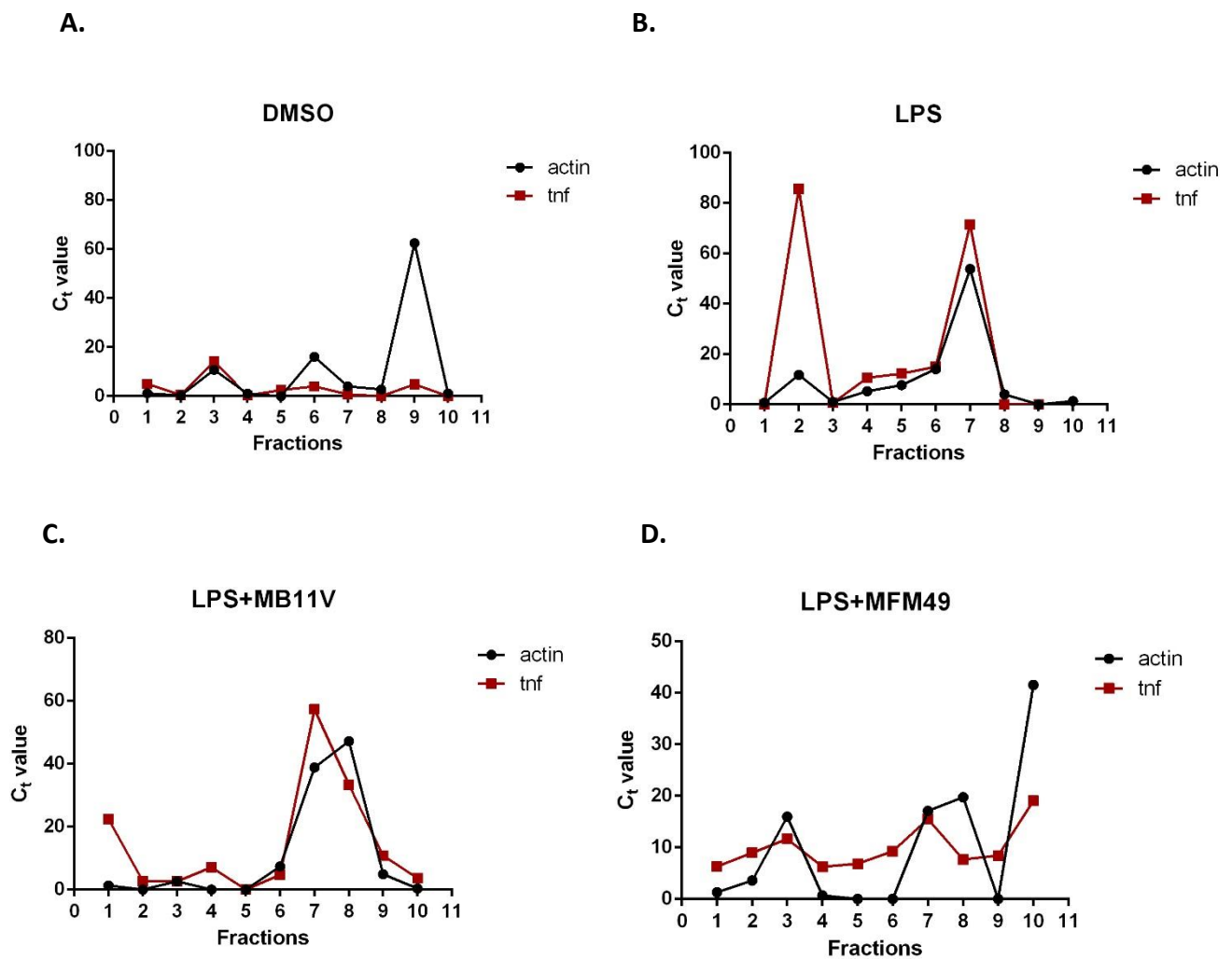


Figure 39 RT-qPCR analysis of actin and TNF mRNA levels in polysomal RNA fractions in RAW 264.7 cells. **A)** For DMSO only **B)** LPS+DMSO and **C)** LPS+MB11V **D)** LPS+MFM49 (Experiment has been performed by me, at MHH Hannover).

on the active translation machinery I treated RAW 264.7 with DHTS analogs at their reference doses with LPS co-induction (1 $\mu\text{g}/\text{ml}$) for 3hrs, followed by collection and sucrose gradient sub-polysomal fractionation of DMSO, DMSO+LPS, DHTS+LPS, MFM49+LPS, MB11V+LPS, GD041+LPS treated cells. For the moment we could analyze only 4 samples for their TNF α and actin distribution over the polysomes. Nonetheless I still have to analyze DHTS+LPS and GD041+LPS. From the graph obtained after qPCR analysis of fractionated samples, I could make some observation that relative cytoplasmic TNF α are very low in DMSO treated samples, whereas actin was distributed and its levels are unchanged (**Figure 39A**). In LPS treated cells, TNF α is greatly distributed over the translation machinery after 3 hrs of LPS induction, whereas actin qualitative or quantitative levels were found normally distributed over the

actively translating monosomes or polysomes (**Figure 39B**). However we observed qualitative and quantitative difference among the DMSO and LPS+DSMO treated samples.

MB11V did not influence any polysomal distribution of TNF α , but apparent levels were reduced, if we compare with LPS control, TNF α sub-polysomal and polysomal distribution profile (**Figure 39C**). Conversely, MFM49 has influenced the TNF α level clearly from the active polysomes (**Figure 39D**).

Besides this we have fractionated, samples of TTP-KO cells, treated with DHTS analogs DMSO, DSMO+LPS, DHTS+LPS, MFM49+LPS, MB11V+LPS, GD041+LPS, to investigate the influence of DHTS analogs on TTP-dependent translation of TNF α , after their RNA extraction and consequent steps to quantify the distribution profile of these DHTS analogs.

Effect on mRNA Stability after transcriptional inhibition with Actinomycin D

TNF α a key player in inflammation and Cxcl2 (homologue of human growth-regulated protein (Gro) is a potent attractant of neutrophils, and highly related to innate inflammatory responses [150], [151]. Also CXCL10 (IP10) has been shown as an inflammatory mediator in the liver steatohepatitis, a type of fatty liver disease, characterized by inflammation of the liver [152]. We examined the kinetics of levels of remaining TNF α , CXCL2 and CXCL10 mRNAs in RAW264.7 macrophages. The half-life of TNF α mRNA in LPS withdrawn cells was lowered as compared LPS challenged and LPS co-treated cells with DHTS (1 μ M) and MFM49 (5 μ M). Showing slightly additive effect, our compound further decreased the mRNA stability of TNF α after ActD addition (**Figure 40A**).

Conversely, the half-life of CXCL2 mRNA in LPS withdrawn cells was higher as compared LPS challenged and LPS co-treated cells. This could be due to the very low stability of CXCL-2. Following immediate transcriptional arrest with ActD (in co-treated cells) after LPS stimulation. CXCL2 mRNA levels were strongly reduced upon addition of ActD, where DHTS and MFM49 subsequently decreased CXCL2 stability to significant levels as shown in graph as $t_{1/2}$ half-life (**Figure 40B**).

Similarly CXCL10 stability was also affected upon ActD addition along with DHTS and MFM49 after LPS stimulation, the half-life of CXCL10 mRNA in LPS withdrawn cells was higher as compared to LPS challenged and LPS co-treated cells with DHTS (1 μ M) and MFM49 (5 μ M) (**Figure 40C**).

Based on these observations, the half-life of all the transcripts has been affected to the significant level ($P \leq 0.001$) by DHTS and MFM49. Mentioning HuR again as a target of DHTS and MFM49, influenced stability causing the behavior of HuR protein, within RAW 264.7 macrophages.

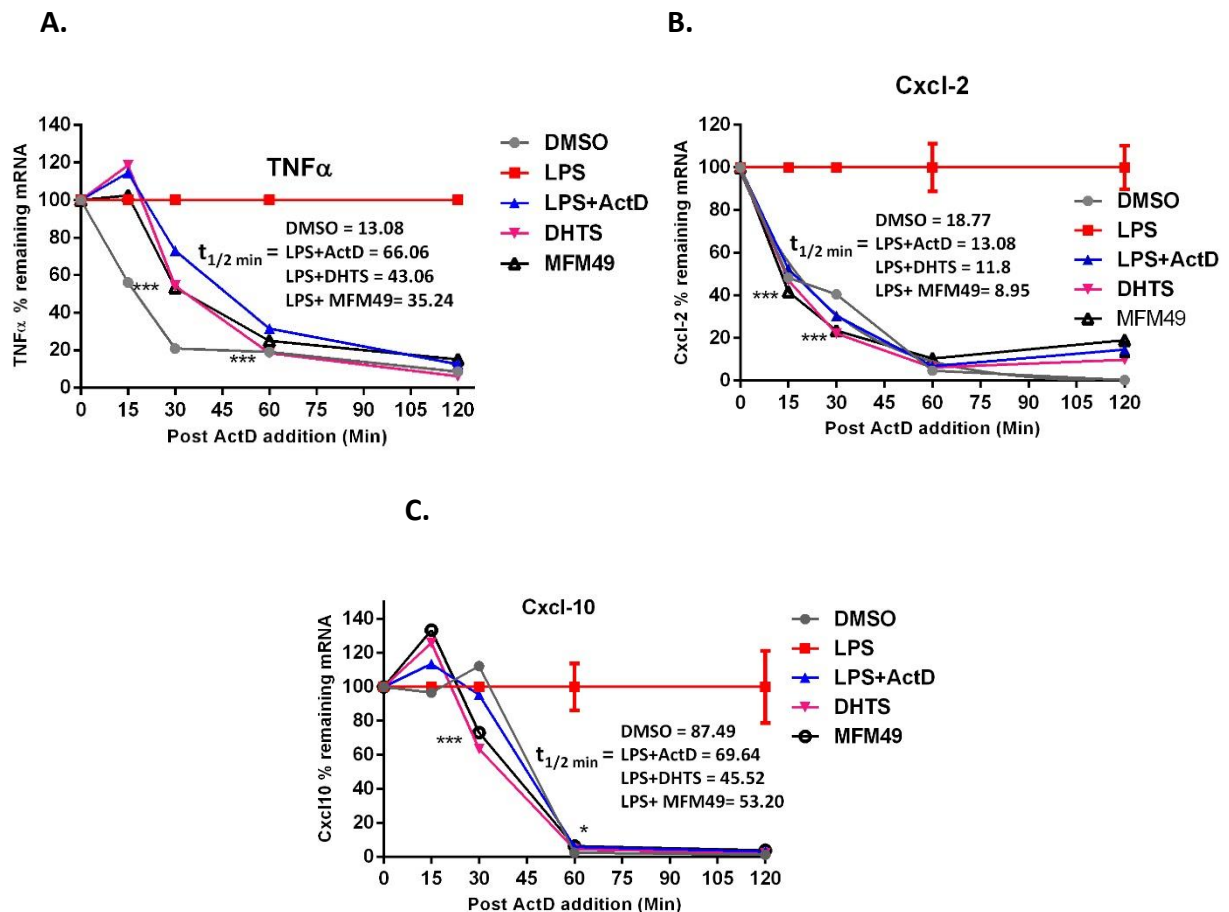


Figure 40 Influence of DHTS and MFM49 on the stability of major cytokines in LPS-exposed RAW 264.7. RAW264.7 cells were co-treated with DMSO, LPS, LPS+ActD, DHTS+ActD and MFM49+ActD for 0, 15, 30, 60 and 120 min. Real-time PCR was performed to assess the remaining **A)** TNF α , **B)** Cxcl12 and **C)** Cxcl-10 mRNA levels. The half-lives of different samples are indicated in the inset and was calculated using GraphPad Prism, using nonlinear regression analysis and then choosing one phase decay function to calculate the half-life of each mRNAs. Each replicate were plotted and compared using Dunnett's Multiple Comparison Test showing P values * $P \leq 0.05$, *** $P \leq 0.001$. (All Experiments has been performed by me).

Other DHTS analogs

Our team together, are involved further involved in screening other potent inhibitors named VB16, VB27, VB35, VB40, VB44, MFM48, VB49, VB062, MFM75, and DHTS again in biochemical and cell-based assays. We observed their low cytotoxic effect, when we

compared with DHTS in a panel of cell lines, e.g. MCF-7, MDA-MB231, PANC-1 and THP-1 cell lines (Figure 41).

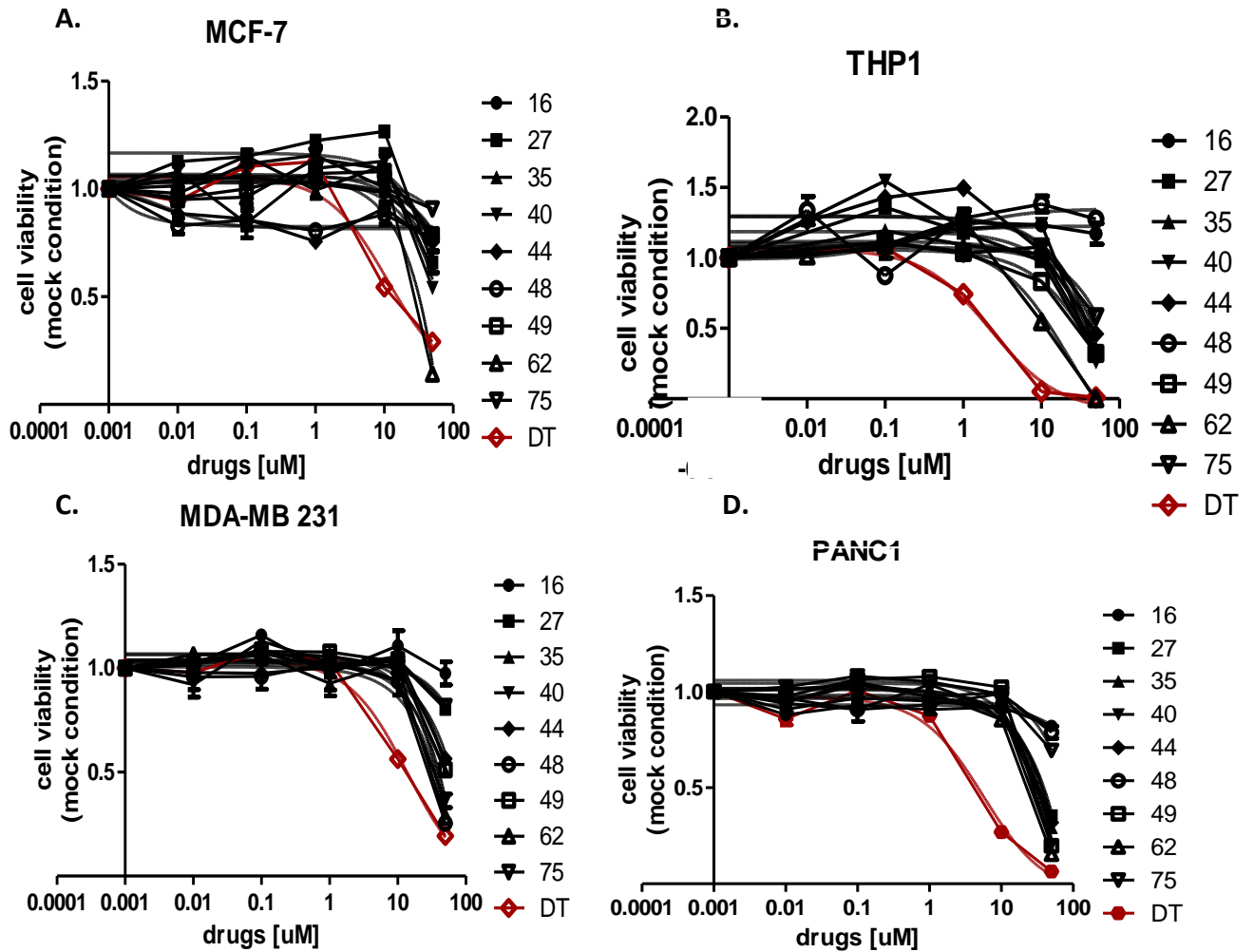


Figure 41 Cell viability assays done on various cell line using HuR inhibitors (shown in legends) (IC50 values are **not shown**). Numbers on the right hand side indicate the name of each compound. (Dr. Natthakan Thongon, Dr. Chiara Zucal and Dr. Vito D'Agostino has contributed to these figures).

CHAPTER 4

Discussion and Conclusion

Discussion

To our knowledge, until now HuR inhibitors are yet not available in the market as anticancer therapy module. This may be due to HuR pleiotropic role in controlling gene expression is very complex, and consequent results of HuR inhibition are difficult to predict. We know that HuR inhibition is not compatible with life, but if we compare thousands of studies of multiple cancer types e.g. Breast cancer, colon cancer [153] oral cancer, Renal cell carcinoma (RCC), non-small lung cancer carcinoma (NSLC), non-muscle invasive bladder cancer (NMIBC), Pancreatic ductal adenocarcinoma (PDAC), and many others, where HuR has been associated with aberrant nucleus/cytoplasmic ratio relating to carcinogenesis and tumor progression [154]; [93]. With reference to these studies, HuR pharmacological modulation is possible and necessary [18]; [97]; [98] and [155]. Here in my dissertation, we used AlphaScreen technology, EMSA assays to target HuR-RNA interaction with small molecules *in-vitro* [156], [98], [139]. We show that DHTS and DHTS analogs are potent inhibitors of HuR-RNA complex formation, and can modulate HuR post-transcriptional control, by limiting association rate of HuR-RNA complex formation at low nanomolar/micromolar range, confirmed *in vitro* in biochemical assays (**Figure 13**).

By using tandem RRM1/2, RRM2/3 biochemical experiments, we showed distinct binding preference of DHTS is within RRM1/2 domain, considering the individual RRMs EMSA, this finding also consistent with the EMSA of RRM1/2 (**Figure 14 and Figure 15**).

Regarding DHTS selectivity, it does not interfere with RNA binding activity of RBPs Lin28b, TDP-43 and TTP (**Figure 16**). This further confirms that these type of molecules binds to site-specific binding pocket of the HuR, was revealed by crystal structure of HuR, usually which possess dynamic conformational changes and selective affinity to its target RNA probe [20].

In last recent years, lot of HuR inhibitors have been screened, however interacting structural residual information between these molecules and HuR is lacking. We tried to dig-out this information based on the output of different biochemical approaches, used to find the basis of this interaction. Our collaboration with Prof. Marco Fragai, University of Florence has resulted in positive outcome, with residual amino acid information on HuR interaction with DHTS, suggesting a locus between first two tandem domains, is crucial for binding with target

RNA [20] or DHTS in our case by NMR studies (interacting residues are mentioned in result section).

The linker region within HuR, between first two tandem domains, navigate the HuR function by altering the conformation of RRM2 at opposite orientation which represents the bound form of HuR. However, this binding is dynamic and affinity-dependent, toward the corresponding interacting RNAs. Titration of HuR with DHTS experienced some conformational changes. Therefore we suggest that linker region is involved in binding to DHTS as it was revealed by delta RRM1 studies, REMSA binding assays. C-terminal region removal within RRM1 resulted in reduced affinity binding of RRM1 domain to the target RNA, hence it also loses important kinetic binding interactions with DHTS, this proved that region next or within linker region are obligatory in order to establish the stable binding of respective proteins (RRM1/2 or FL-HuR) and ligand (DHTS) (**Figure 17**). We also proved binding of Δ RRM1 to target FAM RNA probe in Fluorescence Polarization (FP) experiments, consistent with REMSA data we suggest that 14 amino acid region is critical for RNA binding as we observed K (obs), constant of ~ 8 min (**Figure 17C** and **Table 1**).

Single point mutations in the interacting region at S94, N107, I133, and N134, to Alanine has shown us that these residues are crucial for preserving dynamic equilibrium state of free HuR protein in monomer/dimer form and the closed protein-RNA dimer. Interestingly mutants were fully resistant to DHTS, as DHTS has lost efficacy to interrupt the complexed binding of HuR mutants and target RNA (**Figure 18B**), this further supports that DHTS competes for the same protein regions, interacting with the target RNA probe. Stabilization of this 'closed' conformation alters the protein dynamics, reflecting the observed generalized decrease of signal intensity of the resonances in NMR, observed upon the addition of DHTS to the RRM1_M2 tandem domains. Unfortunately, the non-optimal solubility of DHTS hampered the quantitative assessment of its K_d with rHuR protein. Additionally CD and NMR measurements ruled out the putative interaction between DHTS and RNA Probe (**Figure 19A and 19B**).

Moreover, the alpha signals at the hook point values for protein and RNA probes were significantly lowered in intensity compared to wild-type HuR, indicating a suboptimal environment, compatible with ligand self-aggregation [157]. Indeed, mutants showed significantly lower K_d values, i.e., an increased affinity in saturation binding experiments with

compared to wild-type HuR (**Figure 20, 21**), indicating again these residues are critical for self-dimerization behavior of HuR, as imprudent aggregation was observed in muteins (**Figure 22**). Among well-known HuR inhibitors, naphthofuranone MS-444, which has been identified using fluorescence intensity distribution analysis (FIDA) screening on almost 50,000 natural plant extract, it was shown to inhibit the HuR-RNA binding by inhibiting HuR oligomerization at K_d of 40 nM respectively [18]. About ~23,000 compounds were also tested by using FP-HTS based technique. Consequent validation by Alpha and SPR of ST-3 inhibitor and its analogs has decreased the HuR target mRNAs' half-life and accordingly encoded proteins (Bcl-2, XIAP, and Msi1/2). In this context using DHTS we measure strong nanomolar inhibition of complex formation rate among HuR and RNA *in vitro*, also lowered the level of pre-TNF and TNF half-life followed by the decrease in TNF protein levels [129], [155]. MS-444 was examined for its direct HuR inhibition potential, preventing the association of HuR with miR116, and hence with TDP-43 and FUS mRNA, but at the high level than DHTS [158]. Furthermore, MS-444 has also been exploited for its potential to impact upon HuR inhibition in colorectal cancer tumorigenesis, where it resulted in growth inhibition of induced apoptotic gene expression [136]. We also noted this behavior of DHTS, activating Caspase at 24 hrs at its IC50 [99].

Consequently this biological effects of DHTS were recapitulated in our cell models, where significant downregulation of TNF α , VEGF and other HuR targets were seen, nonetheless RNA Immunoprecipitation experiments also revealed the potential of DHTS to limit the association rate of HuR with target TNF α RNA. [99] (**Figure 23**).

As mentioned already that several studies described in details regarding HuR inhibition. However a link between post-transcriptional control, phenotypic effects, and therapeutic exploitation is far from being elucidated. Here we show the repressive effect on cellular viability together with impact of DHTS at low doses, on cellular proliferation, based on HuR dependency, where DHTS efficacy was counteracted by HuR overexpression in breast cancer cell lines, (**Figure 24**).

Moreover, DHTS belongs to tanshinone family and are known for their anti-inflammatory, anticancer, anti-atherosclerosis and cardio-protective properties. [122], [159].

Nevertheless, DHTS-dependent HuR dysregulation has a strong anti-cancer activity *in vivo*, as observed using a xenograft model of colon cancer (HCT116 cells). These results are consistent

with other findings in colon, leukemia, cervical, and breast cancer cells, and suggests that DHTS can enter tumors effectively [123], [160]–[162]. With no sign of systemic toxicity in treated animals supports the idea that inhibition of HuR by bioactive molecules can be a therapeutic route for future endeavor. Here the DHTS effects on the immune system have to be evaluated in a non-immuno-compromised mouse model. Interestingly, HCT116ΔHuR knockout cells *in-vivo* reflected limited ability to augment tumors, but the extent of DHTS inhibition on growth of those tumors did not match inhibition with that of WT tumors (**Figure 25**). While we cannot dismiss the fact that loss of HuR may affect cancer cell drug uptake, all these results suggest *in vivo* specificity of DHTS and confirm the idea that DHTS requires HuR for its antitumor influence. We uncovered here previously unrecognized mechanism of action of DHTS, targeting post-transcriptional regulation of HuR.

Taken together, these results present DHTS as competitive inhibitor of RNA binding to HuR, and DHTS further has been exploited for its anticancer function in *in vivo* models based on HuR pathology (**Figure 25**).

Another member of Tanshinones, Tan I is well known for its anti-adhesion properties in MDA-MB231 by decreasing intracellular ICAM1 and V-CAM levels [163]. Moreover Tanshinones are also known for their repressive effect on certain mi-RNA (miR155) in colon carcinoma, they have been known for their repressive activity and on numerous other miRNAs [164]; [165]. In fact they have been known for their suppressive function on interleukins cox2, il-6, VEGF, and MMP [166]–[169].

Further, we provide evidence of improved efficacy of HuR inhibitors called DHTS analogs, in terms of loss of HuR and target RNA binding functions *in vitro*. The differences in inhibition quotient OR their activity depends upon the chemical structure they possessed (**Figure 26**) as mentioned in the result section we couldn't provide structural information, but nonetheless, we are describing the experimental outcome of these analogs, in context of HuR posttranscriptional control where they modulate anti-inflammatory and anti-cancer effects.

The most potent MFM49 inhibitor was identified after cumbersome screening among other participant inhibitors (**Figure 26, 27 and 28**). MFM49 specificity with in cell based assays was also exploited using 5 μM of MFM49, This is a highest dose as compared to DHTS which may reflect the global functional potential of DHTS affecting numerous pathway. Indeed DHTS

showed lower IC₅₀, conversely MFM49 being a specific HuR inhibitors its efficacy could be confined to HuR based influences within the cells. Moreover a noteworthy example of HuR inhibitor is MS-444, which has been shown to block HuR oligomerization, came up with its IC₅₀ in 5-40 μ M range, depending upon the cell type used and the pathologic substantial levels of HuR [136].

Cumulatively some of the outcomes, MFM49 has shown differential efficacy compared to DHTS. We did not observe DHTS, and DHTS analogs induced activation of p38 MAPK pathway hence HuR translocation to the cytoplasm, further supporting, the anticancer role of these inhibitors, specifically where cytoplasmic HuR is anticipating in the cause [16]. Additionally DHTS analog's influence on NF- κ B translocation to the nucleus upon LPS stimulation could not reveal any difference concerning control (LPS) in RAW 264.7 cells (**Figure 29 and 30**).

Anti-inflammatory function of DHTS and DHTS analogs, was investigated in normal and TTP-KO RAW264.7 cells macrophages, since HuR and TTP are involved in regulation of AU-rich sequences under the influence of p38 MAPK pathway [43]. Our compounds were efficient in lowering the cytokines TNF α , CXCL-2 and CXCL10 to significant levels depending on the target levels/affinity/preference to HuR (**Figure 31, 32 and 33**) [40] [43]. Nevertheless, initial pool of induced cytokines was lowered upon application of DHTS and MFM49, excluding some of the cytokines, which explains their tight affinity regulation by HuR within cell lines. [16], [170] (**Supplementary Figure 1 and Figure 2**). HuR silencing has confirmed that anti-inflammatory effects of DHTS and MFM49, is really due to inhibition of HuR, as further loss resulted in lower stability of important cytokines (**Figure 34**) [171].

TNF α decrease in TTP-KO upon application of DHTS and DHTS analog also showed that, this decrease was independent of TTP and further explain that p38 Activation stabilizes the AU-rich elements, conversely this effect was counteracted to significant level by our compounds in a HuR dependent manner [171] [172] (**Figure 35**).

Preliminary results

NF- κ B activation upon LPS stimulation in RAW264.7, and consequent blockade of translocation to the nucleus by DHTS and DHTS analogs was visible at the different extent, MFM49 has shown promising action, and nevertheless in immunofluorescence MFM49 didn't show any strong evidence in this regard (**Figure 36**). Again in normal and TTP-KO 264.7 cells, we did not see a DHTS-analog's induced activation of the p38 MAPK pathway, as we saw no

alteration in TTP protein levels, however substantial increase in the levels of p-MK2 (T222) , TTP in case of DHTS treatment was a stability issue, which was resolved later (data not shown) [173] [174] (**Figure 37 and Figure 38**).

Polysomal recruitment profile of DHTS analogs is being investigated analogs, in normal and TTP-KO RAW264.7, to check the influence of these analogs on TTP dependent translation. Interestingly, MFM49 has shown potential to displace TNF α from active polysomes, consistent with the finding in D'Agostino et al., 2015 (**Figure 39**). Moreover changes in major cytokines mRNA levels has been significantly reduced with the application of DHTS and MFM49, nonetheless, biological replicates of these findings need to be confirmed (**Figure 40**). Our lab is further involved in the screening of other HuR inhibitors, in various cell lines. (**Figure 41**).

The mouse model with AOS/DSS induction was tested using the MS-444 HuR inhibitor. Although the general HuR deletion is difficult for cell survival, myeloid specific deletion of the HuR causes augmented tumor formation in size with increased invasiveness in AOS/DSS colitis-associated cancer mouse model when treated with reference doses of MS-444 and potential HuR oligomerization inhibitor. In return, they found reduced induction of apoptosis despite the decrease in proliferation rate in the absence of HuR and presence of MS-444 [176].

In preclinical cell model of pancreatic ductal adenocarcinoma, HuR silencing has impaired proliferation, decreased anchorage-independent growth as well as impaired invasion and migration [177]. HuR's effect on the cancer phenotype is tissue and context type dependent. Typically, HuR as the determinant of cell pro-survival, in lethal stress conditions has been found promoter of cellular apoptosis in HeLa cells [178]. On the other hand HuR role in muscle cell differentiation cannot be avoided where it got cleaves at aspartate 226 to two parts HuR-CP1 (24 kDa) and HuR-CP2 (8 kDa), however HuR-CP1 with the help of transportin-2 got accumulated in the cytoplasm and hence helps in muscle differentiation whereas HuR-CP2 (8 kDa) associates with apoptosome activator PHAPI (putative HLA associated protein) to promote apoptosis [179]. Another advantage of HuR cleavage of HuR was demonstrated by HuRD226A, which further skipped cleavage by caspase and failed to recover apoptosis in cells devoid of endogenous HuR [178].

HuR has been implicated in the regulation of mRNAs controlling the class switch antibody responses by B-cells. HuR absence has caused impaired mitochondrial metabolism with a

significant increase in the levels of ROS (Reactive oxygen species) and subsequent B-cells death [71]. HuR ablation has been reported to arrest the normal embryonic development in mice and where fetus failed to survive, even at halfway of gestation [180]. Myeloid-specific conditional knockout of HuR in mice resulted in aberrant cytokine expression followed by chemical-induced colitis progression and consequent colitis mediated cancer. This shows that HuR plays as coordinator of the mRNAs (Tnf, Tgfb, Il10, Ccr2, and Ccl2) which are further involved in controlling innate inflammatory effects. This further guide us to exploit the HuR related inflammation and cancer like anomalies. Loss of HuR is not compatible with life, or it may lead to systematic inflammation with increase in pro-inflammatory tnf, il-6, ccl2 thus leading to severe colitis [82]. On the other hand HuR role in intestinal homeostasis, cell growth and survival where loss of HuR intestinal tissue reduced the burden of small intestinal polyposis [83]. HuR dosage has been suggested as the important factor in cytokine production level, after confirmation in heterozygous and homozygous conditional HuR knockout mice model in Th2, explaining the implication of HuR in asthma, allergies and autoimmune diseases when is ablated or dysregulated [81]. Considering these HuR based pathologies, it is now necessary to think about the pharmacological targeting of HuR. My thesis described some of the possible strategies to target HuR, when HuR is deregulated or has prognostic significance e.g. in as breast, colon or ovarian cancers or in inflammation-related disorders.

There are many things to be noted for further DHTS usage in therapeutic based strategies, in our study it influenced TNF α level representing its post-transcriptional function to attenuate TNF α levels, instead of depletion induced by targeted antibody-based drugs. We exploited ability of DHTS to inhibit HuR-RNA complex formation and we showed efficacy of DHTS, relating to loss of function of HuR and impacting further on the phenotypic, in terms of proliferation and sensitivity in breast cancer cell models. Overall our findings in context of DHTS a small natural molecule, possesses anti-inflammatory and anticancer properties, which could make the feasible measurement concerning "*genome druggability*" for anticancer therapy based on HuR pathology.

Summing up, to target HuR loss of function, is crucial and is evident from the numerous studies done in inflammation and cancer like conditions. HuR being an important factor at the posttranscriptional regulation channels, whose inhibition may result in ubiquitous, post-

transcriptional alterations in the body nevertheless it depends absolutely on the cell and tissue type, and thus its pharmacological tuning is possible.

CONCLUSIONS

We have shown here previously unrecognized mechanism of DHTS and other analogs interfering with HuR-RNA binding complex *in vitro*, and in *in vivo* experiments. We provided information about residual participating amino acids, binding to DHTS. Mutational analysis has shown that inter-domain region is responsible for the RNA binding and DHTS binding. The most potent compound is MFM49 among other HuR inhibitors, revealed by EMSA or AlphaScreen technology. In cells based assays DHTS and analogs down-regulates the TNF α , and other cytokines. Additionally DHTS and MFM49 downregulates TNF α , CXCL2 and CXCL10 in HuR dependent manner. Moreover DHTS and MFM49 do not influence activation of NF- κ B in RAW 264.7 cells after LPS stimulation. At last DHTS analogs do not change LPS induced activation of p38 pathway, and hence consequently do not affect substantial TTP levels.

References

- [1] T. Glisovic, J. L. Bachorik, J. Yong, and G. Dreyfuss, "RNA-binding proteins and post-transcriptional gene regulation," *FEBS Lett.*, vol. 582, no. 14, pp. 1977–1986, 2008.
- [2] C. Burd and G. Dreyfuss, "Conserved structures and diversity of functions of RNA-binding proteins," *Science (80-.)*, vol. 265, no. 5172, pp. 615–621, 1994.
- [3] M.-H. Lee, "RNA-binding proteins," *WormBook*, 2006.
- [4] M. J. Moore, "From birth to death: the complex lives of eukaryotic mRNAs.," *Science*, vol. 309, no. 5740, pp. 1514–8, 2005.
- [5] S. Robinow and K. White, "Characterization and spatial distribution of the ELAV protein during *Drosophila melanogaster* development.," *J. Neurobiol.*, vol. 22, no. 5, pp. 443–61, 1991.
- [6] A. R. Campos, D. Grossman, and K. White, "Mutant Alleles at the Locus *elav* in *Drosophila melano- gaster* lead to Nervous System Defects . A Develop- men t a 1 - Gene tic An a l y si s," vol. 2, pp. 197–218, 1985.
- [7] A. Szabo *et al.*, "HuD, a paraneoplastic encephalomyelitis antigen, contains RNA-binding domains and is homologous to Elav and Sex-lethal," *Cell*, vol. 67, no. 2, pp. 325–333, 1991.
- [8] P. J. Good, "A conserved family of *elav*-like genes in vertebrates.," *Proc. Natl. Acad. Sci. U. S. A.*, vol. 92, no. 10, pp. 4557–4561, 1995.
- [9] J. Dalmau, H. M. Furneaux, C. Cordon-Cardo, and J. B. Posner, "The expression of the Hu (paraneoplastic encephalomyelitis/sensory neuronopathy) antigen in human normal and tumor tissues.," *Am. J. Pathol.*, vol. 141, no. 4, pp. 881–886, 1992.
- [10] D. Antic and J. D. Keene, "Embryonic Lethal Abnormal Visual RNA-Binding Proteins Involved in Growth , Differentiation , and Posttranscriptional Gene Expression," *Am. J. Hum. Genet.*, vol. 61, pp. 273–278, 1997.
- [11] W. J. Ma and H. Furneaux, "Localization of the human HuR gene to chromosome 19p13.2," *Hum. Genet.*, vol. 99, no. 1, pp. 32–33, 1997.
- [12] R. Treisman, "Transient accumulation of *c-fos* RNA following serum stimulation requires a conserved 5' element and *c-fos* 3' sequences," *Cell*, vol. 42, no. 3, pp. 889–902, 1985.
- [13] D. Caput, B. Beutler, K. Hartog, R. Thayer, S. Brown-Shimer, and A. Cerami, "Identification of a common nucleotide sequence in the 3'-untranslated region of mRNA molecules specifying inflammatory mediators.," *Proc. Natl. Acad. Sci. U. S. A.*, vol. 83, no. 6, pp. 1670–4, 1986.
- [14] D. Kontoyiannis, M. Pasparakis, T. T. Pizarro, F. Cominelli, and G. Kollias, "Impaired On/Off Regulation of TNF Biosynthesis in Mice Lacking TNF AU-Rich Elements," *Immunity*, vol. 10, no. 3, pp. 387–398, 1999.

-
- [15] N. Mukherjee *et al.*, “Integrative regulatory mapping indicates that the RNA-binding protein HuR couples pre-mRNA processing and mRNA stability,” *Mol. Cell*, vol. 43, no. 3, pp. 327–339, Aug. 2011.
- [16] K. Abdelmohsen and M. Gorospe, “Posttranscriptional regulation of cancer traits by HuR,” *Wiley Interdiscip. Rev. RNA*, vol. 1, no. 2, pp. 214–229, 2010.
- [17] C. M. Brennan and J. a Steitz, “HuR and mRNA stability.,” *Cell. Mol. Life Sci.*, vol. 58, no. 2, pp. 266–277, 2001.
- [18] N.-C. Meisner *et al.*, “Identification and mechanistic characterization of low-molecular-weight inhibitors for HuR,” *Nat. Chem. Biol.*, vol. 3, no. 8, pp. 508–515, Aug. 2007.
- [19] M. N. Hinman and H. Lou, “Diverse molecular functions of Hu proteins,” *Cell. Mol. Life Sci.*, vol. 65, no. 20, pp. 3168–3181, 2008.
- [20] H. Wang *et al.*, “The structure of the ARE-binding domains of Hu antigen R (HuR) undergoes conformational changes during RNA binding,” *Acta Crystallogr. Sect. D Biol. Crystallogr.*, vol. 69, no. 3, pp. 373–380, 2013.
- [21] J. D. Keene, “Why is Hu where? Shuttling of early-response-gene messenger RNA subsets,” *Proc. Natl. Acad. Sci. U. S. A.*, vol. 96, no. 1, pp. 5–7, 1999.
- [22] W. Wang *et al.*, “AMP-Activated Kinase Regulates Cytoplasmic HuR,” *Mol. Cell. Biol.*, vol. 22, no. 10, pp. 3425–3436, 2002.
- [23] C. Tiedje, H. Holtmann, and M. Gaestel, “The role of mammalian MAPK signaling in regulation of cytokine mRNA stability and translation.,” *J. Interferon Cytokine Res.*, vol. 34, no. 4, pp. 220–32, 2014.
- [24] H. Tran, F. Maurer, and Y. Nagamine, “Stabilization of urokinase and urokinase receptor mRNAs by HuR is linked to its cytoplasmic accumulation induced by activated mitogen-activated protein kinase-activated protein kinase 2.,” *Mol. Cell. Biol.*, vol. 23, no. 20, pp. 7177–88, 2003.
- [25] X. Yang *et al.*, “Prostaglandin A2-mediated stabilization of p21 mRNA through an ERK-dependent pathway requiring the RNA-binding protein HuR,” *J. Biol. Chem.*, vol. 279, no. 47, pp. 49298–49306, 2004.
- [26] V. Lafarga, A. Cuadrado, I. Lopez de Silanes, R. Bengoechea, O. Fernandez-Capetillo, and A. R. Nebreda, “p38 Mitogen-Activated Protein Kinase- and HuR-Dependent Stabilization of p21Cip1 mRNA Mediates the G1/S Checkpoint,” *Mol. Cell. Biol.*, vol. 29, no. 16, pp. 4341–4351, 2009.
- [27] R. M. Scheiba, Á. Aroca, and I. Díaz-Moreno, “HuR thermal stability is dependent on domain binding and upon phosphorylation,” *Eur. Biophys. J.*, vol. 41, no. 7, pp. 597–605, 2012.
- [28] H. K. Hyeon and M. Gorospe, “Phosphorylated HuR shuttles in cycles,” *Cell Cycle*, vol. 7, no. 20, pp. 3124–3126, 2008.

-
- [29] W. Wang, M. C. Caldwell, S. Lin, H. Furneaux, and M. Gorospe, "HuR regulates cyclin A and cyclin B1 mRNA stability during cell proliferation," *EMBO J.*, vol. 19, no. 10, pp. 2340–2350, 2000.
- [30] K. Masuda *et al.*, "Global dissociation of HuR-mRNA complexes promotes cell survival after ionizing radiation," *EMBO J.*, vol. 30, no. 6, pp. 1040–1053, 2011.
- [31] S. Schulz, A. Doller, N. R. Pardini, J. A. Wilce, J. Pfeilschifter, and W. Eberhardt, "Domain-specific phosphomimetic mutation allows dissection of different protein kinase C (PKC) isotype-triggered activities of the RNA binding protein HuR," *Cell. Signal.*, vol. 25, no. 12, pp. 2485–2495, 2013.
- [32] L. Pang *et al.*, "Loss of CARM1 is linked to reduced HuR function in replicative senescence," *BMC Mol. Biol.*, vol. 14, no. 1, p. 15, 2013.
- [33] H. Li *et al.*, "Lipopolysaccharide-induced methylation of HuR, an mRNA-stabilizing protein, by CARM1," *J. Biol. Chem.*, vol. 277, no. 47, pp. 44623–44630, 2002.
- [34] C. Lucchesi, M. S. Sheikh, and Y. Huang, "Negative regulation of RNA-binding protein HuR by tumor-suppressor ECRG2," *Oncogene*, vol. 35, no. April, pp. 1–9, 2015.
- [35] A. Kotlyarov *et al.*, "MAPKAP kinase 2 is essential for LPS-induced TNF-alpha biosynthesis," *Nat. Cell Biol.*, vol. 1, no. 2, pp. 94–7, 1999.
- [36] A. Neining *et al.*, "MK2 targets AU-rich elements and regulates biosynthesis of tumor necrosis factor and interleukin-6 independently at different post-transcriptional levels," *J. Biol. Chem.*, vol. 277, no. 5, pp. 3065–3068, 2002.
- [37] C. A. Chrestensen *et al.*, "MAPKAP Kinase 2 Phosphorylates Tristetraprolin on in Vivo Sites Including Ser178, a Site Required for 14-3-3 Binding," *J. Biol. Chem.*, vol. 279, no. 11, pp. 10176–10184, 2004.
- [38] S. Rousseau, N. Morrice, M. Pegg, D. G. Campbell, M. Gaestel, and P. Cohen, "Inhibition of SAPK2a/p38 prevents hnRNP A0 phosphorylation by MAPKAP-K2 and its interaction with cytokine mRNAs," *EMBO J.*, vol. 21, no. 23, pp. 6505–6514, 2002.
- [39] P. Briata *et al.*, "p38-Dependent phosphorylation of the mRNA decay-promoting factor KSRP controls the stability of select myogenic transcripts," *Mol. Cell*, vol. 20, no. 6, pp. 891–903, 2005.
- [40] G. Stoecklin *et al.*, "MK2-induced tristetraprolin:14-3-3 complexes prevent stress granule association and ARE-mRNA decay," *EMBO J.*, vol. 23, no. 6, pp. 1313–24, 2004.
- [41] F. Bollig, R. Winzen, M. Gaestel, S. Kostka, K. Resch, and H. Holtmann, "Affinity purification of ARE-binding proteins identifies poly(A)-binding protein 1 as a potential substrate in MK2-induced mRNA stabilization," *Biochem. Biophys. Res. Commun.*, vol. 301, no. 3, pp. 665–670, 2003.
- [42] V. Lafarga, A. Cuadrado, I. Lopez de Silanes, R. Bengoechea, O. Fernandez-Capetillo, and A. R. Nebreda, "p38 Mitogen-activated protein kinase- and HuR-dependent stabilization of p21(Cip1) mRNA mediates the G(1)/S checkpoint," *Mol. Cell. Biol.*, vol.

-
- 29, no. 16, pp. 4341–51, 2009.
- [43] C. Tiedje *et al.*, “The p38/MK2-Driven Exchange between Tristetraprolin and HuR Regulates AU-Rich Element-Dependent Translation,” *PLoS Genet.*, vol. 8, no. 9, 2012.
- [44] P. Anderson, “Post-transcriptional control of cytokine production,” *Nat Immunol*, vol. 9, no. 4, pp. 353–359, 2008.
- [45] S. Srikantan and M. Gorospe, “UneCLIPsing HuR Nuclear Function,” *Mol. Cell*, vol. 43, no. 3, pp. 319–321, 2011.
- [46] L. P. Ford, J. Watson, J. D. Keene, and J. Wilusz, “ELAV proteins stabilize deadenylated intermediates in a novel in vitro mRNA deadenylation/degradation system,” *Genes Dev.*, vol. 13, no. 2, pp. 188–201, 1999.
- [47] T. Kawai, A. Lal, X. Yang, S. Galban, K. Mazan-Mamczarz, and M. Gorospe, “Translational control of cytochrome c by RNA-binding proteins TIA-1 and HuR,” *Mol. Cell. Biol.*, vol. 26, no. 8, p. 3295, 2006.
- [48] V. Katsanou *et al.*, “HuR as a negative posttranscriptional modulator in inflammation,” *Mol. Cell*, vol. 19, no. 6, pp. 777–789, 2005.
- [49] E. Carballo, W. S. Lai, and P. J. Blakeshear, “Feedback Inhibition of Macrophage Tumor Necrosis Factor- α Production by Tristetraprolin,” *Science (80-.)*, vol. 281, no. 5379, pp. 1001–1005, 1998.
- [50] C. W. Muller, “DNA Recognition by NF κ B and STAT Transcription Factors,” *Ernst Scher. Res. Found. Work.* 34, 2001.
- [51] A. R. Brasier, “The NF- κ B Regulatory Network,” *Cardiovasc. Toxicol.*, vol. 6, no. 2, pp. 111–130, 2006.
- [52] A. Neri *et al.*, “B cell lymphoma-associated chromosomal translocation involves candidate oncogene *lyt-10*, homologous to NF- κ B p50,” *Cell*, vol. 67, no. 6, pp. 1075–1087, 1991.
- [53] R. Meyer *et al.*, “Cloning of the DNA-binding subunit of human nuclear factor kappa B: the level of its mRNA is strongly regulated by phorbol ester or tumor necrosis factor alpha,” *Proc. Natl. Acad. Sci. U. S. A.*, vol. 88, no. 3, pp. 966–70, 1991.
- [54] M. Kieran *et al.*, “The DNA binding subunit of NF- κ B is identical to factor KBF1 and homologous to the *rel* oncogene product,” *Cell*, vol. 62, no. 5, pp. 1007–1018, 1990.
- [55] G. P. Nolan, S. Ghosh, H. C. Liou, P. Tempst, and D. Baltimore, “DNA binding and I kappa B inhibition of the cloned p65 subunit of NF-kappa B, a *rel*-related polypeptide,” *Cell*, vol. 64, no. 5, pp. 961–9, 1991.
- [56] D. W. Ballard *et al.*, “The 65-kDa subunit of human NF-kappa B functions as a potent transcriptional activator and a target for v-Rel-mediated repression,” *Proc. Natl. Acad. Sci. U. S. A.*, vol. 89, no. 5, pp. 1875–9, 1992.
- [57] U. Sieben, G. Franzoso, and K. Brown, “STRUCTURE, REGULATION AND FUNCTION OF

-
- NF-1d3," *Annu. Rev. Cell Biol.*, vol. 10, pp. 405–55, 1994.
- [58] M. J. Kang *et al.*, "NF- κ B Activates Transcription of the RNA-Binding Factor HuR, via PI3K-AKT Signaling, to Promote Gastric Tumorigenesis," *Gastroenterology*, vol. 135, no. 6, p. 2030–2042.e3, 2008.
- [59] T. D. Gilmore, "Introduction to NF- κ B: players, pathways, perspectives," *Oncogene*, vol. 25, no. 51, pp. 6680–6684, 2006.
- [60] N. D. Perkins, "Integrating cell-signalling pathways with NF-kappaB and IKK function," *Nat. Rev. Mol. Cell Biol.*, vol. 8, no. 1, pp. 49–62, 2007.
- [61] B. Samarasinghe, "The Hallmarks of Cancer 8: Tumor-Promoting Inflammation," *Sci. Am. Blog Netw.*, pp. 1–10, 2014.
- [62] B. Modrek, A. Resch, C. Grasso, and C. Lee, "Genome-wide detection of alternative splicing in expressed sequences of human genes," *Nucleic Acids Res.*, vol. 29, no. 13, pp. 2850–2859, 2001.
- [63] H. Zhu, M. N. Hinman, R. A. Hasman, P. Mehta, and H. Lou, "Regulation of neuron-specific alternative splicing of neurofibromatosis type 1 pre-mRNA," *Mol. Cell. Biol.*, vol. 28, no. 4, pp. 1240–51, 2008.
- [64] Y. I. G. Chen, R. E. Moore, H. Y. Ge, M. K. Young, T. D. Lee, and S. W. Stevens, "Proteomic analysis of in vivo-assembled pre-mRNA splicing complexes expands the catalog of participating factors," *Nucleic Acids Res.*, vol. 35, no. 12, pp. 3928–3944, 2007.
- [65] J. M. Izquierdo, "Hu antigen R (HuR) functions as an alternative pre-mRNA splicing regulator of Fas apoptosis-promoting receptor on exon definition," *J. Biol. Chem.*, vol. 283, no. 27, pp. 19077–19084, 2008.
- [66] W. Zhao *et al.*, "HuR and TIA1/TIAL1 are involved in regulation of alternative splicing of SIRT1 pre-mRNA," *Int. J. Mol. Sci.*, vol. 15, no. 2, pp. 2946–2958, 2014.
- [67] K. Abdelmohsen *et al.*, "Phosphorylation of HuR by Chk2 Regulates SIRT1 Expression," *Mol. Cell*, vol. 25, no. 4, pp. 543–557, 2007.
- [68] S. Lebedeva *et al.*, "Transcriptome-wide Analysis of Regulatory Interactions of the RNA-Binding Protein HuR," *Mol. Cell*, vol. 43, no. 3, pp. 340–352, 2011.
- [69] M. Dutertre *et al.*, "A recently evolved class of alternative 3'-terminal exons involved in cell cycle regulation by topoisomerase inhibitors," *Nat. Commun.*, vol. 5, p. 3395, 2014.
- [70] J. Naipauer *et al.*, "The use of alternative polyadenylation sites renders integrin β 1 (Itgb1) mRNA isoforms with differential stability during mammary gland development," *Biochem. J.*, vol. 454, no. 2, pp. 345–57, 2013.
- [71] M. D. Diaz-Muñoz *et al.*, "The RNA-binding protein HuR is essential for the B cell antibody response," *Nat. Immunol.*, vol. 16, no. 4, pp. 415–25, 2015.
- [72] Y. Akaike *et al.*, "HuR Regulates Alternative Splicing of the TRA2 β Gene in Human Colon Cancer Cells under Oxidative Stress," *Mol. Cell. Biol.*, vol. 34, no. 15, pp. 2857–73, 2014.

-
- [73] W. Al-Ahmadi, M. Al-Ghamdi, L. Al-Haj, M. Al-Saif, and K. S. A. Khabar, "Alternative polyadenylation variants of the RNA binding protein, HuR: abundance, role of AU-rich elements and auto-Regulation," *Nucleic Acids Res.*, vol. 37, no. 11, pp. 3612–3624, Jun. 2009.
- [74] C. Denkert *et al.*, "Expression of the ELAV-like protein HuR in human colon cancer: association with tumor stage and cyclooxygenase-2.," *Mod. Pathol.*, vol. 19, no. 9, pp. 1261–9, 2006.
- [75] R. Calaluce *et al.*, "The RNA binding protein HuR differentially regulates unique subsets of mRNAs in estrogen receptor negative and estrogen receptor positive breast cancer.," *BMC Cancer*, vol. 10, p. 126, 2010.
- [76] I. Kotta-Loizou, S. N. Vasilopoulos, R. H. A. Coutts, and S. Theocharis, "Current Evidence and Future Perspectives on HuR and Breast Cancer Development, Prognosis, and Treatment," *Neoplasia*, vol. 18, no. 11, pp. 674–688, 2016.
- [77] L. A. Licata, C. L. Hostetter, J. Crismale, A. Sheth, and J. C. Keen, "The RNA-binding protein HuR regulates GATA3 mRNA stability in human breast cancer cell lines," *Breast Cancer Res. Treat.*, vol. 122, no. 1, pp. 55–63, 2010.
- [78] H. Janakiraman *et al.*, "Repression of caspase-3 and RNA-binding protein HuR cleavage by cyclooxygenase-2 promotes drug resistance in oral squamous cell carcinoma," *Oncogene*, no. October, pp. 1–12, 2016.
- [79] F. Baldan *et al.*, "Identification of tumorigenesis-related mRNAs associated with RNA-binding protein HuR in thyroid cancer cells," *Oncotarget*, vol. 7, no. 39, pp. 63388–63407, 2016.
- [80] P. Anderson, "Post-transcriptional regulons coordinate the initiation and resolution of inflammation.," *Nat. Rev. Immunol.*, vol. 10, no. 1, pp. 24–35, 2010.
- [81] M. M. Gubin *et al.*, "Conditional knockout of the RNA-binding protein HuR in CD4⁺ T cells reveals a gene dosage effect on cytokine production," *Mol. Med.*, vol. 20, pp. 93–108, Mar. 2014.
- [82] A. Yiakouvaki, M. Dimitriou, I. Karakasiliotis, C. Eftychi, S. Theocharis, and D. L. Kontoyiannis, "Myeloid cell expression of the RNA-binding protein HuR protects mice from pathologic inflammation and colorectal carcinogenesis," *J. Clin. Invest.*, vol. 122, no. 1, pp. 48–61, 2012.
- [83] A. Giammanco *et al.*, "Intestinal epithelial HuR modulates distinct pathways of proliferation and apoptosis and attenuates small intestinal and colonic tumor development," *Cancer Res.*, vol. 74, no. 18, pp. 5322–5335, 2014.
- [84] T. Herjan *et al.*, "HuR is required for IL-17-induced Act1-mediated CXCL1 and CXCL5 mRNA stabilization.," *J. Immunol.*, vol. 191, no. 2, pp. 640–9, 2013.
- [85] J. Chen *et al.*, "Posttranscriptional gene regulation of IL-17 by the RNA-binding protein HuR is required for initiation of experimental autoimmune encephalomyelitis.," *J. Immunol.*, vol. 191, no. 11, pp. 5441–5450, 2013.

-
- [86] C. Wheeler *et al.*, "Sex hormone-dependent attenuation of EAE in a transgenic mouse with astrocytic expression of the RNA regulator HuR," *J. Neuroimmunol.*, vol. 246, no. 1–2, pp. 34–37, 2012.
- [87] H. Park *et al.*, "A distinct lineage of CD4 T cells regulates tissue inflammation by producing interleukin 17.," *Nat. Immunol.*, vol. 6, no. 11, pp. 1133–41, 2005.
- [88] L. A. Tesmer, S. K. Lundy, S. Sarkar, and D. A. Fox, "Th17 cells in human disease," *Immunol Rev*, vol. 223, pp. 87–113, 2008.
- [89] a Skliris *et al.*, "Neuroprotection requires the functions of the RNA-binding protein HuR.," *Cell Death Differ.*, vol. 22, no. 5, pp. 1–16, 2014.
- [90] P. C. Chu, H. C. Chuang, S. K. Kulp, and C. S. Chen, "The mRNA-stabilizing factor HuR protein is targeted by β -TrCP protein for degradation in response to glycolysis inhibition," *J. Biol. Chem.*, vol. 287, no. 52, pp. 43639–43650, 2012.
- [91] W. Wang *et al.*, "HuR regulates p21 mRNA stabilization by UV light," *Mol. Cell. Biol.*, vol. 20, no. 3, pp. 760–769, Feb. 2000.
- [92] R. Upadhyay, S. Sanduja, V. Kaza, and D. A. Dixon, "Genetic polymorphisms in RNA binding proteins contribute to breast cancer survival," *Int. J. Cancer*, vol. 132, no. 3, pp. 128–138, 2013.
- [93] C. Zhang *et al.*, "Cytoplasmic expression of the ELAV-like protein HuR as a potential prognostic marker in esophageal squamous cell carcinoma," *Tumor Biol.*, vol. 35, no. 1, pp. 73–80, 2014.
- [94] D. Jeong-Dan Cha, ShengJin Li, MD, PhD, In-Ho Cha, "Association between expression of embryonic lethal abnormal vision-like protein HuR and cyclooxygenase-2 in oral squamous cell carcinoma," *Head Neck*, vol. 36, no. 10, p. 1391, 2014.
- [95] D. P. Sun *et al.*, "Clinicopathological significance of HuR expression in gallbladder carcinoma: With special emphasis on the implications of its nuclear and cytoplasmic expression," *Tumor Biol.*, vol. 34, no. 5, pp. 3059–3069, 2013.
- [96] Z. Zhu *et al.*, "Cytoplasmic HuR expression correlates with P-gp, HER-2 positivity, and poor outcome in breast cancer," *Tumor Biol.*, vol. 34, no. 4, pp. 2299–2308, 2013.
- [97] M.-J. Chae *et al.*, "Chemical inhibitors destabilize HuR binding to the AU-rich element of TNF- α mRNA," *Exp. Mol. Med.*, vol. 41, no. 11, pp. 824–831, Nov. 2009.
- [98] V. G. D'Agostino, V. Adami, and A. Provenzani, "A Novel High Throughput Biochemical Assay to Evaluate the HuR Protein-RNA Complex Formation," *PLoS One*, vol. 8, no. 8, pp. 1–9, 2013.
- [99] V. G. D'Agostino *et al.*, "Dihydrotanshinone-I interferes with the RNA-binding activity of HuR affecting its post-transcriptional function.," *Sci. Rep.*, vol. 5, no. October, p. 16478, 2015.
- [100] X. Wu *et al.*, "Identification and Validation of Novel Small Molecule Disruptors of HuR-

-
- mRNA Interaction," *ACS Chem. Biol.*, Mar. 2015.
- [101] Z. Wang, A. Bhattacharya, and D. N. Ivanov, "Identification of Small-Molecule Inhibitors of the HuR/RNA Interaction using a fluorescence polarization screening assay followed by NMR validation," *PLoS One*, vol. 10, no. 9, pp. 1–13, 2015.
- [102] F. Bollmann *et al.*, "Resveratrol post-transcriptionally regulates pro-inflammatory gene expression via regulation of KSRP RNA binding activity," *Nucleic Acids Res.*, vol. 42, no. 20, pp. 12555–12569, 2014.
- [103] R. Muralidharan *et al.*, "Folate receptor-targeted nanoparticle delivery of HuR-RNAi suppresses lung cancer cell proliferation and migration," *J. Nanobiotechnology*, vol. 14, no. 1, p. 47, 2016.
- [104] R. Muralidharan, J. Panneerselvam, A. Chen, Y. D. Zhao, A. Munshi, and R. Ramesh, "HuR-targeted nanotherapy in combination with AMD3100 suppresses CXCR4 expression, cell growth, migration and invasion in lung cancer," *Cancer Gene Ther.*, vol. 22, no. 12, pp. 581–590, 2015.
- [105] J. Guo *et al.*, "Inhibiting cytoplasmic accumulation of HuR synergizes genotoxic agents in urothelial carcinoma of the bladder," vol. 7, no. 29.
- [106] Y.-C. Cheng *et al.*, "MPT0B098, a Novel Microtubule Inhibitor That Destabilizes the Hypoxia-Inducible Factor-1 mRNA through Decreasing Nuclear-Cytoplasmic Translocation of RNA-Binding Protein HuR," *Mol. Cancer Ther.*, vol. 12, no. 7, pp. 1202–1212, 2013.
- [107] S. Galban *et al.*, "RNA-Binding Proteins HuR and PTB Promote the Translation of Hypoxia-Inducible Factor 1," *Mol. Cell. Biol.*, vol. 28, no. 1, pp. 93–107, 2008.
- [108] J. Y. Lee *et al.*, "A novel cantharidin analog N-Benzylcantharidinamide reduces the expression of MMP-9 and invasive potentials of Hep3B via inhibiting cytosolic translocation of HuR," *Biochem. Biophys. Res. Commun.*, vol. 447, no. 2, pp. 371–377, 2014.
- [109] L. Sun *et al.*, "Triptolide inhibits COX-2 expression by regulating mRNA stability in TNF- α -treated A549 cells," *Biochem. Biophys. Res. Commun.*, vol. 416, no. 1–2, pp. 99–105, 2011.
- [110] Q. Liu *et al.*, "Triptolide impairs dendritic cell migration by inhibiting CCR7 and COX-2 expression through PI3-K/Akt and NF- κ B pathways," *Mol. Immunol.*, vol. 44, no. 10, pp. 2686–2696, 2007.
- [111] Y. S. Hwang, K.-K. Park, and W.-Y. Chung, "Kalopanaxsaponin A inhibits the invasion of human oral squamous cell carcinoma by reducing metalloproteinase-9 mRNA stability and protein trafficking," *Biol. Pharm. Bull.*, vol. 35, no. 3, pp. 289–300, 2012.
- [112] B. Annabi, J. C. Currie, A. Moghrabi, and R. Béliveau, "Inhibition of HuR and MMP-9 expression in macrophage-differentiated HL-60 myeloid leukemia cells by green tea polyphenol EGCg," *Leuk. Res.*, vol. 31, no. 9, pp. 1277–1284, 2007.

-
- [113] H. Cao *et al.*, "Green tea increases anti-inflammatory tristetraproline and decreases pro-inflammatory tumor necrosis factor mRNA levels in rats.," *J. Inflamm. (Lond).*, vol. 4, p. 1, 2007.
- [114] K. R. Houser, D. K. Johnson, and F. T. Ishmael, "Anti-inflammatory effects of methoxyphenolic compounds on human airway cells," *J. Inflamm.*, vol. 9, no. 1, p. 6, 2012.
- [115] H. M. Chang *et al.*, "Structure Elucidation and Total Synthesis of New Tanshinones Isolated from *Salvia miltiorrhiza* Bunge (Danshen)," *J. Org. Chem.*, vol. 55, no. 11, pp. 3537–3543, 1990.
- [116] H. J. Sung, S. M. Choi, Y. Yoon, and K. S. An, "Tanshinone IIA, an ingredient of *Salvia miltiorrhiza* BUNGE, induces apoptosis in human leukemia cell lines through the activation of caspase-3," *Exp. Mol. Med.*, vol. 31, no. 4, pp. 174–178, 1999.
- [117] W. W. L. C. and C. F.-C. Wu Lung, "Cytotoxic Activities of Tanshinones against Human Carcinoma Cell Lines," *Am. J. Chin. Med.*, vol. XIX, no. 8 August 1991, pp. 207–216, 1991.
- [118] S. I. Jang *et al.*, "Tanshinone IIA from *Salvia miltiorrhiza* inhibits inducible nitric oxide synthase expression and production of TNF- α , IL-1 β and IL-6 in activated RAW 264.7 cells.," *Planta Med.*, no. 69, pp. 1057–1059, 2003.
- [119] J. Xie *et al.*, "The antitumor effect of tanshinone IIA on anti-proliferation and decreasing VEGF/VEGFR2 expression on the human non-small cell lung cancer A549 cell line," *Acta Pharm. Sin. B*, vol. 5, no. 6, pp. 554–563, 2015.
- [120] C.-Y. Lee *et al.*, "Anticancer effects of tanshinone I in human non-small cell lung cancer," *Mol. Cancer Ther.*, vol. 7, no. 11, pp. 3527–3538, 2008.
- [121] J. W. Park *et al.*, "15,16-Dihydrotanshinone I, a major component from *Salvia miltiorrhiza* Bunge (Danshen), inhibits rabbit platelet aggregation by suppressing intracellular calcium mobilization," *Arch. Pharm. Res.*, vol. 31, no. 1, pp. 47–53, 2008.
- [122] X. Wang, S. L. Morris-Natschke, and K. H. Lee, "New developments in the chemistry and biology of the bioactive constituents of Tanshen," *Med. Res. Rev.*, vol. 27, no. 1, pp. 133–148, 2007.
- [123] L. Wang *et al.*, "Dihydrotanshinone I induced apoptosis and autophagy through caspase dependent pathway in colon cancer," *Phytomedicine*, vol. 22, no. 12, pp. 1079–1087, 2015.
- [124] L. Wang *et al.*, "Dihydrotanshinone I induces p53-independent but ROS-dependent apoptosis in colon cancer cells," *Life Sci.*, vol. 93, no. 8, pp. 344–351, 2013.
- [125] J. Li, C. Mi, J. Ma, K. S. Wang, J. J. Lee, and X. Jin, "Dihydrotanshinone I inhibits the translational expression of hypoxia-inducible factor-1 α ," *Chem. Biol. Interact.*, vol. 240, pp. 48–58, 2015.
- [126] F. Wang, J. Ma, K. S. Wang, C. Mi, J. J. Lee, and X. Jin, "Blockade of TNF- α -induced NF- κ B signaling pathway and anti-cancer therapeutic response of dihydrotanshinone I,"

-
- Int. Immunopharmacol.*, vol. 28, no. 1, pp. 764–772, 2015.
- [127] C. Zucal *et al.*, “Targeting the multifaceted HuR protein, benefits and caveats,” *Curr. Drug Targets*, vol. 16, no. 5, pp. 499–515, 2015.
- [128] X. Ouyang *et al.*, “Protective effect of *Salvia miltiorrhiza* on angiotensin II-induced hypertrophic responses in neonatal rat cardiac cells,” *Jpn. J. Pharmacol.*, vol. 87, no. 4, pp. 289–96, 2001.
- [129] V. G. D’Agostino *et al.*, “Dihydrotanshinone-I interferes with the RNA-binding activity of HuR affecting its post-transcriptional function,” *Sci. Rep.*, vol. 5, 2015.
- [130] P. Lal *et al.*, “Regulation of HuR structure and function by dihydrotanshinone-I,” *Nucleic Acids Res.*, 2017.
- [131] T. Peritz *et al.*, “Immunoprecipitation of mRNA-protein complexes,” *Nat. Protoc.*, vol. 1, no. 2, pp. 577–580, 2006.
- [132] X. Guo and R. S. Hartley, “HuR contributes to cyclin E1 deregulation in MCF-7 breast cancer cells,” *Cancer Res.*, vol. 66, no. 16, pp. 7948–7956, Aug. 2006.
- [133] C. K. Chang and T. H. Huang, “Untangling the structure of the TDP-43 N-terminal domain,” *FEBS J.*, vol. 283, no. 7, pp. 1239–1241, 2016.
- [134] H. Wang, F. Zeng, H. Liu, M. Teng, and X. Li, “Crystal structure of two tandem RNA recognition motifs of Human antigen R,” *To be Publ.*, p. null-null, Mar. 2012.
- [135] K. L. Morrison and G. A. Weiss, “Combinatorial alanine-scanning,” *Curr. Opin. Chem. Biol.*, vol. 5, no. 3, pp. 302–307, Jun. 2001.
- [136] F. F. Blanco *et al.*, “Impact of HuR inhibition by the small molecule MS-444 on colorectal cancer cell tumorigenesis,” *Oncotarget*, vol. 7, no. 45, 2016.
- [137] S. Lal, Cheung, E.C., Zarei, M., Preet, L. et al. (2017) C. knockout of the H. gene Causes, lethal phenotype. *M. C. Res.*, and Doi:10.1158/1541-7786.MCR-16-0361., “CRISPR knockout of the HuR gene causes a xenograft lethal phenotype.”
- [138] X. C. Fan and J. A. Steitz, “HNS, a nuclear-cytoplasmic shuttling sequence in HuR,” *Proc. Natl. Acad. Sci. U. S. A.*, vol. 95, no. 26, pp. 15293–15298, Dec. 1998.
- [139] J. L. Dean, R. Wait, K. R. Mahtani, G. Sully, A. R. Clark, and J. Saklatvala, “The 3’ untranslated region of tumor necrosis factor alpha mRNA is a target of the mRNA-stabilizing factor HuR,” *Mol. Cell. Biol.*, vol. 21, no. 3, pp. 721–730, Feb. 2001.
- [140] C. Y. Chen *et al.*, “AU binding proteins recruit the exosome to degrade ARE-containing mRNAs,” *Cell*, vol. 107, no. 4, pp. 451–464, 2001.
- [141] C. Barreau, L. Paillard, and H. B. Osborne, “AU-rich elements and associated factors: Are there unifying principles?,” *Nucleic Acids Res.*, vol. 33, no. 22, pp. 7138–7150, 2005.
- [142] G. Stoecklin, T. Mayo, and P. Anderson, “ARE-mRNA degradation requires the 5’-3’ decay pathway,” *EMBO Rep.*, vol. 7, no. 1, pp. 72–7, 2006.

-
- [143] T. Bakheet, M. Frevel, B. R. Williams, W. Greer, and K. S. Khabar, "ARED: human AU-rich element-containing mRNA database reveals an unexpectedly diverse functional repertoire of encoded proteins.," *Nucleic Acids Res.*, vol. 29, no. 1, pp. 246–54, 2001.
- [144] C. Tiedje *et al.*, "The RNA-binding protein TTP is a global post-transcriptional regulator of feedback control in inflammation," *Nucleic Acids Res.*, vol. 44, no. 15, pp. 7418–7440, 2016.
- [145] L.-Q. Qiu, W. S. Lai, A. Bradbury, D. C. Zeldin, and P. J. Blakeshear, "Tristetraprolin (TTP) coordinately regulates primary and secondary cellular responses to proinflammatory stimuli," *J. Leukoc. Biol.*, vol. 97, no. 4, pp. 723–736, 2015.
- [146] G. Grigoriadis *et al.*, "The Rel subunit of NF-kappaB-like transcription factors is a positive and negative regulator of macrophage gene expression: distinct roles for Rel in different macrophage populations.," *EMBO J.*, vol. 15, no. 24, pp. 7099–107, 1996.
- [147] E. Hitti *et al.*, "Mitogen-activated protein kinase-activated protein kinase 2 regulates tumor necrosis factor mRNA stability and translation mainly by altering tristetraprolin expression, stability, and binding to adenine/uridine-rich element.," *Mol. Cell. Biol.*, vol. 26, no. 6, pp. 2399–2407, 2006.
- [148] R. Cheng, J. Chen, Y. Wang, Y. Ge, Z. Huang, and G. Zhang, "Dihydrotanshinone induces apoptosis of SGC7901 and MGC803 cells via activation of JNK and p38 signalling pathways," *Pharm. Biol.*, vol. 54, no. 12, pp. 3019–3025, 2016.
- [149] J. L. E. Dean, R. Wait, K. R. Mahtani, A. R. Clark, J. Saklatvala, and G. Sully, "The 3' Untranslated Region of Tumor Necrosis Factor Alpha mRNA Is a Target of the mRNA-Stabilizing Factor HuR The 3' Untranslated Region of Tumor Necrosis Factor Alpha mRNA Is a Target of the mRNA-Stabilizing Factor HuR Downloaded from <http://mcb.asm.org/>," vol. 21, no. 3, pp. 721–730, 2001.
- [150] K. De Filippo *et al.*, "Mast cell and macrophage chemokines CXCL1 / CXCL2 control the early stage of neutrophil recruitment during tissue inflammation," *Blood*, vol. 121, no. 24, pp. 4930–4937, 2013.
- [151] A. Zlotnik and O. Yoshie, "The Chemokine Superfamily Revisited," *Immunity*, vol. 36, no. 5, pp. 705–712, 2012.
- [152] X. Zhang *et al.*, "CXCL10 plays a key role as an inflammatory mediator and a non-invasive biomarker of non-alcoholic steatohepatitis," *J. Hepatol.*, vol. 61, no. 6, pp. 1365–1375, 2014.
- [153] I. Loez De Silanes *et al.*, "Role of the RNA-binding protein HuR in colon carcinogenesis," *Oncogene*, vol. 22, pp. 7146–7154, 2003.
- [154] H. Ronkainen, M. H. Vaarala, P. Hirvikoski, and A. Ristimäki, "HuR expression is a marker of poor prognosis in renal cell carcinoma," *Tumor Biol.*, vol. 32, no. 3, pp. 481–487, 2011.
- [155] X. Wu *et al.*, "Abstract 2449: Targeting an 'undruggable' RNA-binding protein: Discovery of small molecule inhibitors of HuR for novel breast cancer therapy," *Cancer Res.*, vol.

-
- 75, no. 15 Supplement, pp. 2449–2449, Aug. 2015.
- [156] J. Viiri *et al.*, “Autophagy Activation Clears ELAVL1/HuR-Mediated Accumulation of SQSTM1/p62 during Proteasomal Inhibition in Human Retinal Pigment Epithelial Cells,” *PLoS One*, vol. 8, no. 7, pp. 1–16, 2013.
- [157] M. R. Arkin, M. A. Glicksman, H. Fu, J. J. Havel, and Y. Du, “Inhibition of Protein-Protein Interactions: Non-Cellular Assay Formats,” in *Assay Guidance Manual*, G. S. Sittampalam, N. P. Coussens, H. Nelson, M. Arkin, D. Auld, C. Austin, B. Bejcek, M. Glicksman, J. Inglese, P. W. Iversen, Z. Li, J. McGee, O. McManus, L. Minor, A. Napper, J. M. Peltier, T. Riss, O. J. Trask, and J. Weidner, Eds. Bethesda (MD): Eli Lilly & Company and the National Center for Advancing Translational Sciences, 2004.
- [158] L. Lu *et al.*, “Hu antigen R (HuR) is a positive regulator of the RNA-binding proteins TDP-43 and FUS/TLS: Implications for amyotrophic lateral sclerosis,” *J. Biol. Chem.*, vol. 289, no. 46, pp. 31792–31804, 2014.
- [159] X. H. Tian and J. H. Wu, “Tanshinone derivatives: A patent review (January 2006 - September 2012),” *Expert Opin. Ther. Pat.*, vol. 23, no. 1, pp. 19–29, 2013.
- [160] S. L. Tsai *et al.*, “Anti-tumor potential of 15,16-dihydrotanshinone I against breast adenocarcinoma through inducing G1 arrest and apoptosis,” *Biochem. Pharmacol.*, vol. 74, no. 11, pp. 1575–1586, 2007.
- [161] Y. Ye, W. Xu, W. Zhong, Y. Li, and C. Wang, “Combination treatment with dihydrotanshinone I and irradiation enhances apoptotic effects in human cervical cancer by HPV E6 down-regulation and caspases activation,” *Mol. Cell. Biochem.*, vol. 363, no. 1–2, pp. 191–202, 2012.
- [162] J.-J. Liu, H.-H. Wu, T.-H. Chen, W. Leung, and Y.-C. Liang, “15,16-Dihydrotanshinone I from the Functional Food *Salvia miltiorrhiza* Exhibits Anticancer Activity in Human HL-60 Leukemia Cells: in Vitro and in Vivo Studies,” *Int. J. Mol. Sci.*, vol. 16, no. 8, pp. 19387–19400, 2015.
- [163] I. T. Nizamutdinova *et al.*, “Tanshinone I suppresses growth and invasion of human breast cancer cells, MDA-MB-231, through regulation of adhesion molecules,” *Carcinogenesis*, vol. 29, no. 10, pp. 1885–1892, 2008.
- [164] N. S. Levy, S. Chung, H. Furneaux, and A. P. Levy, “Hypoxic stabilization of vascular endothelial growth factor mRNA by the RNA-binding protein HuR,” *J. Biol. Chem.*, vol. 273, no. 11, pp. 6417–6423, Mar. 1998.
- [165] D. a Dixon *et al.*, “Altered expression of the mRNA stability factor HuR promotes cyclooxygenase-2 expression in colon cancer cells,” *Cell*, vol. 108, no. 11, pp. 1657–1665, 2001.
- [166] L. Cerofolini *et al.*, “Examination of matrix metalloproteinase-1 in solution: a preference for the pre-collagenolysis state,” *J. Biol. Chem.*, vol. 288, no. 42, pp. 30659–30671, Oct. 2013.
- [167] U. H. Jin *et al.*, “Tanshinone IIA from *Salvia miltiorrhiza* BUNGE inhibits human aortic

-
- smooth muscle cell migration and MMP-9 activity through AKT signaling pathway," *J Cell Biochem*, vol. 104, no. 1, pp. 15–26, 2008.
- [168] Y. Xing, J. Tu, L. Zheng, L. Guo, and T. Xi, "Anti-angiogenic effect of tanshinone IIA involves inhibition of the VEGF/VEGFR2 pathway in vascular endothelial cells," *Oncol. Rep.*, vol. 33, no. 1, pp. 163–170, 2015.
- [169] D. Cox- *et al.*, "Cryptotanshinone Attenuates Cardiac Fibrosis via," vol. 64, no. 1, pp. 28–37, 2014.
- [170] J. Fan *et al.*, "Chemokine transcripts as targets of the RNA-binding protein HuR in human airway epithelium.," *J. Immunol.*, vol. 186, no. 4, pp. 2482–94, 2011.
- [171] Y. Ke *et al.*, "Erratum: PARP1 promotes gene expression at the post-transcriptional level by modulating the RNA-binding protein HuR," *Nat. Commun.*, vol. 8, p. 15191, 2017.
- [172] J. L. E. Dean, G. Sully, A. R. Clark, and J. Saklatvala, "The involvement of AU-rich element-binding proteins in p38 mitogen-activated protein kinase pathway-mediated mRNA stabilisation," *Cell. Signal.*, vol. 16, no. 10, pp. 1113–1121, 2004.
- [173] S. A. Brooks, J. E. Connolly, and W. F. C. Rigby, "The role of mRNA turnover in the regulation of tristetraprolin expression: evidence for an extracellular signal-regulated kinase-specific, AU-rich element-dependent, autoregulatory pathway.," *J. Immunol.*, vol. 172, no. 12, pp. 7263–7271, 2004.
- [174] C. R. Tchen, M. Brook, J. Saklatvala, and A. R. Clark, "The stability of tristetraprolin mRNA is regulated by mitogen-activated protein kinase p38 and by tristetraprolin itself," *J. Biol. Chem.*, vol. 279, no. 31, pp. 32393–32400, 2004.
- [175] K. R. Mahtani, M. Brook, J. L. Dean, G. Sully, J. Saklatvala, and A. R. Clark, "Mitogen-activated protein kinase p38 controls the expression and posttranslational modification of tristetraprolin, a regulator of tumor necrosis factor alpha mRNA stability.," *Mol. Cell. Biol.*, vol. 21, no. 19, pp. 6461–9, 2001.
- [176] M. Lang *et al.*, "Mo1670 Systemic HuR Inhibition Augments Tumorigenesis in the AOM/DSS Mouse," *Gastroenterology*, vol. 146, no. 5, p. S-632, 2014.
- [177] M. Jimbo *et al.*, "Targeting the mRNA-binding protein HuR impairs malignant characteristics of pancreatic ductal adenocarcinoma cells," *Oncotarget*, vol. 6, no. 29, pp. 27312–27331, 2015.
- [178] C. von Roretz *et al.*, "Apoptotic-induced cleavage shifts HuR from being a promoter of survival to an activator of caspase-mediated apoptosis," *Cell Death Differ.*, pp. 154–168, 2012.
- [179] P. Beauchamp *et al.*, "The cleavage of HuR interferes with its transportin-2-mediated nuclear import and promotes muscle fiber formation.," *Cell Death Differ.*, vol. 17, no. 10, pp. 1588–1599, 2010.
- [180] V. Katsanou *et al.*, "The RNA-binding protein Elavl1/HuR is essential for placental branching morphogenesis and embryonic development.," *Mol. Cell. Biol.*, vol. 29, no.

APPENDIX

TABLE 3 IC-50 values for DHTS and its analogs at 24 & 72 hrs.

	GD041	MB11V	VB062	MFM49	MB39	DHTS
IC50 (μM) 24 hrs	~24.17	9.938	21.079	~9.813	8.813	~3.687
R ²	0.9693	0.9927	0.9734	0.9772	0.9428	0.9972
IC50 (μM) 72 hrs	~29.68	16.12	~32.98	14.22	~11.36	2.564
R ²	0.991	0.99	0.96	0.9945	0.997	0.967

TABLE 4 qPCR Primer sequences

NAME	SEQUENCE 5' to 3' (F and R)
TNFα Human	5'-GGGACCTCTCTAATCAGC 5' TCAGCTTGAGGGTTTGCTAC
VEGF Human	5'-CCGCAGACGTGTAAATGTTCT 5'-CGGCTTGTCACATCTGCAAGTA'
GAPDH Human	5'-CAAGGTCATCCATGACAACTT 5'-GTCCACCACCCTGTTGCTGTA
Zfp36 Mouse	5'-GGACTTTGGAACATAAACTCGGACT 5'-GAAGTAGGTGAGGGTGACAGCTCA
CXCL-2 Mouse	5'-CCACCAACCACCAGGCTACA 5'-GCTTCAGGGTCAAGGCAAAC
CXCL-10 Mouse	5'-TCAGCACCATGAACCCAAG 5'-CTATGGCCCTCATTCTCACTG
18S mouse	5'-GTA ACCCGTTGAACCCATT 5'-CCATCCAATCGGTAGTAGCG

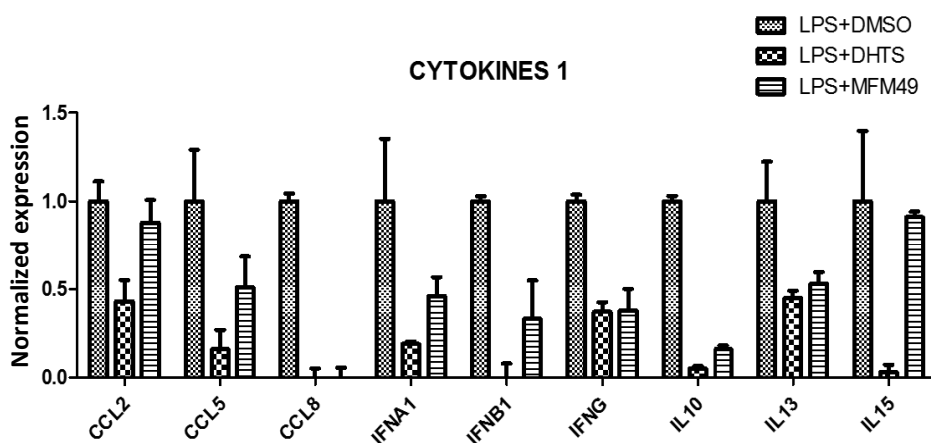
TNFa Taqman	5'-CATCTTCTCAAATTCGAGTGACA 5'-TGGGAGTAGACAAGGTACAACCC
Actin Taqman Mouse	Actin Probe Mix: Mouse ACTB, Applied Biosystems/Thermo Fisher, VIC-labelled #4352341E

TABLE 5 HuR RRM Primers and Muteins Primers

NAME	SEQUENCE 5' to 3' (F and R)
RRM1/2	5'-CCGCATATGATGTCTAATGGTTATG 5'-TATACTCGAGGCGAGAGGAGTGCC
RRM2/3	5'-CCGCATATGATGACCCAGAAGGACGTA 5'-GGCCTCGAGTTTGTGGGACTTGT
RRM1	5'-CCGCATATGATGTCTAATGGTTATG 5'-CCGCTCGAGTACGTCCTTCTGGG
ΔRRM1	5'-CCGCATATGATGTCTAATGGTTATG 5'-GGCCTCGAGCACCTTAATGGTTTTTGAC
RRM2	5'-CCGCATATGATGACCCAGAAGGACGTA 5'-GGCTCGAGTCGCGCTGGCGAGT
RRM3	5'-GGCATATGTCCTCCGGCTGGTGCAT 5'-GGCCTCGAGTTTGTGGGACTTGT
HuR S94A	5'-AACCATTAAGGTGGCGTATGCTCGCCC 5'-GGGCGAGCATA CGCCACCTTAATGGTT
HuR N107A	5'-ATCAAAGACGCCGCTTGTACATCAGC 5'-GCTGATGTACAAGGCGGCGTCTTTGAT
HuR I133A	5'-TTGGGCGGATCGCCAACTCGCGGGTCC 5'-GGACCCGCGAGTTGGCGATCCGCCCAA
HuR N134A	5'-GGGCGGATCATCGCCTCGCGGGTCTC 5'-GAGGACCCGCGAGGCGATGATCCGCC

Supplementary Figures

1.



2.

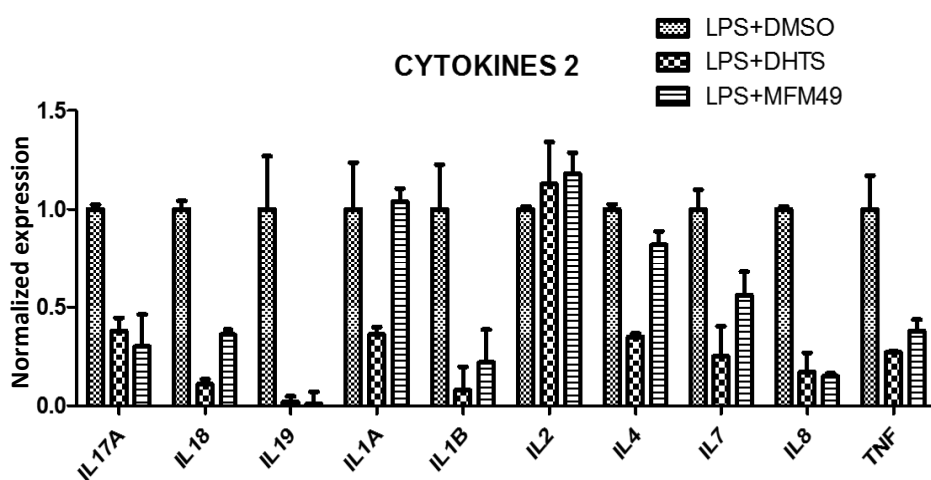


Figure 42 (1 & 2) Evaluation of anti-inflammatory effect of DHTS and MFM49, by checking number of fold reduced target gene, upon LPS co treatment with DHTS and MFM49 application in THP-1 cells (3hrs). The relative expression was normalized with Gapdh. (qPCR Primer used for these targets are not listed). (Dr. Vito D'Agostino has contributed to these figures).

Contribution in Publications

Regulation of HuR structure and function by dihydrotanshinone-I

Lal P et al., Nucleic Acid Res. 2017.....p115.

Dihydrotanshinone-I interferes with the RNA-binding activity of HuR affecting its posttranscriptional function

D'Agostino VG, Lal P et al., Sci. Rep. 2015.....p130.

Regulation of HuR structure and function by dihydrotanshinone-I

Preet Lal^{1,†}, Linda Cerofolini^{2,†}, Vito Giuseppe D'Agostino¹, Chiara Zucal¹, Carmelo Fuccio², Isabelle Bonomo¹, Erik Dassi¹, Stefano Giuntini², Danilo Di Maio^{3,4}, Vikalp Vishwakarma⁵, Ranjan Preet⁵, Sha Neisha Williams⁵, Max S. Fairlamb⁵, Rachel Munk⁶, Elin Lehrmann⁶, Kotb Abdelmohsen⁶, Saioa R. Elezgarai⁷, Claudio Luchinat², Ettore Novellino⁸, Alessandro Quattrone¹, Emiliano Biasini^{1,7}, Leonardo Manzoni⁹, Myriam Gorospe⁶, Dan A. Dixon⁵, Pierfausto Seneci¹⁰, Luciana Marinelli^{8,*}, Marco Fragai^{2,*} and Alessandro Provenzani^{1,*}

¹Centre for Integrative Biology, CIBIO, University of Trento, Trento 38122, Italy, ²Centre for Magnetic Resonance, CERM, University of Florence, Sesto Fiorentino 50019, Italy, ³Scuola Normale Superiore, Pisa 56126, Italy, ⁴Istituto Nazionale di Fisica Nucleare (INFN), Pisa 56127, Italy, ⁵Department of Cancer Biology and University of Kansas Cancer Center, University of Kansas Medical Center, Kansas City, KS 66160, USA, ⁶National Institute on Aging, National Institutes of Health, Baltimore, MD 21224, USA, ⁷Istituto di Ricerche Farmacologiche Mario Negri, Milan 20156, Italy, ⁸Department of Pharmacy, University of Naples Federico II, Naples 80138, Italy, ⁹Istituto di Scienze e Tecnologie Molecolari (ISTM), CNR, Milan 20133, Italy and ¹⁰Dipartimento di Chimica, Università degli Studi di Milano, Milan 20133, Italy

Received January 30, 2017; Revised July 04, 2017; Editorial Decision July 06, 2017; Accepted July 07, 2017

ABSTRACT

The Human antigen R protein (HuR) is an RNA-binding protein that recognizes U/AU-rich elements in diverse RNAs through two RNA-recognition motifs, RRM1 and RRM2, and post-transcriptionally regulates the fate of target RNAs. The natural product dihydrotanshinone-I (DHTS) prevents the association of HuR and target RNAs *in vitro* and in cultured cells by interfering with the binding of HuR to RNA. Here, we report the structural determinants of the interaction between DHTS and HuR and the impact of DHTS on HuR binding to target mRNAs transcriptome-wide. NMR titration and Molecular Dynamics simulation identified the residues within RRM1 and RRM2 responsible for the interaction between DHTS and HuR. RNA Electromobility Shifts and Alpha Screen Assays showed that DHTS interacts with HuR through the same binding regions as target RNAs, stabilizing HuR in a locked conformation that hampers RNA binding competitively. HuR ribonucleoprotein immunoprecipitation followed by microarray (RIP-chip) analysis showed that DHTS

treatment of HeLa cells paradoxically enriched HuR binding to mRNAs with longer 3'UTR and with higher density of U/AU-rich elements, suggesting that DHTS inhibits the association of HuR to weaker target mRNAs. *In vivo*, DHTS potently inhibited xenograft tumor growth in a HuR-dependent model without systemic toxicity.

INTRODUCTION

The Human antigen R (ELAVL1, HuR) is an ubiquitously expressed RNA-binding protein, belonging to the ELAVL (Embryonic Lethal Abnormal Vision)-like family, that preferentially binds U- and AU-rich elements (AREs) abundant in the 3' untranslated regions (3'UTRs) of certain mRNAs. It is mainly localized within the nucleus (90%), where it exerts post-transcriptional functions such as splicing (1–4) and alternative polyadenylation (5–7), and is able to shuttle to the cytoplasm, where it mainly regulates the fate of target RNAs (8). HuR regulates cellular responses to differentiation, senescence, inflammatory factors, and immune stimuli by tightly controlling the post-transcriptional fate of specific mRNAs (9–12). Notably, HuR binds to and regulates the half-life of mRNAs and/or the translation of

*To whom correspondence should be addressed. Tel: +39 046 1283094; Fax: +39 046 1283239; Email: alessandro.provenzani@unitn.it
Correspondence may also be addressed to Marco Fragai. Tel: +39 055 4574261; Fax: +39 055 4574923; Email: fragai@cerm.unifi.it
Correspondence may also be addressed to Luciana Marinelli. Tel: +39 081 679899; Fax: +39 081 676569; Email: lmarinel@unina.it

[†]These authors contributed equally to this work as first authors.

mRNAs encoding key inflammatory cytokines and interleukins, such as tumor necrosis factor- α (TNF α) (13) and interleukin IL-1 β , IL-3 (14), IL-6 (15), IL-8, IL-10, IL-4, CXCL1 (16–18), in turn governing the development and maturation of B and T lymphocytes (19,20). HuR is highly expressed in many cancer types, and is believed to promote tumorigenesis by interacting with mRNAs encoding proteins implicated in cell proliferation and survival, angiogenesis, invasion, pharmacoresistance and metastasis (21–27). The role of HuR in inflammation and cancer has prompted the search for inhibitors/modulators to interfere with its biological activity (28–32).

A number of natural and synthetic molecules have been found to interfere with the formation of HuR/mRNA complexes *in vitro* (29,32–35). The structural basis of the interaction of such molecules with HuR is still poorly characterized. HuR contains three highly conserved RNA recognition motifs (RRMs) among which the first two, RRM1 and RRM2, bind with high affinity to U/AU-rich RNA (36). By contrast, the third domain, RRM3, contributes to the interaction of HuR with poly(A) tails of target mRNA, and is believed to be involved in mRNA-induced cooperative assembly of HuR oligomers (37) (Figure 1A). Each RRM domain adopts a β_1 - α_1 - β_2 - β_3 - α_2 - β_4 topology with the two α -helices packed in an antiparallel four-stranded β -sheet. Residues at conserved positions located on β -strands 1 and 3 are essential for mRNA binding, and are either involved in stacking interactions with mRNA bases or inserted between two sugar rings (38). At present, two crystal structures of the isolated RRM1 domain (PDB codes 3HI9 and 4FXV (39)) and two of the RRM1–RRM2 domains (PDB codes 4ED5 (40) and 4EGL) are available in the Protein Data Bank (PDB). Conformational changes occurring on the tandem RRM1–RRM2 domains are crucial for mRNA binding (40). As suggested by the crystal structures, the tandem construct adopts an ‘open’ conformation in the free form and a ‘closed’ conformation when the RRM1 and RRM2 domains bind mRNA (Figure 1B and C). This hypothesis is supported by SAXS data that show an equilibrium among ‘closed’ and ‘open’ conformations for HuR in solution, in the absence of mRNA. When a target mRNA sequence is present, the two domains form a stable complex with mRNA and adopt a ‘closed’ globular conformation around the mRNA strand (41).

Dihydroanthranone-I (DHTS) is a natural compound present in *Salvia miltiorrhiza* that interferes with the formation of HuR/RNA complexes (31). However, there is currently no detailed information about the specific interaction of DHTS with HuR or about the perturbations of the RNA-binding abilities of HuR transcriptome-wide. Here, we report the analysis of the interaction between DHTS and HuR by NMR, Molecular Dynamics simulation, and mutagenesis experiments. We have characterized the internal dynamics of the HuR RRM1–RRM2 domains, and have used this information to analyze the role of the two domains in ligand binding. In this respect, the identification of the flexibility of the two domains, RRM1 and RRM2, was particularly interesting. Moreover, ribonucleoprotein immunoprecipitation followed by microarray analysis revealed that DHTS dysregulates HuR by enriching HuR binding towards longer mRNAs highly rich in U/AU-rich 3'UTRs,

including the mRNAs that encode apoptotic and cell-cycle regulatory proteins in cells, and inhibits cancer cell growth *in vivo*.

MATERIALS AND METHODS

Cell lines and reagents

Human cervical adenocarcinoma HeLa cells (ATCC[®] CCL2[™]), colon carcinoma cells HCT116 (ATCC; Manassas, VA) were cultured in standard Dulbecco's Modified Eagle Medium (DMEM) supplemented with 10% fetal bovine serum (Gibco/Invitrogen), 1% L-glutamine (Gibco/Invitrogen), 1% penicillin–streptomycin (Invitrogen), and growth conditions at 37°C in 5% humidified CO₂ incubators. Creation and characterization of CRISPR/Cas9-mediated knockout of the *ELAVL1* gene in HCT116 cells was accomplished as described (42). Dihydroanthranone I (D0947) was purchased from Sigma and dissolved in ultrapure dimethylsulfoxide (DMSO, Amresco, N182) to 10 mM final concentration. Antibodies used recognized HuR (sc-71290; from Santa Cruz Biotechnology), His tag (anti-6x His (ab1187; from Abcam)) and β -actin (Clone C4; MP Biomedicals).

Cell and tumor growth assays

Transient transfection of cells with a HuR expression construct (pcDNA3.1/Zeo/HuR-Flag) or empty vector was accomplished using Lipofectamine Plus (Gibco/Invitrogen) as described (43) for 48 h, following addition of 10 μ M DHTS or vehicle. Cell survival was assayed using the MTT-based cell growth determination kit (Sigma-Aldrich) as previously described (30).

Anchorage- and serum-independent growth assays were accomplished by plating cells (20 cells per well) on 96-well ultra-low attachment plates (Corning) in spheroid growth medium (DMEM supplemented with 10 mM HEPES, N2 supplement (1 \times ; Gibco), B-27 supplement (1 \times ; Gibco), Insulin Transferrin Selenium (1 \times ; Gibco), FGF (10 ng/ml; Gibco) and EGF (20 ng/ml; Gibco)). After 3 days of growth, spheroids were treated with 10 μ M DHTS or vehicle for 15 days changing medium every 3 days. Individual spheroids ($n = 5$ –10/time point) were imaged every 3 days and area was measured using ImageJ software.

Six week-old athymic nude (Nu/Nu) mice were purchased from Jackson Laboratories and maintained under sterile conditions in cage micro-isolators according to approved IACUC guidelines. Parental HCT116 and a representative HuR knockout clone (2×10^6 cells) used between passages 14 and 23 were resuspended in PBS containing 50% Matrigel (Corning) and injected into the dorsal subcutaneous tissue (three mice/group with two tumors/mouse). Mice (three per group) received intraperitoneal (IP) injections of DHTS (10 mg/kg) dissolved in PBS/5% *N*-methyl pyrrolidine (NMP) (Sigma-Aldrich) or vehicle control every 48 h. Tumor volumes and body weight were measured three times per week using a caliper, and tumor volumes were calculated using the formula: volume = length \times width²/2. Upon termination of the experiment, mice were euthanized and tumors were harvested.

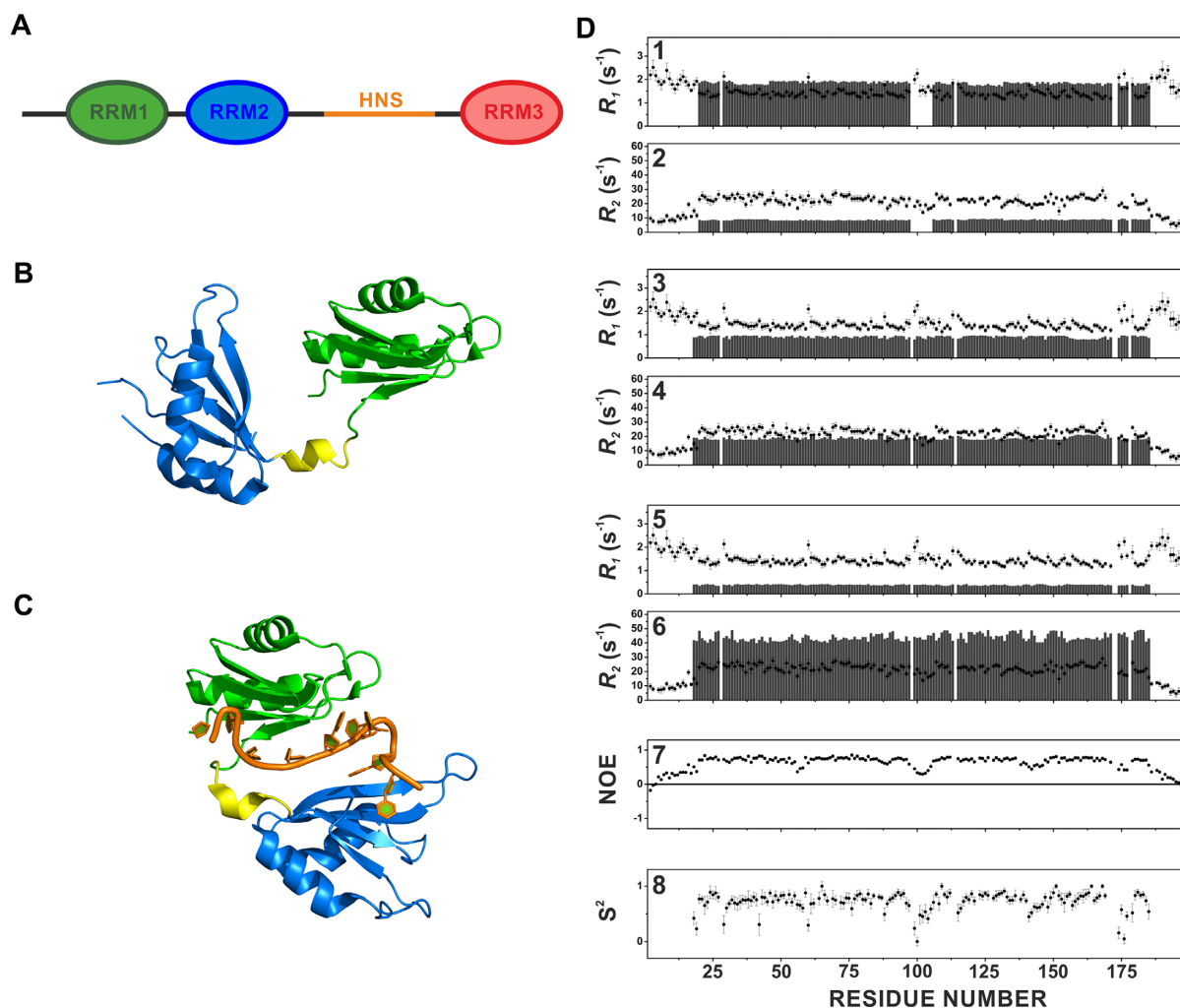


Figure 1. Multidomain organization of HuR (A). The RRM1–RRM2 tandem domains (RRM1 aminoacids (aa) Thr20–Pro98 and RRM2 aa Ala106–Asn186) are separated by a short linker of 7 residues (aa Ser99–Asp105), while RRM3 (aa Trp244–Asn322) is connected to the other two domains by a long hinge region of about 60 residues (aa Pro187–Gly243), which includes the HuR Nucleocytoplasmic Shuttling (HNS) sequence, responsible for nuclear/cytoplasmic shuttling of HuR. RRM1 is represented in green, RRM2 in blue and RRM3 in red. The HuR Nucleocytoplasmic Shuttling Sequence (HNS) is indicated in orange. Cartoon representation of the ‘open’ structure of the tandem RRM1–RRM2 domains crystallized in the absence of RNA (pdb code 4ED5) (B), and of the ‘closed’ structure of the tandem RRM1–RRM2 domains in complex with RNA (pdb code 4EGL) (C). The two domains and the linker are highlighted with different colors (RRM1 in green, linker in yellow and RRM2 in blue). (D) Comparison of experimental backbone ^{15}N R_1 values for RRM1–RRM2 (data collected at 298 K, black filled circles) with the calculated values (grey bars) for isolated RRM1 and RRM2 domains (1), for monomeric RRM1–RRM2 construct (3) and for rigid dimeric adduct (5). Comparison of experimental backbone ^{15}N R_2 values for RRM1–RRM2 (data collected at 298 K, black filled circles) with the calculated values (grey bars) for isolated RRM1 and RRM2 domains (2), for monomeric RRM1–RRM2 construct (4) and for rigid dimeric adduct (6). Experimental NOE values for RRM1–RRM2 (data collected at 298 K) (7) and S^2 order parameter calculated with the program TENSOR2 (8).

AlphaScreen and RNA electromobility shift (REMSA) assays

Amplified Luminescent Proximity Homogenous Assay (Alpha) with a 5'-Biotinylated RNA probe (Bi-TNF, 5'-AUUAUUUAUUUUUUUUUUUUUUUUUA) was used with FL-HuR and four studied mutants. 384-well optiplates (PerkinElmer; 6007299) were used with 20 μl final volume in each well. Hooking points of all the respective proteins were determined. Reagents were used in the nanomolar range using the AlphaScreen His detection kit (PerkinElmer) in alpha buffer (25 mM HEPES pH 7.4, 100 mM NaCl, 0.1% BSA). Donor and acceptor beads were used at 10 $\mu\text{g}/\text{ml}$ as their final concentration, proteins and constructs were ac-

ording to their hooking points and incubated for 1 hour at room temperature. Plates were read for fluorescence signals in an Enspire plate reader instrument (PerkinElmer; 2300-001A), and specific binding was calculated by subtracting the background, obtained in the absence of the protein. For REMSA experiments, equimolar concentrations of purified RRMs and FAM-TNF RNA probes were used (32) in REMSA buffer (20 mM HEPES pH 7.5, 50 mM KCl, 0.5 μg BSA, 0.25% glycerol) together with reference doses of DHTS were run on the native Polyacrylamide (6%) gel, in 0.5 \times TBE buffer at 55 V for 90 min. The gel was analysed by a Typhoon instrument (GE Healthcare; 00-4277-85 AC).

R_1 , R_2 and NOE measurements

The experiments for the determination of ^{15}N longitudinal and transverse relaxation rates and ^{15}N - ^1H NOE (44) were recorded at 298 K and 700 MHz on ^{15}N -enriched samples of the RRM1–RRM2 tandem domains of HuR. ^{15}N Longitudinal relaxation rates (R_1) were measured using a sequence modified to remove cross-correlation effects during the relaxation delay (45). Inversion recovery times ranging between 2.0 and 2500 ms, with a recycle delay of 3.5 s, were used for the experiments. ^{15}N transverse relaxation rates (R_2) were measured using a Carr-Purcell-Meiboom-Gill (CPMG) sequence (45,46), with delays ranging between 8.5 and 237.4 ms and a refocusing delay of 450 μs . Longitudinal and transverse relaxation rates were determined by fitting the cross-peak intensities as a function of the delay to a single-exponential decay using the Origin software. Heteronuclear NOE values were obtained from the ratio of the peak height for ^1H -saturated and unsaturated spectra. Theoretical predictions of NH R_1 and R_2 values for RRM1–RRM2 tandem domains were made using HYDRONMR (47) and the pdb structure 4ED5 (40), considering (i) the isolated domains, (ii) the monomeric and (iii) the dimeric constructs.

Molecular dynamics simulation and analysis

The HuR-DHTS complex, as issuing from docking calculations (see SI for details), was submitted to MD simulation with NAMD (48) using the ff99SBildn Amber force field parameters (49,50) for proteins and the parameters recently developed by Allnér and co-workers for ions (51). Parameters for DHTS were generated in two steps. Initially, charges were computed using the restrained electrostatic potential (RESP) fitting procedure (52). The ESP was first calculated by means of the Gaussian09 package (53) using a 6–31G* basis set at Hartree-Fock level of theory, and then the RESP charges were obtained by a two-stages fitting procedure using the program RED (54,55). Missing bond, angle, torsion and improper torsion angle parameters were then generated using Antechamber (56). The complex was then solvated in a 15 Å layer cubic water box using the TIP3P water model parameters. Neutrality was ensured by adding five further Cl^- ions. The final system size was $\sim 74 \text{ \AA} \times 93 \text{ \AA} \times 74 \text{ \AA}$ for a total number of atoms of $\sim 48\,000$. A 10 Å cutoff (switched at 8.0 Å) was used for atom pair interactions. The long-range electrostatic interactions were computed by means of the particle mesh Ewald (PME) method using a 1.0 Å grid spacing in periodic boundary conditions. The RATTLE algorithm was applied to constrain bonds involving hydrogen atoms, and thus a 2 fs integration time step could be used. More details in the Supplementary Methods

RIP-chip protocol

To analyze the influence of DHTS on the interaction of HuR with endogenous mRNAs, immunoprecipitation (IP) of endogenous ribonucleoprotein complexes was performed as described previously (57). Briefly, HeLa cells were lysed in 20 mM Tris–HCl at pH 7.5, 100 mM KCl, 5 mM MgCl_2 , and 0.5% NP-40 for 10 min on ice and centrifuged at 15 000 $\times g$ for 10 min at 4°C. The supernatants were incubated for

2 h at 4°C with protein G Sepharose beads (GE Healthcare) coated either with anti-HuR or with control IgG antibodies (both from Santa Cruz Biotechnology). The beads were washed with NT2 buffer (50 mM Tris–HCl [pH 7.5], 150 mM NaCl, 1 mM MgCl_2 , 0.05% NP-40), followed by incubation with 20 units of RNase-free DNase I for 15 min at 37°C to remove the DNA. The samples were then incubated for 15 min at 55°C with 0.1% SDS–0.5 mg/ml proteinase K to digest proteins. Microarray analysis was performed in duplicate (GEO number GSE94360). The RNA from the IP samples was extracted using phenol–chloroform, precipitated, and used for cDNA microarray analysis or RT-qPCR validation.

Analysis of enriched mRNAs

GC content, length and secondary structure density (computed as the fraction of unpaired nucleotides) for the UTRs of DEC and INC genes were obtained from the AURA 2 database (58), and plotted with the R software. The enrichment of post-transcriptional regulatory elements was performed with the *Regulatory element enrichment* feature of AURA 2. Gene ontology and pathway enrichment analyses were performed with the Enrichr tool (59) on GO (Biological process, Molecular function and Cellular Component) and pathways (KEGG and Reactome) libraries, using a five genes overlap and minimum combined score of 2 as significance threshold. GO terms were clustered by semantic similarity with the GoSemSim R package (60), and the cluster score computed as the average combined score of composing terms.

RESULTS

NMR resonance assignment

The 2D ^1H - ^{15}N HSQC spectrum of tandem RRM1–RRM2 domains shows well-dispersed signals in agreement with a uniform and folded protein structure (Supplementary Figure S1). All the residues (but Pro172), including those forming the linker region that is crucial for the protein function, have been assigned (Supplementary Table S1, BMRB code: 27002). Our assignment of the tandem RRM1–RRM2 domains was also compared with the ones reported for the isolated RRM1 domain (61) as in the RRM1–RRM2 tandem domains (35). The resonances of residues forming the RRM1 domain are almost the same in the isolated domain (61), and in the RRM1–RRM2 construct. As reported by Wang and coworkers (35), this observation suggests that the RRM1 and RRM2 domains do not interact with each other when they form the tandem construct. Based on TALOS+ predictions, each domain in the RRM1–RRM2 construct is constituted by two α -helices and four β -strands, in agreement with the previously reported crystal structures of the RRM1 and RRM1–RRM2 domains of HuR (39,40,62) (Supplementary Figure S2).

Internal dynamics of RRM1–RRM2 tandem domains

To characterize protein dynamics, measurements of longitudinal (R_1) and transverse (R_2) relaxation rates of backbone amide nitrogens at 700 MHz, ^1H Larmor frequency,

and 298 K were performed on ^{15}N -enriched samples of the RRM1–RRM2 construct. Theoretical estimates of R_1 and R_2 values were calculated for the following model structures: (i) the isolated RRM1 (T20–P98) and RRM2 (A106–N186) domains (Figure 1D, panels 1, 2), (ii) the monomeric RRM1–RRM2 construct (Figure 1D, panels 3, 4) and, (iii) the dimeric adduct (Figure 1D, panels 5, 6) (PDB 4ED5). Figure 1D shows the experimental R_1 and R_2 values (black circles) as well as the theoretical ones (grey bars). The comparison of experimental R_1 and R_2 data with theoretical values calculated for the isolated RRM1 and RRM2 domains shows that experimental R_1 values were smaller and R_2 values are larger than their theoretical counterparts (Figure 1D, panels 1, 2). At the same time, experimental R_1 values were higher than theoretical estimates calculated for the monomeric construct in solution (Figure 1D, panel 3), indicating that the RRM1–RRM2 construct did not behave as a rigid body but instead displayed inter-domain flexibility, simulating a protein of lower molecular weight (63–65). Experimental R_2 values were instead slightly higher than their theoretical counterparts, indicating the occurrence of possible aggregation phenomena (Figure 1D, panel 4). On the other hand, experimental R_1 values were dramatically higher, and R_2 dramatically lower than theoretical values calculated for the rigid dimer (Figure 1D, panel 5, 6), suggesting that the RRM1–RRM2 dimer was not present in solution as a stable complex. Further indication of the presence of inter-domain flexibility was provided by the ^{15}N – ^1H NOE values for the linker residues Ser99 (0.46), Ser100 (0.34), Glu101 (0.31), Val102 (0.30), Ile103 (0.32) and Lys104 (0.40) (Figure 1D, panel 7). The small NOE values of the residues in the linker between the two domains are evidence of fast motions on ps–ns timescale (faster than the overall protein-tumbling rate). Very small NOE values are found also for the N- and C-terminal tails, and for some residues in the loops of RRM1 (Val56, Ala57, Gly58) and RRM2 (Gln141, Thr142, Leu145) domains. The order parameter S^2 calculated with the program TENSOR2 (66) starting from experimental R_1 , R_2 and NOE values is also reported in Figure 1D, panel 8. The S^2 values confirm the presence of high flexibility between the two domains, and for some loops within each domain.

DHTS stabilizes HuR in a closed conformation and competes with mRNA for binding

The interaction of HuR with DHTS was investigated through solution NMR. The significant precipitation of the ligand in the solution, occurring at the high concentrations required by the NMR analysis, prevented the estimation of the affinity constant. Nevertheless, after the addition of increasing amounts of DHTS to the protein, we observed a generalized decrease in signal intensity, with few residues (Thr20, Asn21, Ile52, Ser94, Tyr95, Ala106, Asn107, Leu108, Ile133, Asn134, Val137, Leu138, Arg147, Ile152, Phe154, Asp155, Lys182) experiencing a larger effect. These residues were located in the β -platform of both RRM domains (Figure 2A and B). The generalized decrease of signal intensity, and the distribution of affected residues over the large surfaces of the β -platform in each domain suggested an alteration of the equilibrium among ‘closed’

and ‘open’ conformations upon ligand binding. Specifically, the decrease of signal intensity was consistent with a mechanism where the small molecule stabilizes a ‘closed’ conformation of HuR. After the addition of DHTS to the protein, only negligible chemical shift changes occur. The residues experiencing the largest chemical shift perturbations are located close to the β -platforms (Supplementary Figure S3).

With the dual aim of bringing some insights into DHTS binding mode and mechanism of action, we carried out a molecular modeling study. We employed a ‘tandem’ approach of docking calculations and molecular dynamics (MD) simulations in the attempt to follow the protein/ligand reciprocal conformational mutations. We first performed a docking calculation to the whole mRNA binding surface of HuR by means of AutoDock 4.2, which converged to a single binding pose. As a result, DHTS was found at the center of the mRNA binding cleft, which is shaped by the RRM1 and RRM2 domains (residues 18–95 and 107–185, respectively), and in proximity of the inter-domain linker. To allow both the ligand and the protein to fully adapt to each other, we performed an extended (0.5- μs) MD simulation. During the first 100 ns of simulation, DHTS was displaced from its starting position laterally along the surface of the RRM domain β -sheets, though always remaining bound to the HuR surface (Supplementary Figure S4A and B). This displacement was accompanied by a HuR conformational shift towards a ‘closed’ form featuring the two RRM domains even closer to each other (Supplementary Figure S4C), and establishing further inter-residues contacts (Supplementary Figure S4D) lacking in the mRNA-bound conformation, e.g. a salt bridge between Asp-105 and Arg-153, a backbone hydrogen bond between Ile-133 and Asn-25 or a hydrophobic contact between Ile-133 and Ile-23. For the sake of comparison, a further 500 ns MD was performed, starting from the X-ray HuR–RNA complex. The simulation resulted in an overall greater structural stability as compared to the HuR–DHTS complex (Supplementary Figure S5A and B). Furthermore, we observed neither a decrease in the distance between the two RRM domains nor a significant increase in the number of inter-domain residue contacts (Supplementary Figure S5C and D).

In the final HuR–DHTS complex, which remained stable for the rest of the simulation, DHTS is accommodated in a narrow, elongated and mostly hydrophobic pocket (Figure 2C) shaped by residues of the two RRM domain β -sheets (RRM1: Ile-23, Asn-25, Tyr-26, Leu-61, Tyr-63, Phe-65; RRM2: Asp-105, Ile-133, Asn-134, Arg-153) and of inter-domain linker (Ile-103 side chain and Lys-104, Arg-97 and Ala-96). The aromatic rings of DHTS establish several π -interactions, among which a cation- π interaction with Arg-153 and a NH- π interaction with the Asn-134 side chain. However, although DHTS is gripped between the two domains, it does not bind HuR rigidly, but rather gently sways along the binding surface (Figure 2D). Taken together, our structural data indicate that DHTS competes with RNA for the binding to HuR, interacting with the β -platform of both RRM domains in the proximity of the interdomain linker, and thus stabilizing HuR in a closed conformation.

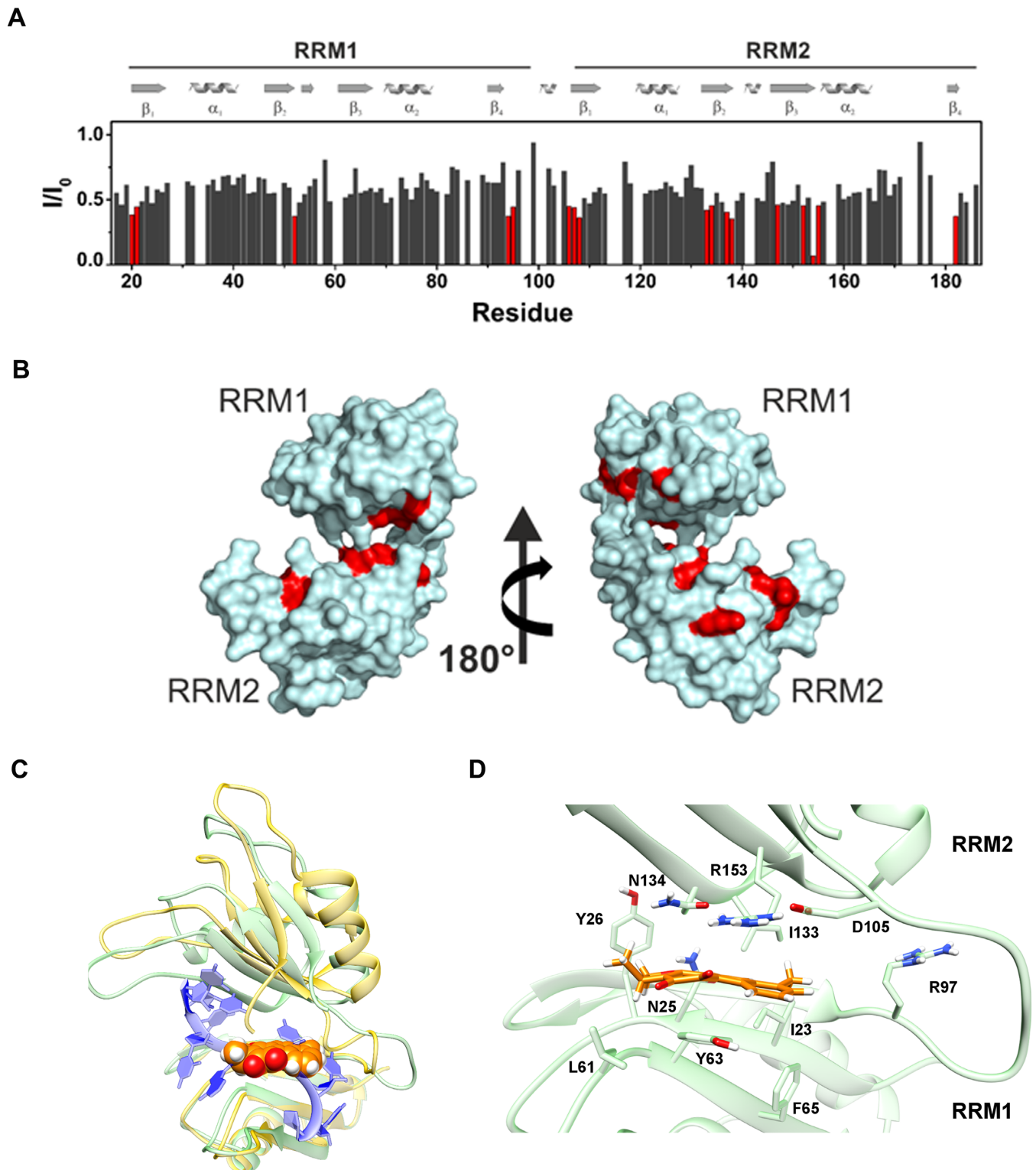


Figure 2. Graphical representation of the intensity changes per residues of RRM1–RRM2 HuR protein (50 μ M in solution) in the presence of DHTS (200 μ M) (A) and surface representation of the closed conformation of HuR (pdb: 4ED5) (B) with the residues exhibiting the highest decreases in signal intensities highlighted in red. (C) Global view of the HuR (green cartoons)-DHTS (orange spheres) complex. Note how the insertion of DHTS into the mRNA binding cleft and the further closure of the latter, as compared to the mRNA-bound conformation (yellow), prevents the accommodation of the mRNA strand (blue ribbons). (D) Theoretical DHTS binding mode, as suggested by our MD simulation. DHTS and HuR residues involved in binding interactions are displayed as sticks.

The β -platforms of RRM domains are involved in DHTS inhibitory activity

To support NMR and molecular modeling that addressed a specific interacting region on HuR, we produced HuR protein domains made of the first RRM domain (RRM1), of the second RRM domain (RRM2), of the RRM1–RRM2 wild-type RRM domains, and of RRM1 lacking 14 aminoacids at the C-terminus (Δ RRM1, missing residues from Ser94 to Asn107) and performed *in vitro* RNA binding experiments. Some of these residues belong to the inter-domain linker (Ser99–Asp105) and the others to the β -platform regions of the two domains, where some aminoacids experienced decreased intensity in the presence of DHTS (Ser94–Tyr95 in RRM1 and Ala106–Asn107 in RRM2). HuR domains were produced in *Escherichia coli* using the pET42 plasmid (31). We obtained the same purity for all the protein isoforms (Supplementary Figure S6). As single domains lose RNA-binding activity very quickly, the *in vitro* activity of the single protein domains and of their combination was evaluated by REMSA, mixing equimolar concentration of each, freshly prepared, with 0.2 μ M of the FAM-ARE ssRNA probe (Figure 3A). The RRM1–RRM2 isoform was used as positive control because it displayed a similar K_d (2.62 ± 0.6 nM (31)) to the FL HuR protein, and because it was used in the NMR experiments (35). RRM1 retained the capability to recognize mRNA substrates (40), however with a lower affinity compared to the RRM1–RRM2 construct, probably indicating a change in the stoichiometry of cooperative protein binding (Figure 3A, Supplementary Figure S7) (40,62).

Importantly, the RRM1–RNA complex was still sensitive to DHTS. After removing 14 aminoacids, the binding capacity of Δ RRM1 to RNA was slightly reduced ($\sim 20\%$) in comparison with the RRM1 domain (Figure 3A). Conversely, Δ RRM1 became resistant to DHTS, suggesting that this region is important for DHTS inhibitory activity (Figure 3A). REMSA performed with RRM2 and *in vitro* complementation of the two domains (RRM1 + M2 and Δ RRM1 + M2) did not provide information about the contact region of DHTS (Supplementary Figure S7B–D). By using fluorescence polarization, we analyzed the binding kinetics of proteins (200 nM) toward the FAM-ARE RNA probe (100 nM). We confirmed that full-length HuR and RRM1–RRM2 tandem domains behave almost similarly (average $K_{obs} \sim 4$ min), reaching equilibrium after 10 min. On the other hand, the RRM1 domain rapidly recognized the substrate ($K_{obs} \sim 1$ min), but this affinity was significantly impaired in the Δ RRM1 construct (K_{obs} of ~ 8 min) (Figure 3B). Circular dichroism (CD) experiments performed at 10 μ M concentration of both reagents, and NMR measurements ruled out a putative interaction between DHTS and RNA (Supplementary Figure S8A and B). Collectively, these findings show that the residues forming the β -platform and placed at the C-terminal in RRM1 domain are critical for RNA binding and the inhibitory activity of DHTS.

Single point mutations in the HuR–DHTS interacting region abolishes DHTS efficacy

Based on NMR data and an initial raw model of DHTS binding as derived by docking calculations, residues Ser94, Asn107, Ile133 and Asn134 of the RRM1–RRM2 inter-domain region were mutated to probe their relevance for DHTS binding. We produced residue-to-Alanine mutations in the full-length HuR sequence by site-directed mutagenesis (67) (Supplementary Figure S9). The preservation of the folding of the mutants was assessed by ^1H 1D NMR spectra (Supplementary Figure S10). By reacting equimolar amount of wild-type HuR or muteins with 0.2 μ M FAM-ssRNA, we observed an inhibitory effect of DHTS only with wild-type HuR, while any functional single point mutation led to resistance to DHTS (Figure 3C). Interestingly, we observed a qualitatively distinct binding profile among muteins: at least three discrete supershifts, numbered according to the molecular weight (1 being the lightest, 2, and 3), were detectable for wild-type HuR. Supershift 3 was markedly enriched in N134A and N107A, and to a lesser extent in I133A muteins (Figure 3C). This behavior could result from a higher efficiency in recognition and dimerization along the mRNA substrate, or alternatively from an aggregation-prone tendency of muteins that therefore aggregate on the same molecule of RNA probe. Indeed, mutants showed significantly lower K_d values, i.e. an increased affinity in saturation binding experiments with respect to wild-type HuR (Figure 3D, Supplementary Figures S11 and S12). Additionally, the raw signals at the hook point values for protein and RNA probes were significantly reduced in intensity compared to wild-type HuR, indicating a sub-optimal assay environment, compatible with ligand self-aggregation (68).

According to these data, when Ser94, Asn107, Ile133 and Asn134 are mutated into Alanine, DHTS does not bind to any mutein. The four residues are thus crucial in providing the required flexibility to HuR for its mRNA binding function.

DHTS prevents HuR binding to low AU-rich density mRNA, but enriches it to high AU-rich density species

We evaluated the ability of DHTS to disrupt the interaction of HuR with its target mRNAs by employing a transcriptome-wide approach. We performed a RIP-chip (ribonucleoprotein immunoprecipitation followed by microarray) experiment in HeLa cells, and observed that, out of the 2306 mRNAs bound to HuR, DHTS only reduced binding of 79 transcripts. Conversely, 558 mRNAs were enriched after treatment with DHTS. Therefore, contrary to our expectations, we observed an overall enrichment of mRNAs bound to HuR after treatment with DHTS. We reasoned that DHTS could displace mRNAs that had lower affinity to HuR than DHTS itself had, and, paradoxically, provide the opportunity for mRNAs with higher affinity for HuR than DHTS to bind in higher copy numbers to HuR. We observed that HuR-bound mRNAs had relatively higher frequency of U/AU-rich segments compared to the frequency transcriptome-wide, as expected (69). However, the U/AU density in UTRs in enriched mRNAs was significantly higher than that in downregulated mRNAs (Sup-

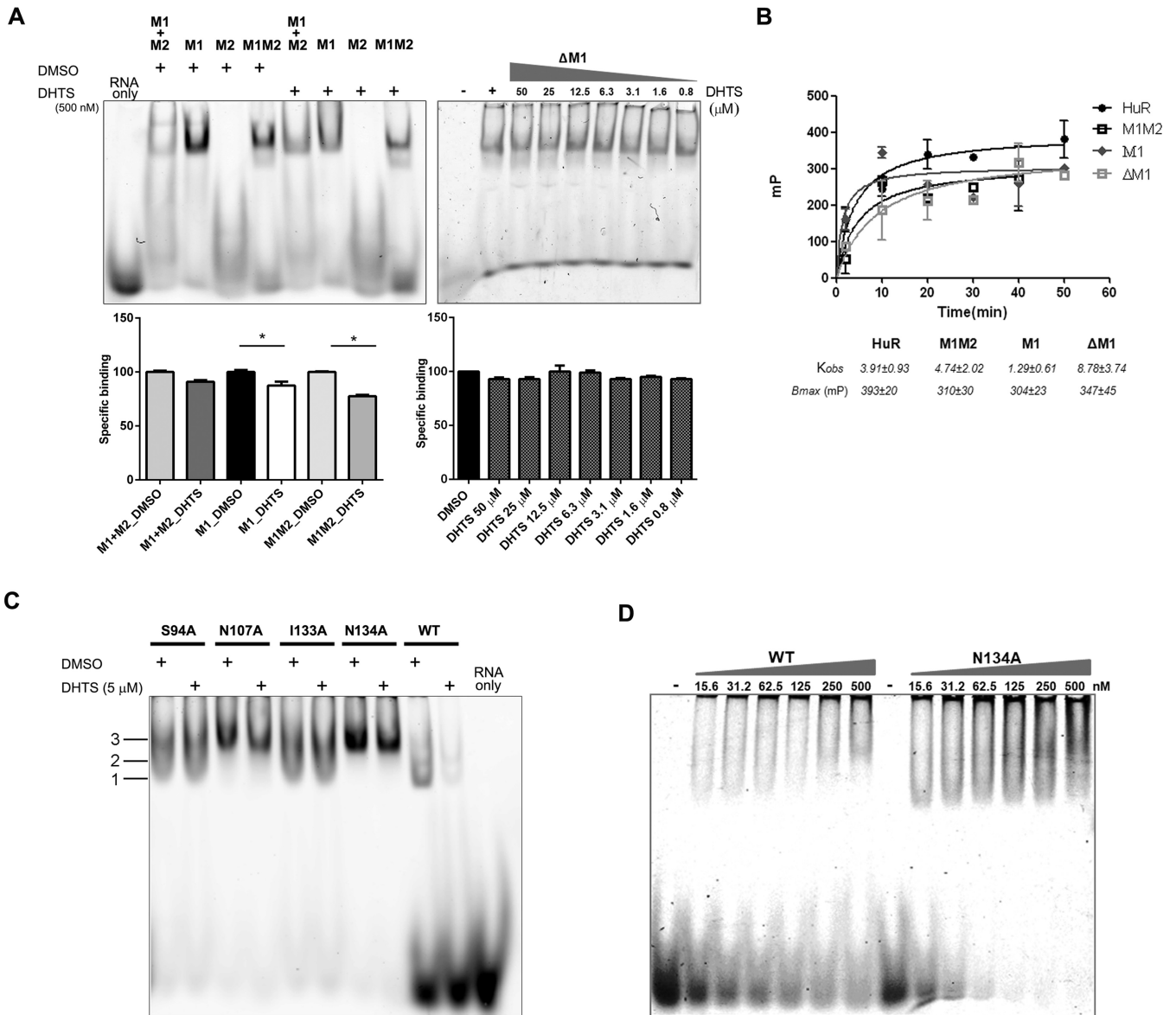


Figure 3. The inter-domain region between RRM1 and RRM2 is crucial for RNA and DHTS binding. (A) On left, representative REMSAs of at least three independent protein preparations of recombinant RRM1 + RRM2 (M1 + M2) domains, RRM1 (M1), RRM2 (M2), RRM1–RRM2 (M1M2) HuR proteins. REMSAs were performed with 0.2 μ M of protein, 0.2 μ M of Cy-3 RNA probe and DMSO or DHTS at indicated doses. On right, representative REMSA performed with 2.5 μ M of Δ RRM1 and 75 fM of probe RNA titrated with DHTS (concentration as shown in the legend). Densitometric quantification plotted below represents specific HuR–RNA binding challenged by DHTS. Mean \pm SD refers to three independent experiments ($n = 3$, * indicates t -test P -value < 0.05). (B) Kinetic saturation binding experiment by fluorescence polarization. 200 nM wild-type protein or mutants were incubated with FAM-ARE RNA probe (100 nM). Full-length HuR and RRM1–RRM2 tandem domains (M1M2) have similar K_{obs} . RRM1 (M1) is binding faster (K_{obs} of ~ 1 min,) but deletion of the inter-domain region abolishes the binding properties of RRM1 (Δ M1) (K_{obs} of ~ 8 min). (C) RNA- and DHTS-interacting amino acids are crucial for DHTS and RNA binding, and for protein dimerization. Representative REMSAs of at least three independent protein preparations of recombinant full-length HuR and indicated mutants. REMSAs were performed with 0.2 μ M of protein, 0.2 μ M of Cy-3 RNA probe, and DMSO or 5 μ M DHTS. Mutants are insensitive to DHTS and show different binding patterns to the RNA probe. (D) Representative REMSAs of at least three independent protein purification performed with increasing concentration of WT and HuR single point mutant N134A with 75 fM of probe RNA.

plementary Table S2, median of 1.37 ARE nts/100 nts for enriched genes, 0.97 for depleted genes; mean of 2.24 ARE nts/100 nts for enriched genes, 1.49 for depleted genes; maximum of 81.97 ARE nts/100 nts for enriched genes, 7.92 for depleted ones). Moreover, the highest differences were observed in the 3'UTR (Figure 4A), where the percentage of AU bases increased from 58% (depleted) to 65% (enriched).

Additionally, 3'UTRs, but not 5'UTRs, were significantly longer for the enriched mRNAs (Figure 4B), while no differences in the density of secondary structure elements were observed (Figure 4C).

Functional analyses of depleted genes provided no considerable enrichment, due to the small size of the set and because it was partially composed of unannotated mRNAs.

UTR properties by response to DHTS

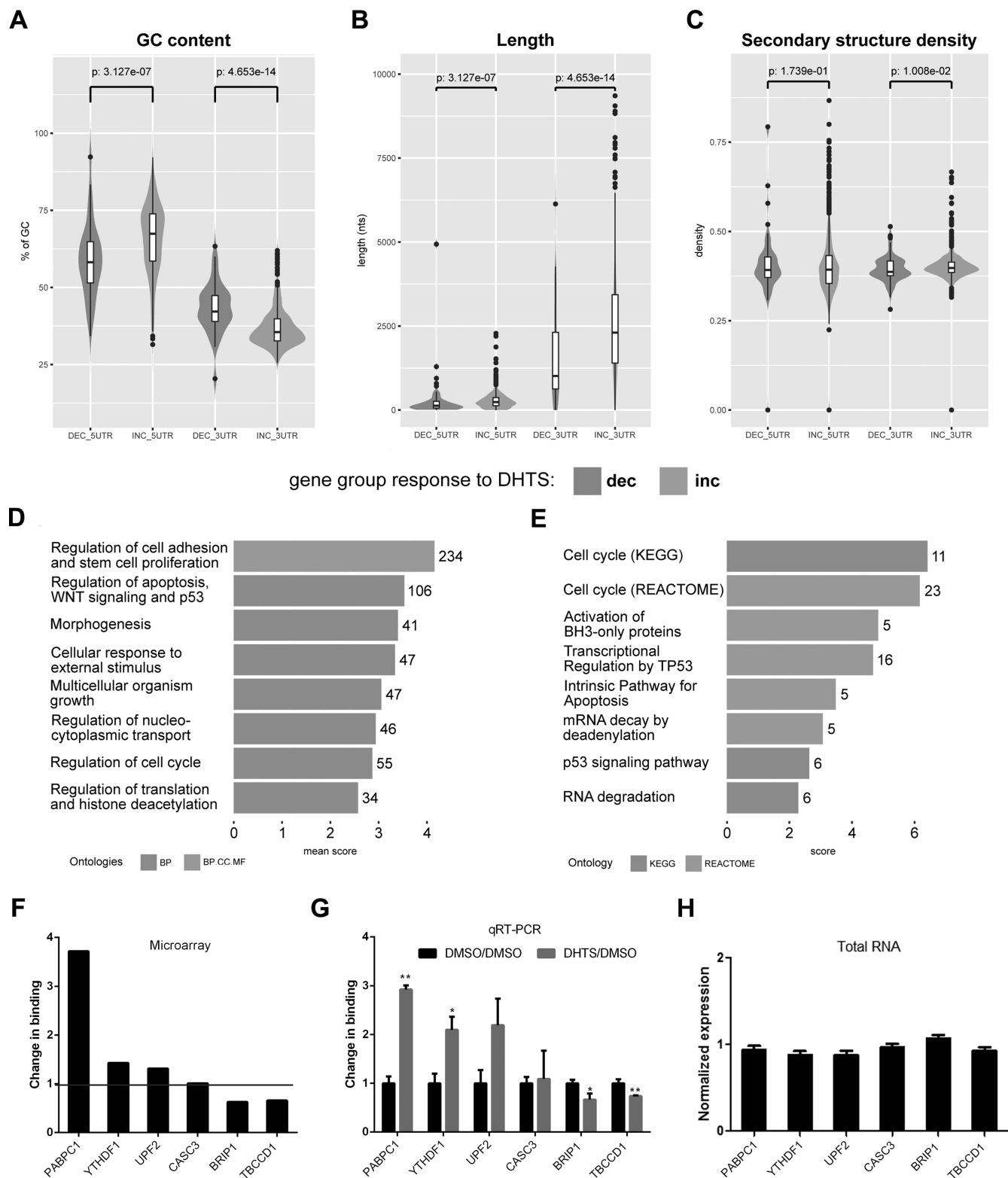


Figure 4. Enriched and depleted mRNAs and their UTRs have distinct properties. (A) Distribution of GC content for depleted (dec) and enriched (inc) UTRs, with Wilcoxon test-*P*-values of the differences. (B) Length distribution for depleted (dec) and enriched (inc) UTRs, with Wilcoxon test-*P*-values of the differences. (C) Secondary structure density (computed as the fraction of unpaired nucleotides) of depleted (dec) and enriched (inc) UTRs, with Wilcoxon test-*P*-values of the differences. (D) Gene Ontology enrichment analysis for the enriched gene set. Number of genes belonging to each terms cluster is shown at the end of the corresponding bar. Mean score represents the mean of the Enrichr combined score for all belonging terms. GO classes

Enriched mRNAs (Figure 4D and E, Supplementary Table S3) showed that, during DHTS treatment, HuR bound preferentially to mRNAs encoding proteins with functions in the regulation of gene expression, cell cycle progression, and apoptosis. Data validation also suggested that the changes in HuR binding were independent of changes in total mRNA levels, as mRNA abundance was generally unchanged (Figure 4F and G). In summary, the ability of DHTS to displace HuR-bound RNAs was specifically limited to mRNAs with a low affinity for HuR, which generally displayed lower AU content in their 3'UTRs.

DHTS is effective on HuR-positive models *in vitro* and *in vivo*

To evaluate this mechanism of action, in which a limited displacement of RNAs from HuR may be effective in HuR-dependent tumor growth, we studied tumor growth *in vitro* and *in vivo*. HCT116 colon cancer cells were used as a model, based on high endogenous levels of HuR and their sensitivity to HuR inhibition (30). Creation and characterization of CRISPR/Cas9-mediated knockout of the *ELAVL1* gene in HCT116 cells was accomplished as described (42). HCT116 and HuR-knockout cells (HCT116ΔHuR) were grown under anchorage- and serum-independent conditions to facilitate tumorspheroid growth, and HuR was observed to be needed for tumorsphere growth (Figure 5A and B). In the presence of DHTS, growth of HCT116 spheroids was attenuated 2-fold, whereas DHTS did not impact HCT116ΔHuR sphere growth (Figure 5A and B). To test the effects of DHTS on tumor growth *in vivo*, mice bearing HCT116 cell xenografts received IP injections of DHTS (10 mg/kg body weight) or vehicle every 48 h. Over the course of the experiment, DHTS was well tolerated and mice did not display any signs of acute toxicity and maintained similar weights. Significant anti-tumor effects of DHTS were observed, with approximately a 4-fold reduction in tumor size (Figure 5C and D). Additionally, the efficacy of DHTS was strictly dependent on the presence of HuR. HCT116ΔHuR cells grew significantly more slowly and formed smaller tumors, but were completely insensitive to DHTS. Furthermore, this decreased growth sensitivity of DHTS in HuR-deficient cells could be restored with expression of HuR in HCT116ΔHuR cells (Figure 5E and F). These results indicate that DHTS has significant antitumor activity *in vitro* and *in vivo* without major systemic toxicity, along with demonstrating specificity of HuR inhibition.

DISCUSSION

Previous efforts targeted towards HuR disruptors (28–30,32,70) identified small molecules that can inhibit the HuR–RNA interaction in the nanomolar range. Here, we have characterized from a structural and functional perspective the mechanism of action of DHTS, a disruptor of the HuR–RNA interaction, identifying the protein regions that promote the interaction, and providing hints for the rational design of more potent HuR inhibitors. Additionally, we showed the cellular effects of DHTS treatment on HuR ability to bind mRNAs, and we described a paradoxical enrichment of mRNAs containing longer 3'UTRs with increased AU content. Such effects result in dysregulation of HuR function, specific to cells that are strictly dependent on HuR function. Starting from the relaxation measurements of RNA-free protein in solution, we described the events preceding RNA binding. The analysis of NMR relaxation data indicates that the free RRM1–RRM2 construct is largely monomeric in solution. However, the observed R_2 values are slightly higher than those expected for a monomeric protein, suggesting the presence of an equilibrium with a fraction of protein experiencing a larger rotational correlation time. On the other hand, the discrepancy of observed R_1 data with respect to the theoretical values calculated for a rigid RRM1–RRM2 monomer are explained by the presence of inter-domain flexibility. The low NOE values suggest a significant conformational plasticity of the protein that is needed for mRNA binding. Therefore, even if it is reported that the RRM1–RRM2 tandem construct forms a separated functional unit from the RRM3 domain (71), RRM1 and RRM2 domains are not rigidly held together but undergo independent motions that can facilitate the recognition of the RNA partner. This confirms observations from the crystal structure of non-complexed HuR, where no contacts between the two domains were detected (40,62) and supports earlier results that phosphorylation at the linker (e.g. Ser100) had a profound impact on HuR binding to target mRNAs (72). Moreover, the large R_1 values and small NOE values seen for the linker indicate that this region highly influences the conformational change of the protein from an open/flexible free conformation towards a closed one bound to mRNA.

As previously reported (40), binding of mRNA to HuR can occur starting from the open/flexible state of the protein, where HuR first binds the mRNA strand via its RRM1 domain. As a result of the subsequent conformational change, the linker and the RRM2 domain bind the mRNA filament to form a stable complex (40). Therefore, the linker takes part in the binding allowing the reciprocal reorienta-

found in each cluster are represented by the bars color. (E) KEGG and REACTOME pathway enrichment analysis for the enriched gene set. Number of genes belonging to each pathway is shown at the end of the corresponding bar. The score is the Enrichr combined score for the pathway. Pathway database of each entry is represented by the bars color. RIP of HuR in DHTS-treated HeLa cells. (F) Microarray data for selected targets. Fold enrichment of each mRNA during DHTS treatment is reported, black bars represent microarray values obtained. (G) Validation of microarray data by RT-qPCR. Gray bars represent fold enrichment of each mRNA during DHTS treatment compared with the control condition (DMSO). Comparison between microarray (F) and RT-qPCR data (G) shows similar results for enriched transcripts (*PABPC1*, *YTHDF1* and *UPF2* mRNAs), unchanged transcripts (*CASC3* mRNA) and depleted transcripts (*BRIP1* and *TBCCD1* mRNAs). In RT-qPCR validation experiments, *RPLP0* mRNA was used as an endogenous control mRNA that did not bind to HuR. Error bars represent SD. P -value is * <0.05 . ** <0.001 . Microarray experiments were done in duplicate ($n = 2$), qRT-PCR in triplicate ($n = 3$). (H) RT-qPCR analysis of mRNAs bound to of HuR showing no changes in total expression levels after DHTS treatment. *RPLP0* mRNA was used as an endogenous control. Error bars represent SD. Experiments were done in triplicate ($n = 3$).

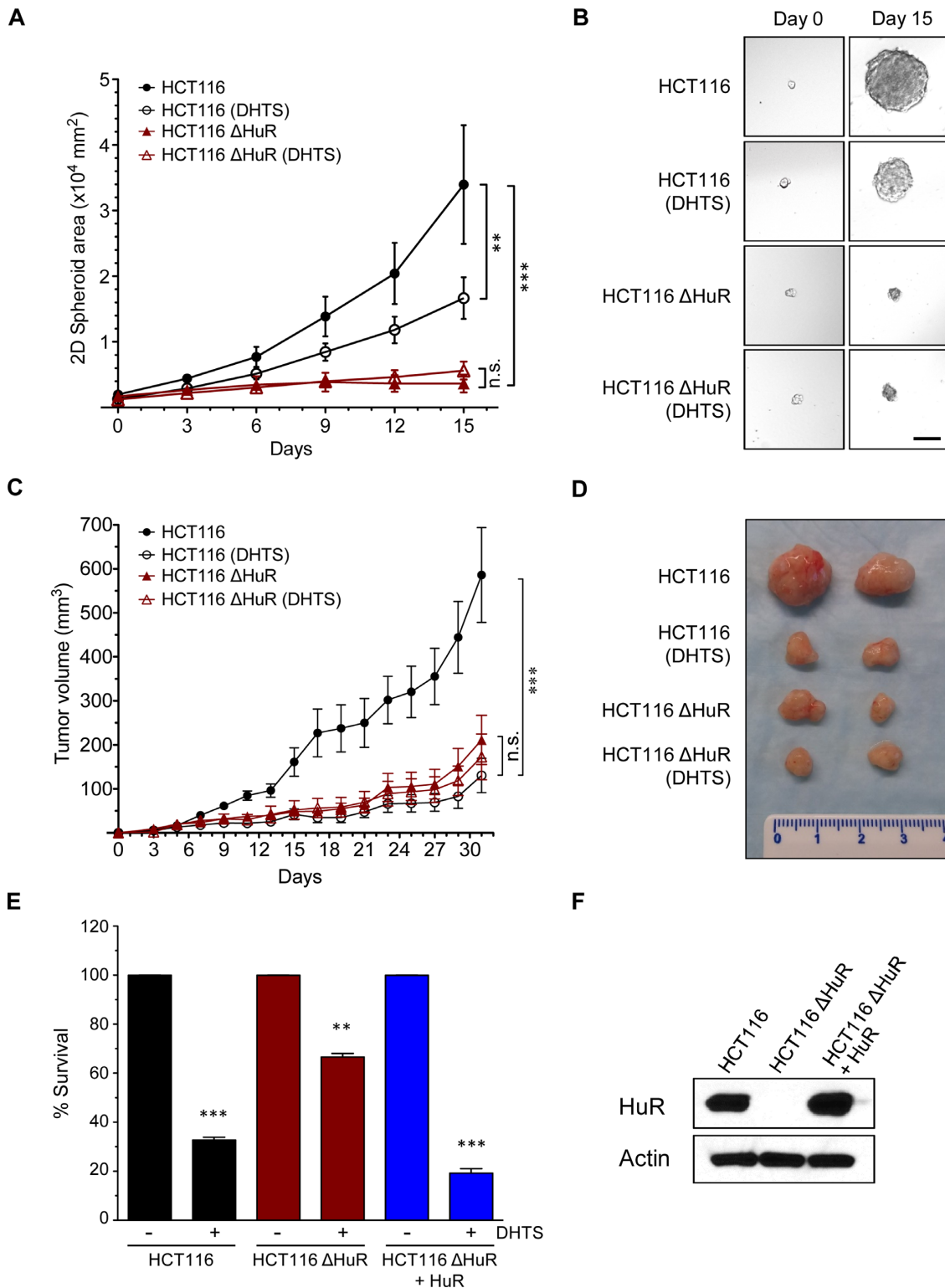


Figure 5. DHTS efficacy relies on HuR presence *in vivo*. (A) Spheroid growth of parental HCT116 (HCT116) and HuR-knockout cells (HCT116 Δ HuR) treated with DHTS (10 μ M) or vehicle. DHTS was added after 3 days of culture in spheroid growth medium on ultra-low adherence substrate and spheroid growth was tracked by imaging for 15 days. *P*-value is ** <0.01 , *** <0.001 , n.s. = not significant. (B) Representative tumorsphere images from day 0 and day 15 of DHTS treatment. Scale bar = 100 μ m. (C) Tumor growth of parental HCT116 and HuR-knockout cells (HCT116 Δ HuR) xenografts in nude mice treated with 10 mg/kg DHTS or vehicle control every 48 h. *P*-value is *** <0.001 , n.s. = not significant. (D) Representative tumors excised at day 31 are shown. (E) HuR-knockout cells (HCT116 Δ HuR) were transfected a HuR-expression construct (+HuR), along with empty vector transfected parental HCT116 and HCT116 Δ HuR cells. Cells were treated with DHTS (10 μ M) or vehicle, and cell growth was assessed 6 days after the treatment using MTT assay. Cell survival was normalized to the respective control and are the average of three experiments. *P*-value is ** <0.01 , *** <0.001 . (F) Western blot showing HuR complementation in HCT116 Δ HuR+HuR cells and absence of HuR in HCT116 Δ HuR cells. Actin was used as a loading control.

tion of the two domains and establishing interactions with the RNA strand. Addition of DHTS to unbound HuR results in a generalized decrease of the signal intensity of the NMR resonances, with some residues experiencing larger effects. It is likely that this behavior is due, at least in part, to a change in the conformational dynamics of the protein. Accordingly, upon complex formation with DHTS, in our MD simulation we observed a rather limited inter-domain flexibility, as a result of the shift in the conformational equilibrium between HuR forms in favor of a closed conformation. This result was not anticipated since, at least in principle, a change in the conformational dynamics of HuR could also have been achieved by stabilizing an open form of HuR. Indeed, residues located on the β -platforms of RRM1 and RRM2 domains, in the same regions involved in the binding with the mRNA strand, experience a deep quenching.

In our MD simulation, we observed a further closure of the RNA-binding groove, as compared to the RNA-bound conformation of HuR, and an ensuing increase in the number of inter-domain contacts, which could explain why the largest decreases in signal intensity were observed in residues belonging to these β -platforms. Deletion of the C-terminus region of RRM1 reduces the binding affinity of RRM1 to the mRNA probe but, importantly, abolishes the interaction between RRM1 and DHTS. This experimental validation of the NMR data and molecular modeling points to the residues next to the linker as being key structural elements responsible of the interaction between DHTS and HuR. Single aminoacid mutagenesis of Ser94, Asn107, Ile133, and Asn134 into alanine highlighted the importance of these residues in maintaining the equilibrium between the free protein in the monomer/dimer form and the closed-bound-to-RNA protein dimer, avoiding its aggregation on the RNA target. Interestingly, muteins are fully resistant to DHTS, further supporting that this small molecule competes for the same protein regions interacting with the target RNA. Collectively, these results suggest that DHTS stabilizes an unproductive 'closed' conformation of HuR and prevents the physiological re-orientation of the two domains needed to bind the target mRNA. Stabilization of such 'closed' conformation alters the protein dynamics, producing the observed generalized decrease of signal intensity of the resonances observed upon the addition of DHTS to the RRM1–RRM2 tandem domains. Unfortunately, the non-optimal solubility of DHTS hampered the quantitative assessment of its K_d .

In other experiments, we characterized the ability of DHTS to inhibit HuR activity *in vitro*, to modulate its post-transcriptional function in cell models, and its specificity towards other RNA-binding proteins. Additionally, we observed that DHTS inhibits the association step of HuR to its target RNAs, and that its cytotoxicity against cancer cells was HuR-dependent (31). The stable 'closed' form of the protein blocks the access to HuR for low affinity target RNAs. Indeed, paradoxically, the mRNAs with longer 3'UTR and higher U/AU content were more abundantly loaded on HuR after DHTS treatment, as they likely bind more avidly to HuR than DHTS itself. The levels of HuR-target RNAs were not changed during DHTS treatment, so a 'post-binding' mechanism of regulation can be inferred. Nevertheless, DHTS-dependent HuR dysreg-

ulation has a strong anti-cancer activity *in vivo*, as observed using a xenograft model of colon cancer (HCT116 cells). These findings are consistent with other results using colon, leukemia, cervical, and breast cancer cells, and indicate that DHTS can penetrate tumors effectively (73–76). The absence of systemic toxicity in treated animals supports the idea that general inhibition of HuR by small molecules can be a therapeutic avenue for future efforts, although the effects on the immune system should be evaluated in a non-immuno-compromised mouse model. Notably, HCT116 Δ HuR knockout cells *in vivo* showed a limited ability to develop tumors, but the extent of DHTS growth inhibition on these tumors did not match the effects on WT tumors. While we cannot discount that loss of HuR may impact cancer cell drug uptake, these results indicate *in vivo* specificity of DHTS and support the view that DHTS requires HuR for its antitumor influence. Finally, experimental and theoretical studies here reported suggest that the mechanism of action of DHTS is that of a competitive inhibitor of mRNA binding to HuR. These observations will be the ground for a rational design and synthesis of more potent small-molecule HuR disruptors.

SUPPLEMENTARY DATA

Supplementary Data are available at NAR Online.

FUNDING

Associazione Italiana per la Ricerca sul Cancro (AIRC) [17153 to A.P.]; University of Trento [Intramural funding 40201031 to A.P.]; Fondazione Cariplo [40102636 to A.P.]; AXonomIX research project (to A.Q.) financed by the Provincia Autonoma di Trento, Italy; National Institute of Aging Intramural Research Program of the National Institutes of Health [to M.G., K.A., R.M.]; National Institutes of Health [R01 CA134609 to D.D.]; NIH/NCI Cancer Center Support Grant [P30 CA168524 to D.D.]; Prevent Cancer Foundation and an Institutional Development Award (IDeA) from NIH/ NIGMS [P30 GM103495 to R.P.]. Funding for open access charge: Associazione Italiana per la Ricerca sul Cancro (AIRC).

Conflict of interest statement. None declared.

REFERENCES

- Akaike, Y., Masuda, K., Kuwano, Y., Nishida, K., Kajita, K., Kurokawa, K., Satake, Y., Shoda, K., Imoto, I. and Rokutan, K. (2014) HuR regulates alternative splicing of the TRA2 β gene in human colon cancer cells under oxidative stress. *Mol. Cell. Biol.*, **34**, 2857–2873.
- Izquierdo, J.M. (2008) Hu antigen R (HuR) functions as an alternative pre-mRNA splicing regulator of Fas apoptosis-promoting receptor on exon definition. *J. Biol. Chem.*, **283**, 19077–19084.
- Mukherjee, N., Corcoran, D.L., Nusbaum, J.D., Reid, D.W., Georgiev, S., Hafner, M., Asciano, M., Tuschl, T., Ohler, U. and Keene, J.D. (2011) Integrative regulatory mapping indicates that the RNA-binding protein HuR couples pre-mRNA processing and mRNA stability. *Mol. Cell*, **43**, 327–339.
- Lebedeva, S., Jens, M., Theil, K., Schwanhäusser, B., Selbach, M., Landthaler, M. and Rajewsky, N. (2011) Transcriptome-wide analysis of regulatory interactions of the RNA-binding protein HuR. *Mol. Cell*, **43**, 340–352.

5. Al-Ahmadi, W., Al-Ghamdi, M., Al-Haj, L., Al-Saif, M. and Khabar, K.S.A. (2009) Alternative polyadenylation variants of the RNA binding protein, HuR: abundance, role of AU-rich elements and auto-regulation. *Nucleic Acids Res.*, **37**, 3612–3624.
6. Dai, W., Zhang, G. and Makeyev, E. V. (2012) RNA-binding protein HuR autoregulates its expression by promoting alternative polyadenylation site usage. *Nucleic Acids Res.*, **40**, 787–800.
7. Dutertre, M., Chakrama, F.Z., Combe, E., Desmet, F.-O., Mortada, H., Polay Espinoza, M., Grataidou, L. and Auboeuf, D. (2014) A recently evolved class of alternative 3'-terminal exons involved in cell cycle regulation by topoisomerase inhibitors. *Nat. Commun.*, **5**, 3395.
8. Brennan, C.M. and Steitz, J.A. (2001) HuR and mRNA stability. *Cell. Mol. Life Sci.*, **58**, 266–277.
9. Srikantan, S. and Gorospe, M. (2012) HuR function in disease. *Front. Biosci.*, **17**, 189–205.
10. Papadaki, O., Milatos, S., Grammenoudi, S., Mukherjee, N., Keene, J.D. and Kontoyiannis, D.L. (2009) Control of thymic T cell maturation, deletion and egress by the RNA-binding protein HuR. *J. Immunol.*, **182**, 6779–6788.
11. Legnini, I., Morlando, M., Mangiacavalli, A., Fatica, A. and Bozzoni, I. (2014) A feedforward regulatory loop between HuR and the long noncoding RNA linc-MD1 controls early phases of myogenesis. *Mol. Cell*, **53**, 506–514.
12. Wang, W., Yang, X., Cristofalo, V.J., Holbrook, N.J. and Gorospe, M. (2001) Loss of HuR is linked to reduced expression of proliferative genes during replicative senescence. *Mol. Cell Biol.*, **21**, 5889–5898.
13. Sakai, K., Kitagawa, Y. and Hirose, G. (1999) Binding of neuronal ELAV-like proteins to the uridine-rich sequence in the 3'-untranslated region of tumor necrosis factor- α messenger RNA. *FEBS Lett.*, **446**, 157–162.
14. González-Feliciano, J.A., Hernández-Pérez, M., Estrella, L.A., Colón-López, D.D., López, A., Martínez, M., Maurás-Rivera, K.R., Lasalde, C., Martínez, D., Araujo-Pérez, F. *et al.* (2014) The role of HuR in the post-transcriptional regulation of interleukin-3 in T cells. *PLoS One*, **9**, e92457.
15. Zha, W., Wang, G., Pecora, B.S., Studer, E., Hylemon, P.B., Pandak, W.M. and Zhou, H. (2010) Role of RNA-binding protein HuR and CUGBP1 in LPS-induced interleukin-6 expression in macrophages. *FASEB J.*, **24**, 494.7–494.7.
16. Kim, Y., Noren Hooten, N., Dluzen, D.F., Martindale, J.L., Gorospe, M. and Evans, M.K. (2015) Posttranscriptional regulation of the inflammatory marker C-reactive protein by the RNA-binding protein HuR and MicroRNA 637. *Mol. Cell Biol.*, **35**, 4212–4221.
17. Gubin, M.M., Techasintana, P., Magee, J.D., Dahm, G.M., Calaluce, R., Martindale, J.L., Whitney, M.S., Franklin, C.L., Besch-Williford, C., Hollingsworth, J.W. *et al.* (2014) Conditional knockout of the RNA-binding protein HuR in CD4⁺ T cells reveals a gene dosage effect on cytokine production. *Mol. Med.*, **20**, 93–108.
18. Fan, J., Ishmael, F.T., Fang, X., Myers, A., Cheadle, C., Huang, S.-K., Atasoy, U., Gorospe, M. and Stellato, C. (2011) Chemokine transcripts as targets of the RNA-binding protein HuR in human airway epithelium. *J. Immunol.*, **186**, 2482–2494.
19. Diaz-Muñoz, M.D., Bell, S.E., Fairfax, K., Monzon-Casanova, E., Cunningham, A.F., Gonzalez-Porta, M., Andrews, S.R., Bunik, V.I., Zarnack, K., Curk, T. *et al.* (2015) The RNA-binding protein HuR is essential for the B cell antibody response. *Nat. Immunol.*, **16**, 415–425.
20. DeMicco, A., Naradikian, M.S., Sindhava, V.J., Yoon, J.-H., Gorospe, M., Wertheim, G.B., Cancro, M.P. and Bassing, C.H. (2015) B cell-intrinsic expression of the HuR RNA-binding protein is required for the T cell-dependent immune response in vivo. *J. Immunol.*, **195**, 3449–3462.
21. Mazan-Mamczarz, K., Hagner, P.R., Corl, S., Srikantan, S., Wood, W.H., Becker, K.G., Gorospe, M., Keene, J.D., Levenson, A.S. and Gartenhaus, R.B. (2008) Post-transcriptional gene regulation by HuR promotes a more tumorigenic phenotype. *Oncogene*, **27**, 6151–6163.
22. Wang, W., Furneaux, H., Cheng, H., Caldwell, M.C., Hutter, D., Liu, Y., Holbrook, N. and Gorospe, M. (2000) b. HuR regulates p21 mRNA stabilization by UV light. *Mol. Cell Biol.*, **20**, 760–769.
23. Latorre, E., Carelli, S., Raimondi, I., D'Agostino, V., Castiglioni, I., Zucal, C., Moro, G., Luciani, A., Ghilardi, G., Monti, E. *et al.* (2016) The ribonucleic complex HuR-MALAT1 represses CD133 expression and suppresses epithelial-mesenchymal transition in breast cancer. *Cancer Res.*, **76**, 2626–2636.
24. Latorre, E., Tebaldi, T., Viero, G., Sparta, A.M., Quattrone, A. and Provenzani, A. (2012) Downregulation of HuR as a new mechanism of doxorubicin resistance in breast cancer cells. *Mol. Cancer*, **11**, 13.
25. Latorre, E., Castiglioni, I., Gatto, P., Carelli, S., Quattrone, A. and Provenzani, A. (2014) Loss of protein kinase C δ /HuR interaction is necessary to doxorubicin resistance in breast cancer cell lines. *J. Pharmacol. Exp. Ther.*, **349**, 99–106.
26. Abdelmohsen, K. and Gorospe, M. (2010) Posttranscriptional regulation of cancer traits by HuR. *Wiley Interdiscip. Rev. RNA*, **1**, 214–229.
27. Levy, N.S., Chung, S., Furneaux, H. and Levy, A.P. (1998) Hypoxic stabilization of vascular endothelial growth factor mRNA by the RNA-binding protein HuR. *J. Biol. Chem.*, **273**, 6417–6423.
28. Meisner, N.-C., Hintersteiner, M., Mueller, K., Bauer, R., Seifert, J.-M., Naegeli, H.-U., Ottl, J., Oberer, L., Guenat, C., Moss, S. *et al.* (2007) Identification and mechanistic characterization of low-molecular-weight inhibitors for HuR. *Nat. Chem. Biol.*, **3**, 508–515.
29. Wu, X., Lan, L., Wilson, D.M., Marquez, R.T., Tsao, W., Gao, P., Roy, A., Turner, B.A., McDonald, P., Tunge, J. *et al.* (2015) Identification and validation of novel small molecule disruptors of HuR-mRNA interaction. *ACS Chem. Biol.*, doi:10.1021/cb500851u.
30. Blanco, F.F., Preet, R., Aguado, A., Vishwakarma, V., Stevens, L.E., Vyas, A., Padhye, S., Xu, L., Weir, S.J., Anant, S. *et al.* (2016) Impact of HuR inhibition by the small molecule MS-444 on colorectal cancer cell tumorigenesis. *Oncotarget*, doi:10.18632/oncotarget.12189.
31. D'Agostino, V.G., Lal, P., Mantelli, B., Tiedje, C., Zucal, C., Thongon, N., Gaestel, M., Latorre, E., Marinelli, L., Seneci, P. *et al.* (2015) Dihydroanthranone-I interferes with the RNA-binding activity of HuR affecting its post-transcriptional function. *Sci. Rep.*, **5**, 16478.
32. D'Agostino, V.G., Adami, V. and Provenzani, A. (2013) A novel high throughput biochemical assay to evaluate the HuR protein-RNA complex formation. *PLoS One*, **8**, e72426.
33. Chae, M.-J., Sung, H.Y., Kim, E.-H., Lee, M., Kwak, H., Chae, C.H., Kim, S. and Park, W.-Y. (2009) Chemical inhibitors destabilize HuR binding to the AU-rich element of TNF- α mRNA. *Exp. Mol. Med.*, **41**, 824–831.
34. Zucal, C., D'Agostino, V., Loffredo, R., Mantelli, B., Thongon, N., Lal, P., Latorre, E. and Provenzani, A. (2015) Targeting the multifaceted HuR protein, benefits and caveats. *Curr. Drug Targets*, **16**, 499–515.
35. Wang, Z., Bhattacharya, A. and Ivanov, D.N. (2015) Identification of small-molecule inhibitors of the HuR/RNA interaction using a fluorescence polarization screening assay followed by NMR validation. *PLoS One*, **10**, e0138780.
36. Fan, X.C. and Steitz, J.A. (1998) HNS, a nuclear-cytoplasmic shuttling sequence in HuR. *Proc. Natl. Acad. Sci. U.S.A.*, **95**, 15293–15298.
37. Scheiba, R.M., de Opakua, A.I., Diaz-Quintana, A., Cruz-Gallardo, I., Martínez-Cruz, L.A., Martínez-Chantar, M.L., Blanco, F.J. and Diaz-Moreno, I. (2014) The C-terminal RNA binding motif of HuR is a multi-functional domain leading to HuR oligomerization and binding to U-rich RNA targets. *RNA Biol.*, **11**, 1250–1261.
38. Maris, C., Dominguez, C. and Allain, F.H.-T. (2005) The RNA recognition motif, a plastic RNA-binding platform to regulate post-transcriptional gene expression. *FEBS J.*, **272**, 2118–2131.
39. Benoit, R.M., Meisner, N.-C., Kallen, J., Graff, P., Hemmig, R., Cèbe, R., Ostermeier, C., Widmer, H. and Auer, M. (2010) The x-ray crystal structure of the first RNA recognition motif and site-directed mutagenesis suggest a possible HuR redox sensing mechanism. *J. Mol. Biol.*, **397**, 1231–1244.
40. Wang, H., Zeng, F., Liu, Q., Liu, H., Liu, Z., Niu, L., Teng, M. and Li, X. (2013) The structure of the ARE-binding domains of Hu antigen R (HuR) undergoes conformational changes during RNA binding. *Acta Crystallogr. D. Biol. Crystallogr.*, **69**, 373–380.
41. Kim, H.S., Wilce, M.C.J., Yoga, Y.M.K., Pendini, N.R., Gunzburg, M.J., Cowieson, N.P., Wilson, G.M., Williams, B.R.G., Gorospe, M. and Wilce, J.A. (2011) Different modes of interaction by TIAR and HuR with target RNA and DNA. *Nucleic Acids Res.*, **39**, 1117–1130.
42. Lal, S., Cheung, E.C., Zarei, M., Preet, R., Chand, S.N., Mambelli-Lisboa, N.C., Romeo, C., Stout, M.C., Londin, E., Goetz, A. *et al.* (2017) CRISPR knockout of the HuR gene causes a xenograft lethal phenotype. *Mol. Cancer Res.*, doi:10.1158/1541-7786.MCR-16-0361.

43. Young, L.E., Moore, A.E., Sokol, L., Meisner-Kober, N. and Dixon, D.A. (2012) The mRNA stability factor HuR inhibits microRNA-16 targeting of COX-2. *Mol. Cancer Res.*, **10**, 167–180.
44. Barbato, G., Ikura, M., Kay, L.E., Pastor, R.W. and Bax, A. (1992) Backbone dynamics of calmodulin studied by ¹⁵N relaxation using inverse detected two-dimensional NMR spectroscopy: the central helix is flexible. *Biochemistry*, **31**, 5269–5278.
45. Kay, L.E., Nicholson, L.K., Delaglio, F., Bax, A. and Torchia, D. (1992) Pulse sequences for removal of the effects of cross correlation between dipolar and chemical-shift anisotropy relaxation mechanisms on the measurement of heteronuclear T1 and T2 values in proteins. *J. Magn. Reson.*, **97**, 359–375.
46. Peng, J.W. and Wagner, G. (1994) Investigation of protein motions via relaxation measurements. *Methods Enzymol.*, **239**, 563–596.
47. García de la Torre, J., Huertas, M.L. and Carrasco, B. (2000) HYDRONMR: prediction of NMR relaxation of globular proteins from atomic-level structures and hydrodynamic calculations. *J. Magn. Reson.*, **147**, 138–146.
48. Phillips, J.C., Braun, R., Wang, W., Gumbart, J., Tajkhorshid, E., Villa, E., Chipot, C., Skeel, R.D., Kalé, L. and Schulten, K. (2005) Scalable molecular dynamics with NAMD. *J. Comput. Chem.*, **26**, 1781–1802.
49. Cornell, W.D., Cieplak, P., Bayly, C.I., Gould, I.R., Merz, K.M., Ferguson, D.M., Spellmeyer, D.C., Fox, T., Caldwell, J.W. and Kollman, P.A. (1995) A second generation force field for the simulation of proteins, nucleic acids, and organic molecules. *J. Am. Chem. Soc.*, **117**, 5179–5197.
50. Lindorff-Larsen, K., Piana, S., Palmo, K., Maragakis, P., Klepeis, J.L., Dror, R.O. and Shaw, D.E. (2010) Improved side-chain torsion potentials for the Amber ff99SB protein force field. *Proteins*, **78**, 1950–1958.
51. Allnér, O., Nilsson, L. and Villa, A. (2012) Magnesium ion–water coordination and exchange in biomolecular simulations. *J. Chem. Theory Comput.*, **8**, 1493–1502.
52. Bayly, C.I., Cieplak, P., Cornell, W. and Kollman, P.A. (1993) A well-behaved electrostatic potential based method using charge restraints for deriving atomic charges: the RESP model. *J. Phys. Chem.*, **97**, 10269–10280.
53. Gaussian 09, Revision A.02 (2009) *Gaussian 09 Citation*. <http://gaussian.com/g09citation/>.
54. Dupradeau, F.-Y., Pigache, A., Zaffran, T., Savineau, C., Lelong, R., Grivel, N., Lelong, D., Rosanski, W. and Cieplak, P. (2010) The R.E.D. tools: advances in RESP and ESP charge derivation and force field library building. *Phys. Chem. Chem. Phys. PCCP*, **12**, 7821–7839.
55. Vanquelef, E., Simon, S., Marquart, G., Garcia, E., Klimerak, G., Delepine, J.C., Cieplak, P. and Dupradeau, F.-Y. (2011) R.E.D. Server: a web service for deriving RESP and ESP charges and building force field libraries for new molecules and molecular fragments. *Nucleic Acids Res.*, **39**, W511–W517.
56. Wang, J., Wang, W., Kollman, P.A. and Case, D.A. (2006) Automatic atom type and bond type perception in molecular mechanical calculations. *J. Mol. Graph. Model.*, **25**, 247–260.
57. Abdelmohsen, K., Srikantan, S., Yang, X., Lal, A., Kim, H.H., Kuwano, Y., Galban, S., Becker, K.G., Kamara, D., de Cabo, R. et al. (2009) Ubiquitin-mediated proteolysis of HuR by heat shock. *EMBO J.*, **28**, 1271–1282.
58. Dassi, E., Re, A., Leo, S., Tebaldi, T., Pasini, L., Peroni, D. and Quattrone, A. (2014) AURA 2: Empowering discovery of post-transcriptional networks. *Transl. (Austin, Tex.)*, **2**, e27738.
59. Chen, E.Y., Tan, C.M., Kou, Y., Duan, Q., Wang, Z., Meirelles, G.V., Clark, N.R. and Ma'ayan, A. (2013) Enrichr: interactive and collaborative HTML5 gene list enrichment analysis tool. *BMC Bioinformatics*, **14**, 128.
60. Yu, G., Li, F., Qin, Y., Bo, X., Wu, Y. and Wang, S. (2010) GOSemSim: an R package for measuring semantic similarity among GO terms and gene products. *Bioinformatics*, **26**, 976–978.
61. Mujo, A., Lixa, C., Carneiro, L.A.M., Anobom, C.D., Almeida, F.C. and Pinheiro, A.S. (2014) ¹H, ¹⁵N and ¹³C resonance assignments of the RRM1 domain of the key post-transcriptional regulator HuR. *Biomol. NMR Assign.*, doi:10.1007/s12104-014-9592-9.
62. Wang, H., Zeng, F., Liu, H., Teng, M. and Li, X. (2012) Crystal structure of two tandem RNA recognition motifs of Human antigen R. <https://www.ncbi.nlm.nih.gov/Structure/mmdb/mmdbsrv.cgi?uid=4EGL>.
63. Bertini, I., Fragai, M., Luchinat, C., Melikian, M., Mylonas, E., Sarti, N. and Svergun, D.I. (2009) Interdomain flexibility in full-length matrix metalloproteinase-1 (MMP-1). *J. Biol. Chem.*, **284**, 12821–12828.
64. Bertini, I., Calderone, V., Fragai, M., Jaiswal, R., Luchinat, C., Melikian, M., Mylonas, E. and Svergun, D.I. (2008) Evidence of reciprocal reorientation of the catalytic and hemopexin-like domains of full-length MMP-12. *J. Am. Chem. Soc.*, **130**, 7011–7021.
65. Cerofolini, L., Fields, G.B., Fragai, M., Gerales, C.F.G.C., Luchinat, C., Parigi, G., Ravera, E., Svergun, D.I. and Teixeira, J.M.C. (2013) Examination of matrix metalloproteinase-1 in solution: a preference for the pre-collagenolysis state. *J. Biol. Chem.*, **288**, 30659–30671.
66. Dosset, P., Hus, J.-C., Blackledge, M. and Marion, D. (2000) Efficient analysis of macromolecular rotational diffusion from heteronuclear relaxation data. *J. Biomol. NMR*, **16**, 23–28.
67. Morrison, K.L. and Weiss, G.A. (2001) Combinatorial alanine-scanning. *Curr. Opin. Chem. Biol.*, **5**, 302–307.
68. Arkin, M.R., Glicksman, M.A., Fu, H., Havel, J.J. and Du, Y. (2004) Inhibition of protein-protein interactions: non-cellular assay formats. In: Sittampalam, G.S., Coussens, N.P., Nelson, H., Arkin, M., Auld, D., Austin, C., Bejcek, B., Glicksman, M., Ingles, J. and Iversen, P.W. (eds). *Assay Guidance Manual*. Eli Lilly & Company and the National Center for Advancing Translational Sciences, Bethesda.
69. de Silanes, I.L., Zhan, M., Lal, A., Yang, X. and Gorospe, M. (2004) Identification of a target RNA motif for RNA-binding protein HuR. *Proc. Natl. Acad. Sci. U.S.A.*, **101**, 2987–2992.
70. Wu, X., Lan, L., Smith, A., Marquez, R., Wilson, D., Rogers, S., Gao, P., Lovell, S., Karanicolas, J., Dixon, D. et al. (2015) Abstract 2449: Targeting an ‘undruggable’ RNA-binding protein: Discovery of small molecule inhibitors of HuR for novel breast cancer therapy. *Cancer Res.*, **75**, 2449–2449.
71. Scheiba, R.M., Aroca, Á. and Díaz-Moreno, I. (2012) HuR thermal stability is dependent on domain binding and upon phosphorylation. *Eur. Biophys. J.*, **41**, 597–605.
72. Abdelmohsen, K., Pullmann, R., Lal, A., Kim, H.H., Galban, S., Yang, X., Blethrow, J.D., Walker, M., Shubert, J., Gillespie, D. et al. (2007) Phosphorylation of HuR by Chk2 regulates SIRT1 expression. *Mol. Cell*, **25**, 543–557.
73. Wang, L., Hu, T., Shen, J., Zhang, L., Chan, R.L.-Y., Lu, L., Li, M., Cho, C.H. and Wu, W.K.K. (2015) Dihydrotanshinone I induced apoptosis and autophagy through caspase dependent pathway in colon cancer. *Phytomedicine*, **22**, 1079–1087.
74. Liu, J.-J., Wu, H.-H., Chen, T.-H., Leung, W. and Liang, Y.-C. (2015) 15,16-Dihydrotanshinone I from the functional food *Salvia miltiorrhiza* exhibits anticancer activity in human HL-60 leukemia cells: in vitro and in vivo studies. *Int. J. Mol. Sci.*, **16**, 19387–19400.
75. Ye, Y., Xu, W., Zhong, W., Li, Y. and Wang, C. (2012) Combination treatment with dihydrotanshinone I and irradiation enhances apoptotic effects in human cervical cancer by HPV E6 down-regulation and caspases activation. *Mol. Cell. Biochem.*, **363**, 191–202.
76. Tsai, S.-L., Suk, F.-M., Wang, C.-I., Liu, D.-Z., Hou, W.-C., Lin, P.-J., Hung, L.-F. and Liang, Y.-C. (2007) Anti-tumor potential of 15, 16-dihydrotanshinone I against breast adenocarcinoma through inducing G1 arrest and apoptosis. *Biochem. Pharmacol.*, **74**, 1575–1586.

SCIENTIFIC REPORTS



OPEN

Dihydrotanshinone-I interferes with the RNA-binding activity of HuR affecting its post-transcriptional function

Received: 18 March 2015
Accepted: 14 October 2015
Published: 10 November 2015

Vito Giuseppe D'Agostino¹, Preet Lal¹, Barbara Mantelli¹, Christopher Tiedje², Chiara Zucal¹, Natthakan Thongon¹, Matthias Gaestel², Elisa Latorre¹, Luciana Marinelli³, Pierfausto Seneci⁴, Marialaura Amadio⁵ & Alessandro Provenzani¹

Post-transcriptional regulation is an essential determinant of gene expression programs in physiological and pathological conditions. HuR is a RNA-binding protein that orchestrates the stabilization and translation of mRNAs, critical in inflammation and tumor progression, including tumor necrosis factor-alpha (TNF). We identified the low molecular weight compound 15,16-dihydrotanshinone-I (DHTS), well known in traditional Chinese medicine practice, through a validated high throughput screening on a set of anti-inflammatory agents for its ability to prevent HuR:RNA complex formation. We found that DHTS interferes with the association step between HuR and the RNA with an equilibrium dissociation constant in the nanomolar range *in vitro* ($K_i = 3.74 \pm 1.63$ nM). In breast cancer cell lines, short term exposure to DHTS influences mRNA stability and translational efficiency of TNF in a HuR-dependent manner and also other functional readouts of its post-transcriptional control, such as the stability of selected pre-mRNAs. Importantly, we show that migration and sensitivity of breast cancer cells to DHTS are modulated by HuR expression, indicating that HuR is among the preferential intracellular targets of DHTS. Here, we disclose a previously unrecognized molecular mechanism exerted by DHTS, opening new perspectives to therapeutically target the HuR mediated, post-transcriptional control in inflammation and cancer cells.

Post-transcriptional control of messenger RNA, coordinated by RNA-binding proteins (RBPs) and small or long non-coding RNAs, is an essential determinant of protein expression. Altered mRNA stability of pro-inflammatory cytokines tightly correlates with several pathological conditions such as inflammation, autoimmune disorders and cancer¹. A prominent example of cytokine subjected to post-transcriptional control is tumor necrosis factor alpha (TNF-alpha or TNF), one of the main mediators of chronic inflammation associated with malignant cell transformation, growth and tumor progression². Depletion of several RBPs can alter TNF protein production, leading to exacerbated chronic inflammatory disease both in mice and in humans³, supporting the relevance of *in vivo* post-transcriptional control on TNF mRNA. The half-life of this transcript is influenced by competitive binding of RBPs to adenylate- and uridylate-rich elements (AU-rich elements or AREs) and by a constitutive decay element (CDE) in its 3'-untranslated region (UTR)^{4,5}. Notably, it has been shown that the stability and translational

¹Centre For Integrative Biology (CIBIO), University of Trento, Trento, 38123, Italy. ²Department of Biochemistry, Hannover Medical University, Hannover, D-30625, Germany. ³Department of Pharmacy, University of Naples "Federico II", Naples, 80131, Italy. ⁴Chemistry Department, University of Milan, Milan, 20133, Italy. ⁵Department of Drug Sciences, University of Pavia, Pavia, 27100, Italy. Correspondence and requests for materials should be addressed to A.P. (email: alessandro.provenzani@unitn.it)

efficiency of TNF mRNA is dependent on the p38 MAPK pathway, whose activation modulates the cytoplasmic equilibrium of tristetraprolin (TTP or Zfp36) and HuR/ELAVL1 proteins⁶. Whilst TTP is an anti-inflammatory RBP favoring rapid mRNA degradation, HuR stabilizes transcripts and promotes their poly-ribosomes engagement for active translation. This post-transcriptional function of HuR has been described for a wide number of transcripts bearing AU-rich elements, whose turnover is critical for cell proliferation, tumor cell survival, angiogenesis and metastasis^{7–10}. Sporadically, anti-inflammatory agents have been reported to post-transcriptionally modulate cytokines, including TNF, with a variable involvement of the p38 MAPK pathway, as in the case of KL-1037¹¹, s-curvularin¹², LCY-2-CHO¹³. However, the direct and specific modulation of defined *trans*-acting factors has remained elusive. On the other side, systematic investigations, based on the direct evaluation of a post-transcriptional read-out have shown the feasibility of considering RBPs as potential drug targets^{14–16}. Interestingly, resveratrol was found to suppress activation-induced gene expression in T-cell via a post-transcriptional mechanism and its effects were rescued by the RBP HuR. The same molecule was found to exert its post-transcriptional effects by regulating the RBP KSRP, suggesting that resveratrol changes the mRNA stability of HuR-targeted transcripts by enhancing the 3'-UTR binding of KSRP and replacing HuR from the same 3'-UTR sequences¹⁶. Here we demonstrate that 15,16-dihydrotanshinone-I (DHTS), identified through a biochemical high-throughput screening among a set of anti-inflammatory agents, inhibits the HuR-RNA complex formation *in vitro* in low nanomolar range. DHTS belongs to the bioactive family of diterpenic tanshinones, extracted from the roots of *Salvia miltiorrhiza* and well-known in traditional Chinese medicine practice. Tanshinones are anti-inflammatory agents used for treatment of cardiovascular diseases¹⁷ and during the last years they have been proposed as anti-cancer agents due their anti-proliferative, anti-angiogenic and pro-apoptotic activities against a broad spectrum of tumors^{18,19}. We provide evidences that interference of DHTS on HuR activity determines a post-transcriptional influence of TNF mRNA processing, showing a previously unrecognized molecular mechanism for this class of small molecules. In addition, we show that cytotoxicity and migration properties of breast cancer cell lines treated with DHTS are influenced by HuR dosage, supporting the post-transcriptional effect of this compound as a new, therapeutically relevant molecular mechanism.

Results

15,16-Dihydrotanshinone I (DHTS) interferes with HuR-RNA interaction *in vitro*. The mRNA stabilizing effects of HuR have been frequently investigated by studying the post-transcriptional control of key pro-inflammatory genes like *COX-2*, *TNF* or specific cytokines such as *IL17*^{20–22}. We hypothesized that anti-inflammatory small molecules could integrate a post-transcriptional layer of influence on mRNAs, in their mechanism of action, by interfering with HuR function. By using a previously validated biochemical approach²³ involving the 3'UTR ARE of TNF as RNA probe and a recombinant human HuR protein, we screened a set of commercially available anti-inflammatory compounds (a total of 107 listed in Supplementary Table S1) for their ability to prevent the rHuR-RNA complex formation. Eight positive hits were obtained (DHTS, hydrocortisone acetate, amiprilose, flurbiprofen, deracoxib, fluocinolone, triamcinolone, dexamethasone). The most potent hit, DHTS (ChEMBL227075 ID in ChEMBL database, Z-Score = -2.69, Fig. 1A and Supplementary Table S1), among the other compounds, confirmed this inhibitory activity in RNA electrophoresis mobility shift assays. DHTS did not alter the electrophoretic mobility or the stability of the RNA probe even when a 200 fold molar excess (100 μ M) was used in the assay (Fig. 1B and Supplementary Fig. S1A), behaving as a validated hit. Saturation binding competitive experiments at equilibrium, either by REMSA (Fig. 1C) or AlphaScreen assays (Fig. 1D), indicated an equilibrium dissociation constant for DHTS (K_d) of 3.74 ± 1.63 nM, using a K_d equal to 2.5 nM²³, and IC_{50} equaling 149 ± 34 nM and 68 ± 16 nM for REMSA or AlphaScreen assays, respectively and according to the different concentration of the reagents used. The range of K_d values was also confirmed by competitive binding kinetics experiments (Fig. 1E), that revealed an association rate constant (k_3) of $5.38 \pm 1.64 \times 10^6 M^{-1} min^{-1}$ and a dissociation rate constant (k_4) of $0.016 \pm 0.01 min^{-1}$ for DHTS ($k_4/k_3 = 2.97 \pm 0.7$ nM). From these data, representing the law of mass action parameters of DHTS, it can be inferred that DHTS has a much higher probability to associate with one or both the free ligands, rather than to displace a pre-formed protein-RNA complex. Consistently, binding kinetic experiments performed either upon pre-incubation of rHuR with different concentrations of DHTS (Fig. 1F), or upon pre-incubation of protein and RNA (Fig. 1G), provided evidence that DHTS mainly prevents the association between the two ligands. Since the recognition of RNA substrate is determined by the RNA recognition domains (RRMs) of HuR, we purified two recombinant HuR isoforms (Supplementary Fig. S1B) retaining two different arrangements of RRM, as depicted in Fig. 2A. As RRM1 and RRM2 are the rate-limiting domains for HuR binding activity²⁴, the M1_M2 construct was expected to best recapitulate the ability of full-length HuR to bind to RNA, and to be the best target for DHTS. Accordingly, at equilibrium, M1_M2 isoform showed a K_d value (2.66 nM) similar to full-length HuR. DHTS similarly inhibited the M1_M2-RNA complex formation ($K_i = 4.12 \pm 0.81$ nM). Notably, the M2_M3 construct expressed a labile protein characterized by higher K_d value (~24 nM) and only limited effects of DHTS were observed. In addition, we purified each single RRM domain (M1, M2, M3) from *E. coli* cells (Supplementary Fig. S1C) and analyzed their binding to the RNA probe in the presence of DHTS. The binding of M2 and M3 was not affected even using 10 μ M of DHTS, while M1 was only marginally affected, being 74% of the protein still binding RNA with 5 μ M of DHTS (Supplementary Fig. S1C). Taken together, these results

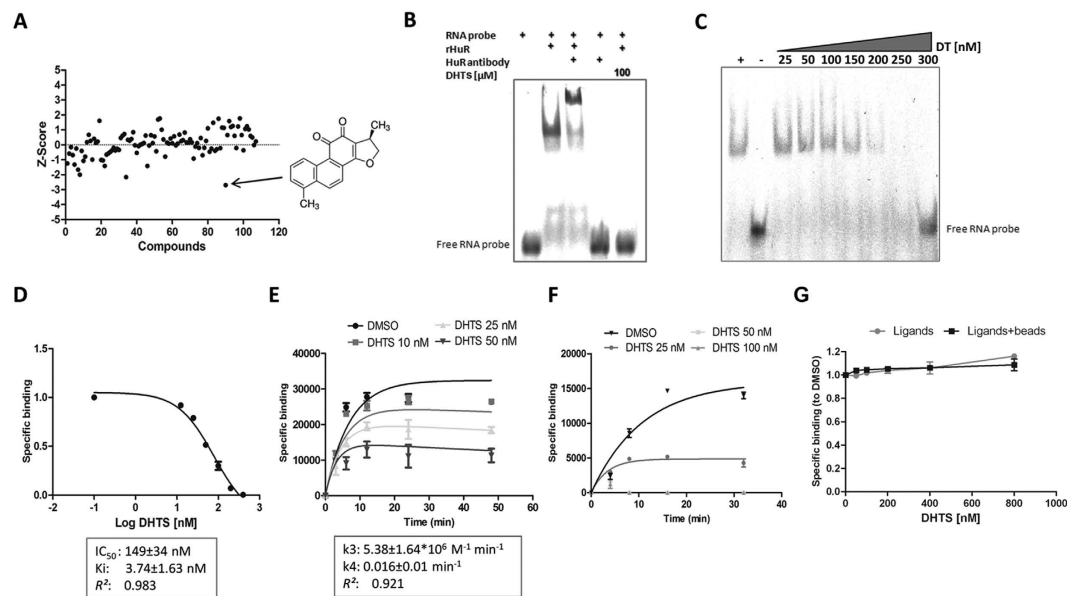


Figure 1. DHTS is an inhibitor of the rHuR-RNA interaction. (A) AlphaScreen HTS carried out using 1 nM of rHuR, 50 nM of BiTNF RNA probe and 50 nM of 107 anti-inflammatory compounds (see Table S1). (B) Representative REMSA performed with 0.5 μ M of rHuR and 0.5 μ M of Cy-3 RNA probe at equilibrium, showing the inhibitory activity of DHTS and its un-efcacy to electrophoretic mobility of the free RNA even at 100 μ M. (C) Saturation binding by REMSA or (D) by AlphaScreen assays evaluating DHTS activity in low micromolar or nanomolar range, respectively. (E) Kinetic experiments showing association (k_3) and dissociation (k_4) rate constants of DHTS. (F) Kinetic experiments performed upon pre-incubation of 1 nM of rHuR with different concentrations of DHTS before addition of 50 nM of BiTNF probe. (G) Dissociation experiments performed upon 30 min pre-incubation of 1 nM of rHuR and 50 nM of RNA (Ligands), or 30 min pre-incubation of Ligands+beads, before addition of DHTS. Mean \pm SD refers to three independent experiments ($n = 3$).

suggest that the compound interferes with RNA binding by affecting a different site from the domain of RNA recognition. A putative explanation could reside in the interference by DHTS with the allosteric conformational changes of the first two RRM, disturbing the additional contacts formed with the inter-domain linker region during RNA binding²⁴. The *in vitro* activity of three commercially available members of the tanshinone family of compounds was evaluated in our biochemical model. Each tested tanshinone showed inhibitory activity (Supplementary Fig. S1D). However, while cryptotanshinone and tanshinone IIA were less potent (micromolar range), the potency of tanshinone I was comparable to DHTS at equilibrium (Fig. 2B). This indicates how this kind of interference requires either an aromatic furan ring (as in tanshinone I), or a reduced dihydrofuran (as in DHTS) on the right portion of the molecule. Conversely, the left side of tanshinones must contain a planar, aromatic methyl-substituted ring (as in DHTS and tanshinone I), rather than a non-planar, dimethyl-substituted cyclohexene ring (as in cryptotanshinone and tanshinone IIA). As tanshinone I is poorly soluble in buffers of biochemical assays (producing visible precipitates at the highest doses), we used DHTS as reference compound/inhibitor to exploit this bioactivity for further experiments.

Albeit the selective profile of DHTS and tanshinones has to be systematically characterized, we selected four other RBPs, i.e. Lin28b, TTP, TDP-43 and ELAVL4/HuD, with different structural similarity compared with HuR and tested DHTS as a modulator of their specific protein-RNA interactions (Fig. 2C). As expected considering the 78% structural similarity with HuR, only HuD-RNA complex formation was affected by DHTS at the reference doses. Conversely, the binding of Lin28b, TTP, and TDP-43 to RNA did not appear substantially affected. Taken together, these biochemical data allowed to quantitatively determine the DHTS-mediated inhibition of the HuR-RNA complex formation *in vitro*, the highest potency of DHTS among the tested analogs and its selective profile towards other RBPs. Then, we decided to deeply investigate the post-transcriptional role of DHTS in a panel of breast cancer cell lines, characterized by HuR over-expression²⁵.

DHTS down-regulates TNF mRNA and protein levels. Viability assays measuring intracellular ATP levels in different breast cancer cell lines (MCF-7, MDA-MB-231 and SKBR3), showed that about 50% of cells were not viable after 24 h treatment with 1 μ M DHTS (MCF-7, $IC_{50} = 0.84 \mu$ M, Fig. 3A; MDA-MB-231, $IC_{50} = 0.92 \mu$ M, and SKBR3, $IC_{50} = 1.2 \mu$ M, graphs not shown). In MCF-7 cells, caspase activation was clearly visible after 24 h of treatment using as low as 0.5 μ M of DHTS. Conversely, at an

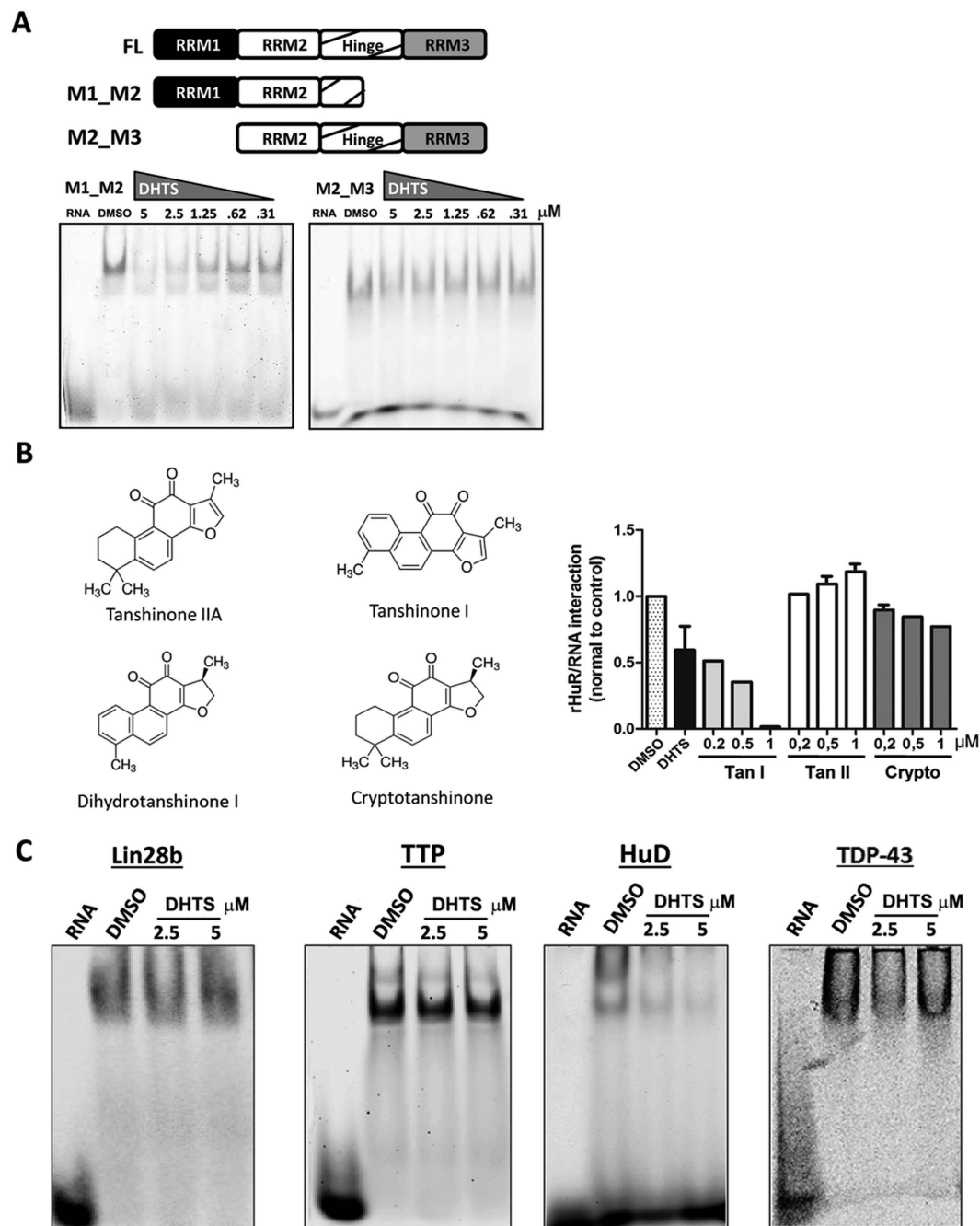


Figure 2. DHTS inhibits HuR's first RRM1s and is not effective against other RBPs, HuD excluded; *in vitro* activity of other tanshinones. (A) Representative gels of at least three independent protein preparations of recombinant M1_M2 and M2_M3 HuR proteins. REMSAs were performed with 0.5 μM of protein, 0.5 μM of Cy-3 RNA probe and DMSO or DHTS at indicated doses. (B) Quantification of specific HuR-RNA binding challenged by indicated concentrations of commercially available tanshinones, including cryptotanshinone; TanI and TanII that were not included in the first screening. (C) Evaluation of DHTS activity at the indicated concentrations against Lin28b, TTP, HuD, and TDP-43 RNA-binding proteins tested by REMSA with 0.5 μM of Cy-3 RNA as indicated in methods. Mean ± SD refers to three independent experiments (n = 3).

earlier time point (3 h), no caspase activation was observed with 1 μM of DHTS (Fig. 3B) and total RNA was actively transcribed (Fig. 3C and Supplementary Fig. S2A). Therefore, we used 1 μM DHTS treatment at 3 h as reference condition to further characterize the impact of DHTS on HuR activity, and to reasonably exclude the induction of dramatic molecular events associated with cytotoxicity of the compound. DHTS alone or in combination with 3 h LPS stimulation (100 ng/ml) reduced TNF levels in stimulated

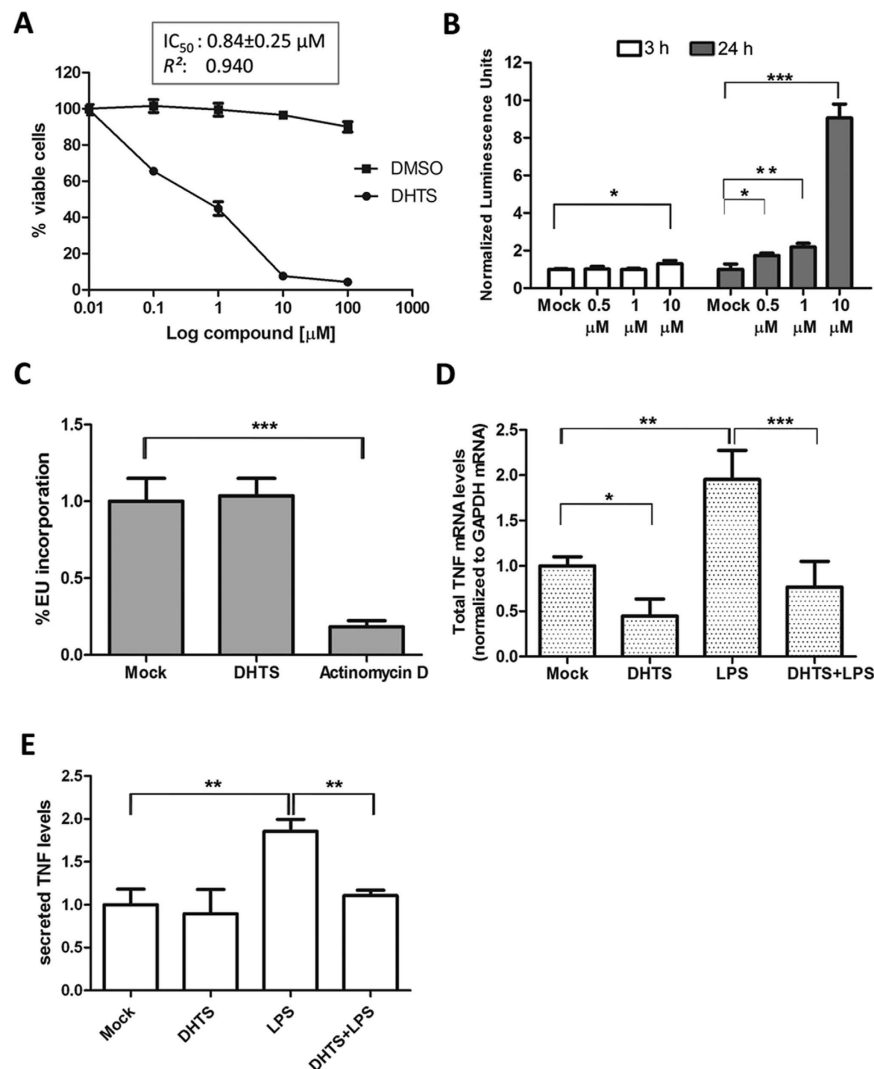


Figure 3. DHTS toxicity and inhibition of TNF in MCF-7 cells. (A) CellTiter-Glo assays upon exposure of MCF-7 cells to DHTS for 24 h. Relative IC₅₀ was calculated by nonlinear regression curve fitting. (B) Apoptosis evaluation by 3/7 Caspase-Glo luminescent assays (Promega) and normalization to trypan blu negative cells (n = 3). (C) High content imaging quantification of fluorescence intensity/cell population of EU-conjugated Alexa-488 after 3 h treatment of MCF-7 cells with 1 μM of DHTS or 2 μM of actinomycin D. (D) Q-RT-PCR of TNF mRNA levels. Relative abundance was normalized with GAPDH mRNA in MCF-7 cells. (E) ELISA measuring secreted TNF protein levels. We detected in Mock condition an average of 15 pg/ml of sTNF as obtained by titration with standards. Where not indicated, mean ± SD refers to four independent experiments (n = 4).

mouse RAW264.7 cell line (Supplementary Fig. S2B)²⁶. Since chronic production of TNF influences the phenotype of breast cancer cells by inducing secondary cytokines production and by impacting their growth and metastatic potential²⁷, we studied the effect of DHTS on the regulation of TNF in human breast cancer cell lines. Exposure of breast cancer cells to 1 μM of DHTS for 3 h significantly reduced total TNF mRNA levels to ≈40% (P < 0.05) of the control levels (Fig. 3D and Supplementary Fig. S2C). Treatment with 1 μg/ml of LPS to MCF-7 (TLR4 positive) enhanced the TNF mRNA levels (P < 0.01), while treatment with DHTS counteracted the LPS-induced up-regulation (P < 0.001) (Fig. 3D). MCF-7 cells expressed almost undetectable levels of TNF protein, and the endogenous (pro-TNF) protein could not be detected by immunoblotting in standard conditions. However, massive stimulation of pro-TNF production *via* exposure of MCF-7 cells to *E. coli* cells, and subsequent administration of DHTS, showed the efficacy of the compound in attenuating the production of pro-TNF (Supplementary Fig. S2D). Similarly, endogenous secreted TNF (sTNF, Fig. 3E) was hardly detectable under basal conditions, but protein level increased after LPS treatment and decreased markedly after 3 h treatment by DHTS (P < 0.01). These data show that DHTS first reduces the TNF mRNA expression level, and subsequently

the translation and secretion of the encoded protein, confirming the anti-inflammatory properties of the compound in these cellular models.

DHTS inhibits post-transcriptional effects of HuR in MCF-7 cells. To test whether DHTS influences the post-transcriptional control of TNF mRNA mediated by HuR we performed ribonucleoprotein immunoprecipitation (RIP) analyses. DHTS reduced the number of copies of TNF mRNA selectively bound by HuR in MCF-7 cells (Fig. 4A). The strong enrichment observed in LPS-stimulated cell extracts confirmed the functional role of HuR in the post-transcriptional control of TNF in human cancer cells ($P < 0.001$). Notably, this effect is not specific for TNF mRNA, since RIP analysis on other HuR regulated transcript demonstrated that the copy number of ERBB2, VEGF, and CCND1 mRNAs bound by HuR in the presence of DHTS is, with different extent, significantly less with respect to the control (Supplementary Fig. S3A). RNA pull-down experiments in lysates from DHTS-treated MCF-7 cells confirmed the inhibition of the association step leading to the HuR:RNA complex formation (Fig. 4B), being the differences of precipitated HuR protein in DHTS treated cells statistically significant ($P < 0.05$) comparing DHTS vs Mock using the biotinylated probe. The same trend was observed for DHTS+LPS vs LPS condition, although with a non-significant effect in these experiments. Another ARE-binding RBP, hnRNP-D/AUF1, also displayed differential RNA-binding activity, however we observed these differences exclusively upon stimulation with LPS. To understand whether DHTS influences the stability of TNF mRNA in a HuR-dependent manner, we used both a stable HuR-silenced MCF-7 clone (siHuR) and transiently HuR over-expressing MCF-7 (HuROE) cells in actinomycin D chase experiments (Fig. 4C). The expression level of HuR positively correlated with the relative abundance of total TNF mRNA in MCF-7 cells, upon simultaneous transcriptional block. Interestingly, DHTS significantly reduced TNF mRNA stability compared with mock cells ($P < 0.01$ at 60 min time point), and caused a slightly additive effect in siHuR cells. On the contrary, DHTS displayed less efficacy in HuROE cells, suggesting that HuR expression is able to counteract the destabilizing effect of DHTS on mature TNF mRNA. To better understand these functional relationships, we evaluated the stability of nuclear immature (pre-) TNF transcripts, confirming, although with different kinetics, the HuR-dependency of mRNA stability and the same effects induced by DHTS on mature RNA transcripts; Similar effects were not observed for GAPDH mRNA under the same experimental conditions (Fig. 4C). Given the emerging evidences regarding HuR functionality in pre-mRNA processing events²⁸, candidate HuR pre-mRNA targets were chosen according to Mukherjee *et al.*²⁸, and CD14 was chosen as a negative control lacking AREs¹⁴. The mRNA stability of individual mRNAs, in actinomycin D chase experiment at single time point, was differently regulated by HuR expression and, except for pre-CTCF mRNA, HuR silencing caused a reduction of pre-BRCA1, pre-MDM2, pre-MYBL2 and pre-NFATC3 mRNA stability (Supplementary Fig. S3B, compare bar 1 and 3), in agreement with reported data²⁸. To a different extent, DHTS diminished the stability of all the pre-mRNAs except the non-target, ARE-lacking, CD14 pre-mRNA (Supplementary Fig. S3B, compare bars 1 to 2). The compound exhibited further destabilization of pre-mRNAs in HuR depleted cells (siHuR), with the exception of pre-NFATC3 mRNA (Supplementary Fig. S3B, compare bars 3 to 4 and 5 to 6). Strikingly, over-expression of HuR in HuROE cells rescued the destabilization effect of DHTS to control levels (Supplementary Fig. S3B, compare bars 7 and 8), supporting the idea that HuR RNA-binding activity is a target of DHTS, and that this compound early impacts this post-transcriptional modulation.

DHTS reduces polysomal recruitment of cytoplasmic TNF mRNA. To evaluate if DHTS modifies the recruitment of TNF mRNA to the translational machinery, we performed nuclear and cytoplasmic RNA purifications from MCF-7 cells treated with DHTS and/or LPS, respectively, and evaluated TNF mRNA levels by real-time PCR (Fig. 5A). Nuclear levels of the transcript were significantly reduced by DHTS both in case-control and in LPS-treated cells (of ~55% and ~31%, $P < 0.001$ and $P < 0.05$, respectively). The relative amount of cytoplasmic TNF mRNA was unchanged in DHTS-treated versus control cells, but was significantly reduced by DHTS treatment (~44%, $P < 0.01$) in LPS-stimulated cells. Therefore, DHTS down-regulated nuclear TNF mRNA and reduced cytoplasmic TNF mRNA only after LPS stimulation.

To functionally investigate the translational efficiency of TNF mRNA, we performed sucrose-gradient fractionations of cytoplasmic sub-polysomal (representative of non-translating monosomes) and polysomal RNAs (representative of actively translating poly-ribosomes). DHTS treatment was performed on MCF-7 cells as such (Fig. 5B), and on LPS-treated MCF-7 and RAW264.7 cells (Supplementary Fig. S4A, S4B, S4C). Overall polysomal profiles showed no qualitative differences between the conditions analyzed, but the distribution analysis of single mRNAs, i.e. GAPDH and TNF (Fig. 5C) demonstrated that treatment with DHTS clearly reduced the polysomal loading of TNF mRNA paralleled by an increased amount in the sub-polysomal fractions. These data are also supported by the quantification of the TNF mRNA in collected sub-polysomal (fraction 1 to 6) and polysomal (fraction 7 to 12) compartments (Supplementary Fig. S4B). Notably, the effect of DHTS on poly/sub ratios increased significantly with concomitant LPS stimulation ($P < 0.001$). Accordingly, polysomal loading of mouse TNF mRNA was also affected by DHTS in stimulated RAW264.7 cells (Supplementary Fig. S4C), supporting the hypothesis that DHTS interferes with the cytoplasmic TNF mRNA fraction loaded on polysomes for its translation. Extensive literature data show that HuR enhances the stability and translation of its bound

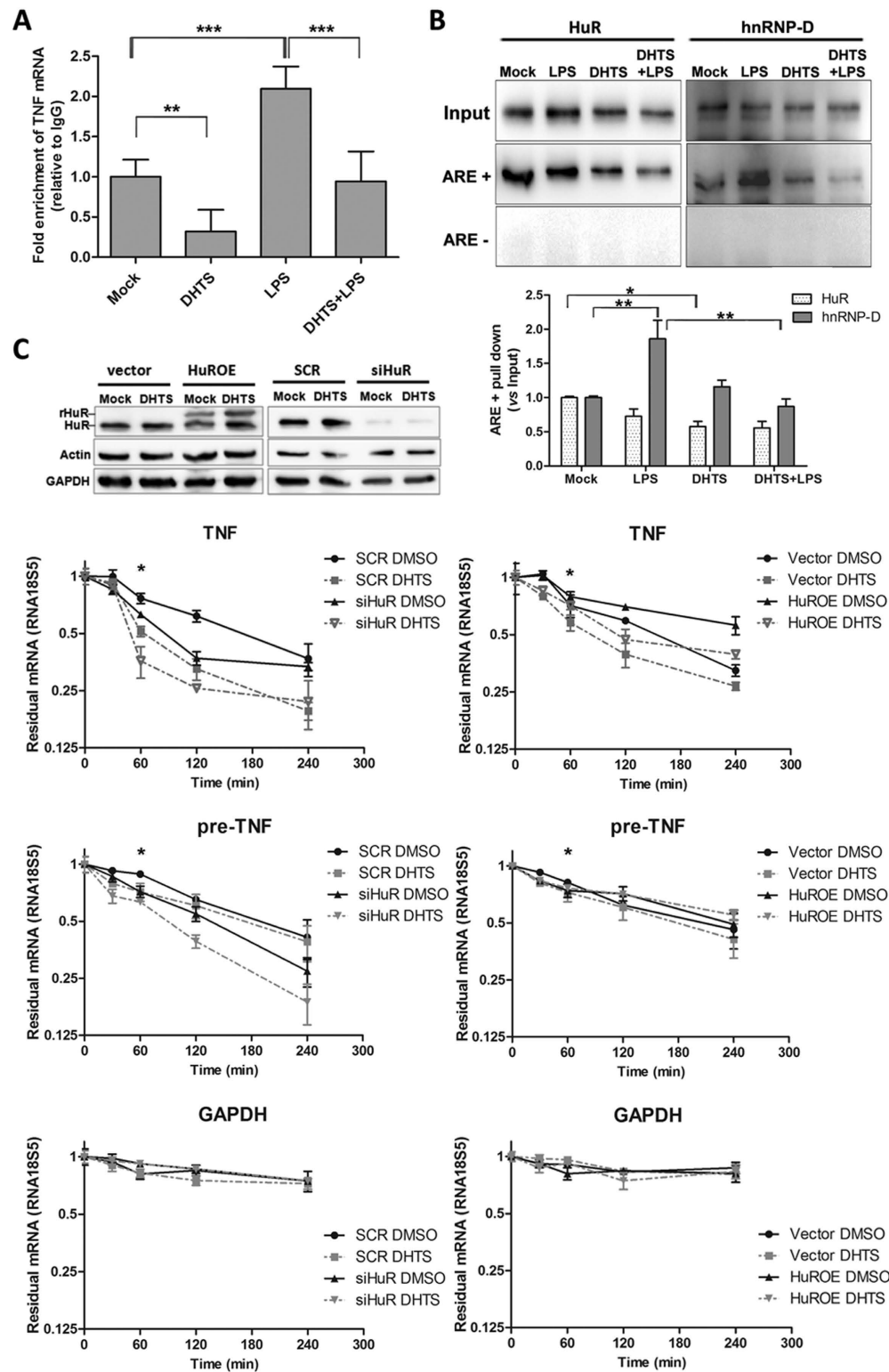


Figure 4. DHTS inhibits intracellular HuR-mRNA association, influencing mRNA stability. (A) RNA immunoprecipitation using MCF-7 lysates obtained after 3 h of treatment with DMSO, 1 μ M of DHTS, 1 μ g/ml of LPS, or DHTS+LPS co-treatment. (B) RNA pull down assays on MCF-7 lysates obtained as in (A) after 2 h incubation with BiTNF (ARE+) or BiTNFneg (ARE-) exogenous RNA probes. Graph shows densitometric analyses by Image J software (NIH). (C) mRNA stability evaluation of TNF, pre-TNF, and GAPDH after co-treatment with actinomycin (D) and DHTS of scramble, vector, HuR silenced (siHuR) and HuR over-expressing (HuROE) MCF-7 cells. Relative HuR expression levels are shown in the representative WB. Residual mRNA, plotted in log scale, was normalized to relative RNA18S5 mRNA levels. Mean \pm SD refers to three independent experiments ($n = 3$).

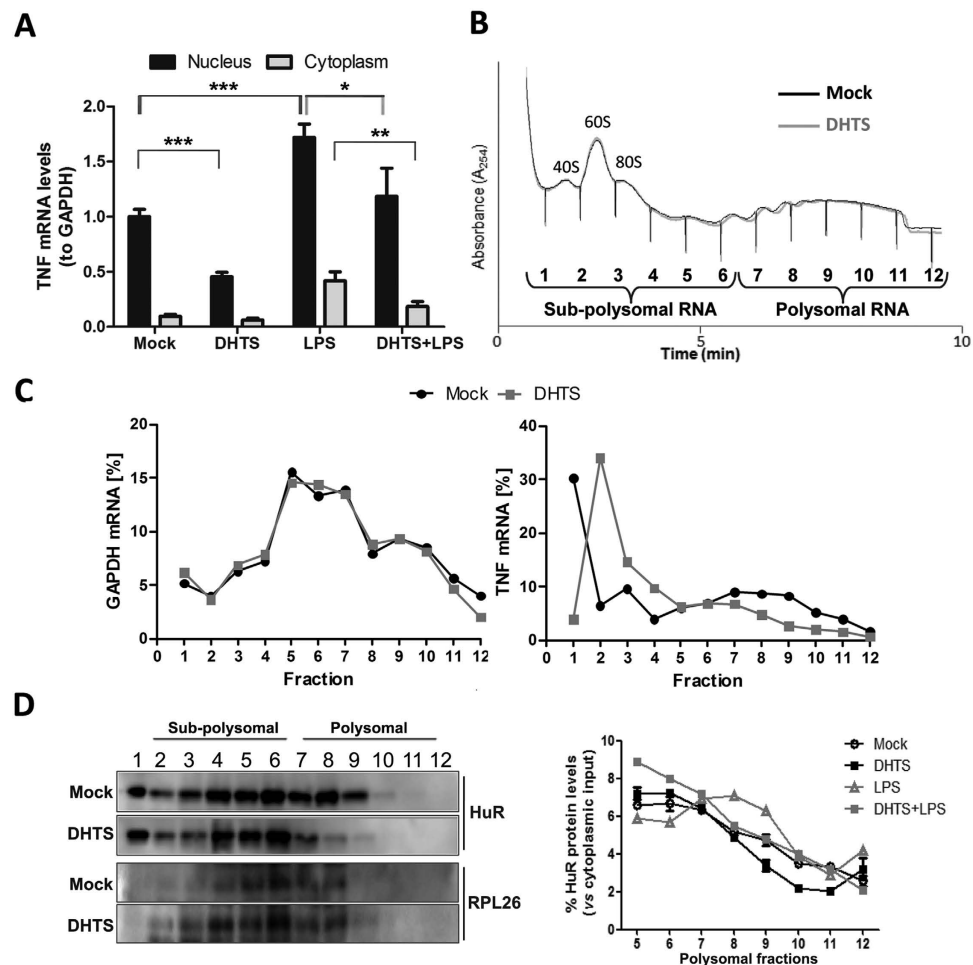


Figure 5. DHTS decreases TNF mRNA translational efficiency in MCF-7 cells. (A) Q-RT-PCR showing relative nuclear or cytoplasmic amounts of TNF mRNA after 3 h treatment, normalized with GAPDH mRNA levels. (B) Polysomal profiles of cytoplasmic RNA of MCF-7 treated for 3 h with DMSO or 1 μ M of DHTS. (C) Q-RT-PCR analysis of GAPDH and TNF mRNA levels in single cytoplasmic RNA fractions. (D) Representative WB showing the distribution of HuR and RPL26 ribosomal protein in single fractions (left); densitometric analysis of relative cytoplasmic HuR protein levels in polysomal fractions. Mean \pm SD refers to three independent experiments ($n = 3$).

mRNA by favoring the polysomal recruitment of the transcript²¹. Western blot analyses on protein samples precipitated from polysomal fractions revealed that DHTS displaces HuR from heavy polysomal fractions in un-stimulated and LPS-stimulated cells (Fig. 5D). Notably, we could not detect alterations in the activation of the p38 MAPK pathway in RAW264.7 cells (Supplementary Fig. S4D), which is responsible for cytoplasmic re-localization of HuR and stabilization of TNF mRNA upon LPS stimulation⁶. Similarly, treatment of 3 h with 1 μ M of DHTS did not affect sub-cellular localization of HuR in MCF-7 cells (Fig. 6A) and did not change HuR protein expression level (Fig. 6B). Nucleo-cytoplasmic fractionation confirmed DHTS-induced HuR nuclear localization (Fig. 6C) further supporting the loss of function of HuR in the cytoplasm and its reduced polysomal loading. Our data suggests that, at early time points, pharmacological inhibition of RNA loading on HuR by DHTS confines HuR into the nuclear compartment.

HuR expression influences the sensitivity of breast cancer cells to DHTS. Dose-response assays on HuR-silenced or -over-expressing MCF-7 cells revealed a different sensitivity to DHTS (IC₅₀ at 24 h of 0.45 or 1.3 μ M compared with scramble or vector MCF-7 cells, respectively) (Fig. 7A), showing a compensatory effect of HuR against DHTS. Interestingly, ectopic expression of TNF CDS alone, with 3'UTR and ARE or with 3'UTR but without ARE, did not influence the sensitivity of cells to 1 μ M of DHTS (Fig. 7B). This indicates that TNF itself is not responsible for this phenotypic response and that it can depend on the dysregulation of other factors regulated by HuR or, also, on independent events triggering the apoptotic pathways (Figs 3B, 7A). Real-time cell analysis assays demonstrated that DHTS exerts anti-proliferative effects at low doses (1 μ M), in MCF-7 cells after about 12 h of treatment (Fig. 7C). At

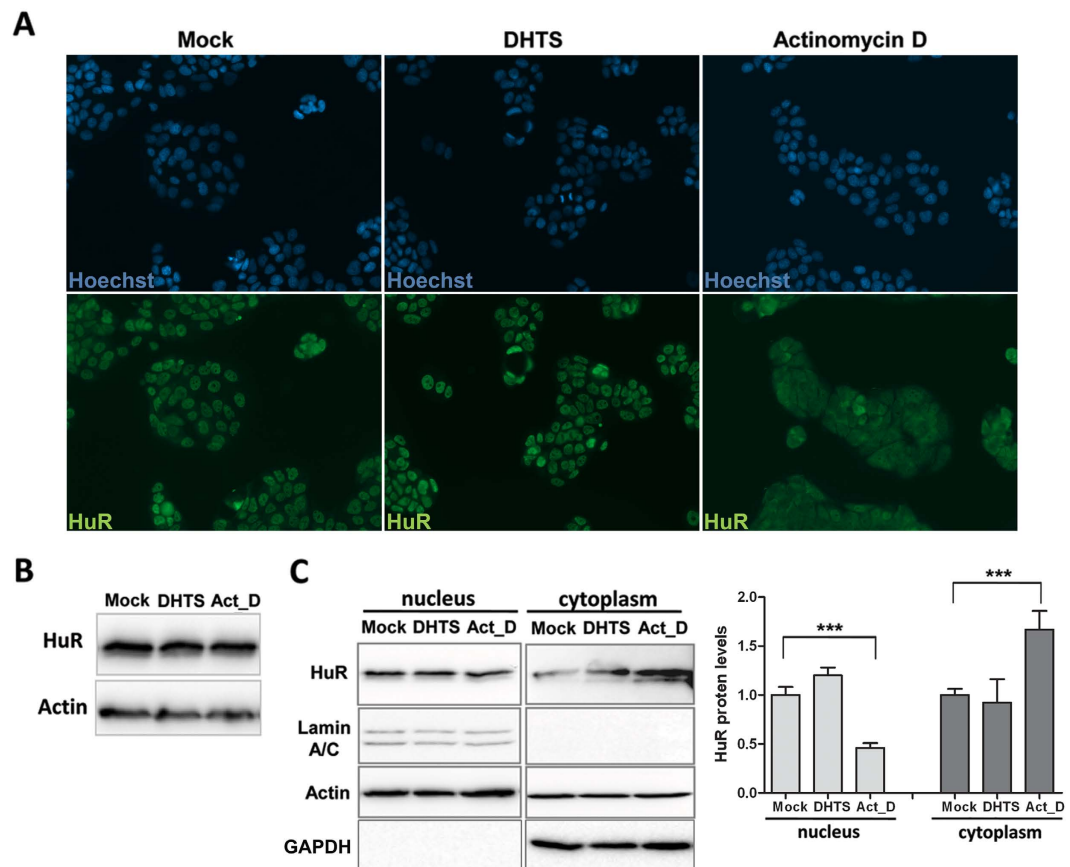


Figure 6. Effect of DHTS on HuR sub-cellular localization. (A) Representative immunofluorescence showing nuclei (Hoechst) or endogenous HuR (green) in MCF-7 cells treated with 1 μ M DHTS or 2 μ M of Actinomycin for 3 hD. (B) Representative western blot of total protein levels of HuR. (C) Western blot analysis on nuclear and cytoplasmic extracts of MCF-7 treated as in A. Densitometric analysis plot data of three independent experiments (n = 3).

higher doses (10 μ M) cytotoxic effects of the compound appeared in this experimental system, and were confirmed by MTT (data not shown). HuR-silenced MCF-7 cells showed a decreased proliferative rate, and DHTS treatment completely blocked cell proliferation. Conversely, the proliferative potential of HuR over-expressing cells was considerably influenced by 1 μ M of DHTS compared with control (Fig. 7D), indicating that HuR dosage can modulate phenotypic response of these cells to low DHTS doses.

To better understand the phenotypic effect related with down-regulation of HuR-dependent and/or signaling molecules such as TNF, we then investigated the chemotactic potential of DHTS-treated, MCF-7 conditioned medium using MDA-MB-231 trans-well migration as read-out, because the migration ability of MDA-MB-231 cells also depends on the presence of TNF and other cytokines in the surrounding environment²⁹. DHTS treated medium strongly inhibited MDA-MB-231 migration more effectively than HuR depletion, whereas the DHTS treatment in siHuR cells produced an almost chemotactic inactive medium (Fig. 7E, left panel). Once again, HuR over-expression completely rescued DHTS efficacy and the corresponding medium was equally effective as the control medium. Notably, HuR over-expression *per se* did not produce an increased chemotactic medium (Fig. 7E, right panel). Taken all together, these data show that HuR completely rescues at least three phenotypic effects of DHTS, such as direct viability and proliferation inhibition on cancer cells and autocrine/paracrine inhibition of cancer cell migration. This suggests that HuR is a pivotal intracellular target of DHTS and that multi-target effects of DHTS, and eventually of tanshinones, can be explained by the inhibition of RNA-binding activity of HuR.

Discussion

In this study we show that DHTS is a potent inhibitor of the HuR:RNA interaction, active in the low nanomolar range, mainly by limiting the association rate of HuR with RNA. This inhibition is functionally recapitulated in our cellular models, in which the known, DHTS induced down-regulation of TNF expression can be largely ascribed to the loss of function of HuR, that no longer stabilizes TNF mRNA neither mediates its polysomal loading. This molecular mechanism of action has a therapeutic relevance, as shown by the inhibitory effect on viability, proliferation and chemotaxis of breast cancer cell lines and

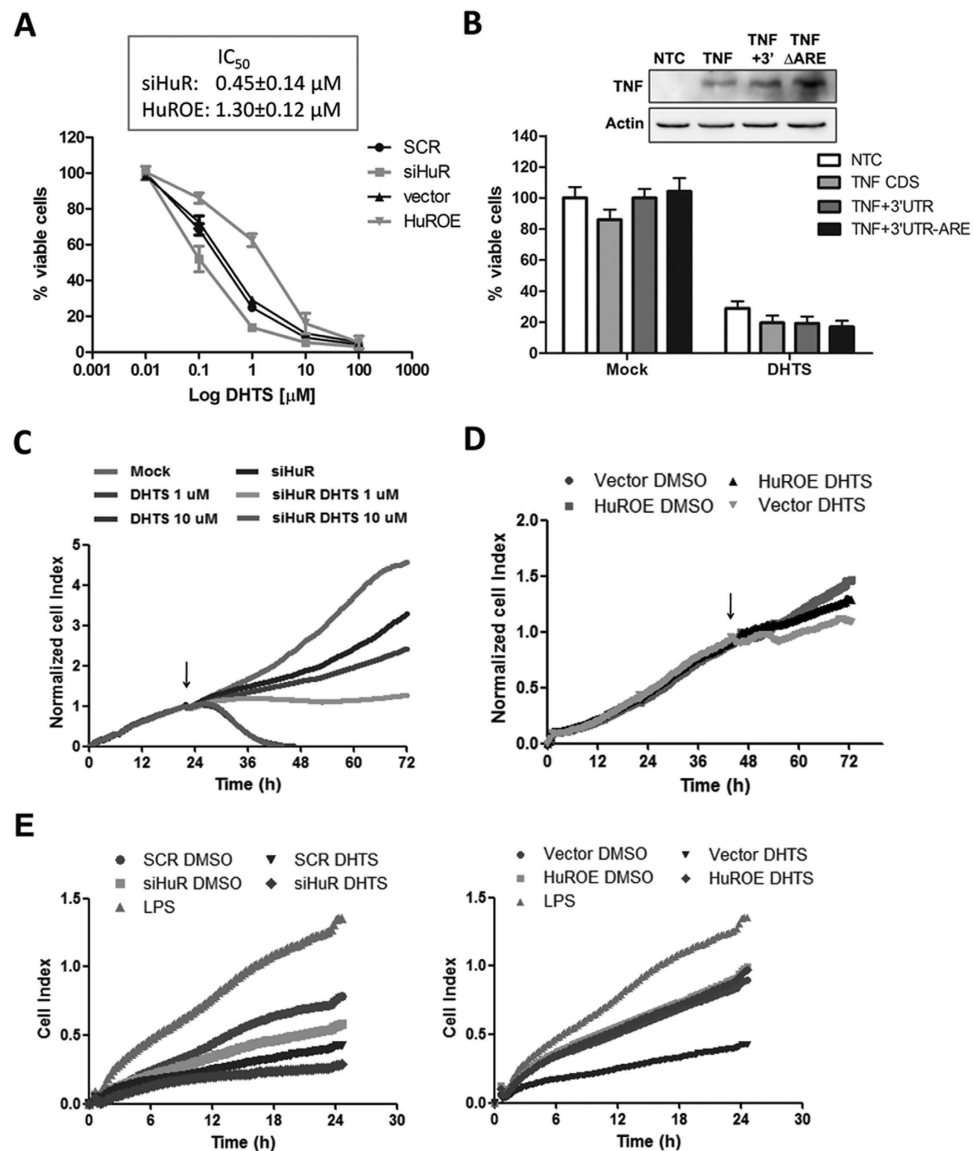


Figure 7. Efficacy of DHTS is dependent on HuR in breast cancer cell lines. (A) MTT assays on MCF-7 cells genetically ablated or over-expressing HuR and treated for 24 h with DMSO or DHTS. (B) MTT assays on MCF-7 un-transfected or transfected with pUNO1-hTNFA (TNF), pUNO1-hTNFA/3' UTR (TNF+3'), or pUNO1-hTNFA/3' UTR-ARE (TNFΔARE) plasmids, then treated as in A. Western blot shows relative amount resulting from ectopic expression of TNF. (C,D) RTCA proliferation assays. Arrows indicate the treatment point with DMSO or the indicated doses of DHTS (symbol of vector DMSO condition is behind HuROE DHTS in the figure). (E) RTCA migration assays. Complete media of SCR, vector, siHuR, and HuROE MCF-7 cells treated for 3 h with DMSO, 1 μM of DHTS 1 μg/ml of LPS (vector cells only for positive control) were diluted to obtain 1% FBS final concentration. MDA-MB-231 cells were equally seeded (20,000/well) in each well of the upper chamber. SCR; stably transfected cells with non targeting shRNA, siHuR; stably transfected cells with HuR targeting shRNA, vector; transiently transfected cells with empty vector, HuROE; transiently transfected cells with HuR expressing vector. Mean ± SD refers to three independent experiments (n = 3).

by the decreased TNF production in macrophages cells. Remarkably, the molecular and phenotypic effects induced by short-term and low doses of DHTS in breast cancer cell lines are rescued by the over-expression of HuR, confirming the cellular interaction between these two molecules. HuR over-expression in cancer tissues and the mechanistic role in mediating the inflammatory process has suggested that its inhibition could be beneficial in these pathologies^{22,30,31}. In addition, HuR has been proposed as a drug target in cardiovascular diseases, nephropathy and diabetic retinopathy^{32–34}. Several *in vitro* studies^{14,23,35} introduced some naturally occurring small molecule as HuR inhibitors, however the correlation among their post-transcriptional mechanism, biological effect and specificity, and therapeutic

usefulness remains elusive. The most noteworthy example is the naphthofuranone MS-444, that was identified by a screening campaign on $\approx 50,000$ natural product extracts using confocal fluctuation spectroscopic assays¹⁴. MS-444 has been shown to inhibit the HuR:RNA interaction by blocking the dimerization of HuR upon binding to the target RNA with a K_d around 40 nM. We did not investigate if DHTS acts via a similar inhibition of HuR dimerization. MS-444 has been recently used as a mechanistic tool to prevent HuR binding to miR-16³⁶ and to TDP-43 and FUS mRNA³⁷, although at higher concentrations than DHTS. In a recent effort compounds with a coumarin-derived core, which interfere with the function of HuR in the nanomolar range, have been identified using fluorescence polarization. This class of compounds shows anticancer properties in cell lines by inhibition of the expression of anti-apoptotic HuR targets, such as Bcl-2, Msi1 and XIAP³⁸. In our case, having RNA-binding activity as functional read-out, we measured a strong, nanomolar inhibition of the association rate constant between HuR and RNA *in vitro* that was also specific to HuR and not to other RBPs as Lin28b, TDP-43 and TTP. In particular, we observed a $\approx 60\%$ reduction in the number of TNF mRNA copies, as well as, with different extent, for ERBB2, VEGF, and CCND1 transcripts, using 1 μ M of DHTS by RIP experiments. Consistently, pull down experiments confirmed this effect although the magnitude of the interference was smaller ($\sim 40\%$), being limited by the use of a competitive exogenous RNA probe. The inhibitory effect of DHTS on AUF1 protein upon stimulation with LPS (Fig. 4B) could be ascribed to different mechanisms such as a diminished affinity for RNA or to an increased affinity for DHTS due to post-translational modifications, therefore we can not exclude a multi-targeting effect of DHTS in this condition. We did not observe a DHTS-induced activation of the p38 MAPK pathway nor HuR localization to the cytoplasm, further supporting the DHTS-induced HuR inhibition within cells and the utilization of DHTS in those cancer where HuR cytoplasmic localization plays a relevant role³¹. DHTS belongs to a family of natural diterpenes called tanshinones. Their anti-inflammatory, anti-atherosclerosis, cardioprotective and anti-cancer properties have been exploited in traditional Chinese medicine and are now under clinical investigation, but their exact mechanism of action is still unclear^{17,39}. In this context we disclose a previously unrecognized molecular mechanism of action, involving post-transcriptional regulation, that might contribute to explain the wide spectrum of activities of DHTS correlated with their well-known inhibition of TNF. In particular, tanshinone I inhibits growth, invasion and angiogenesis on human breast cancer cells MDA-MB-231, both *in vitro* and *in vivo*, by decreasing the TNF-induced VEGF production. Moreover it reduces the MDA-MB-231 adhesion properties by decreasing the TNF dependent pivotal intercellular adhesion molecule-1 (ICAM-1) and vascular adhesion molecule-1 (V-CAM) of endothelial cells²⁹. The efficacy of tanshinones has also been related with reduced expression of interleukins such as *IL-6*¹⁸, *MMPs*⁴⁰, *VEGF*⁴¹ and *COX-2*⁴². There are also indications that the modulatory properties on an inflammatory state upon administration of tanshinones occurs via post-transcriptional repression of specific miRNAs, as in the case of miRNA-155 in colon cancer cells⁴³. Interestingly, many of these key mRNAs and miRNAs are post-transcriptionally regulated by HuR^{8,20,44–47}. Tanshinones have been shown to target or modulate several transcription factors, ion channels or hormone receptors within the cell³⁹. We show that an intriguing explanation to the multi-target spectrum of tanshinones, could rely on the inhibition of the post-transcriptional function of HuR. Importantly resveratrol that has been shown to post-transcriptionally modulate TNF through KSRP regulation, providing a valuable example of the importance of post-transcriptional modulation of mRNA processing in the control of inflammation¹⁶. We provide mechanistic data indicating that HuR-mediated post-transcriptional inhibition is a major component of the cellular response to DHTS and that its relevance is shown by the HuR dosage modulation of cytotoxicity and migratory potential in breast cancer cells in response to DHTS. These findings suggest several important avenues for further research: (i) *HuR-dependent regulation of TNF expression levels*. Modulation of cytokines is a validated therapeutic strategy for the treatment of inflammatory disorders, and due to its predicted post-transcriptional regulation, it might be expected that administration of DHTS could attenuate the TNF protein levels rather than deplete TNF at systemic levels, such as a consequence of antibody-based therapeutic strategies⁴⁸; (ii) *DHTS as a tool to investigate the connections between cancer and inflammation based on modulation of post-transcriptional events*. Once validated *in vivo*, the use of DHTS (or of some of its analogues with a better drug-like profile) for therapeutic purposes could be conceived. A functional screening of anti-inflammatory agents allowed the identification of 15,16-dihydrotanshinone-I (DHTS) for its ability to inhibit a specific protein-RNA interaction. First, we have characterized the biochemical parameters of DHTS in virtue of its interference on the dynamic of HuR-RNA binding and anticipated a new molecular scaffold exerting a previous unrecognized bioactivity. Second, we have reported mechanistic evidences, in human tumor and mouse macrophages cell lines, suggesting HuR among the early intracellular targets of DHTS. The loss of function of HuR in response to this agent explains the modulation of the stability and translational efficiency of target mRNAs. Third, we have shown that phenotypic response, in terms of migration and sensitivity, of breast cancer cells to DHTS is remarkably influenced by HuR expression. Overall, these findings advance the understanding of contribution of post-transcriptional control in mediating anti-inflammatory and anti-cancer effects of a class of natural compounds and expand the concept of “genome druggability” by adding the post-transcriptional activity of the RNA binding protein HuR as feasible event that can occur during a pharmacological treatment. Finally, we suggest a novel rationale for the use of tanshinones in human diseases where HuR is deregulated or has prognostic significance, as breast, colon or ovarian cancers.

supernatants were collected (cytoplasmic lysates), whereas pelleted nuclei were re-suspended in buffer N (10 mM Tris-HCl pH 8, 25 mM NaCl, 5 mM MgCl₂, 1% p/w sodium deoxycholate, 1% Triton, 0.2% SDS, 1 mM DTT) plus protease and RNase inhibitors and sonicated as above. TRIzol reagent (Life Technologies, 12183-555) was used for RNA isolation. Quantitative PCRs, after cDNA Synthesis (Thermo Scientific, K1612) with equimolar mix of random and oligo-dT primers and two micrograms of template RNA, were performed using Universal SYBR Master Mix (KAPA Biosystems, KR0389) on CFX-96/384 thermal cyclers (BIO-RAD). $2^{-\Delta\Delta Ct}$ method was used for quantification of mRNAs. Forward and reverse primers used: RNA18S5 (GCAGCTAGGAATAATGGAATAG and TGGCAAATGCTTTCGCTCTG), TNF (5'-GGGACCTCTCTCTAATCAGC and 5'-TCAGCTTGAGGGTTTGCTAC), GAPDH (5'-CAAGGTCA TCCATGACAACCTT and 5'-GTCCACCACCCTGTTGCTGTA), CD14 (5'-GAAGCTAAAGCACTTCCA GAGC and 5'-TTCATCGTCCAGCTCACAAG), ERBB2 (GGTACTGAAAGCCTTAGGGAAGC and AC ACCATTGCTGTTCCCTCCTC), VEGF (CCGCAGACGTGTAAATGTTCCCT and CGGCTTGTCACAT CTGCAAGTA), and CCND1 (CAGAACACGGCTCACGCTTAC and CTTGCCCCATCACGACAGAC). Primers for pre-TNF, pre-BRCA1, pre-CTCF, pre-MDM2, pre-MYBL2, and pre-NFATC3 are described elsewhere²⁸.

Polysomal profiling and protein/RNA isolation. For polysomal RNA profiling, cytoplasmic lysates of 2×10^7 MCF-7 cells/sample were subjected to 15–50% sucrose gradient ultracentrifugation and fractionation following reported protocols^{6,54,55}. Aliquots of cytoplasmic lysates were considered for normalization. From each sub-polysomal or polysomal fraction, protein samples were obtained by precipitation with 10% final concentration of trichloroacetic acid (TCA), while RNAs were isolated by TRIzol reagent (1:5 v/v). Fractions 1 to 6 were pooled to represent sub-polysomal RNA samples, while pooling of fractions 7 to 12 represented polysomal RNA samples.

RNA immunoprecipitation (RIP) and RNA pull-down assays. Five $\times 10^6$ cells/sample were used for each RIP experiment, performed as described in⁵⁶ without cross-linking steps and using 0.8 μ g/ml of anti-Hu antibody or of mouse IgG isotype (negative control). TRIzol reagent was added directly to the beads for HuR-bound RNA isolation. Fold enrichment was calculated as $2e^{-\Delta Ct}$, $\Delta Ct = \text{target mRNA IP HuR}/(\text{target mRNA IgG})$. For RNA pull-down assays, MCF-7 cells were lysed in buffer R (20 mM HEPES pH 7.5, 50 mM KCl, 0.5 μ g BSA, 0.25% Glycerol, + protease and RNase inhibitors) by sonication (80 amplitude with 6–7 cycles of 7" on and 45" off) at 4°C. Clear lysates (0.2 μ m-filtered) were incubated for 1 h at 4°C with 0.5 μ M of positive (BiTNF) or negative biotinylated (BiTNFneg, 5'-ACCACCCACCACCCACCACCCCA) RNA probes²³. Solutions were incubated for further 2 h with 30 μ l/samples of streptavidin magnetic beads (Life technologies, 11205D). Specific protein enrichments in beads-precipitated samples were analyzed by immunoblotting and densitometric analysis obtained using Image J 1.4 software (NIH).

RNA stability assays. SCR, siHuR, vector, and HuROE MCF-7 cells were co-treated with Act-D (2 μ M) and DMSO or DHTS for 3 h. Kinetics for mRNA stability evaluation has been carried out by extracting RNA in five time points (0, 30, 60, 120, 240 min) to be used for cDNA synthesis and quantitative PCR analyses. Residual levels of target mRNAs were normalized to those of RNA18S5, and data were plotted as function of time with respect 0 min condition.

Cytotoxicity, Click-iT and RTCA assays. Sensitivity to DHTS was evaluated by CellTiter-Glo[®] (Promega, G7570), alamarBlue or MTT reagents following suggested protocols.

Ectopic expression of human TNF has been obtained with the pUNO1-hTNFA (Invivogen) plasmid. Inserts for recombinant pUNO-hTNFA/3'UTR and pUNO-hTNFA/3'UTR Δ ARE plasmids have been obtained by digestion of pBS vectors^{57,58}, respectively, with XbaI and then blunt-end ligated in pUNO1-hTNFA vector digested with NheI restriction enzyme. Sequencing confirmed the results.

Apoptosis was evaluated by Caspase-Glo[®] 3/7 luminescent assay (Promega, G8090) upon normalization to the number of trypan blue negative cells. RNA transcription was assessed using Click-iT[®] RNA Alexa Fluor[®] 488 Imaging Kit (Life Technologies, C10330). EthynylUridine (EU) was added 30 min before fixation, permeabilization and Click-iT reaction. Fluorescence signals relative to nascent RNA and nuclei (Hoechst 33342) were detected with Operetta instrument (PerkinElmer) and analyzed with Harmony 3.5.2 software (PerkinElmer). Proliferation assays were carried out with the xCELLigence RTCA DP Instrument (Roche) by plating 5,000 cells/well at t_0 in E-Plate-16 format. Parallel plates were used to check the magnitude of HuR silencing or over-expression. Migration assays were performed using the same instrument and settings for CIM-Plates-16 (Roche), using media (1% FBS) of MCF-7 cells in the lower chamber and MDA-MB-231 cells equally seeded (20,000/well/160 μ l) in the upper chamber.

Immunoblotting and Enzyme-linked immunosorbent (ELISA) assay. Total, nuclear, and cytoplasmic cell extracts were subjected to 15%-SDS-PAGE and resolved proteins were transferred to nitrocellulose membrane (Millipore, IPVH00010) as previously described⁵⁹. ELISA assays were carried out using Human TNF kit (Thermo Scientific, EH3TNFA) and the suggested protocol using supernatants of 95%-confluent MCF-7 cells at time of treatment, seeded in 12-well plates.

Statistical analysis. All data are expressed as means \pm SD from three to four independent experiments and statistics was performed using one-way ANOVA with Bonferroni's multiple comparison test and Alpha level of 0.05. Magnitude of significance was also evaluated by student *t*-test and probability (P) values <0.05 , <0.01 , and <0.001 were indicated with *, **, *** symbols, respectively.

References

- Anderson, P. Post-transcriptional regulons coordinate the initiation and resolution of inflammation. *Nat. Rev. Immunol.* **10**, 24–35 (2010).
- Grivnenkov, S. I. & Karin, M. Inflammatory cytokines in cancer: tumour necrosis factor and interleukin 6 take the stage. *Ann. Rheum. Dis.* **70** Suppl 1, i104–8 (2011).
- Khera, T. K., Dick, A. D. & Nicholson, L. B. Mechanisms of TNF α regulation in uveitis: focus on RNA-binding proteins. *Prog. Retin. Eye Res.* **29**, 610–21 (2010).
- Schlundt, A. *et al.* Structural basis for RNA recognition in roquin-mediated post-transcriptional gene regulation. *Nat. Struct. Mol. Biol.* **21**, 671–8 (2014).
- Wang, E., Ma, W. J., Aghajanian, C. & Spriggs, D. R. Posttranscriptional regulation of protein expression in human epithelial carcinoma cells by adenine-uridine-rich elements in the 3'-untranslated region of tumor necrosis factor-alpha messenger RNA. *Cancer Res.* **57**, 5426–33 (1997).
- Tiedje, C. *et al.* The p38/MK2-Driven Exchange between Tristetraprolin and HuR Regulates AU-Rich Element-Dependent Translation. *PLoS Genet.* **8**, e1002977 (2012).
- Simone, L. E. & Keene, J. D. Mechanisms coordinating ELAV/Hu mRNA regulons. *Curr. Opin. Genet. Dev.* **23**, 35–43 (2013).
- Levy, N. S., Chung, S., Furneaux, H. & Levy, A. P. Hypoxic stabilization of vascular endothelial growth factor mRNA by the RNA-binding protein HuR. *J. Biol. Chem.* **273**, 6417–23 (1998).
- Lal, A. *et al.* Concurrent versus individual binding of HuR and AUF1 to common labile target mRNAs. *EMBO J.* **23**, 3092–102 (2004).
- Abdelmohsen, K. *et al.* Phosphorylation of HuR by Chk2 regulates SIRT1 expression. *Mol. Cell* **25**, 543–557 (2007).
- Kim, W.-K. *et al.* A new anti-inflammatory agent KL-1037 represses proinflammatory cytokine and inducible nitric oxide synthase (iNOS) gene expression in activated microglia. *Neuropharmacology* **47**, 243–52 (2004).
- Schmidt, N. *et al.* Transcriptional and post-transcriptional regulation of iNOS expression in human chondrocytes. *Biochem. Pharmacol.* **79**, 722–32 (2010).
- Ho, F.-M. *et al.* The anti-inflammatory carbazole, LCY-2-CHO, inhibits lipopolysaccharide-induced inflammatory mediator expression through inhibition of the p38 mitogen-activated protein kinase signaling pathway in macrophages. *Br. J. Pharmacol.* **141**, 1037–47 (2004).
- Meisner, N.-C. *et al.* Identification and mechanistic characterization of low-molecular-weight inhibitors for HuR. *Nat. Chem. Biol.* **3**, 508–15 (2007).
- Mukherjee, N., Lager, P. J., Friedersdorf, M. B., Thompson, M. A. & Keene, J. D. Coordinated posttranscriptional mRNA population dynamics during T-cell activation. *Mol. Syst. Biol.* **5**, 288 (2009).
- Bollmann, F. *et al.* Resveratrol post-transcriptionally regulates pro-inflammatory gene expression via regulation of KSRP RNA binding activity. *Nucleic Acids Res.* **42**, 12555–69 (2014).
- Wang, X., Morris-Natschke, S. L. & Lee, K.-H. New developments in the chemistry and biology of the bioactive constituents of Tanshen. *Med. Res. Rev.* **27**, 133–48 (2007).
- Lin, C. *et al.* Tanshinone IIA inhibits breast cancer stem cells growth *in vitro* and *in vivo* through attenuation of IL-6/STAT3/NF- κ B signaling pathways. *J. Cell. Biochem.* **114**, 2061–70 (2013).
- Lee, C.-Y. *et al.* Anticancer effects of tanshinone I in human non-small cell lung cancer. *Mol. Cancer Ther.* **7**, 3527–38 (2008).
- Dixon, D. A. *et al.* Altered expression of the mRNA stability factor HuR promotes cyclooxygenase-2 expression in colon cancer cells. **108**, 1657–1665 (2001).
- Dean, J. L. *et al.* The 3' untranslated region of tumor necrosis factor alpha mRNA is a target of the mRNA-stabilizing factor HuR. *Mol. Cell. Biol.* **21**, 721–30 (2001).
- Chen, J. *et al.* Posttranscriptional gene regulation of IL-17 by the RNA-binding protein HuR is required for initiation of experimental autoimmune encephalomyelitis. *J. Immunol.* **191**, 5441–50 (2013).
- D'Agostino, V. G., Adami, V. & Provenzani, A. A novel high throughput biochemical assay to evaluate the HuR protein-RNA complex formation. *PLoS One* **8**, e72426 (2013).
- Wang, H. *et al.* The structure of the ARE-binding domains of Hu antigen R (HuR) undergoes conformational changes during RNA binding. *Acta Crystallogr. D. Biol. Crystallogr.* **69**, 373–80 (2013).
- Xu, F. *et al.* Loss of repression of HuR translation by miR-16 may be responsible for the elevation of HuR in human breast carcinoma. *J. Cell. Biochem.* **111**, 727–34 (2010).
- Jang, S.-I. *et al.* Tanshinone IIA from *Salvia miltiorrhiza* inhibits inducible nitric oxide synthase expression and production of TNF-alpha, IL-1beta and IL-6 in activated RAW 264.7 cells. *Planta Med.* **69**, 1057–9 (2003).
- Yu, M. *et al.* Targeting transmembrane TNF- α suppresses breast cancer growth. *Cancer Res.* **73**, 4061–74 (2013).
- Mukherjee, N. *et al.* Integrative regulatory mapping indicates that the RNA-binding protein HuR couples pre-mRNA processing and mRNA stability. *Mol. Cell* **43**, 327–39 (2011).
- Nizamutdinova, I. T. *et al.* Tanshinone I suppresses growth and invasion of human breast cancer cells, MDA-MB-231, through regulation of adhesion molecules. *Carcinogenesis* **29**, 1885–92 (2008).
- Krishnamurthy, P. *et al.* Myocardial knockdown of mRNA-stabilizing protein HuR attenuates post-MI inflammatory response and left ventricular dysfunction in IL-10-null mice. *FASEB J.* **24**, 2484–94 (2010).
- Abdelmohsen, K. & Gorospe, M. Posttranscriptional regulation of cancer traits by HuR. *Wiley Interdiscip. Rev. RNA* **1**, 214–29 (2010).
- Amadio, M. *et al.* The PKCbeta/HuR/VEGF pathway in diabetic retinopathy. *Biochem. Pharmacol.* **80**, 1230–7 (2010).
- Misquitta, C. M., Iyer, V. R., Werstuck, E. S. & Grover, A. K. The role of 3'-untranslated region (3'-UTR) mediated mRNA stability in cardiovascular pathophysiology. *Mol. Cell. Biochem.* **224**, 53–67 (2001).
- Yu, C. *et al.* Human antigen R mediated post-transcriptional regulation of epithelial-mesenchymal transition related genes in diabetic nephropathy. *J. Diabetes* (2014). doi: 10.1111/1753-0407.12220.
- Chae, M.-J. *et al.* Chemical inhibitors destabilize HuR binding to the AU-rich element of TNF-alpha mRNA. *Exp. Mol. Med.* **41**, 824–31 (2009).
- Young, L. E., Moore, A. E., Sokol, L., Meisner-Kober, N. & Dixon, D. A. The mRNA stability factor HuR inhibits microRNA-16 targeting of COX-2. *Mol. Cancer Res.* **10**, 167–80 (2012).
- Lu, L. *et al.* Hu Antigen R (HuR) Is a Positive Regulator of the RNA-binding Proteins TDP-43 and FUS/TLS: IMPLICATIONS FOR AMYOTROPHIC LATERAL SCLEROSIS. *J. Biol. Chem.* **289**, 31792–804 (2014).
- Wu, X. *et al.* Identification and Validation of Novel Small Molecule Disruptors of HuR-mRNA Interaction. *ACS Chem. Biol.* doi: 10.1021/cb500851u (2015).

39. Tian, X.-H. & Wu, J. H. Tanshinone derivatives: a patent review (January 2006—September 2012). *Expert Opin. Ther. Pat.* **23**, 19–29 (2013).
40. Jin, U.-H. *et al.* Tanshinone IIA from *Salvia miltiorrhiza* BUNGE inhibits human aortic smooth muscle cell migration and MMP-9 activity through AKT signaling pathway. *J. Cell. Biochem.* **104**, 15–26 (2008).
41. Xing, Y., Tu, J., Zheng, L., Guo, L. & Xi, T. Anti-angiogenic effect of tanshinone IIA involves inhibition of the VEGF/VEGFR2 pathway in vascular endothelial cells. *Oncol. Rep.* **33**, 163–70 (2015).
42. Ma, Y. *et al.* Cryptotanshinone attenuates cardiac fibrosis via downregulation of COX-2, NOX-2, and NOX-4. *J. Cardiovasc. Pharmacol.* **64**, 28–37 (2014).
43. Tu, J. *et al.* TanshinoneIIA ameliorates inflammatory microenvironment of colon cancer cells via repression of microRNA-155. *Int. Immunopharmacol.* **14**, 353–61 (2012).
44. Gurgis, F. M. S. *et al.* The p38-MK2-HuR pathway potentiates EGFRvIII-IL-1 β -driven IL-6 secretion in glioblastoma cells. *Oncogene* doi: 10.1038/onc.2014.225 (2014).
45. Kurosu, T. *et al.* HuR keeps an angiogenic switch on by stabilising mRNA of VEGF and COX-2 in tumour endothelium. *Br. J. Cancer* **104**, 819–29 (2011).
46. Akoel, E.-S. *et al.* Nitric oxide increases the decay of matrix metalloproteinase 9 mRNA by inhibiting the expression of mRNA-stabilizing factor HuR. *Mol. Cell. Biol.* **23**, 4901–16 (2003).
47. Chang, S.-H. & Hla, T. Post-transcriptional gene regulation by HuR and microRNAs in angiogenesis. *Curr. Opin. Hematol.* **21**, 235–40 (2014).
48. Kim, S. Y. & Solomon, D. H. Tumor necrosis factor blockade and the risk of viral infection. *Nat. Rev. Rheumatol.* **6**, 165–74 (2010).
49. Mahtani, K. R. *et al.* Mitogen-activated protein kinase p38 controls the expression and posttranslational modification of tristetraprolin, a regulator of tumor necrosis factor alpha mRNA stability. *Mol. Cell. Biol.* **21**, 6461–9 (2001).
50. Viiri, J. *et al.* Autophagy Activation Clears ELAVL1/HuR-Mediated Accumulation of SQSTM1/p62 during Proteasomal Inhibition in Human Retinal Pigment Epithelial Cells. *PLoS One* **8**, e69563 (2013).
51. Kundu, P., Fabian, M. R., Sonenberg, N., Bhattacharyya, S. N. & Filipowicz, W. HuR protein attenuates miRNA-mediated repression by promoting miRISC dissociation from the target RNA. *Nucleic Acids Res.* **40**, 5088–100 (2012).
52. Motulsky, H. J. & Mahan, L. C. The kinetics of competitive radioligand binding predicted by the law of mass action. *Mol. Pharmacol.* **25**, 1–9 (1984).
53. Ali, P. S. S., Ghoshdastider, U., Hoffmann, J., Brutschy, B. & Filipek, S. Recognition of the let-7g miRNA precursor by human Lin28B. *FEBS Lett.* **586**, 3986–90 (2012).
54. Provenzani, A. *et al.* Global alterations in mRNA polysomal recruitment in a cell model of colorectal cancer progression to metastasis. *Carcinogenesis* **27**, 1323–33 (2006).
55. Bisio, A. *et al.* Functional analysis of CDKN2A/p16INK4a 5'-UTR variants predisposing to melanoma. *Hum. Mol. Genet.* **19**, 1479–91 (2010).
56. Peritz, T. *et al.* Immunoprecipitation of mRNA-protein complexes. *Nat. Protoc.* **1**, 577–80 (2006).
57. Henneke, M. *et al.* Composition and arrangement of genes define the strength of IRES-driven translation in bicistronic mRNAs. *Nucleic Acids Res.* **29**, 3327–34 (2001).
58. Kontoyiannis, D., Pasparakis, M., Pizarro, T. T., Cominelli, F. & Kollias, G. Impaired on/off regulation of TNF biosynthesis in mice lacking TNF AU-rich elements: implications for joint and gut-associated immunopathologies. *Immunity* **10**, 387–98 (1999).
59. Latorre, E. *et al.* Downregulation of HuR as a new mechanism of doxorubicin resistance in breast cancer cells. *Mol. Cancer* **11**, 13 (2012).

Acknowledgements

We thank prof. Alessandro Quattrone, CIBIO, University of Trento, for providing us with the expression plasmids for TDP-43, Lin28b and TTP. A.P. thank prof. Dan Dixon, University of Kansas, for helpful discussion. C.T. and M.G. would like to thank Kathrin Laass for expert technical assistance. Funding: This work was supported by the CIBIO intramural start-up funds to A.P. and by the AXonomIX research project to A. P. financed by the Provincia Autonoma di Trento, Italy. C.T. and M.G. were supported by a Deutsche Forschungsgemeinschaft (DFG) grant [Ga453/13-1].

Author Contributions

V.D.A. ideated and performed most of the experiments, drafted and critically revised the manuscript, P.L. performed REMSAs with DHTS analogs and with RBPs, B.M. performed ActD chase experiments, C.T. performed most of the experiments in RAW cells, C.Z. performed IF experiments, N.T. helped with immunoprecipitation, M.A. performed ActD chase experiment and critically revised the manuscript, M.G., L.M. and P.S. critically discussed the project and revised the manuscript, E.L. performed RIP experiments, and A.P. ideated the project and the experiments, coordinated the work, wrote and revised the manuscript. All authors reviewed the manuscript.

Additional Information

Supplementary information accompanies this paper at <http://www.nature.com/srep>

Competing financial interests: The authors declare no competing financial interests.

How to cite this article: D'Agostino, V. G. *et al.* Dihydrotanshinone-I interferes with the RNA-binding activity of HuR affecting its post-transcriptional function. *Sci. Rep.* **5**, 16478; doi: 10.1038/srep16478 (2015).



This work is licensed under a Creative Commons Attribution 4.0 International License. The images or other third party material in this article are included in the article's Creative Commons license, unless indicated otherwise in the credit line; if the material is not included under the Creative Commons license, users will need to obtain permission from the license holder to reproduce the material. To view a copy of this license, visit <http://creativecommons.org/licenses/by/4.0/>

ACKNOWLEDGEMENTS

I am very grateful to my supervisor, **Dr. Alessandro Provenzani** for guiding and training me. I sincerely thank him for giving me a lot of freedom, motivation, and his efforts for my perfection. I also thank my advisor **Dr. Vito D'Agostino** for his kind support during my PhD. It was a pleasure to work with my lab members (**Rosa, Barbara, Chiara, Nat, Isabelle, Nausica, Daniele and Maria**), thanks to them for their friendliness, time, help in practical things throughout my PhD. I specially thank **Nat** for assisting me in the Immunofluorescence and electroporation experiments during the revision of my thesis.

My sincere thanks to **Prof. Dr. Matthias Gaestel** and **Dr. Christopher Tiedje** from MHH Germany for their supervision during my internship period. It was a wonderful experience to work with you, during my PhD.

I also would also like to thank **Betty** for her kind help throughout PhD period. I am grateful to the **Erasmus Plus traineeship** program to sponsor me for two months period at MHH Germany. I also would like to express my sincere gratitude to **Erasmus Mundus program, India4EU** for selecting me as a capable candidate with PhD fellowship for 3 years at CIBIO, University of Trento, Italy.

My special thanks and appreciation goes to my parents as well as my family for their blessings, love, patience, support and understanding throughout my studies and most of all to the Almighty God who made everything possible.

Preet Lal

